



University of Kentucky
UKnowledge

Theses and Dissertations--Mechanical
Engineering

Mechanical Engineering


2018

DISCRETE-TIME ADAPTIVE CONTROL ALGORITHMS FOR REJECTION OF SINUSOIDAL DISTURBANCES

Mohammadreza Kamaldar

University of Kentucky, mkamaldar@uky.edu

Author ORCID Identifier:

 <https://orcid.org/0000-0002-4774-9794>

Digital Object Identifier: <https://doi.org/10.13023/etd.2018.478>

[Right click to open a feedback form in a new tab to let us know how this document benefits you.](#)

Recommended Citation

Kamaldar, Mohammadreza, "DISCRETE-TIME ADAPTIVE CONTROL ALGORITHMS FOR REJECTION OF SINUSOIDAL DISTURBANCES" (2018). *Theses and Dissertations--Mechanical Engineering*. 129.
https://uknowledge.uky.edu/me_etds/129

This Doctoral Dissertation is brought to you for free and open access by the Mechanical Engineering at UKnowledge. It has been accepted for inclusion in Theses and Dissertations--Mechanical Engineering by an authorized administrator of UKnowledge. For more information, please contact UKnowledge@lsv.uky.edu.

STUDENT AGREEMENT:

I represent that my thesis or dissertation and abstract are my original work. Proper attribution has been given to all outside sources. I understand that I am solely responsible for obtaining any needed copyright permissions. I have obtained needed written permission statement(s) from the owner(s) of each third-party copyrighted matter to be included in my work, allowing electronic distribution (if such use is not permitted by the fair use doctrine) which will be submitted to UKnowledge as Additional File.

I hereby grant to The University of Kentucky and its agents the irrevocable, non-exclusive, and royalty-free license to archive and make accessible my work in whole or in part in all forms of media, now or hereafter known. I agree that the document mentioned above may be made available immediately for worldwide access unless an embargo applies.

I retain all other ownership rights to the copyright of my work. I also retain the right to use in future works (such as articles or books) all or part of my work. I understand that I am free to register the copyright to my work.

REVIEW, APPROVAL AND ACCEPTANCE

The document mentioned above has been reviewed and accepted by the student's advisor, on behalf of the advisory committee, and by the Director of Graduate Studies (DGS), on behalf of the program; we verify that this is the final, approved version of the student's thesis including all changes required by the advisory committee. The undersigned agree to abide by the statements above.

Mohammadreza Kamaldar, Student

Dr. Jesse B. Hoagg, Major Professor

Dr. Alexandre Martin, Director of Graduate Studies

DISCRETE-TIME ADAPTIVE CONTROL ALGORITHMS FOR
REJECTION OF SINUSOIDAL DISTURBANCES

DISSERTATION

A dissertation submitted in partial fulfillment of the requirements for the
degree of Doctor of Philosophy in the College of Engineering at the
University of Kentucky

By
Mohammadreza Kamaldar

Advisor: Jesse B. Hoagg, Professor of Mechanical Engineering

Lexington, Kentucky, 2018

Copyright© Mohammadreza Kamaldar 2018

ABSTRACT OF DISSERTATION

DISCRETE-TIME ADAPTIVE CONTROL ALGORITHMS FOR REJECTION OF SINUSOIDAL DISTURBANCES

We present new adaptive control algorithms that address the problem of rejecting sinusoids with known frequencies that act on an unknown asymptotically stable linear time-invariant system. To achieve asymptotic disturbance rejection, adaptive control algorithms of this dissertation rely on limited or no system model information. These algorithms are developed in discrete time, meaning that the control computations use sampled-data measurements. We demonstrate the effectiveness of algorithms via analysis, numerical simulations, and experimental testings. We also present extensions to these algorithms that address systems with decentralized control architecture and systems subject to disturbances with unknown frequencies.

KEYWORDS: Adaptive, Disturbance Rejection, Harmonic, Unknown System

Author's signature: Mohammadreza Kamaldar

Date: December 14, 2018

Discrete-Time Adaptive Control Algorithms for Rejection of Sinusoidal Disturbances

By
Mohammadreza Kamaldar

Director of Dissertation: Prof. Jesse B. Hoagg

Director of Graduate Studies: Prof. Alexandre Martin

Date: December 14, 2018

*To my parents,
for their love and sacrifice*

ACKNOWLEDGMENTS

First and foremost, I would like to truly thank my mentor and advisor, Professor Jesse Hoagg, for his continued guidance, support, and technical resourcefulness over the course of my studies. Through the years, I have had the valuable opportunity of learning and benefiting from his incisive way of thinking, insightful recommendations, vibrant-yet-meticulous presentation style, and his discipline and sense of responsibility. His impact on my personal and professional development is indeed remarkable and unforgettable.

In addition, I want to acknowledge Professors Michael Seigler, David Herrin, Yu-Ming Zhang, and Olivier Thibault for being on my dissertation committee and for their helpful discussions.

Finally, I would like to especially thank my parents Hosein and Azam, and my siblings Ehsan, Elham, Negar, and Zohre for their love, support, and encouragement. I am genuinely grateful to them for greatly caring for me over the years and always motivating me to the pursuit of knowledge.

CONTENTS

Acknowledgments	iii
Contents	iv
List of Figures	v
List of Tables	vi
Chapter 1 — Introduction and Motivation	1
1.1 Problem Statement	1
1.2 Motivating Applications	3
1.3 Literature Review	7
1.4 Summary of Contributions	11
Chapter 2 — Frequency-Domain Adaptive Higher Harmonic Control	14
2.1 Introduction	14
2.2 Notation	16
2.3 Problem Formulation	16
2.4 Review of Frequency-Domain Higher Harmonic Control	19
2.5 Frequency-Domain Adaptive Higher Harmonic Control	20
2.6 FD-AHHC Stability Analysis	22
2.7 Numerical Study of the Steady-State and Transient Performance of FD-AHHC	25
2.8 FD-AHHC for Multi-Tone Disturbances	27
2.9 Numerical Examples	29
2.10 Conclusions	33
2.11 Proofs of Theorems 2.1 and 2.2	34
2.12 Proofs of Proposition 2.1 and Theorems 2.3 and 2.4	39
Chapter 3 — Time-Domain Adaptive Higher Harmonic Control . . .	44
3.1 Introduction	44
3.2 Notation	46
3.3 Problem Formulation	46
3.4 Mathematical Preliminaries	47
3.5 Time-Domain Higher Harmonic Control	50
3.6 Stability Analysis of TD-HHC	51
3.7 Time-Domain Adaptive Higher Harmonic Control	52
3.8 Stability Analysis of TD-AHHC	55
3.9 Numerical Examples	56
3.10 Results from Active Noise Control Experiments	64
3.11 Conclusions	74

3.12	Proof of Proposition 3.1	75
3.13	Proof of Theorem 3.2	79
3.14	Proof of Theorem 3.3	82
3.15	Proof of Lemma 3.2	83
3.16	Proofs of Proposition 3.2 and Theorem 3.4	83
3.17	Lemma 3.3 used in proof of Theorems 3.3 and 3.4	94
Chapter 4 — Frequency-Domain Adaptive Harmonic Control		95
4.1	Introduction	95
4.2	Notation	97
4.3	Problem Formulation	97
4.4	Frequency-Domain Adaptive Harmonic Control	99
4.5	FD-AHC Stability Analysis	101
4.6	FD-AHC for Multi-Tone Disturbances	102
4.7	Numerical Examples	104
4.8	Conclusions	106
4.9	Proof of Theorem 4.2	106
Chapter 5 — Time-Domain Adaptive Harmonic Control		111
5.1	Introduction	111
5.2	Notation	113
5.3	Problem Formulation	113
5.4	Time-Domain Adaptive Harmonic Control	116
5.5	Stability Analysis	118
5.6	Numerical Examples Comparing TD-AHC To FD-HHC	119
5.7	Results From Active Noise Control Experiments	123
5.8	Conclusions	133
5.9	Proof of Theorem 5.2	134
Chapter 6 — Frequency-Domain Adaptive Harmonic Control for De-		
centralized Control Systems		140
6.1	Introduction	140
6.2	Notation	142
6.3	Problem Formulation	142
6.4	Decentralized Frequency-Domain Adaptive Harmonic Control	145
6.5	Stability and Performance Analysis	147
6.6	Numerical Examples	149
6.7	Conclusions	150
6.8	Proof of Theorem 6.2	151
Chapter 7 — Frequency-Domain Adaptive Higher Harmonic Control		
with Unknown Disturbance Frequencies		157
7.1	Introduction	157
7.2	Notation	159
7.3	Problem Formulation	159

7.4	FD-AHHC with Unknown Disturbance Frequency	160
7.5	Adaptive Law for \hat{u}_k	161
7.6	Adaptive Law for $\hat{\omega}_k$	162
7.7	Stability Analysis	163
7.8	Numerical Examples	164
7.9	Conclusions	167
7.10	Proof of Proposition 7.1	167
7.11	Proof of Theorem 7.1.	170
7.12	Lemma 7.1 Used in Proof of Theorem 7.1	176
Chapter 8 — Conclusions and Future Work		179
8.1	Trade-offs for Adaptive Algorithms	179
8.2	Concluding Remarks	181
8.3	Recommendations for Future Work	183
Bibliography		184
Vita		200

LIST OF FIGURES

1.1	Schematic of the discrete-time control architecture used in this dissertation.	2
1.2	Schematic of FD-HHC used for helicopter vibration suppression.	9
1.3	FD-HHC is robust to small changes in the system dynamics, and yields disturbance attenuation. If the changes in the system dynamics are not sufficiently small, then FD-HHC does not achieve disturbance attenuation and can cause closed-loop instabilities.	10
2.1	Schematic of FD-HHC given by (2.9) and (2.11).	19
2.2	Schematic of FD-AHHC given by (2.9), (2.16), and (2.20).	22
2.3	Steady-state performance P_{ss} for 30,000 systems. For all systems, the steady-state performance with FD-AHHC converges. For all 20,000 systems with $m \geq \ell$, FD-AHHC yields $y_k \rightarrow 0$ as $k \rightarrow \infty$. For 9,952 out of 10,000 systems with $m < \ell$, FD-AHHC yields improvement relative to open loop (i.e., $P_{ss} < 0$).	26
2.4	Peak transient performance P_t for 30,000 systems. For approximately 39% of the systems, the transient performance with FD-AHHC is never worse than the initial performance $\ y_1\ $. Furthermore, for 75% of the systems with $\lambda_m > 0$, the transient performance with FD-AHHC is never worse than $\ y_1\ $	26
2.5	The acoustic duct used in Examples 2.2–2.5.	29
2.6	FD-HHC and FD-AHHC for a SISO system with $ \angle(M_0/M_*) < \frac{\pi}{2}$. Both FD-HHC and FD-AHHC yield $y(t) \rightarrow 0$ as $t \rightarrow \infty$. The dashed lines show $\pm u_* $	31
2.7	FD-HHC and FD-AHHC for a SISO system with $ \angle(M_0/M_*) > \frac{\pi}{2}$. The response y with FD-HHC diverges, whereas FD-AHHC yields $y(t) \rightarrow 0$ as $t \rightarrow \infty$. The dashed lines show $\pm u_* $	31
2.8	Trajectory of M_k with FD-AHHC for a SISO system where $ \angle(M_0/M_*) > \frac{\pi}{2}$. The dashed line shows the locus of M such that $ \angle(M/M_*) = \frac{\pi}{2}$, which is the FD-HHC stability boundary for M_e . Selecting $M_e = M_0$ from the lower region, where $ \angle(M/M_*) > \frac{\pi}{2}$, results in an unstable response with FD-HHC, whereas FD-AHHC yields asymptotic disturbance rejection for all $M_0 \in \mathcal{M}$	32
2.9	FD-HHC and FD-AHHC for a two-input single-output system that satisfies (2.14). Both FD-HHC and FD-AHHC yield $y(t) \rightarrow 0$ as $t \rightarrow \infty$	33
2.10	FD-HHC and FD-AHHC for a two-input single-output system that does not satisfy (2.14). The response y with FD-HHC diverges, whereas FD-AHHC yields $y(t) \rightarrow 0$ as $t \rightarrow \infty$	34
2.11	FD-HHC and FD-AHHC for a single-input two-output system that satisfies (2.14). Both FD-HHC and FD-AHHC minimize $\lim_{k \rightarrow \infty} \ y_k\ $. The dashed lines show $\pm u_* $	35

2.12	FD-HHC and FD-AHHC for a single-input two-output system that does not satisfy (2.14). The response y with FD-HHC diverges, whereas FD-AHHC minimizes $\lim_{k \rightarrow \infty} \ y_k\ $. The dashed lines show $\pm u_* $	36
2.13	FD-HHC and FD-AHHC for a MIMO system that satisfies (2.14) with a 2-tone disturbance. Both FD-HHC and FD-AHHC yield $y(t) \rightarrow 0$ as $t \rightarrow \infty$	37
2.14	FD-HHC and FD-AHHC for a MIMO system that does not satisfy (2.14) with a 2-tone disturbance. The response y with FD-HHC diverges, whereas FD-AHHC yields $y(t) \rightarrow 0$ as $t \rightarrow \infty$	38
3.1	Schematic of TD-HHC given by (3.4) and (3.10).	50
3.2	Schematic of TD-AHHC given by (3.4) and (3.13)–(3.18).	55
3.3	The two-mass structure used in Examples 3.1 and 3.2.	57
3.4	For a SISO system with a settling time smaller than the period of disturbance, and where $G_{1,e}$ is 30° away from $G_{yu}(j\omega_1)$, both FD-HHC and TD-HHC yield $y(t) \rightarrow 0$ as $t \rightarrow \infty$. However, the convergence time is improved with TD-HHC relative to FD-HHC. The dashed lines show $\pm\ u_{1,*}\ $	58
3.5	For a SISO system with a settling time smaller than the period of disturbance, and where $G_{1,e}$ is 60° away from $G_{yu}(j\omega_1)$, both FD-HHC and TD-HHC yield $y(t) \rightarrow 0$ as $t \rightarrow \infty$. However, the convergence time is significantly improved with TD-HHC relative to FD-HHC. The dashed lines show $\pm\ u_{1,*}\ $	59
3.6	For a SISO system with a settling time larger than the period of disturbance, and where $G_{1,e}$ is 30° away from $G_{yu}(j\omega_1)$, both FD-HHC and TD-HHC yield $y(t) \rightarrow 0$ as $t \rightarrow \infty$, with approximately the same convergence time. The dashed lines show $\pm\ u_{1,*}\ $	60
3.7	For a SISO system with a settling time larger than the period of disturbance, and where $G_{1,e}$ is 60° away from $G_{yu}(j\omega_1)$, both FD-HHC and TD-HHC yield $y(t) \rightarrow 0$ as $t \rightarrow \infty$, with approximately the same convergence time. The dashed lines show $\pm\ u_{1,*}\ $	60
3.8	The acoustic duct used in Examples 3.3–3.5.	61
3.9	For a SISO system, where $G_{1,0}$ is 30° away from $G_{yu}(j\omega_1)$, FD-HHC, TD-HHC, and TD-AHHC yield $y(t) \rightarrow 0$ as $t \rightarrow \infty$, with approximately the same convergence time. The dashed lines show $\pm\ u_{1,*}\ $	63
3.10	For a SISO system, where $G_{1,0}$ is 85° away from $G_{yu}(j\omega_1)$, FD-HHC, TD-HHC, and TD-AHHC yield $y(t) \rightarrow 0$ as $t \rightarrow \infty$; however, the convergence time with TD-AHHC is smaller than the convergence time with FD-HHC and TD-HHC. The dashed lines show $\pm\ u_{1,*}\ $	63
3.11	For a SISO system, where $G_{1,0}$ is not within 90° of $G_{yu}(j\omega)$, the response y with both FD-HHC and TD-HHC diverges, whereas TD-AHHC yields $y(t) \rightarrow 0$ as $t \rightarrow \infty$. The dashed lines show $\pm\ u_{1,*}\ $	64

3.12	Trajectory of $G_{1,k}$ with TD-AHHC for a SISO system where $ \angle(G_{1,0}/G_{yu}(j\omega_i)) > \frac{\pi}{2}$. The dashed line shows the locus of G such that $ \angle(G/G_{yu}(j\omega_i)) = \frac{\pi}{2}$, which is FD-HCC and TD-HHC stability boundary for selection of $G_{1,e}$. Selecting $G_{1,e} = G_{1,0}$ from the upper region, where $ \angle(G_{1,e}/G_{yu}(j\omega_i)) > \frac{\pi}{2}$, results in an unstable response with FD-HCC and TD-HHC, whereas TD-AHHC moves the initial condition $G_{1,0}$ towards $G_{yu}(j\omega_1)$ and yields asymptotic disturbance rejection.	65
3.13	For a SISO system subject to measurement noise, TD-AHHC yields asymptotic disturbance rejection. Increasing the parameter r can improve the transient performance and the convergence time. The dashed lines show $\pm\ u_{1,*}\ $	66
3.14	For a MIMO system subject to a multi-tone disturbance, where $G_{i,0}$ satisfies the condition $\Lambda \subset \text{ORHP}$, both TD-HHC and TD-AHHC yield $y(t) \rightarrow 0$ as $t \rightarrow \infty$	67
3.15	For a MIMO system subject to a multi-tone disturbance, where $G_{i,0}$ does not satisfy the condition $\Lambda \subset \text{ORHP}$, the response y with TD-HHC diverges, whereas TD-AHHC yields $y(t) \rightarrow 0$ as $t \rightarrow \infty$	68
3.16	Photograph of the experimental setup.	69
3.17	Schematic of the experimental setup.	69
3.18	For a SISO system, and for a given $G_{1,0}$, both TD-HHC and TD-AHHC yield near-zero steady-state performance, which suggests that $G_{1,0}$ is within 90° of $G_{yu}(j\omega_1)$	70
3.19	For the same SISO system as in Fig. 3.18, but with an initial condition $G_{1,0}$ that is 180° from the initial condition used to obtain Fig. 3.18, the response y with TD-HHC diverges, which suggests that $G_{1,0}$ is not within 90° of $G_{yu}(j\omega_1)$. In contrast, TD-AHHC yields near-zero steady-state performance.	71
3.20	TD-HHC can accommodate sufficiently small changes in control speaker location, and yields disturbance attenuation. If the changes in control speaker location are not sufficiently small, TD-HHC does not achieve disturbance attenuation.	72
3.21	TD-AHHC adapts to changes in control speaker location, and yields disturbance attenuation.	73
3.22	TD-HHC and TD-AHHC can cause actuator saturation during the transient. However, in this case, both TD-HHC and TD-AHHC yield near-zero steady-state performance. The dotted lines show $\pm u_m$	74
3.23	TD-AHHC causes actuator saturation during the transient. Perfect asymptotic disturbance rejection is not achieved even though $\ u_{1,*}\ < \ u_m\ $. The dotted lines show $\pm u_m$, and the dashed lines show $\pm\ u_{1,*}\ $	75
3.24	Modified TD-AHHC yields near-zero steady-state performance despite actuator saturation. The dotted lines show $\pm u_m$, and the dashed lines show $\pm\ u_{1,*}\ $	76
3.25	For the same SISO system used to obtain Fig. 3.22, modified TD-HHC and modified TD-AHHC improve the transient response and convergence rate. The dotted lines show $\pm u_m$	76

3.26	For a MIMO system subject to a two-tone disturbance, and for given $G_{1,0}$ and $G_{2,0}$, both TD-HHC and TD-AHHC yield asymptotic disturbance rejection.	77
3.27	For the same MIMO system as in Fig. 3.26, but with initial conditions $G_{1,0}$ and $G_{2,0}$ that are negative of those initial conditions used to obtain Fig. 3.26, the response y with TD-HHC diverges, while TD-AHHC yields near-zero steady-state performance.	78
4.1	Schematic of FD-AHC given by (4.9)–(4.16).	100
4.2	Two-mass structure used in Examples 4.1–4.3.	105
4.3	For a SISO system, where $M_{1,0}$ is within 90° of $M_{*,1}$, both FD-HHC and FD-AHC yield $y(t) \rightarrow 0$ as $t \rightarrow \infty$. The dashed lines show $\pm \ u_{*,1}\ $	106
4.4	For a SISO system, where $M_{1,0}$ is not within 90° of $M_{*,1}$, y with FD-HHC diverges, whereas FD-AHC yields $y(t) \rightarrow 0$ as $t \rightarrow \infty$. The dashed lines show $\pm \ u_{*,1}\ $	107
4.5	For a MIMO system with a two-tone disturbance, FD-AHC yields $y(t) \rightarrow 0$ as $t \rightarrow \infty$	107
5.1	Schematic of TD-AHC given by (5.7)–(5.13).	117
5.2	Two-mass structure used in Examples 5.1–5.5.	120
5.3	For a SISO system, where $G_{1,0}$ is within 90° of $G_{yu}(j\omega_1)$, both FD-HHC and TD-AHC yield $y(t) \rightarrow 0$ as $t \rightarrow \infty$. The dashed lines show $\pm \ u_{1,*}\ $	121
5.4	TD-AHC can be implemented with larger gains γ_d and γ_H , or with a smaller update period T_s if the gains γ_d and γ_H are reduced to ensure that the HSS approximation is valid. The dashed lines show $\pm \ u_{1,*}\ $	122
5.5	For a SISO system, where $G_{1,0}$ is not within 90° of $G_{yu}(j\omega_1)$, y with FD-HHC diverges, whereas TD-AHC yields $y(t) \rightarrow 0$ as $t \rightarrow \infty$. The dashed lines show $\pm \ u_{1,*}\ $	123
5.6	For a SISO system subject to measurement noise, TD-AHC yields near-zero steady-state performance. The noise v does not cause drift in $d_{1,k}$ or $H_{1,k}$	124
5.7	For a SISO system subject to a sinusoidal disturbance with time-varying frequency, TD-AHC can yield disturbance rejection if the time variation is known, and the rate of change of the disturbance frequency is sufficiently small.	125
5.8	For a MIMO system with a two-tone disturbance, TD-AHC yields $y(t) \rightarrow 0$ as $t \rightarrow \infty$	126
5.9	Photograph of the experimental setup.	127
5.10	Schematic of the experimental setup.	127
5.11	TD-AHC yields near-zero steady-state performance. After TD-AHC is turned on, the amplitude of y decreases monotonically, which suggests that $G_{1,0}$ satisfies the FD-HHC stability condition (i.e., $G_{1,0}$ is within 90° of $G_{yu}(j\omega_1)$). The dotted lines show $\pm u_m$	128

5.12	TD-AHC yields near-zero steady-state performance for the same SISO system as in Fig. 5.11 but with an initial condition $G_{1,0}$ that is 180° from the initial condition used to obtain Fig. 5.11. After TD-AHC is turned on, the amplitude of y initially grows, which suggests that $G_{1,0}$ does not satisfy the FD-HHC stability condition (i.e., $G_{1,0}$ is not within 90° of $G_{yu}(j\omega_1)$). The dotted lines show $\pm u_m$.	129
5.13	With increased gains γ_d and γ_H , TD-AHC yields near-zero steady-state performance, and the convergence rate is faster than that in Fig. 5.11. The dotted lines show $\pm u_m$.	130
5.14	With increased gains γ_d and γ_H , TD-AHC causes actuator saturation during the transient. However, in this case, TD-AHC yields near-zero steady-state performance. The dotted lines show $\pm u_m$.	131
5.15	TD-AHC causes actuator saturation during the transient. Perfect asymptotic disturbance rejection is not achieved even though $\ u_{1,*}\ < u_m$. The dotted lines show $\pm u_m$, and the dashed lines show $\pm \ u_{1,*}\ $.	132
5.16	Modified TD-AHC yields near-zero steady-state performance despite actuator saturation. The dotted lines show $\pm u_m$, and the dashed lines show $\pm \ u_{1,*}\ $.	133
5.17	Modified TD-AHC adapts to changes in control speaker location, and yields disturbance attenuation.	134
5.18	For a SISO system, where the disturbance frequency is not known accurately, modified TD-AHC can yield disturbance attenuation if the frequency of the control is sufficiently close to the disturbance frequency.	135
5.19	For a MIMO system with a two-tone disturbance, modified TD-AHC yields asymptotic disturbance rejection.	136
6.1	Schematic of decentralized FD-AHC with r subsystems, where each local controller has access only to local measurements.	147
6.2	The 10-mass structure used in Examples 6.1 and 6.2.	149
6.3	For a completely unknown system with several control inputs and several performance measurements subject to measurement noise, where only a decentralized control architecture is feasible, decentralized FD-AHC with $r = 10$ rejects the sinusoidal disturbances asymptotically. The convergence time is approximately as small as the convergence time implied by (6.18).	151
6.4	For the same unknown system used to obtain Fig. 6.3, but where a centralized control architecture is feasible, decentralized FD-AHC with $r = 1$ rejects the sinusoidal disturbances asymptotically. The convergence time is approximately equal to convergence time of the decentralized control architecture used to obtain Fig. 6.3.	152
7.1	Schematic of FD-AHHC with unknown disturbance frequency.	163
7.2	The acoustic duct used in Examples 7.1–7.4.	165
7.3	For a SISO plant with a step change in frequency, the control is capable of adapting to the change. The dashed lines in the u and $\hat{\omega}_k$ plots show $\pm u_* $ and ω_* , respectively.	166

7.4	For a SISO plant subject to measurement noise, the control reduces the power of y relative to open loop. The dashed lines in the u and $\hat{\omega}_k$ plots show $\pm u_* $ and ω_* , respectively.	167
7.5	For a single-input two-output plant, the control yields $u_k \rightarrow u_*$ as $t \rightarrow \infty$, which minimizes $\lim_{k \rightarrow \infty} \ y_k\ $. The dashed lines in the u and $\hat{\omega}_k$ plots show $\pm u_* $ and ω_* , respectively.	168
7.6	Control yields $y(t) \rightarrow 0$ as $t \rightarrow \infty$. The dashed lines in the u and $\hat{\omega}_k$ plots show $\pm u_* $ and ω_* , respectively.	169
8.1	Trade-offs for adaptive algorithms of this dissertation	180

LIST OF TABLES

2.1	Percent of systems satisfying a steady-state P_{ss} or peak transient P_t performance condition.	27
-----	--------------------------------------------------------------------------------------------------------------	----

Chapter 1

Introduction and Motivation

The problem of sinusoidal disturbance rejection arises in a wide variety of engineering applications, including helicopter vibration suppression [1–15], active rotor balancing [16–31], active noise cancellation [32–49], vibration reduction in spacecraft [50–66], and vibration compensation in computer hard disk drives [67–80]. Most existing methods require some model information regarding the dynamic system that is to be controlled. However, modeling often requires simplification of physical phenomena and employs idealized assumptions. Therefore, developing reliable models can be challenging, expensive, or impractical. Moreover, system dynamics and external disturbances can be uncertain or subject to change during the operation. Thus, we need methods that address highly uncertain systems. In this dissertation, we present new adaptive control methods that achieve sinusoidal disturbance rejection with limited or even no system model information.

1.1 Problem Statement

Consider the linear time-invariant (LTI) system

$$\dot{x}(t) = Ax(t) + Bu(t) + D_1d(t), \quad (1.1)$$

$$y(t) = Cx(t) + Du(t) + D_2d(t), \quad (1.2)$$

where $t \geq 0$, $x(t) \in \mathbb{R}^n$ is the state, $x(0) = x_0 \in \mathbb{R}^n$ is the initial condition, $u(t) \in \mathbb{R}^m$ is the control, $y(t) \in \mathbb{R}^\ell$ is the measured performance, $d(t) \in \mathbb{R}^p$ is the unmeasured disturbance, and $A \in \mathbb{R}^{n \times n}$ is asymptotically stable. Let $\omega_1, \omega_2, \dots, \omega_q > 0$, and consider the tonal disturbance

$$d(t) = \sum_{i=1}^q d_{c,i} \cos \omega_i t + d_{s,i} \sin \omega_i t, \quad (1.3)$$

where $d_{c,1}, \dots, d_{c,q}, d_{s,1}, \dots, d_{s,q} \in \mathbb{R}^p$ determine the disturbance amplitude and phase at each frequency.

The objective is to design a control u that reduces or even eliminates the effect of the disturbance d on the performance y . We seek a control that relies on limited or no model information regarding the system (1.1) and (1.2), and requires knowledge of only the disturbance frequencies $\omega_1, \dots, \omega_q$. Thus, the disturbance amplitudes $d_{c,1}, \dots, d_{c,q}, d_{s,1}, \dots, d_{s,q}$ and the state-space matrices A, B, C, D, D_1 , and D_2 are completely unknown.

To achieve the objective of disturbance rejection, consider a sinusoidal control with frequencies $\omega_1, \dots, \omega_q$, where the amplitudes and phases are updated in discrete time. Let $T_s > 0$ be the control update period. Then, for each $k \in \mathbb{N}$ and for all $t \in [kT_s, (k+1)T_s)$, the control is

$$u(t) = \sum_{i=1}^q u_{c,i,k} \cos \omega_i t + u_{s,i,k} \sin \omega_i t, \quad (1.4)$$

where for all $i \in \{1, 2, \dots, q\}$, $u_{c,i,k}, u_{s,i,k} \in \mathbb{R}^m$ are the control amplitudes at each frequency, which are determined from update equations. This dissertation presents novel algorithms for updating the control parameters $u_{c,i,k}$ and $u_{s,i,k}$ in order to accomplish disturbance rejection with minimal or even no system model information. The control (1.4) can be expressed more compactly as

$$u(t) = \sum_{i=1}^q (f_i^T(t) \otimes I_m) u_{i,k},$$

where \otimes denotes the Kronecker product, and for all $k \in \mathbb{N}$ and all $i \in \{1, 2, \dots, q\}$,

$$f_i(t) \triangleq \begin{bmatrix} \cos \omega_i t \\ \sin \omega_i t \end{bmatrix} \in \mathbb{R}^2, \quad u_{i,k} \triangleq \begin{bmatrix} u_{c,i,k} \\ u_{s,i,k} \end{bmatrix} \in \mathbb{R}^{2m}.$$

The control parameter update equations presented in this dissertation use sampled-data measurements, and the control methods are thus developed in discrete time. Figure 1.1 shows a schematic of the control architecture used in this dissertation.

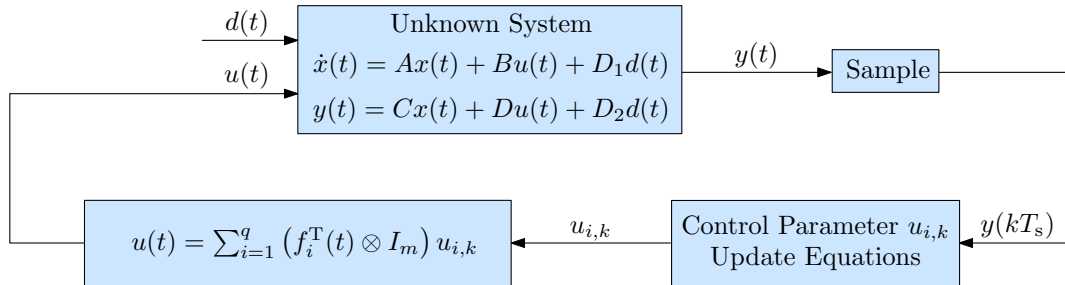


Figure 1.1: Schematic of the discrete-time control architecture used in this dissertation.

1.2 Motivating Applications

Many engineering applications require active rejection of sinusoidal disturbances. However, most existing methods require some model information regarding the dynamic system in order to achieve disturbance rejection. If the system's dynamics are uncertain or change during operation, then existing control methods can cause closed-loop instabilities [7, 81, 82]. Thus, we need methods that address highly uncertain systems and can adapt to changes in the system's dynamics during the operations. We now discuss motivating applications, where the adaptive control methods of this dissertation can achieve disturbance rejection.

Helicopter Vibration Suppression:

The fuselage of a helicopter is subject to undesirable vibrations that negatively impact ride quality for passengers, result in crew fatigue, and can harm expensive components of the helicopter. The aeroelastic motion of a helicopter's main rotor blades is a primary source of these undesirable vibrations. Moreover, the dominant frequency content of these vibrations is known, because it is a function of the rotor's angular velocity and the number of blades [83, 84]—both of which are known. For helicopters produced in the 1960s, the average vibration level of the fuselage was approximately 0.3 g [15, 85], causing an uncomfortable ride and reoccurring components failure [15, 85, 86]. Active vibration reduction techniques have successfully reduced the levels of vibrations to approximately 0.1 to 0.2 g [15, 87], which is a significant improvement compared to the early days of helicopter production. Next generation of helicopter designs aim to reduce vibration levels to approximately 0.03 to 0.05 g [15].

A detailed discussion of the origin of helicopter vibration is in [84, 88, 89]. In summary, the vibrations stem from the rotation of the main rotor and occur at a frequency equal to the rotor angular velocity multiplied by the number of the blades. The resulting vibration frequency is typically between 15 and 25 Hz. In most helicopters, the vibratory loads (i.e., forces and moments) are directly transmitted to the helicopter fuselage via the main gearbox. Metal or elastomeric isolation mounts are frequently used for isolating foundations from vibrations of industrial equipment. However, isolation mounts cannot be used to isolate a helicopter's fuselage from its main gearbox, because the gearbox is light weight relative to industrial equipment, and the vibration frequencies are relatively low [15].

Since the beginning of the helicopter manufacturing industry, passive vibration absorbers have been used to reduce vibrations, and are still in wide use. The earliest patents (e.g., US2489342) using vibration absorbers for helicopters are from 1945, where pendular absorbers are used to reduce unacceptable vibrations [90]. This patent was granted 5 years after the first flight of the Vought-Sikorsky VS-300, which is widely considered the first demonstration of a practical helicopter [15]. Therefore, the need for vibration suppression on helicopters was obvious from the early days of helicopter flight. One of the earliest uses of vibration absorbers on production helicopters was in the Chinook CH-47B helicopter in the early 1960s [91]. This 40,500-

lbm helicopter with two 3-bladed rotors, incorporated five absorbers each weighing 90 lbm, which accounts for 1.1% of the aircraft gross weight. Thus, one drawback of passive vibration absorbers is that they are heavy. Also, being passive, these absorbers are not adjustable for different flight conditions, meaning that changes to the helicopter dynamics (e.g., changes in the payload) can reduce the level of vibration suppression.

In the 1980s, passive vibration absorbers were often replaced with active vibration systems, for example, in the Sikorsky UH-60M Black Hawk helicopter [15, 92]. The actuators of the active vibration control (AVC) system are placed in the exact location of previous passive absorbers. In this AVC system, the controller receives acceleration measurements from accelerometers placed throughout the helicopter’s fuselage. Then, the controller uses this acceleration feedback to command the AVC actuators to produce vibratory forces to suppress accelerations. The frequency-domain controller implemented in the UH-60M AVC system is based on the seminal work by J. Molisius and F. Farrar described in [93]; this control algorithm is known as higher-harmonic control. In fact, according to [15], higher-harmonic control and its variants are probably used in the vast majority of fielded AVC systems.

The AVC system, has significant advantages over passive vibration absorbers. Specifically, the AVC system can reject the vibrations at locations, where the passengers and crew sit—a feature that passive absorbers rarely provide. If there is no physical room to mount passive absorbers near where we would like to reduce vibrations, then they must be mounted at alternative locations, which are often less effective and less weight-efficient. Thus, AVC is more weight efficient. In addition, AVC reduces fuselage vibration to the same or lower levels than passive systems, and AVC uses lighter and/or fewer actuators, which are the heaviest components in AVC systems [15].

Traditional AVC algorithms are robust to changes in the dynamics of the helicopter; however, since they require some model information regarding the dynamics of the system, these AVC systems are not capable of accommodating all changes that can occur during a helicopter’s flight. In this dissertation, we present new adaptive control methods that can adapt to arbitrary changes in the system’s dynamics.

Active Rotor Balancing:

Balancing rotating machinery is an indispensable task in manufacturing, maintenance, repair, and operation of an industrial plant [16, 17, 21]. During installation of a piece of rotating device, the rotating components are balanced either as an individual item, as an assembly, or in some instances, as a combination of both.

To balance the components or the assembly, the parts are installed in a balancing machine, and once the rotating equipment has been installed, a manual balance correction is made. There is typically a need to make a field balance correction, known as either a trim balance or in-situ balance [21, 94]. Both of these terms refer to performing a manual balance correction without removing the rotor or the associated assembly from the bearings. The field balancing operation begins with a trial run, which is used to establish a baseline of the vibration level. The rotating device is then

stopped, and a trial mass is added. This trial mass allows the amount of unbalance to be identified. A calculation is made in order to determine the balance-mass weight and location required to cancel the unbalance. Once the trial run is completed, the rotating equipment is stopped, and the calculated balance weight is added or removed. The rotating equipment is then started again and measurements are made to determine if the desired level of balance has been achieved. If not, the process is repeated until an acceptable balance level is reached.

Active balancing systems provide an alternative to the traditional on-site field balancing methods. These systems are usually able to detect the unbalance, identify the correction required to offset the unbalance, and automatically make the balance correction while the piece of rotating equipment is running. A balancing system consists of sensors that can measure the undesirable vibrations, and actuators that can produce counterweight to cancel the unbalances. The vibration sensor is mounted on or near the bearing's centerline and continuously samples the vibration level. This information is sent to a controller, where the vibration signal is analyzed and compared to acceptable levels. If the vibration level exceeds the acceptable levels, then the controller determines the amount of unbalance and the correction counterweight required to make a balance correction. The controller also determines the location that the counterweight needs to be located, in order to reduce the vibration. This is often referred to as calculating the magnitude and phase angle of the balance correction. The controller sends a series of commands to a power amplifier, which, in turn, provides modulated power to the actuators, which move the counterweight to the desired location inside the balancer assembly. This automatic balance correction is typically completed in less than one minute. Once the system is installed, there is no need to stop the piece of rotating equipment to perform a balance correction.

Existing control methods for active rotor balancing are model-based (e.g., convergent control [20,95]), meaning that some information regarding the model of dynamic system is required in order to implement rotor balancing. In contrast, the adaptive control methods in this dissertation do not require any model information.

Active Noise Control:

Active noise control (ANC) is the electro-acoustic generation (i.e., typically using loudspeakers) of a sound field for canceling or reducing the influence of an undesirable existing sound field. Although ANC is widely used as a laboratory tool for validating research activity, it has certain industrial applications. For example, ANC systems help reduce low-frequency fan noise levels stemming from industrial air exhaust ducts [96]. Also, rotorcraft and propeller aircraft use ANC systems to reduce noise level in the cabin [97]. However, ANC systems are still not wide-spread in industry. Ideal ANC systems are adaptive, meaning that they can adapt to changing characteristics of the noise, and changing environmental conditions that affect the acoustic field. In practice, non-adaptive noise cancellation systems are not very effective, except in noise-canceling headsets and ear muffs [42, 98, 99]. Many industries deal with low-frequency noise, which is difficult and expensive to control passively, because large mufflers and enclosures are needed to accommodate the long acoustic wavelengths

of the low-frequency noise. Industries are interested in ANC because it is likely to provide a lower-cost alternative to passive noise control [42].

Although Thompson observed the phenomenon of sound cancellation using two Bell telephones in 1878, it was not until 1930 that the French engineer H. Coanda patented the concept of sound cancellation via destructive interference [42,100]. In 1933, German physicist P. Lueg patented the idea of using active noise cancellation as an alternative to passive control for low-frequency noise in an acoustic duct [101]. In the 1950s, American engineers Harry F. Olson and W. B. Conover independently modernized Lueg’s idea by utilizing feedback control theory, and investigating possibilities of active noise cancellation in rooms, acoustic ducts, headsets, and earmuffs [102–104]. However, limitations in control methods and electronic hardware made their ideas commercially impractical [42].

Since the early days of ANC, researchers have been dealing with practical complications of ANC schemes. Progress in the areas of control, signal processing, electronics, acoustics, and vibrations facilitated practical and commercial implementations in the 1980s. Surveys of ANC algorithms are in [33,42,105,106]. Most available ANC algorithms require some model information regarding the acoustic system, whereas the adaptive control techniques of this dissertation are applicable to unknown acoustic systems and do not require any model information.

Spacecraft Vibration Control:

Many spacecraft are equipped with lightweight but large-and-complex appendages, such as antennas and solar arrays, in order to facilitate communication, remote sensing, and other similar tasks. These large lightweight structural appendages are extremely flexible and have low-frequency fundamental oscillatory modes [58, 60]. These fundamental modes are excited during many tasks and missions such as slewing and pointing maneuvers. In addition, large-angle and fast rotational maneuvers of spacecraft are indispensable in order to meet certain mission requirements.

Effective cancellation or attenuation of the induced vibrations is a challenging control objective. Modern spacecraft control systems use different types of actuation mechanisms including thrusters and internal momentum exchange devices (e.g., momentum or reaction wheels, and control moment gyros) to accomplish increased functionality during the space flight [107, 108].

For certain maneuvering and precision pointing tasks, active disturbance rejection techniques have been increasingly used for flexible spacecraft to achieve the desired level of vibration attenuation. Significant progress has been made in designing control systems for simultaneous attitude control and vibration suppression of flexible spacecraft [109, 110]. Due to uncertainties in the dynamics of spacecraft, adaptive control techniques are essential in vibration control system design; however, current techniques require knowledge of some model information regarding the spacecraft’s dynamics (e.g., relative degree, upper bounds on the magnitude of uncertainties). In this dissertation, we present adaptive control methods that can reject sinusoidal vibrations of spacecraft without requiring any model information.

In a hard disk drive, data is stored in circular paths of magnetization recognized as tracks. For the read and write operations, the disk rotates, and the read-write head is commanded to follow certain circular tracks. Modern hard disk drives are equipped with track following servo control systems, which are responsible for keeping the read-write head at the desired track accurately. This process is facilitated by the track misregistration diagnosis mechanism, which uses the standard deviation of the position error signal. See [73] for more details.

Tracking errors can be induced by many sources including disk and bearing run-out, servo-track-writer induced irregularities, electronic noise, spindle and actuator resonances, and external shock and rotary vibration [111]. External shock and rotary vibrations, contain frequency components with time-varying phases and magnitudes at unknown frequencies. In addition, turbulent air flow within the hard disk assembly or imperfections in the spindle bearing can cause harmful vibrations and result in non-repeatable narrow-band disturbances, whose energy is highly concentrated at multiple unknown frequencies. More details are available in [112–114]. These disturbances differ from track to track and disk to disk. Moreover, frequencies of the narrowband components can be higher than the bandwidth of the existing servo loops as reported in [112, 113]. Therefore, the uncertain nature of these disturbances, makes vibration compensation in hard disk drives a challenging control task. If the dynamics of hard disk drive are also unknown or subject to change, disturbance rejection becomes more challenging. The adaptive controllers in Chapter 7 of this dissertation are not model-based and are applicable to vibrations with unknown frequencies as is common in hard disk drives.

1.3 Literature Review

For an accurately modeled LTI system, the internal-model principle can be used to design a feedback controller capable of rejecting sinusoidal disturbances of known frequencies [115–120]. In this case, disturbance rejection is accomplished by incorporating copies of the disturbance dynamics in the feedback loop. For sinusoids with unknown frequencies, a model-based disturbance observer can be implemented [121–128].

If, on the other hand, an accurate model of the system is not available, but the open-loop dynamics are asymptotically stable, then adaptive feedforward cancellation can be used to accomplish disturbance rejection [129–138]. These approaches use a harmonic regressor consisting of sinusoids at the known disturbance frequencies. The control is generated by updating the amplitudes and phases of these sinusoids in a manner that achieves asymptotic disturbance rejection. Adaptive feedforward approaches require certain model information or assumptions regarding the open-loop transfer function. In the simplest case where the system is single-input single-output (SISO), the only required model information is the sign of the control-to-performance transfer function at the disturbance frequencies. However, if the system is multi-

input multi-output (MIMO), then stronger assumptions (e.g., strict positive realness, a nominal system model, or upper bounds on uncertainties) are invoked.

Feedback (rather than feedforward) adaptive control methods are also capable of rejecting sinusoids of known or even unknown frequencies (e.g., [139–151]); however, these approaches generally rely on some model information (e.g., relative degree) and structural assumptions regarding the system (e.g., minimum phase, or state feedback).

The filtered-X least-mean-squares algorithm is an approach from the digital signal processing literature [152, 153]. Filtered-X can be used in cases where the disturbance frequencies are uncertain or unknown; however, filtered-X relies on a model of the control-to-performance transfer function (referred to as the secondary path in the noise control literature). If this model is inaccurate, then filtered-X can destabilize the closed loop [33]. To reduce the required model information, algorithms have been proposed which incorporate real-time identifiers [154, 155]. However, these methods require injection of white-noise excitation to ensure convergence of the parameter identifier.

Another approach to sinusoidal disturbance rejection takes advantage of an asymptotically stable LTI system’s harmonic steady-state (HSS) response, that is, the sinusoidal response that remains after the system’s transient response decays to zero. This HSS approach was developed independently in several research communities, specifically: i) active sound and vibration control [32], ii) helicopter vibration reduction [10, 156], and iii) active rotor balancing [20]. For active rotor balancing, this approach is called convergent control, whereas for helicopter vibration reduction, the approach is known as higher-harmonic control (HHC). This approach is a frequency-domain method, meaning that all control computations are performed using discrete Fourier transform (DFT) data. In this dissertation, we refer to this approach as frequency-domain higher-harmonic control (FD-HHC).

To further explain FD-HHC, consider an LTI system that is acted on by a sinusoidal disturbance with known frequency ω . The FD-HHC control signal is a sinusoid with frequency ω , but where the amplitude and phase are updated at discrete times. Let $T_s > 0$ denote the FD-HHC update period. Then, at each time step $k \in \mathbb{N}$, the control amplitude and phase are updated using DFT data, which are computed from a sampling of the performance measurement over the time interval $[(k-1)T_s, kT_s]$. FD-HHC relies on the key assumption that the update period T_s is sufficiently large relative to the settling time of the system. This assumption ensures that by the end of each time interval between control updates, the closed-loop response approximates the HSS response. If T_s is too small, then the HSS approximation is not accurate, and the closed-loop system can become unstable. In practice, T_s can be increased to achieve closed-loop stability; however, increasing T_s also increases convergence time. In fact, large convergence time is one shortcoming of FD-HHC [81].

Another potential drawback of FD-HHC is that it requires an estimate of the control-to-performance transfer function evaluated at the disturbance frequency. In the SISO case, this estimate must have an angle within 90° of the actual value for closed-loop stability. The closed-loop stability conditions for the MIMO case are given in [82, Theorem 2]. If there are multiple disturbance frequencies, then estimates of the control-to-performance transfer function are required at each frequency. For certain

applications, this transfer function can be difficult to estimate or subject to change.

The following example demonstrates a limitation of FD-HHC for the case, where the system's dynamics are subject to changes.

Example 1.1. Consider a 4-blade helicopter rotor system, where we denote the swash-plate vertical displacement by $u \in \mathbb{R}$, the vertical speed of the rotor system by $v \in \mathbb{R}$, and the coning angle of the blades by $\beta \in \mathbb{R}$. Let $N \triangleq 4$ denote the number of blades, and let $\Omega \triangleq 300$ RPM be the angular velocity of the rotor. Note that helicopters are subject to sinusoidal disturbances due to the vibration of the blades at frequencies equal to $N\Omega$ as well as frequencies equal to the integer multiples of $N\Omega$, that is, higher harmonics $2N\Omega, 3N\Omega, 4N\Omega$, etc. See [15, 83] for more details.

The control objective is to determine a control u , such that $\lim_{t \rightarrow \infty} v(t) = 0$. Thus, we let $y = v$. The equations of motion for the rotor system are given by (1.1), where

$$A = \begin{bmatrix} -0.08 & -241.4 & -11.23 \\ 0 & 0 & 1 \\ 0.12 & -142.7 & -1.14 \end{bmatrix}, \quad x(t) = \begin{bmatrix} v(t) \\ \beta(t) \\ \dot{\beta}(t) \end{bmatrix}, \quad B = \begin{bmatrix} -2.82 \\ 0 \\ 2.2 \end{bmatrix}, \quad D_1 = \begin{bmatrix} 0.1 \\ 0 \\ -0.2 \end{bmatrix},$$

and $d(t)$ is given by (1.3), where we consider the first harmonic due to the vibration of the blades (i.e., $q = 1$ and $\omega_1 = N\Omega$). Let $d_{c,1} = d_{s,1} = 400$ mm. We use FD-HHC to eliminate the effects of d on y . We implement FD-HHC according to [82, Eq. (11)], where $u_0 = 0$, $\rho = 1.57 \times 10^3$, and $G_e = (-8 + j16) \times 10^{-3}$, which is the estimate of control-to-performance transfer function at disturbance frequency. Figure 1.2 shows a schematic of the control architecture. Figure 1.3 shows y and u with FD-HHC. The control is turned on at $t = 2$ s, and disturbance rejection is achieved. At time $t = 20$ s, the first row of the matrix A is changed from $[-0.08 \quad -241.4 \quad -11.23]$ to $[-0.2 \quad -603.5 \quad -28.1]$. The controller is robust to this change and rejects the disturbance. At time $t = 35$ s, the the first row of the matrix A is changed from $[-0.2 \quad -603.5 \quad -28.1]$ to $[-0.32 \quad -965.6 \quad -44.92]$. In this case, the response y with FD-HHC diverges. \triangle

Example 1.1 demonstrates that FD-HHC yields unstable response if the fixed estimate of control-to-performance transfer function at disturbance frequency is no longer sufficiently accurate due to changes in the system's dynamics. To address uncertainty, adaptive HHC methods have been proposed [81, 157, 158]. However, the

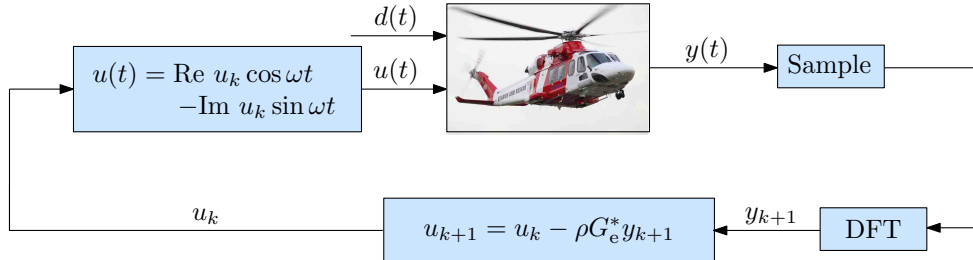


Figure 1.2: Schematic of FD-HHC used for helicopter vibration suppression.

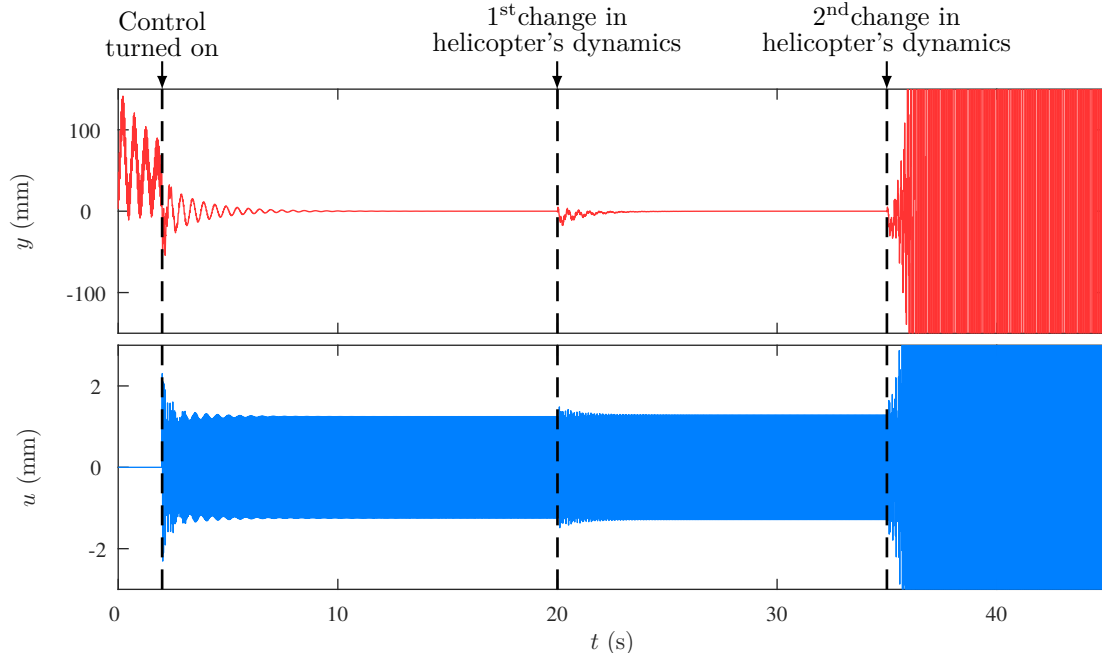


Figure 1.3: FD-HHC is robust to small changes in the system dynamics, and yields disturbance attenuation. If the changes in the system dynamics are not sufficiently small, then FD-HHC does not achieve disturbance attenuation and can cause closed-loop instabilities.

methods in [81, 157] require an external excitation signal to ensure stability, and the analysis in [158] is restricted to an averaged system. In Chapters 2–5 of this dissertation, we present adaptive control techniques that address the problem of uncertainty, and achieve asymptotic disturbance rejection for completely unknown MIMO LTI systems.

Another challenge for active disturbance rejection is large-scale dynamic system, where practical constraints can necessitate decentralized control architecture. In a decentralized control architecture, the control system is designed with the constraint that none of local controllers has information regarding the nonlocal performance measurements [159].

For large-scale uncertain systems, decentralized adaptive control techniques that require limited model information are proposed in [160–168]. For example, the technique in [162] concerns systems with strong nonlinear interconnections, and the method in [163] is applicable to large-scale dynamical systems with unknown interconnections. The methods presented in [161, 162] develop decentralized adaptive controllers that require local full-state feedback for closed-loop stabilization. These local full-state feedback adaptive methods have been extended in [169–171]. Existing decentralized control techniques for disturbance rejection are given in [144, 151, 170, 172]. However, these methods require some model information regarding the system to be controlled and may not yield perfect tonal disturbance rejection.

The adaptive disturbance rejection algorithms that we present in Chapters 2–5 are for unknown systems, however, these methods are centralized control schemes. Ref. [172] presents a decentralized HHC technique. If the value at frequency ω of

the control-to-performance transfer function is a diagonally-dominant matrix, then [172] provides sufficient-but-not-necessary conditions for tonal disturbance rejection. Therefore, the decentralized control technique requires some model information, and is not applicable to unknown systems. In Chapter 6 of this dissertation, we present a decentralized control algorithm for rejection of sinusoidal disturbances acting on an unknown MIMO LTI system.

Next, we consider the problem of rejecting sinusoids for unknown frequency. Consider the case where an accurate model of the system is known, but the frequencies of the sinusoidal disturbance are unknown. This case is related to the problem of estimating the frequency of a sinusoidal signal. Frequency estimation is addressed with discrete-time adaptive notch filters [173–177] and related continuous-time methods [178–181]. The recent survey [182] provides a comparison of frequency-estimation techniques.

For control, the rejection of unknown-frequency sinusoids can be addressed by combining a frequency estimator with a controller capable of rejecting known-frequency sinusoids (e.g., internal-model control) [183]. Related adaptive control methods (both direct and indirect) for rejection of unknown-frequency sinusoids are presented in [147, 184–187] for continuous time and [147, 187] for discrete time.

For the case, where both the system model and the disturbance frequencies are unknown, adaptive feedback (rather than feedforward) control methods are capable of asymptotic disturbance rejection for both LTI systems [140–143, 188–190] and certain classes of nonlinear systems [191, 192]. However, these approaches generally rely on some model information (e.g., relative degree) and structural assumptions regarding the system (e.g., minimum phase, or state feedback). Note that [141] does not require a minimum-phase assumption, but instead relies on estimates of the nonminimum-phase zeros. In Chapter 7 of this dissertation, we present an adaptive control method that rejects a sinusoidal disturbance with unknown frequency that act on an unknown MIMO LTI system.

1.4 Summary of Contributions

Chapter 2 presents a new control algorithm named frequency-domain adaptive higher-harmonic control (FD-AHHC), which addresses the problem of rejecting sinusoids with known frequencies that act on a completely unknown asymptotically stable LTI system. We analyze the stability and closed-loop performance of FD-AHHC for MIMO systems that are square (i.e., the number of controls equals the number of performance measurements). In this case, we show that FD-AHHC asymptotically rejects disturbances, that is, the performance measurement tends to zero. We also present a numerical study of the steady-state and transient performance of FD-AHHC for square and nonsquare systems. The result of this chapter appears in [82, 193].

Chapter 3 presents two new time-domain feedback control algorithms for rejection of known-frequency sinusoidal disturbances that act on an asymptotically stable LTI system. The first algorithm is time-domain higher-harmonic control (TD-HHC),

which is effective for uncertain LTI systems. However, TD-HHC requires an estimate of the control-to-performance transfer function evaluated at the disturbance frequency. The second algorithm is time-domain adaptive higher-harmonic control (TD-AHHC), which is effective for completely unknown LTI systems. We analyze the stability and performance of TD-HHC and TD-AHHC. For both TD-HHC and TD-AHHC, we show that the controller asymptotically rejects the disturbance. We also present numerical simulations comparing TD-HHC and TD-AHHC with FD-HHC. We also present results from an active disturbance rejection experiment in an acoustic environment. These experimental results demonstrate the practical effectiveness of the TD-HHC and TD-AHHC. The result of this chapter appears in [194, 195].

Chapter 4 presents a new control algorithm named frequency-domain adaptive harmonic control (FD-AHC), which rejects sinusoids with known frequencies that act on a completely unknown asymptotically stable LTI system. We analyze the stability and closed-loop performance for systems with at least as many controls as performance measurements. We show that the closed-loop system is Lyapunov stable and that the adaptive controller asymptotically rejects the disturbances. We demonstrate the controller on numerical simulations of SISO and MIMO acoustic ducts. The result of this chapter appears in [196, 197].

Chapter 5 presents a new control algorithm named time-domain adaptive harmonic control (TD-AHC), which rejects sinusoids with known frequencies that act on a completely unknown asymptotically stable LTI system. We analyze the stability and closed-loop performance for systems with at least as many controls as performance measurements. We show that the closed-loop system is uniformly Lyapunov stable and that the adaptive controller asymptotically rejects the disturbances. We present numerical simulations comparing TD-AHC with FD-HHC. We also present results from an active disturbance rejection experiment in an acoustic environment. These experimental results demonstrate the practical effectiveness of the adaptive harmonic controller. The result of this chapter appears in [198, 199].

Chapter 6 extends FD-AHC to address decentralized control systems. The decentralized control architecture consists of MIMO subsystems, where each local controller does not have access to any information regarding the system or the nonlocal measurements. We analyze stability and performance properties of the closed-loop for MIMO subsystems. We show that the decentralized control rejects sinusoidal disturbances asymptotically. In addition, we present a result regarding the transient properties of the decentralized controller, which provides an estimate for the convergence rate of the closed-loop system. We show that the convergence rate can be significantly improved by choice of certain control parameters. We also demonstrate the effectiveness of the controller through numerical simulations. The result of this chapter appears in [196, 197].

Chapter 7 extends TD-AHHC to address the problem of rejecting a sinusoidal disturbance with unknown frequency that acts on an unknown MIMO LTI system that is asymptotically stable. For SISO systems, we analyze the closed-loop stability and performance of the adaptive controller. In this case, we show that the controller asymptotically rejects disturbances. We demonstrate the controller on numerical simulations of SISO and MIMO acoustic ducts. The result of this chapter appears

in [200].

In this dissertation, the notation is defined and valid within each chapter.

Chapter 2

Frequency-Domain Adaptive Higher Harmonic Control

In this chapter, we present frequency-domain adaptive higher harmonic control (FD-AHHC) algorithm that addresses the problem of rejecting sinusoids with known frequencies that act on a completely unknown asymptotically stable linear time-invariant system. We analyze the stability and closed-loop performance of FD-AHHC for multi-input multi-output systems that are square (i.e., the number of controls equals the number of performance measurements). In this case, we show that FD-AHHC asymptotically rejects disturbances, that is, the performance measurement tends to zero. We also present a numerical study of the steady-state and transient performance of FD-AHHC for square and nonsquare systems. The result of this chapter appears in [82, 193].

2.1 Introduction

Sinusoidal disturbance rejection is a fundamental control objective, which arises in a wide variety of applications, including active noise cancellation [33], helicopter vibration suppression [10], active rotor balancing [20], and vibration reduction in spacecraft [59].

For an accurately modeled linear time-invariant (LTI) system, the internal-model principle can be used to design a feedback controller capable of rejecting sinusoidal disturbances of known frequencies [115–117, 119]. In this case, disturbance rejection is accomplished by incorporating copies of the disturbance dynamics in the feedback loop. For sinusoids with unknown frequencies, a model-based disturbance observer can be implemented [121–125].

If, on the other hand, an accurate model of the system is not available, but the open-loop dynamics are asymptotically stable, then adaptive feedforward cancellation can be used to accomplish disturbance rejection [129–135]. These approaches use a harmonic regressor consisting of sinusoids at the known disturbance frequencies. The control is generated by updating the amplitudes and phases of these sinusoids

in a manner that achieves asymptotic disturbance rejection. Adaptive feedforward approaches require certain model information or assumptions regarding the open-loop transfer function. In the simplest case where the system is single-input single-output (SISO), the only required model information is the sign of the control-to-performance transfer function at the disturbance frequencies. However, if the system is multi-input multi-output (MIMO), then stronger assumptions (e.g., strict positive realness, a nominal system model, or upper bounds on uncertainties) are invoked. Feedback (rather than feedforward) adaptive control methods are also capable of rejecting sinusoids of known or even unknown frequencies (e.g., [139–146]); however, these approaches generally rely on some model information (e.g., relative degree) and structural assumptions regarding the system (e.g., minimum phase, or state feedback).

The filtered-X least-mean-squares algorithm is an approach from the digital signal processing literature [152, 153]. Filtered-X can be used in cases where the disturbance frequencies are uncertain or unknown; however, filtered-X relies on a model of the control-to-performance transfer function (referred to as the secondary path in the noise control literature). If this model is inaccurate, then filtered-X can destabilize the closed loop [33]. To reduce the required model information, algorithms have been proposed which incorporate real-time identifiers [154, 155]. However, these methods require injection of white-noise excitation to ensure convergence of the parameter identifier.

Another approach to sinusoidal disturbance rejection takes advantage of an asymptotically stable LTI system’s harmonic steady-state (HSS) response, that is, the sinusoidal response that remains after the system’s transient response decays to zero. This HSS approach was developed independently in several research communities, specifically, i) active sound and vibration control [32], ii) helicopter vibration reduction [10, 156], and iii) active rotor balancing [20]. For active rotor balancing, this approach is called convergent control, whereas for helicopter vibration reduction, the approach is known as higher harmonic control. In this chapter, we refer to the approach as frequency-domain higher harmonic control (FD-HHC).

To discuss FD-HHC control further, let G_{yu} denote the control-to-performance transfer function, and assume that there is a single known disturbance frequency ω . Then, FD-HHC requires an estimate of $G_{yu}(j\omega)$, that is, an estimate of the transfer function evaluated at the disturbance frequency. In the SISO case, FD-HHC stabilizes the closed-loop if the estimate of $G_{yu}(j\omega)$, which is a single complex number, has an angle within 90° of $\angle G_{yu}(j\omega)$. In the MIMO case, closed-loop stability is ensured if the estimate of $G_{yu}(j\omega)$ is sufficiently accurate. If there are multiple disturbance frequencies, then estimates are required at each frequency.

For certain applications $G_{yu}(j\omega)$ can be difficult to estimate or subject to change. For example, a helicopter’s structural dynamics may vary depending on payload. To address this uncertainty, online estimation methods have been combined with HSS control [81, 157, 158]. For example, a recursive-least-squares identifier is used in [81, 157] to estimate $G_{yu}(j\omega)$ in real time; however, an external excitation signal is required to ensure stability.

In this chapter, we present a new adaptive higher harmonic control (FD-AHHC), which is effective for rejecting sinusoids with known frequencies that act on a comple-

tely unknown MIMO LTI system. We analyze the stability and closed-loop performance of FD-AHHC for MIMO systems that are square (i.e., the number of controls equals the number of performance measurements). We provide conditions such that the measured performance tends to zero, that is, the disturbance is asymptotically rejected. We also review FD-HHC control and its stability properties in order to compare FD-HHC to FD-AHHC. In contrast to FD-HHC [10, 20, 32, 156] and other existing adaptive feedforward methods [129–135], FD-AHHC requires no model information.

The new FD-AHHC algorithm presented in this chapter is a frequency-domain method, meaning that all computations use discrete Fourier transform (DFT) data rather than time-domain data. The FD-AHHC algorithm (including DFT) is demonstrated on a numerical simulation of an acoustic duct.

Section 2.3 presents the tonal disturbance rejection problem. Section 2.4 reviews FD-HHC, and Section 2.5 presents the new FD-AHHC algorithm. The main analytic results regarding FD-AHHC stability and convergence are given in Section 2.6. Section 2.7 provides a numerical study of the FD-AHHC’s steady-state and transient performance for square and nonsquare systems. Section 2.8 extends FD-AHHC to address multi-tone disturbances rejection, and Section 2.9 demonstrates the FD-AHHC algorithm on a numerical simulation of an acoustic duct.

2.2 Notation

Let \mathbb{F} be either \mathbb{R} or \mathbb{C} . Let $x_{(i)}$ denote the i th element of $x \in \mathbb{F}^n$, and let $A_{(i,j)}$ denote the element in row i and column j of $A \in \mathbb{F}^{m \times n}$. Let $\|\cdot\|$ be the 2-norm on \mathbb{F}^n . Next, let A^* denote the complex conjugate transpose of $A \in \mathbb{F}^{m \times n}$, and define $\|A\|_F \triangleq \sqrt{\text{tr } A^*A}$, which is the Frobenius norm of $A \in \mathbb{F}^{m \times n}$.

Let $\text{spec}(A) \triangleq \{\lambda \in \mathbb{C} : \det(\lambda I - A) = 0\}$ denote the spectrum of $A \in \mathbb{F}^{n \times n}$. Let $\lambda_{\min}(A)$ and $\lambda_{\max}(A)$ denote the minimum and maximum eigenvalues, respectively, of the Hermitian positive-semidefinite matrix $A \in \mathbb{F}^{n \times n}$. Let $\angle \lambda$ denote the argument of $\lambda \in \mathbb{C}$ defined on the interval $(-\pi, \pi]$ rad. Let OLHP, ORHP, OUD, and CUD denote the open-left-half plane, open-right-half plane, open unit disk, and closed unit disk in \mathbb{C} , respectively.

Define $\mathbb{N} \triangleq \{0, 1, 2, \dots\}$ and $\mathbb{Z}^+ \triangleq \mathbb{N} \setminus \{0\}$. Define the *open ball of radius $r > 0$ centered at $C \in \mathbb{C}^{m \times n}$* by $\mathbb{B}_r(C) \triangleq \{X \in \mathbb{C}^{m \times n} : \|X - C\|_F < r\}$.

2.3 Problem Formulation

Consider the LTI system

$$\dot{x}(t) = Ax(t) + Bu(t) + D_1d(t), \quad (2.1)$$

$$y(t) = Cx(t) + Du(t) + D_2d(t), \quad (2.2)$$

where $t \geq 0$, $x(t) \in \mathbb{R}^n$ is the state, $x(0) = x_0 \in \mathbb{R}^n$ is the initial condition, $u(t) \in \mathbb{R}^m$ is the control, $y(t) \in \mathbb{R}^\ell$ is the measured performance, $d(t) \in \mathbb{R}^p$ is the unmeasured

disturbance, and $A \in \mathbb{R}^{n \times n}$ is asymptotically stable. Define the transfer functions $G_{yu} : \mathbb{C} \rightarrow \mathbb{C}^{\ell \times m}$ and $G_{yd} : \mathbb{C} \rightarrow \mathbb{C}^{\ell \times p}$ by

$$\begin{aligned} G_{yu}(s) &\triangleq C(sI - A)^{-1}B + D, \\ G_{yd}(s) &\triangleq C(sI - A)^{-1}D_1 + D_2. \end{aligned}$$

Let $\omega_1, \omega_2, \dots, \omega_q > 0$, and consider the tonal disturbance

$$d(t) = \sum_{i=1}^q d_{c,i} \cos \omega_i t + d_{s,i} \sin \omega_i t, \quad (2.3)$$

where $d_{c,1}, \dots, d_{c,q}, d_{s,1}, \dots, d_{s,q} \in \mathbb{R}^p$ determine the disturbance amplitude and phase at each frequency.

The objective is to design a control u that reduces or even eliminates the effect of the disturbance d on the performance y . We seek a control that relies on no model information regarding the system (2.1) and (2.2), and requires knowledge of only the disturbance frequencies $\omega_1, \dots, \omega_q$. Thus, the disturbance amplitudes $d_{c,i}$ and $d_{s,i}$, and the system (2.1) and (2.2) are completely unknown.

We first focus on the case where d is the single-tone disturbance

$$d(t) = d_c \cos \omega t + d_s \sin \omega t.$$

However, the adaptive controller presented in this chapter generalizes to the case, where d consists of multiple tones. We discuss the extension to multiple tones in Section 2.8.

For the moment, assume that G_{yu} , G_{yd} , d_c , and d_s are known. In this case, consider the harmonic control

$$u(t) = u_c \cos \omega t + u_s \sin \omega t, \quad (2.4)$$

where $u_c, u_s \in \mathbb{R}^m$. Define $\hat{u} \triangleq u_c - j u_s$, which is the DFT at frequency ω obtained from a sampling of u . In addition, define

$$\begin{aligned} M_* &\triangleq G_{yu}(j\omega) \in \mathbb{C}^{\ell \times m}, \\ d_* &\triangleq G_{yd}(j\omega)(d_c - j d_s) \in \mathbb{C}^{\ell}. \end{aligned}$$

Then, the harmonic steady-state (HSS) performance of (2.1) and (2.2) with control (2.4) is

$$\begin{aligned} y_{\text{hss}}(t, \hat{u}) &\triangleq \text{Re} \left[\left(G_{yu}(j\omega) \hat{u} + G_{yd}(j\omega)(d_c - j d_s) \right) e^{j\omega t} \right] \\ &= \text{Re} (M_* \hat{u} + d_*) \cos \omega t - \text{Im} (M_* \hat{u} + d_*) \sin \omega t. \end{aligned} \quad (2.5)$$

The HSS performance y_{hss} is the steady-state output y of (2.1) and (2.2) with control

(2.4), that is, $\lim_{t \rightarrow \infty} [y_{\text{hss}}(t) - y(t)] = 0$ [201, Chap. 12.12]. Define

$$\hat{y}_{\text{hss}}(\hat{u}) \triangleq M_* \hat{u} + d_*, \quad (2.6)$$

which is the DFT at frequency ω obtained from a sampling of y_{hss} . Consider the cost function

$$J(\hat{u}) \triangleq \lim_{t \rightarrow \infty} \frac{1}{t} \int_0^t \|y_{\text{hss}}(\tau, \hat{u})\|^2 d\tau, \quad (2.7)$$

which is the average power of y_{hss} . Using (2.5) and (2.6), it follows that

$$\begin{aligned} J(\hat{u}) &= \lim_{t \rightarrow \infty} \frac{1}{t} \int_0^t \|\text{Re } \hat{y}_{\text{hss}}(\hat{u}) \cos \omega\tau - \text{Im } \hat{y}_{\text{hss}}(\hat{u}) \sin \omega\tau\|^2 d\tau \\ &= \begin{bmatrix} \text{Re } \hat{y}_{\text{hss}}(\hat{u}) \\ \text{Im } \hat{y}_{\text{hss}}(\hat{u}) \end{bmatrix}^T \left(\lim_{t \rightarrow \infty} \frac{1}{t} \int_0^t \begin{bmatrix} \cos^2 \omega\tau & -(\cos \omega\tau)(\sin \omega\tau) \\ -(\cos \omega\tau)(\sin \omega\tau) & \sin^2 \omega\tau \end{bmatrix} d\tau \right) \\ &\quad \times \begin{bmatrix} \text{Re } \hat{y}_{\text{hss}}(\hat{u}) \\ \text{Im } \hat{y}_{\text{hss}}(\hat{u}) \end{bmatrix} \\ &= \frac{1}{2} \hat{y}_{\text{hss}}^*(\hat{u}) \hat{y}_{\text{hss}}(\hat{u}). \end{aligned} \quad (2.8)$$

The following result provides an expression for a control $\hat{u} = u_*$ that minimizes J . The proof is in Section 2.11.

Theorem 2.1. Consider the cost function (2.7), and assume that $\text{rank } M_* = \min\{\ell, m\}$. Then, the following statements hold:

- i)* Assume $\ell > m$, and define $u_* \triangleq -(M_*^* M_*)^{-1} M_*^* d_*$. Then, $\hat{y}_{\text{hss}}(u_*) = (I_\ell - M_* (M_*^* M_*)^{-1} M_*^*) d_*$, $J(u_*) = \frac{1}{2} d_*^* (I_\ell - M_* (M_*^* M_*)^{-1} M_*^*) d_*$, and for all $\hat{u} \in \mathbb{C}^m \setminus \{u_*\}$, $J(u_*) < J(\hat{u})$.
- ii)* Assume $\ell = m$, and define $u_* \triangleq -M_*^{-1} d_*$. Then, $\hat{y}_{\text{hss}}(u_*) = 0$, $J(u_*) = 0$, and for all $\hat{u} \in \mathbb{C}^m \setminus \{u_*\}$, $J(u_*) < J(\hat{u})$.
- iii)* Assume $\ell < m$, and let $u_* \in \{-M_*^* (M_* M_*^*)^{-1} d_* + (I_m - M_*^* (M_* M_*^*)^{-1} M_*) v : v \in \mathbb{C}^m\}$. Then, $\hat{y}_{\text{hss}}(u_*) = 0$ and $J(u_*) = 0$.

Theorem 2.1 provides an expression for a control u_* that minimizes J , but u_* requires knowledge of M_* and d_* .

In this chapter, we consider a sinusoidal control with frequency ω but where the amplitude and phase are updated in discrete time. Let $T_s > 0$ be the update period, and for each $k \in \mathbb{N}$, let $u_k \in \mathbb{C}^m$ contain information regarding the control amplitude and phase, which is determined from control update equations presented later. Then, for each $k \in \mathbb{N}$ and for all $t \in [kT_s, (k+1)T_s)$, the control is

$$u(t) = \text{Re } u_k \cos \omega t - \text{Im } u_k \sin \omega t. \quad (2.9)$$

For each $k \in \mathbb{Z}^+$, let $y_k \in \mathbb{C}^\ell$ denote DFT at frequency ω of the sequence obtained by sampling y on the interval $[(k-1)T_s, kT_s]$. If T_s is sufficiently large relative to the settling time of G_{yu} , then for all $k \in \mathbb{N}$, $y_{k+1} \approx \hat{y}_{\text{hss}}(u_k)$. For the remainder of this chapter, we assume that for all $k \in \mathbb{N}$, $y_{k+1} = \hat{y}_{\text{hss}}(u_k)$. In this case, (2.6) implies that for all $k \in \mathbb{N}$,

$$y_{k+1} = M_* u_k + d_*. \quad (2.10)$$

The HSS assumption $y_{k+1} = \hat{y}_{\text{hss}}(u_k)$ is used for stability analyses only. For the remainder of this chapter, we also assume that $\text{rank } M_* = \min\{\ell, m\}$, which is a technical assumption that depends on sensor and actuator placement.

2.4 Review of Frequency-Domain Higher Harmonic Control

In this section, we review FD-HHC control, which relies on knowledge of an estimate $M_e \in \mathbb{C}^{\ell \times m}$ of M_* . Let $\rho > 0$, and for all $k \in \mathbb{N}$, consider the control

$$u_{k+1} = u_k - \rho M_e^* y_{k+1}, \quad (2.11)$$

where $u_0 \in \mathbb{C}^m$ is the initial condition. The control architecture of FD-HHC is shown in Figure 2.1.

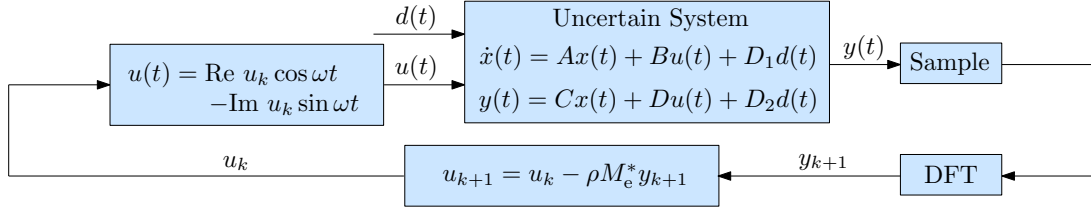


Figure 2.1: Schematic of FD-HHC given by (2.9) and (2.11).

Note that, it follows from (2.10) that

$$M_*(u_k - u_{k-1}) = y_{k+1} - y_k. \quad (2.12)$$

Multiplying (2.11) by M_* and using (2.12) implies that for all $k \in \mathbb{Z}^+$,

$$y_{k+1} = y_k - \rho M_* M_e^* y_k, \quad (2.13)$$

where $y_1 = M_* u_0 + d_*$ is the initial condition. Define the set

$$\Lambda \triangleq \text{spec}(M_e^* M_*) \cap \text{spec}(M_* M_e^*),$$

where the location of the elements of Λ affects the stability of (2.13). The following result provides the stability properties of the closed-loop system (2.13). The proof is in Section 2.11.

Theorem 2.2. Consider the closed-loop system (2.13), which consists of (2.10) and (2.11). Assume that $\Lambda \subset \text{ORHP}$, and assume that ρ satisfies

$$0 < \rho < \min_{\lambda \in \Lambda} \frac{2\text{Re } \lambda}{|\lambda|^2}. \quad (2.14)$$

Then, for all $u_0 \in \mathbb{C}^m$, $u_\infty \triangleq \lim_{k \rightarrow \infty} u_k$ exists and $y_\infty \triangleq \lim_{k \rightarrow \infty} y_k$ exists. Furthermore, for all $u_0 \in \mathbb{C}^m$, the following statements hold:

- i)* If $\ell > m$, then $u_\infty = -(M_e^* M_*)^{-1} M_e^* d_*$ and $y_\infty = [I_\ell - M_* (M_e^* M_*)^{-1} M_e^*] d_*$.
- ii)* If $\ell = m$, then $u_\infty = -M_*^{-1} d_*$ and $y_\infty = 0$.
- iii)* If $\ell < m$, then $u_\infty = u_0 - M_e^* (M_* M_e^*)^{-1} (M_* u_0 + d_*)$ and $y_\infty = 0$.

Theorem 2.2 relies on the conditions that $\Lambda \subset \text{ORHP}$ and ρ satisfies (2.14). These conditions depend on the estimate M_e . In the SISO case, $\Lambda \subset \text{ORHP}$ if and only if M_e is within 90° of M_* , that is, $|\angle(M_e/M_*)| < \frac{\pi}{2}$. In this case, (2.14) is satisfied by a sufficiently small $\rho > 0$. If $\Lambda \cap \text{OLHP}$ is not empty, then for all $\rho > 0$, $I_\ell - \rho M_* M_e^*$ has at least one eigenvalue outside the CUD. In this case, (2.13) implies that y_k diverges.

For MIMO systems with at least as many controls as performance signals (i.e., $m \geq \ell$), Theorem 2.2 implies that if $\Lambda \subset \text{ORHP}$ and ρ satisfies (2.14), then the FD-HHC (2.11) achieves asymptotically perfect disturbance rejection (i.e., $\lim_{k \rightarrow \infty} y_k = 0$). In contrast, for underactuated systems (i.e., $m < \ell$), asymptotically perfect disturbance rejection is impossible. In this case Theorem 2.2 implies that the steady-state performance depends on the estimate M_e . The next result is a corollary of Theorems 2.1 and 2.2 and addresses the case, where $M_e = M_*$.

Corollary 2.1. Consider the closed-loop system (2.13), which consists of (2.10) and (2.11). Assume that $M_e = M_*$, and assume that ρ satisfies

$$0 < \rho < \frac{2}{\lambda_{\max}(M_*^* M_*)}. \quad (2.15)$$

Then, for all $u_0 \in \mathbb{C}^m$, $u_\infty \triangleq \lim_{k \rightarrow \infty} u_k$ exists and $y_\infty \triangleq \lim_{k \rightarrow \infty} y_k$ exists, and for all $\hat{u} \in \mathbb{C}^m$, $J(u_\infty) \leq J(\hat{u})$.

Corollary 2.1 demonstrates that if $M_e = M_*$ and ρ satisfies (2.15), then u_k converges to a minimizer of J . In this case, $\lim_{k \rightarrow \infty} \|y_k\|$ exists and is minimized.

2.5 Frequency-Domain Adaptive Higher Harmonic Control

We now develop FD-AHHC algorithm, which does not require any information regarding M_* . Let $\mu \in (0, 1]$, $\nu_1 > 0$, and $u_0 \in \mathbb{C}^m$, and for all $k \in \mathbb{N}$, consider the control

$$u_{k+1} = u_k - \frac{\mu}{\nu_1 + \|M_k\|_{\text{F}}^2} M_k^* y_{k+1}, \quad (2.16)$$

where $M_k \in \mathbb{C}^{\ell \times m}$ is an estimate of M_* obtained from the adaptive equation developed below. Note that (2.16) is reminiscent of the FD-HHC (2.11) except the fixed estimate M_e is replaced by the adaptive estimate M_k , and the fixed gain ρ is replaced by the M_k -dependent gain $\mu/(\nu_1 + \|M_k\|_F^2)$, which normalizes the update equation (2.16).

To determine the adaptive equation for M_k , note that $M_*(u_k - u_{k-1}) - (y_{k+1} - y_k) = 0$, and consider the cost function $\mathcal{J} : \mathbb{R}^{\ell \times m} \times \mathbb{R}^{\ell \times m} \rightarrow [0, \infty)$ defined by

$$\mathcal{J}(M_r, M_i) \triangleq \frac{1}{2} \left\| (M_r + jM_i)(u_k - u_{k-1}) - (y_{k+1} - y_k) \right\|^2.$$

Note that $\mathcal{J}(\text{Re } M_*, \text{Im } M_*) = 0$, that is, M_* minimizes \mathcal{J} . Define the complex gradient

$$\begin{aligned} \nabla \mathcal{J}(M_r, M_i) &\triangleq \frac{\partial \mathcal{J}(M_r, M_i)}{\partial M_r} + j \frac{\partial \mathcal{J}(M_r, M_i)}{\partial M_i} \\ &= [(M_r + jM_i)(u_k - u_{k-1}) - (y_{k+1} - y_k)](u_k - u_{k-1})^*, \end{aligned} \quad (2.17)$$

which is the direction of the maximum rate of change of \mathcal{J} with respect to $M_r + jM_i$ [202]. Let $M_0 \in \mathbb{C}^{\ell \times m} \setminus \{0\}$, $\gamma \in (0, 1]$, and $\nu_2 > 0$, and for all $k \in \mathbb{Z}^+$, consider the adaptive equation

$$M_k \triangleq M_{k-1} - \eta_k \nabla \mathcal{J}(M_r, M_i) \Big|_{M_r = \text{Re } M_{k-1}, M_i = \text{Im } M_{k-1}}, \quad (2.18)$$

where for all $k \in \mathbb{Z}^+$,

$$\eta_k \triangleq \frac{\gamma(\nu_1 + \|M_{k-1}\|_F^2)^2}{\nu_2 \mu^2 + (\nu_1 + \|M_{k-1}\|_F^2)^2 \|u_k - u_{k-1}\|^2}. \quad (2.19)$$

Using (2.17)–(2.19), it follows that, for all $k \in \mathbb{Z}^+$,

$$M_k = M_{k-1} - \frac{\gamma(\nu_1 + \|M_{k-1}\|_F^2)^2 \left[M_{k-1}(u_k - u_{k-1}) - (y_{k+1} - y_k) \right] (u_k - u_{k-1})^*}{\nu_2 \mu^2 + (\nu_1 + \|M_{k-1}\|_F^2)^2 \|u_k - u_{k-1}\|^2}. \quad (2.20)$$

Thus, FD-AHHC is given by (2.9), (2.16), and (2.20). The control architecture is shown in Figure 2.2. All FD-AHHC computations are performed using complex DFT signals. At time kT_s , the control u is updated using (2.9) and the complex signal u_k . Note that u_k is calculated using y_k , which is the DFT of y at frequency ω sampled over the interval $[(k-1)T_s, kT_s)$, which corresponds to the time between time step $k-1$ and time step k . The update period T_s must be sufficiently large such that the harmonic steady-state assumption $y_{k+1} \approx \hat{y}_{\text{hss}}(u_k)$ is valid. Numerical testing suggests that T_s should be at least as large as the settling time associated with the slowest mode of A , that is, $T_s > 4/(\zeta\omega_n)$, where ζ and ω_n are the damping ratio and natural frequency of the slowest mode of A .

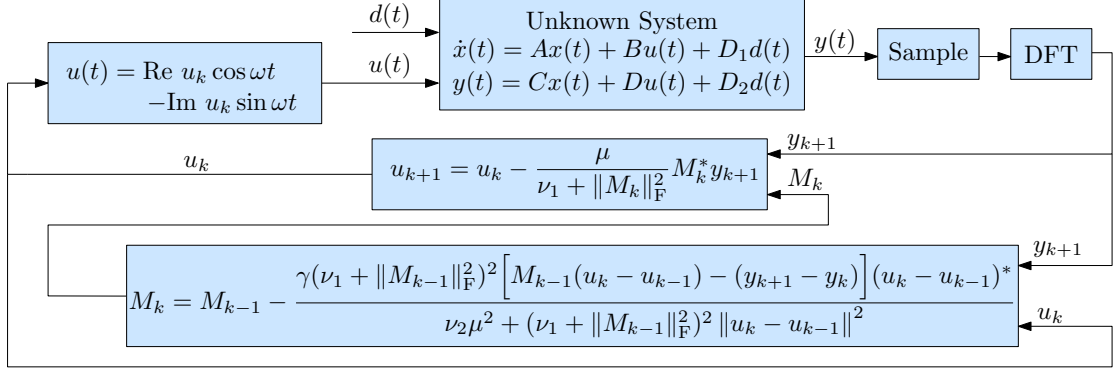


Figure 2.2: Schematic of FD-AHHC given by (2.9), (2.16), and (2.20).

The FD-AHHC parameters are $\mu \in (0, 1]$, $\gamma \in (0, 1]$, $\nu_1 > 0$, and $\nu_2 > 0$. The adaptive gains μ and γ influence the step size of the u_k and M_k update equations, respectively. The stability analysis in the next section demonstrates that μ and γ can be selected as large as 1. However, numerical testing suggests that smaller gains (e.g., $\mu = 0.2$ and $\gamma = 0.2$) tend to yield better performance. The parameters ν_1 and ν_2 influence the normalization of the u_k and M_k update equations, respectively. Numerical testing suggests $\nu_1 \ll \|M_0\|_F^2$ and $\nu_2 \ll \|M_0\|_F^2$ are good choices.

The FD-AHHC update equations (2.16) and (2.20) do not depend explicitly on the disturbance frequency ω . However, the open-loop equation (2.10) is based on the HSS approximation $y_{k+1} \approx \hat{y}_{\text{hss}}(u_k)$, and for a given T_s , the accuracy of this HSS approximation can be affected by the disturbance frequency ω . Numerical simulations suggest that if ω is large relative to the spectral radius of A (i.e., $\max\{|\lambda| : \lambda \in \text{spec}(A)\}$), then larger ω tends to result in smaller peak transient $\max_{k \in \mathbb{Z}^+} \|y_k\|$. In contrast, if ω is small relative to the spectral radius of A , then the relationship between ω and peak transient depends on the parameters of the system (2.1) and (2.2). Numerical simulations also suggest that the convergence speed of FD-AHHC is independent of ω .

2.6 FD-AHHC Stability Analysis

In this section, we analyze the stability of the closed-loop system that consists of (2.10), (2.16), and (2.20). The analysis focuses on systems that are square, that is, the number m of controls equals the number ℓ of performance signals.

Multiplying (2.16) by M_* and using (2.12) implies that for all $k \in \mathbb{Z}^+$,

$$y_{k+1} = y_k - \frac{\mu}{\nu_1 + \|M_{k-1}\|_F^2} M_* M_{k-1}^* y_k, \quad (2.21)$$

where $y_1 = M_* u_0 + d_*$ is the initial condition. Substituting (2.12) and (2.16) into (2.20) yields

$$M_k = M_{k-1} - \eta_k (M_{k-1} - M_*) (u_k - u_{k-1}) (u_k - u_{k-1})^*$$

$$\begin{aligned}
&= M_{k-1} - \eta_k \frac{\mu^2}{(\nu_1 + \|M_{k-1}\|_{\mathbb{F}}^2)^2} (M_{k-1} - M_*) M_{k-1}^* y_k y_k^* M_{k-1} \\
&= M_{k-1} - \frac{\gamma \mu^2}{\nu_2 \mu^2 + (\nu_1 + \|M_{k-1}\|_{\mathbb{F}}^2) \|u_k - u_{k-1}\|^2} (M_{k-1} - M_*) M_{k-1}^* y_k y_k^* M_{k-1},
\end{aligned}$$

and using (2.16) again implies that

$$M_k = M_{k-1} - \frac{\gamma}{\nu_2 + \|M_{k-1}^* y_k\|^2} (M_{k-1} - M_*) M_{k-1}^* y_k y_k^* M_{k-1}. \quad (2.22)$$

The following result provides properties of (2.22). The proof is in Section 2.12.

Proposition 2.1. Consider the closed-loop system (2.21) and (2.22), which consists of (2.10), (2.16), and (2.20), where $\mu \in (0, 1]$, $\gamma \in (0, 1]$, $\nu_1 > 0$, and $\nu_2 > 0$. Then, for all $u_0 \in \mathbb{C}^m$ and $M_0 \in \mathbb{C}^{\ell \times m}$, the estimate M_k is bounded, and for all $k \in \mathbb{Z}^+$,

$$\|M_k - M_*\|_{\mathbb{F}}^2 - \|M_{k-1} - M_*\|_{\mathbb{F}}^2 \leq -\frac{\gamma \|(M_{k-1} - M_*) M_{k-1}^* y_k\|^2}{\nu_2 + \|M_{k-1}^* y_k\|^2}. \quad (2.23)$$

Proposition 2.1 implies that $\|M_k - M_*\|_{\mathbb{F}}^2$ is nonincreasing. Note that Proposition 2.1 does not impose assumptions on the number m of controls or the number ℓ of performance signals.

For the remainder of this section, we assume $\ell = m$. In this case, define $u_* \triangleq -M_*^{-1} d_*$, which exists because $\text{rank } M_* = \ell = m$. Note that it follows from (2.10) that if $u_k \equiv u_*$, then $y_k \equiv 0$. The following result provides the stability properties of the closed-loop system (2.10), (2.16), and (2.20), where $\ell = m$. The proof is in Section 2.12.

Theorem 2.3. Consider the closed-loop system (2.21) and (2.22), which consists of (2.10), (2.16), and (2.20), where $\ell = m$, $\mu \in (0, 1]$, $\gamma \in (0, 1]$, $\nu_1 > 0$, and $\nu_2 > 0$. Then, the following statements hold:

- i)* $(y_k, M_{k-1}) \equiv (0, M_*)$ is a Lyapunov stable equilibrium of (2.21) and (2.22).
- ii)* There exists $r > 0$ such that for all $(u_0, M_0) \in \mathbb{C}^\ell \times \mathbb{B}_r(M_*)$, $\lim_{k \rightarrow \infty} u_k = u_*$ and $\lim_{k \rightarrow \infty} y_k = 0$.
- iii)* Let $u_0 \in \mathbb{C}^\ell$, and let $M_0 \in \mathbb{C}^{\ell \times \ell}$ be nonsingular. Assume that there exist $k_s \geq 0$ and $\varepsilon > 0$ such that for all $k \geq k_s$, $\lambda_{\min}(M_k^* M_k) \geq \varepsilon$. Then, $\lim_{k \rightarrow \infty} u_k = u_*$ and $\lim_{k \rightarrow \infty} y_k = 0$.

Part *iii)* of Theorem 3 invokes the assumption that there exist $k_s \geq 0$ and $\varepsilon > 0$ such that for all $k \geq k_s$, $\lambda_{\min}(M_k^* M_k) \geq \varepsilon$. This assumption, which implies that M_k is asymptotically nonsingular, cannot be verified *a priori*. However, the assumption $\lambda_{\min}(M_k^* M_k) \geq \varepsilon$, for some arbitrarily small $\varepsilon > 0$, can be verified at each time step. In fact, if the condition $\lambda_{\min}(M_k^* M_k) \geq \varepsilon$ is violated on a time step, then the estimate M_k can be perturbed to ensure $\lambda_{\min}(M_k^* M_k) \geq \varepsilon$. For example, M_k could

be perturbed to the nearest point such that $\lambda_{\min}(M_k^* M_k) = \varepsilon$. However, analyzing the stability of such a perturbation is an open problem. Nevertheless, the numerical simulations in the following sections suggest that for almost all initial conditions $(u_0, M_0) \in \mathbb{C}^\ell \times \mathbb{C}^{\ell \times \ell}$, the estimate M_k is asymptotically nonsingular, and thus, satisfies $\lambda_{\min}(M_k^* M_k) \geq \varepsilon$.

In the SISO (i.e., $\ell = m = 1$) case, the assumption $\lambda_{\min}(M_k^* M_k) \geq \varepsilon$ is satisfied for all initial conditions $(u_0, M_0) \in \mathbb{C} \times \mathbb{C} \setminus \{0\}$ except those where M_0 is exactly 180° from M_* , which is a set of Lebesgue measure zero. Define $\mathcal{M} \triangleq \mathbb{C} \setminus \{x \in \mathbb{C} : |\angle x - \angle M_*| = \pi\}$, which is the set of all complex numbers except those numbers that are exactly 180° from M_* . The following result provides the SISO stability properties. The proof is in Section 2.12.

Theorem 2.4. Consider the closed-loop system (2.21) and (2.22), which consists of (2.10), (2.16), and (2.20), where $\ell = m = 1$, $\mu \in (0, 1]$, $\gamma \in (0, 1]$, $\nu_1 > 0$, and $\nu_2 > 0$. Then, $(y_k, M_{k-1}) \equiv (0, M_*)$ is a Lyapunov stable equilibrium of (2.21) and (2.22). Furthermore, for all initial conditions $u_0 \in \mathbb{C}$ and $M_0 \in \mathcal{M} \setminus \{0\}$, M_k is bounded, $\lim_{k \rightarrow \infty} u_k = u_*$, and $\lim_{k \rightarrow \infty} y_k = 0$.

Theorem 2.4 demonstrates that in the SISO case, $\lim_{k \rightarrow \infty} y_k = 0$ for almost all initial conditions $(u_0, M_0) \in \mathbb{C} \times \mathbb{C}$. In fact, Theorem 2.4 provides the set of initial conditions (i.e., $M_0 \in \{0\} \cup \mathbb{C} \setminus \mathcal{M}$) for which the performance y_k may not converge to zero. In the square (i.e., $\ell = m$) MIMO case, there are also initial conditions for which the performance y_k does not converge to zero. The following example demonstrates this scenario.

Example 2.1. Consider (2.10), where

$$M_* = \begin{bmatrix} -1 & 1 \\ 0 & 1 \end{bmatrix}, \quad d_* = \begin{bmatrix} 1 \\ -1 \end{bmatrix}.$$

For all $k \in \mathbb{Z}^+$, u_k and M_k are given by (2.16) and (2.20), where

$$M_0 = \begin{bmatrix} 1 & 0 \\ 0 & 1 \end{bmatrix}, \quad u_0 = \begin{bmatrix} 1 \\ 1 \end{bmatrix}, \quad \mu = \gamma = 1, \quad \nu_1 = \nu_2 = 1.$$

Then, computing (2.10), (2.16), and (2.20) for $k = 0$ and $k = 1$ yields

$$y_2 = \begin{bmatrix} 4/3 \\ 0 \end{bmatrix}, \quad u_1 = \begin{bmatrix} 2/3 \\ 1 \end{bmatrix}, \quad M_1 = \begin{bmatrix} 0 & 0 \\ 0 & 1 \end{bmatrix}.$$

Since $M_1^* y_2 = 0$, it follows from (2.10), (2.16), and (2.20) that for all $k \in \mathbb{Z}^+$, $u_k = u_1$, $M_k = M_1$, and $y_{k+1} = y_2$. Thus, y_k does not converge to zero. \triangle

In Example 2.1, the initial conditions u_0 and M_0 are such that for all $k \in \mathbb{Z}^+$, M_k is singular and thus, $\lambda_{\min}(M_k^* M_k) = 0$. In this case, part *iii*) of Theorem 2.3 does not apply, and convergence of y_k to zero is not guaranteed. However, parts *i*) and *ii*) of Theorem 2.3 still apply.

In the SISO case, the set of initial conditions for which the performance y_k does not converge to zero is a set of Lebesgue measure zero. In the square MIMO case, determining the set of initial conditions for which the performance y_k does not converge to zero and examining its Lebesgue measure is an open problem. In the next section, we present a numerical study of FD-AHHC, which suggests that for MIMO systems with $m \geq \ell$, the performance y_k converges to zero for almost all initial conditions.

2.7 Numerical Study of the Steady-State and Transient Performance of FD-AHHC

In this section, we numerically investigate the steady-state and transient performance properties of not only square systems but also nonsquare (i.e., $m > \ell$ or $m < \ell$) systems. We consider 3 cases: *i*) $\ell = m \leq 5$; *ii*) $\ell < m \leq 5$; *iii*) $m < \ell \leq 5$. For each case, we simulate 10,000 random systems (2.10). For each system in case *i*), ℓ is a uniformly distributed random integer (UDRI) on $[1, 5]$, and $\ell = m$. For each system in case *ii*), m is a UDRI on $[2, 5]$, and ℓ is a UDRI on $[1, m - 1]$. For each system in case *iii*), ℓ is a UDRI on $[2, 5]$, and m is a UDRI on $[1, \ell - 1]$. For each system, each element of $\text{Re } M_*$, $\text{Im } M_*$, $\text{Re } M_0$, and $\text{Im } M_0$ is a uniformly distributed random variable (UDRV) on $[-2, 2]$, and each element of $\text{Re } u_0$, $\text{Im } u_0$, $\text{Re } d_*$, and $\text{Im } d_*$ is a UDRV on $[-1, 1]$.

For each simulation, $\mu = \gamma = 1$ and $\nu_1 = \nu_2 = 10^{-3} \|M_0\|_F^2$. Each simulation stops at time step k_f if, for all $i \in [k_f - 50, k_f]$, $\|u_i - u_{i-1}\| / \|u_{k_f}\| < 10^{-6}$ (i.e., u_k has converged). Note that all 30,000 systems tested satisfied this convergence criteria.

For each simulation, we consider the steady-state performance

$$P_{\text{ss}} \triangleq \log(\|y_{k_f}\| / \|d_*\|),$$

and the peak transient performance

$$P_t \triangleq \max_{k \in \mathbb{Z}^+} (\|y_k\| / \|y_1\|).$$

Note that $P_{\text{ss}} < 0$ implies that $\|y_{k_f}\|$ is improved relative to the uncontrolled open-loop performance. In addition, $P_{\text{ss}} \rightarrow -\infty$ as $y_{k_f} \rightarrow 0$. For peak transient performance, $P_t = 1$ implies that the performance $\|y_k\|$ is never worse (i.e., larger) than the initial performance $\|y_1\|$.

For each system, we consider $\lambda_m \triangleq \text{argmin}_{\lambda \in \Lambda_0} \text{Re } \lambda$, where

$$\Lambda_0 \triangleq \text{spec}(M_0^* M_*) \cap \text{spec}(M_* M_0^*).$$

Recall from Section 2.4 that the control (2.11) for FD-HHC with $M_e = M_0$ requires $\lambda_m > 0$ for y_k to be bounded. In contrast, FD-AHHC requires no assumption on λ_m .

Figure 2.3 shows P_{ss} for the 3 cases. For all 20,000 systems with $m \geq \ell$, FD-AHHC yields $\lim_{k \rightarrow \infty} y_k = 0$. For all 10,000 systems with $m < \ell$, the performance y_k converges, and for 99.5% of those systems, $P_{\text{ss}} < 0$, which means the steady-state performance is improved relative to the uncontrolled open-loop performance.

Figure 2.4 shows P_t for the 3 cases. For approximately 39% of the 30,000 systems, $P_t = 1$, which implies that the performance $\|y_k\|$ is never worse (i.e., larger) than the initial performance $\|y_1\|$. Note that P_t tends to be better (i.e., smaller) for systems where $\lambda_m > 0$, which is the region where FD-HHC is stable. Table 2.1 summarizes P_{ss} and P_t for each case. Note that 99.0% of the systems have a peak transient no worse than 2 times the initial performance $\|y_1\|$ (i.e., $P_t \leq 2$). For brevity, the numerical study of FD-HHC is not presented; however, for all systems, the steady-state and peak transient performance with FD-AHHC is at least as good as that with FD-HHC, where the estimate of M_* is $M_e = M_0$.

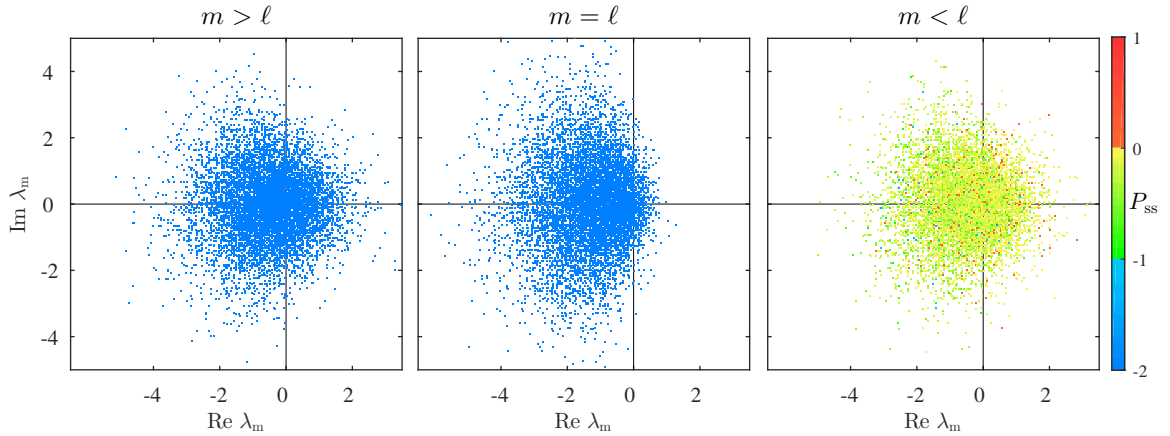


Figure 2.3: Steady-state performance P_{ss} for 30,000 systems. For all systems, the steady-state performance with FD-AHHC converges. For all 20,000 systems with $m \geq \ell$, FD-AHHC yields $y_k \rightarrow 0$ as $k \rightarrow \infty$. For 9,952 out of 10,000 systems with $m < \ell$, FD-AHHC yields improvement relative to open loop (i.e., $P_{ss} < 0$).

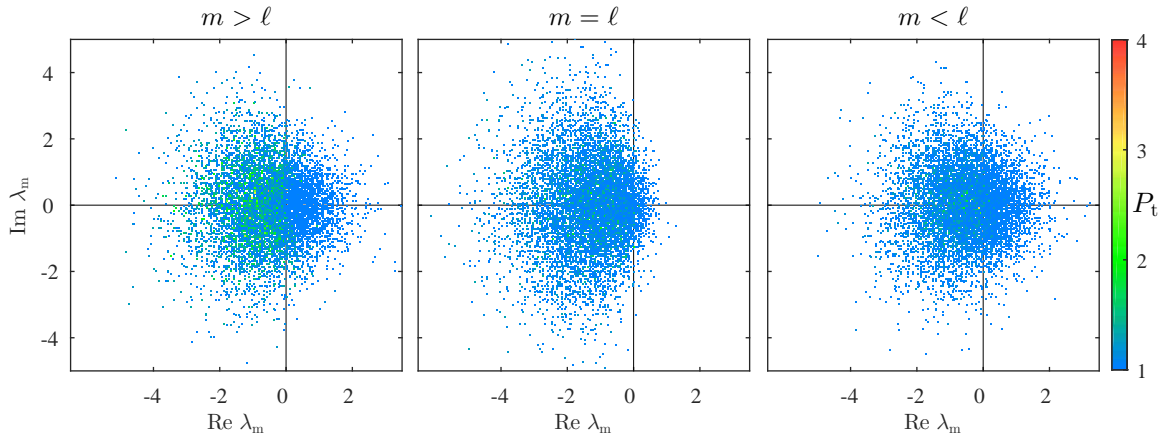


Figure 2.4: Peak transient performance P_t for 30,000 systems. For approximately 39% of the systems, the transient performance with FD-AHHC is never worse than the initial performance $\|y_1\|$. Furthermore, for 75% of the systems with $\lambda_m > 0$, the transient performance with FD-AHHC is never worse than $\|y_1\|$.

Table 2.1: Percent of systems satisfying a steady-state P_{ss} or peak transient P_t performance condition.

	Steady-State Performance				Peak Transient Performance			
	$P_{ss} \leq 1$	$P_{ss} \leq 0$	$P_{ss} \leq -1$	$P_{ss} \leq -2$	$P_t \leq 4$	$P_t \leq 3$	$P_t \leq 2$	$P_t = 1$
$m > \ell$	100	100	100	100	100	99.9	98.3	40.1
$m = \ell$	100	100	100	100	100	100	100	39.4
$m < \ell$	100	99.5	0.85	0	100	99.9	98.7	36.8

2.8 FD-AHHC for Multi-Tone Disturbances

In this section, we extend FD-AHHC to address the multi-tone disturbance (2.3). For the moment, assume that G_{yu} , G_{yd} , $d_{c,1}, \dots, d_{c,q}$, and $d_{s,1}, \dots, d_{s,q}$ are known, and consider the harmonic control

$$u(t) = \sum_{i=1}^q u_{c,i} \cos \omega_i t + u_{s,i} \sin \omega_i t, \quad (2.24)$$

where $u_{c,1}, \dots, u_{c,q}, u_{s,1}, \dots, u_{s,q} \in \mathbb{C}^m$. For $i = 1, \dots, q$, define $\hat{u}_i \triangleq u_{c,i} - j u_{s,i}$, which is the DFT at frequency ω_i obtained from a sampling of u . In addition, for $i = 1, \dots, q$, define

$$\begin{aligned} M_{*,i} &\triangleq G_{yu}(j\omega_i) \in \mathbb{C}^{\ell \times m}, \\ d_{*,i} &\triangleq G_{yd}(j\omega_i)(d_{c,i} - j d_{s,i}) \in \mathbb{C}^\ell. \end{aligned}$$

Then, the HSS performance of (2.1) and (2.2) with control (2.24) is

$$\begin{aligned} y_{m,\text{hss}}(t, \hat{u}_1, \dots, \hat{u}_q) &\triangleq \sum_{i=1}^q \text{Re} \left[\left(G_{yu}(j\omega_i) \hat{u}_i + G_{yd}(j\omega_i)(d_{c,i} - j d_{s,i}) \right) e^{j\omega_i t} \right] \\ &= \sum_{i=1}^q \text{Re} (M_{*,i} \hat{u}_i + d_{*,i}) \cos \omega_i t - \text{Im} (M_{*,i} \hat{u}_i + d_{*,i}) \sin \omega_i t, \end{aligned} \quad (2.25)$$

which is the multi-tone generalization of (2.5). For $i = 1, \dots, q$, define

$$\hat{y}_{\text{hss},i}(\hat{u}_i) \triangleq M_{*,i} \hat{u}_i + d_{*,i}, \quad (2.26)$$

which is DFT at frequency ω_i obtained from a sampling of $y_{m,\text{hss}}$. Consider the cost function

$$J_m(\hat{u}_1, \dots, \hat{u}_q) \triangleq \lim_{t \rightarrow \infty} \frac{1}{t} \int_0^t \|y_{m,\text{hss}}(\tau, \hat{u}_1, \dots, \hat{u}_q)\|^2 d\tau. \quad (2.27)$$

Using (2.25) and (2.26), it follows that

$$J_m(\hat{u}_1, \dots, \hat{u}_q) = \lim_{t \rightarrow \infty} \frac{1}{t} \int_0^t \left\| \sum_{i=1}^q \left[\text{Re} \hat{y}_{\text{hss},i}(\hat{u}_i) \right] \cos \omega_i \tau - \left[\text{Im} \hat{y}_{\text{hss},i}(\hat{u}_i) \right] \sin \omega_i \tau \right\|^2 d\tau$$

$$\begin{aligned}
&= \frac{1}{2} \sum_{i=1}^q \hat{y}_{\text{hss},i}^*(\hat{u}_i) \hat{y}_{\text{hss},i}(\hat{u}_i) \\
&= \sum_{i=1}^q \lim_{t \rightarrow \infty} \frac{1}{t} \int_0^t \|y_{\text{hss},i}(\tau, \hat{u}_i)\|^2 d\tau,
\end{aligned}$$

where for $i = 1, \dots, q$, the steady-state response at frequency ω_i is given by

$$y_{\text{hss},i}(t, \hat{u}_i) \triangleq \text{Re}(M_{*,i}\hat{u}_i + d_{*,i}) \cos \omega_i t - \text{Im}(M_{*,i}\hat{u}_i + d_{*,i}) \sin \omega_i t,$$

Thus, if for each $i = 1, \dots, q$, the average power $\lim_{t \rightarrow \infty} \frac{1}{t} \int_0^t \|y_{\text{hss},i}(\tau, \hat{u}_i)\|^2 d\tau$ at frequency ω_i is minimized, then the average power (2.27) is minimized. Therefore, we can use q copies of the FD-AHHC algorithm (2.16) and (2.20)—one at each disturbance frequency.

For $i = 1, \dots, q$, let $y_{i,k} \in \mathbb{C}^\ell$ denote the DFT at frequency ω_i of the sequence obtained by sampling y on the interval $[(k-1)T_s, kT_s)$. For each $k \in \mathbb{N}$ and for all $t \in [kT_s, (k+1)T_s)$, the control is

$$u(t) = \sum_{i=1}^q \text{Re } u_{i,k} \cos \omega_i t - \text{Im } u_{i,k} \sin \omega_i t, \quad (2.28)$$

where for all $i = 1, \dots, q$,

$$u_{i,k+1} = u_{i,k} - \frac{\mu_i}{\nu_{1,i} + \|M_{i,k}\|_{\text{F}}^2} M_{i,k}^* y_{i,k+1}, \quad (2.29)$$

$$\begin{aligned}
M_{i,k} &= M_{i,k-1} - \frac{\gamma_i (\nu_{1,i} + \|M_{i,k-1}\|_{\text{F}}^2)^2}{\nu_{2,i} \mu_i^2 + (\nu_{1,i} + \|M_{i,k-1}\|_{\text{F}}^2)^2 \|u_{i,k} - u_{i,k-1}\|^2} \\
&\quad \times \left[M_{i,k-1} (u_{i,k} - u_{i,k-1}) - (y_{i,k+1} - y_{i,k}) \right] (u_{i,k} - u_{i,k-1})^*, \quad (2.30)
\end{aligned}$$

where $\mu_i \in (0, 1]$, $\gamma_i \in (0, 1]$, $\nu_{1,i} > 0$, $\nu_{2,i} > 0$, and $u_{i,0}$ and $M_{i,0}$ are the initial conditions.

If T_s is sufficiently large relative to the settling time of G_{yu} , then for $i = 1, \dots, q$, and for all $k \in \mathbb{N}$, $y_{i,k+1} \approx \hat{y}_{\text{hss},i}(u_{i,k})$. We assume that for $i = 1, \dots, q$, and for all $k \in \mathbb{N}$, $y_{i,k+1} = \hat{y}_{\text{hss},i}(u_{i,k})$. In this case, (2.26) implies that for all $k \in \mathbb{N}$,

$$y_{i,k+1} = M_{*,i} u_{i,k} + d_{*,i}. \quad (2.31)$$

The following result is a corollary of Theorem 2.3 and provides the stability properties of the closed-loop system (2.29)–(2.31) with multi-tone disturbance.

Corollary 2.2. Assume $m = \ell$, and for $i = 1, \dots, q$, consider the open-loop system (2.31), and the control (2.29) and (2.30), where $\mu_i \in (0, 1]$, $\gamma_i \in (0, 1]$, $\nu_{1,i} > 0$, and $\nu_{2,i} > 0$. Then, the following statements hold:

- i*) For $i = 1, \dots, q$, $(y_{i,k}, M_{i,k-1}) \equiv (0, M_{*,i})$ is a Lyapunov stable equilibrium of (2.29)–(2.31).

- ii) There exists $r > 0$ such that for $i = 1, \dots, q$ and for all $(u_{i,0}, M_{i,0}) \in \mathbb{C}^\ell \times \mathbb{B}_r(M_{*,i})$, $\lim_{k \rightarrow \infty} u_{i,k} = u_{*,i}$ and $\lim_{k \rightarrow \infty} y_{i,k} = 0$.
- iii) For $i = 1, \dots, q$, let $u_{i,0} \in \mathbb{C}^\ell$, and let $M_{i,0} \in \mathbb{C}^{\ell \times \ell}$ be nonsingular. Assume that there exist $k_s \geq 0$ and $\varepsilon > 0$ such that for $i = 1, \dots, q$, and for all $k \geq k_s$, $\lambda_{\min}(M_{i,k}^* M_{i,k}) \geq \varepsilon$. Then, for $i = 1, \dots, q$, $\lim_{k \rightarrow \infty} u_{i,k} = u_{*,i}$ and $\lim_{k \rightarrow \infty} y_{i,k} = 0$.

The following result is a corollary of Theorem 2.4 and provides the SISO stability properties with multi-tone disturbance.

Corollary 2.3. Assume $m = \ell = 1$, and for $i = 1, \dots, q$, consider the open-loop system (2.31), and the control (2.29) and (2.30), where $\mu_i \in (0, 1]$, $\gamma_i \in (0, 1]$, $\nu_{1,i} > 0$, and $\nu_{2,i} > 0$. Then, for $i = 1, \dots, q$, $(y_{i,k}, M_{i,k-1}) \equiv (0, M_{*,i})$ is a Lyapunov stable equilibrium of (2.29)–(2.31). Furthermore, for $i = 1, \dots, q$ and for all initial conditions $u_{i,0} \in \mathbb{C}$ and $M_{i,0} \in \mathbb{C} \setminus \{x \in \mathbb{C} : x = 0 \text{ or } |\angle x - \angle M_{*,i}| = \pi\}$, $M_{i,k}$ is bounded, $\lim_{k \rightarrow \infty} u_{i,k} = u_{i,*}$, and $\lim_{k \rightarrow \infty} y_{i,k} = 0$.

2.9 Numerical Examples

Consider the acoustic duct of length $L = 2$ m shown in Figure 2.5, where all measurements are from the left end of the duct. A disturbance speaker is at location $\xi_d = 0.95$ m, while control speakers are at locations $\xi_{\psi_1} = 0.4$ m and $\xi_{\psi_2} = 1.25$ m. All speakers have cross-sectional area $A_s = 0.0025$ m². The equation of motion for the acoustic duct is given by

$$\frac{1}{c^2} \frac{\partial^2 p(\xi, t)}{\partial t^2} = \frac{\partial^2 p(\xi, t)}{\partial \xi^2} + \rho_0 \dot{\psi}_1(t) \delta(\xi - \xi_{\psi_1}) + \rho_0 \dot{\psi}_2(t) \delta(\xi - \xi_{\psi_2}) + \rho_0 \dot{d}(t) \delta(\xi - \xi_d),$$

where $p(\xi, t)$ is the acoustic pressure, δ is the Dirac delta, $c = 343$ m/s is the phase speed of the acoustic wave, ψ_1 and ψ_2 are the speaker cone velocities of the control speakers, d is the speaker cone velocity of the disturbance speaker, and $\rho_0 = 1.21$ kg/m³ is the equilibrium density of air at room conditions. See [203] for more details.

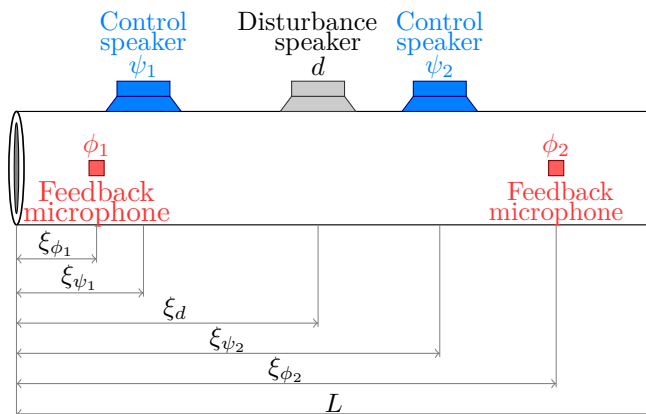


Figure 2.5: The acoustic duct used in Examples 2.2–2.5.

Using separation of variables and retaining r modes, the solution $p(\xi, t)$ is approximated by $p(\xi, t) = \sum_{i=1}^r q_i(t)V_i(\xi)$, where for $i = 1, \dots, r$, $V_i(\xi) \triangleq c\sqrt{2/L} \sin i\pi\xi/L$, and q_i satisfies the differential equation (2.1), where

$$x(t) = \begin{bmatrix} \int_0^t q_1(\sigma) d\sigma \\ q_1(t) \\ \vdots \\ \int_0^t q_r(\sigma) d\sigma \\ q_r(t) \end{bmatrix}, \quad u(t) = \begin{bmatrix} \psi_1(t) \\ \psi_2(t) \end{bmatrix},$$

$$A = \text{diag} \left(\begin{bmatrix} 0 & 1 \\ -\omega_{n_1}^2 & -2\zeta_1\omega_{n_1} \end{bmatrix}, \dots, \begin{bmatrix} 0 & 1 \\ -\omega_{n_r}^2 & -2\zeta_r\omega_{n_r} \end{bmatrix} \right),$$

$$B = \frac{\rho_0}{A_s} \begin{bmatrix} 0 & V_1(\xi_{\psi_1}) & \cdots & 0 & V_r(\xi_{\psi_1}) \\ 0 & V_1(\xi_{\psi_2}) & \cdots & 0 & V_r(\xi_{\psi_2}) \end{bmatrix}^T, \quad D_1 = \frac{\rho_0}{A_s} \begin{bmatrix} 0 & V_1(\xi_d) & \cdots & 0 & V_r(\xi_d) \end{bmatrix}^T,$$

and for $i = 1, \dots, r$, $\omega_{n_i} \triangleq i\pi c/L$ is the natural frequency of the i th mode, and $\zeta_i = 0.2$ is the assumed damping ratio of the i th mode.

Two feedback microphones are in the duct at locations $\xi_{\phi_1} = 0.3$ m and $\xi_{\phi_2} = 1.7$ m, and they measure the acoustic pressures $\phi_1(t) = p(\xi_{\phi_1}, t)$ and $\phi_2(t) = p(\xi_{\phi_2}, t)$, respectively. Thus, for $i = 1, 2$, $\phi_i(t) = C_i x(t)$, where

$$C_i = \frac{\rho_0}{A_s} [0 \quad V_1(\xi_{\phi_i}) \quad \cdots \quad 0 \quad V_r(\xi_{\phi_i})].$$

For all examples, $r = 5$ and $x(0) = 0$. The DFT is performed using a 1-kHz sampling frequency. The settling time of the slowest mode is approximately $4/(\zeta_1\omega_{n_1}) = 0.037$ s. Thus, we select $T_s \geq 0.037$; specifically, we let $T_s = 0.1$ s. The parameters for FD-HHC and FD-AHHC are $u_0 = 0$, $\mu = \gamma = 0.2$, $\nu_1 = \nu_2 = 0.1\|M_0\|_F^2$, $\rho = \mu/(\nu_1 + \|M_0\|_F^2)$, and $M_e = M_0$, where M_0 is specified in each example. The following examples consider the acoustic duct with different control speaker and feedback microphone configurations. Let $\omega_1 = 251$ rad/s and $\omega_2 = 628$ rad/s.

Example 2.2. Consider the SISO ($\ell = m = 1$) system, where we let $u = \psi_1$, $y = \phi_1$, $\psi_2 = 0$, and $d = \sin \omega_1 t + 2 \cos \omega_1 t$. First, consider the case where M_0 is within 90° of M_* , specifically, $M_0 = 2e^{j\frac{\pi}{3}} M_*$. Figure 2.6 shows the response y and control u for FD-HHC and FD-AHHC. The control is turned on after 1 s. Both FD-HHC and FD-AHHC yield asymptotic disturbance rejection. However, FD-AHHC converges more quickly than FD-HHC.

Next, let $M_0 = 2e^{j\frac{2\pi}{3}} M_*$ which is not within 90° of M_* . Figure 2.7 shows the response y and control u for FD-HHC and FD-AHHC. In this case, the response y with FD-HHC diverges, whereas the response y with FD-AHHC converges to zero. Figure 2.8 shows the trajectory of the estimate M_k , which moves toward M_* . Proposition 1 states that $|M_k - M_*|$ is nondecreasing; however, this result assumes that y reaches harmonic steady state (i.e., $y_{k+1} = y_{\text{hss}}(u_k)$ for all $k \in \mathbb{N}$). Figure 2.8 shows that $M_k - M_*$ may increase slightly in practice but generally decreases. \triangle

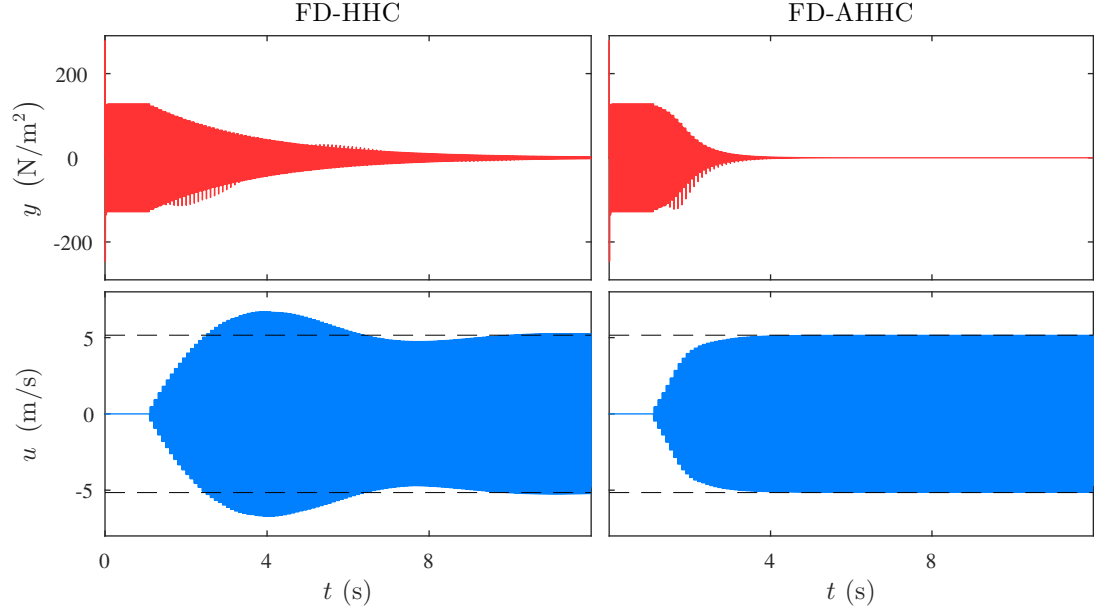


Figure 2.6: FD-HHC and FD-AHHC for a SISO system with $|\angle(M_0/M_*)| < \frac{\pi}{2}$. Both FD-HHC and FD-AHHC yield $y(t) \rightarrow 0$ as $t \rightarrow \infty$. The dashed lines show $\pm|u_*|$.

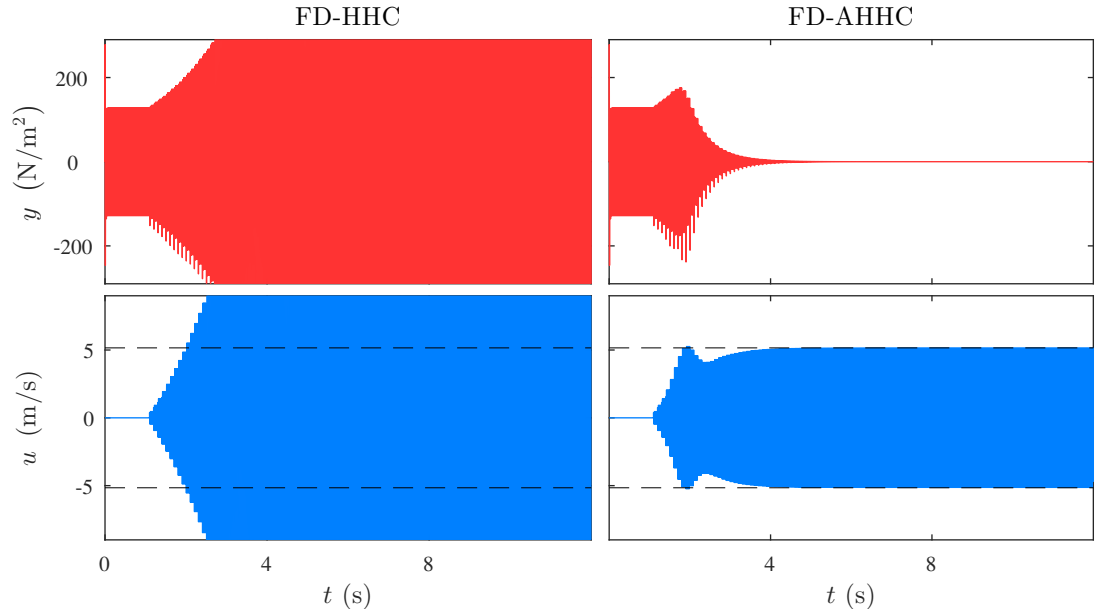


Figure 2.7: FD-HHC and FD-AHHC for a SISO system with $|\angle(M_0/M_*)| > \frac{\pi}{2}$. The response y with FD-HHC diverges, whereas FD-AHHC yields $y(t) \rightarrow 0$ as $t \rightarrow \infty$. The dashed lines show $\pm|u_*|$.

Example 2.3. Consider the two-input single-output ($m = 2$ and $\ell = 1$) system, where we let $u = [\psi_1 \ \psi_2]^\top$, $y = \phi_1$, and $d = \sin \omega_1 t + 2 \cos \omega_1 t$. First, consider the case where M_0 is selected such that (2.14) is satisfied, specifically, $M_0 = [1.5e^{j\frac{\pi}{4}}(M_*)_{(1,1)} \ 0.5e^{j\frac{\pi}{3}}(M_*)_{(1,2)}]$. Figure 2.9 shows the response y and the control u for FD-HHC and FD-AHHC. The control is turned on after 1 s. Both FD-HHC and FD-AHHC yield asymptotic disturbance rejection. Next, let $M_0 = [1.5e^{j\frac{3\pi}{4}}(M_*)_{(1,1)} \ 0.5e^{j\frac{2\pi}{3}}(M_*)_{(1,2)}]$, which does not satisfy (2.14). Figure 2.10 shows

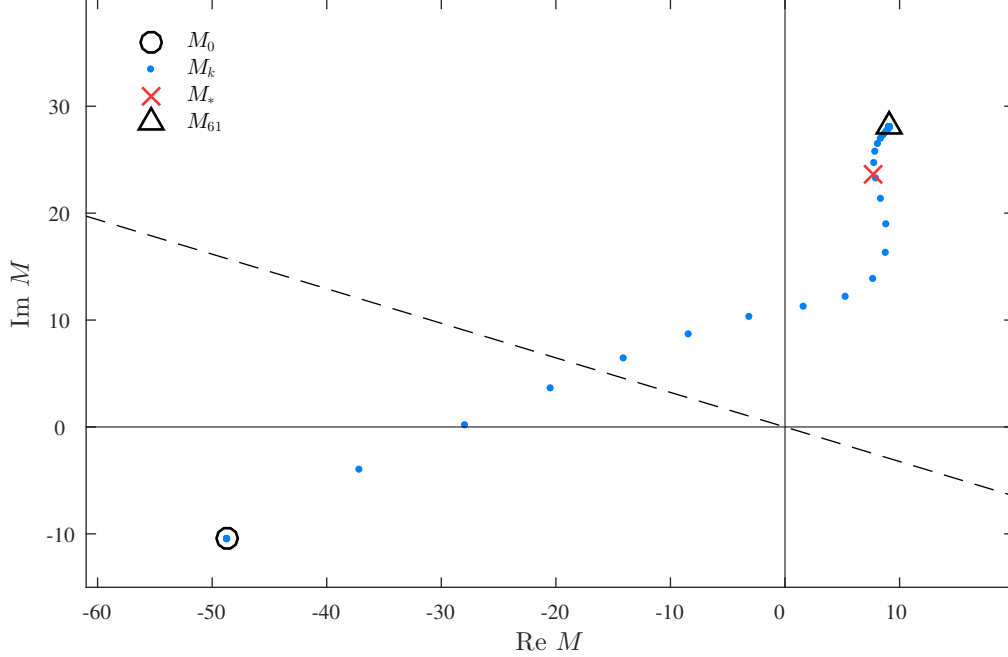


Figure 2.8: Trajectory of M_k with FD-AHHC for a SISO system where $|\angle(M_0/M_*)| > \frac{\pi}{2}$. The dashed line shows the locus of M such that $|\angle(M/M_*)| = \frac{\pi}{2}$, which is the FD-HHC stability boundary for M_e . Selecting $M_e = M_0$ from the lower region, where $|\angle(M/M_*)| > \frac{\pi}{2}$, results in an unstable response with FD-HHC, whereas FD-AHHC yields asymptotic disturbance rejection for all $M_0 \in \mathcal{M}$.

the response and control for FD-HHC and FD-AHHC. In this case, the response y with FD-HHC diverges, whereas the response y with FD-AHHC converges to 0. \triangle

Example 2.4. Consider the single-input two-output ($m = 1$ and $\ell = 2$) system, where we let $u = \psi_1$, $y = [\phi_1 \ \phi_2]^T$, $\psi_2 = 0$, and $d = \sin \omega_1 t + 2 \cos \omega_1 t$. First, consider the case where M_0 is selected such that (2.14) is satisfied, specifically, $M_0 = [1.5e^{j\frac{\pi}{4}}(M_*)_{(1,1)} \ 0.5e^{j\frac{\pi}{3}}(M_*)_{(2,1)}]^T$. Note that the control $u_* = -1.66 + j0.98$ minimizes the average power (2.7). Figure 2.11 shows the response y and the control u for FD-HHC and FD-AHHC. The control is turned on after 1 s. In this case, FD-HHC and FD-AHHC each yield $\lim_{k \rightarrow \infty} u_k = u_*$ as $k \rightarrow \infty$. Thus, $\lim_{k \rightarrow \infty} \|y_k\|$ is minimized. Note that FD-AHHC converges more quickly than FD-HHC.

Next, let $M_0 = [1.5e^{j\frac{3\pi}{4}}(M_*)_{(1,1)} \ 0.5e^{j\frac{2\pi}{3}}(M_*)_{(2,1)}]^T$, which does not satisfy (2.14). Figure 2.12 shows the response y and control u for FD-HHC and FD-AHHC. In this case, the response y with FD-HHC diverges, whereas FD-AHHC yields $\lim_{k \rightarrow \infty} u_k = u_*$, which implies that $\lim_{k \rightarrow \infty} \|y_k\|$ is minimized. \triangle

Example 2.5. Consider the MIMO ($m = 2$ and $\ell = 2$) system where we let $u = [\psi_1 \ \psi_2]^T$, $y = [\phi_1 \ \phi_2]^T$, and $d = \sin \omega_1 t + \sin \omega_2 t + \cos \omega_1 t + \cos \omega_2 t$, which is a two-tone disturbance. Define $M_{*,1} \triangleq G_{yu}(j\omega_1)$ and $M_{*,2} \triangleq G_{yu}(j\omega_2)$. Since d has

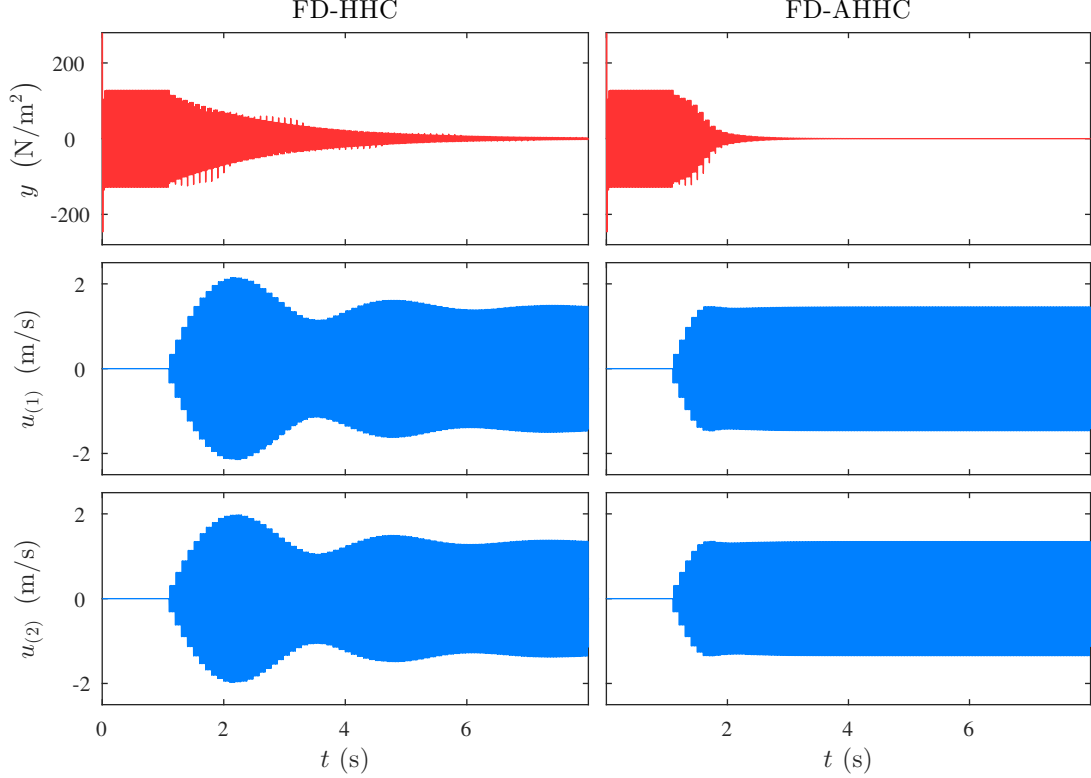


Figure 2.9: FD-HHC and FD-AHHC for a two-input single-output system that satisfies (2.14). Both FD-HHC and FD-AHHC yield $y(t) \rightarrow 0$ as $t \rightarrow \infty$.

2 tones, we use 2 copies of the FD-HHC or FD-AHHC algorithm—one copy at each disturbance frequency. Let $M_{1,0}$ and $M_{2,0}$ denote the initial estimates of $M_{*,1}$ and $M_{*,2}$. First, consider the case where $M_{1,0}$ and $M_{2,0}$ are such that (2.14) is satisfied, specifically, $M_{1,0} = 0.6e^{j\frac{\pi}{6}} M_{*,1}$ and $M_{2,0} = 0.9e^{j\frac{\pi}{3}} M_{*,2}$. Figure 2.13 shows the response y and the control u for FD-HHC and FD-AHHC. The control is turned on after 1 s. Both FD-HHC and FD-AHHC yield asymptotic disturbance rejection.

Next, consider the case where $M_{1,0} = 0.2e^{j\frac{\pi}{7}} M_{*,1}$ and $M_{2,0} = 0.6e^{j\frac{\pi}{14}} M_{*,2}$, which does not satisfy (2.14). Figure 2.14 shows the response y and control u for FD-HHC and FD-AHHC. In this case, the response y with FD-HHC diverges, whereas the response y with FD-AHHC converges to zero. \triangle

2.10 Conclusions

We presented FD-AHHC, which is a new adaptive harmonic controller that is effective for rejecting sinusoidal disturbances with known frequencies that act on a completely unknown asymptotically stable MIMO LTI system. FD-AHHC is a frequency-domain method, where all computations use the DFT of the performance measurement at the disturbance frequencies. We analyzed FD-AHHC stability for square (i.e., $\ell = m$) MIMO systems. In this case, we showed that the closed-loop

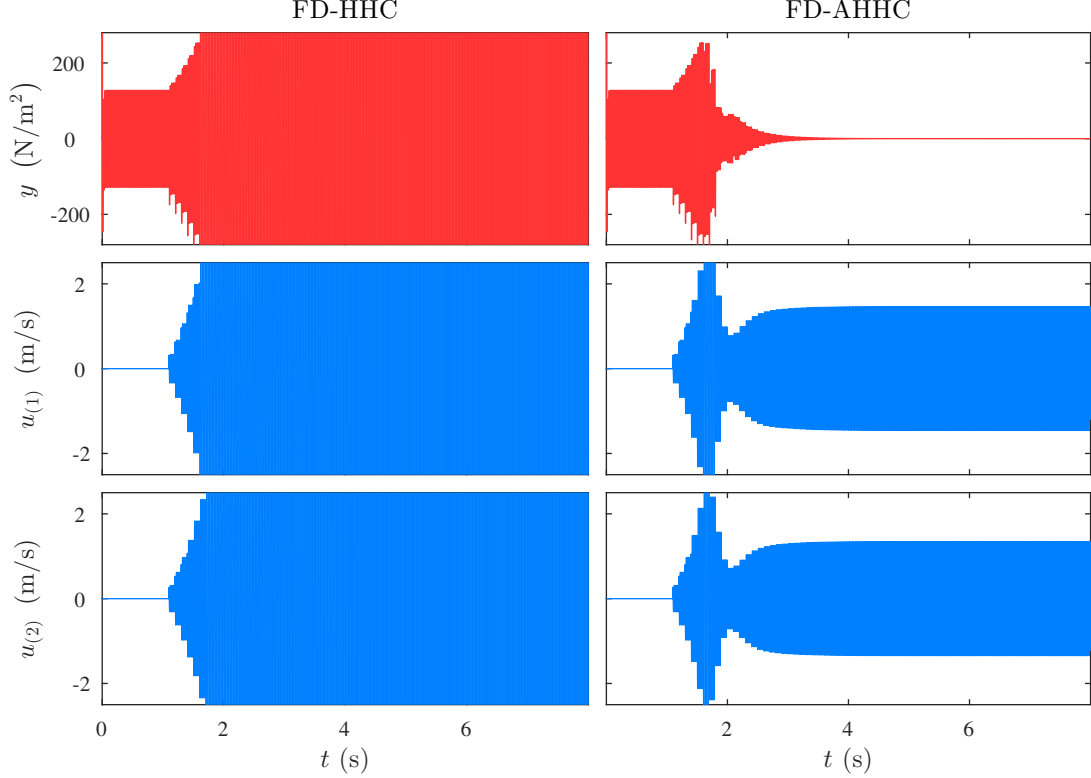


Figure 2.10: FD-HHC and FD-AHHC for a two-input single-output system that does not satisfy (2.14). The response y with FD-HHC diverges, whereas FD-AHHC yields $y(t) \rightarrow 0$ as $t \rightarrow \infty$.

system is Lyapunov stable, and under the technical assumption that the estimate M_k is asymptotically nonsingular, we showed that the performance tends to zero. For SISO systems, this technical assumption is satisfied for almost all initial conditions, and thus, the performance tends to zero for all initial conditions except a set of Lebesgue measure zero.

We presented a numerical study of MIMO FD-AHHC with 30,000 random systems. For all 30,000 systems, the response with MIMO FD-AHHC is bounded and the disturbance attenuation is at least as good as that with FD-HHC. For all 20,000 systems with at least as many controls as performance measurements (i.e., $m \geq \ell$), the performance with FD-AHHC tends to zero. This suggests that FD-AHHC (with $m \geq \ell$) yields zero steady-state performance for almost all initial conditions. Determining the set of initial conditions for which the FD-AHHC (with $m \geq \ell$) performance does not converge to zero is an open problem. In addition, examining the Lebesgue measure of this set is open.

2.11 Proofs of Theorems 2.1 and 2.2

Proof of Theorem 2.1. To show *i*) and *ii*), assume $\ell \geq m$, and define $u_* \triangleq -(M_*^* M_*)^{-1} M_*^* d_*$. It follows from (2.6) that $\hat{y}_{\text{hss}}(u_*) = (I_\ell - M_*(M_*^* M_*)^{-1} M_*^*) d_*$.

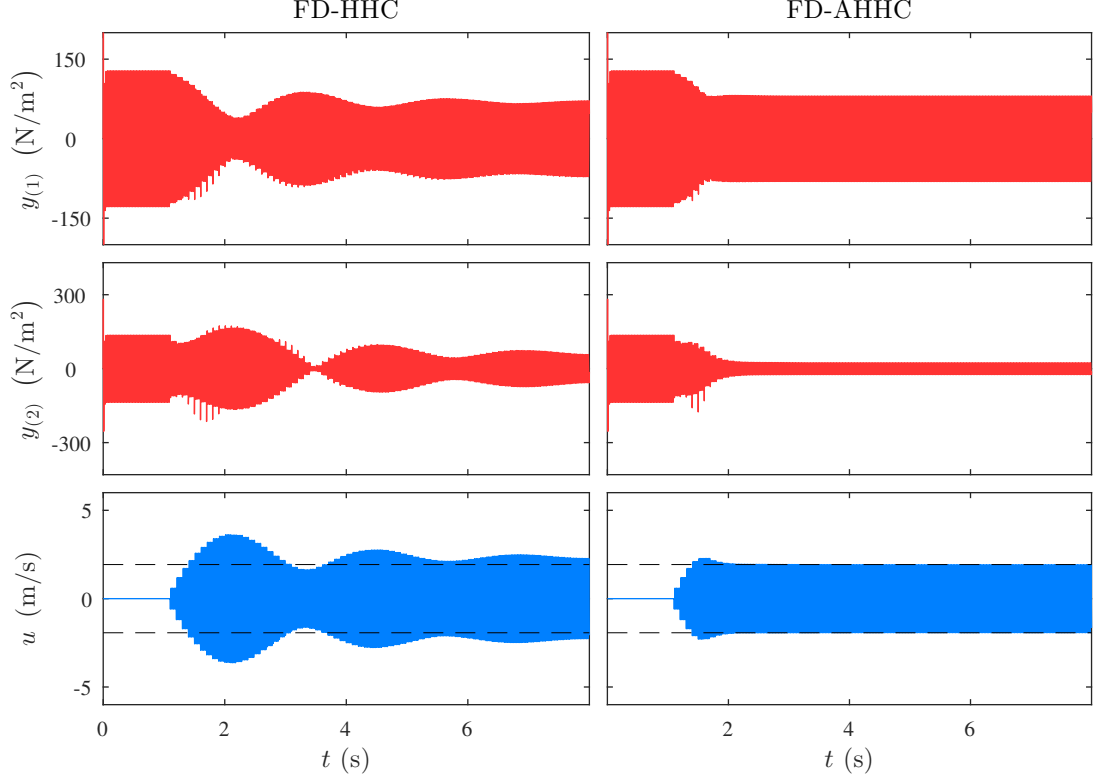


Figure 2.11: FD-HHC and FD-AHHC for a single-input two-output system that satisfies (2.14). Both FD-HHC and FD-AHHC minimize $\lim_{k \rightarrow \infty} \|y_k\|$. The dashed lines show $\pm|u_*|$.

Moreover, (2.6) and (2.8) imply that

$$\begin{aligned}
 J(u_*) &= \frac{1}{2}(u_*^* M_*^* M_* u_* + u_*^* M_*^* d_* + d_*^* M_* u_* + d_*^* d_*) \\
 &= \frac{1}{2} d_*^* (I_\ell - M_* (M_*^* M_*)^{-1} M_*^*) d_*.
 \end{aligned} \tag{2.32}$$

Let $\hat{u} \in \mathbb{C}^m \setminus \{u_*\}$, and it follows from (2.6), (2.8), and (2.32) that

$$\begin{aligned}
 J(\hat{u}) &= \frac{1}{2}(\hat{u}^* M_*^* M_* \hat{u} + 2\text{Re } \hat{u}^* M_*^* d_* + d_*^* d_*) - J(u_*) + J(u_*) \\
 &= \frac{1}{2}(\hat{u} - u_*)^* M_*^* M_* (\hat{u} - u_*) + J(u_*).
 \end{aligned} \tag{2.33}$$

Since $M_*^* M_*$ is positive definite, it follows that $(\hat{u} - u_*)^* M_*^* M_* (\hat{u} - u_*) > 0$. Thus, (2.33) implies that $J(\hat{u}) > J(u_*)$, which confirms *i*) and *ii*) .

To show *iii*), assume $\ell < m$ and let

$$u_* \in \{-M_*^* (M_* M_*^*)^{-1} d_* + (I_m - M_*^* (M_* M_*^*)^{-1} M_*) v : v \in \mathbb{C}^m\}.$$

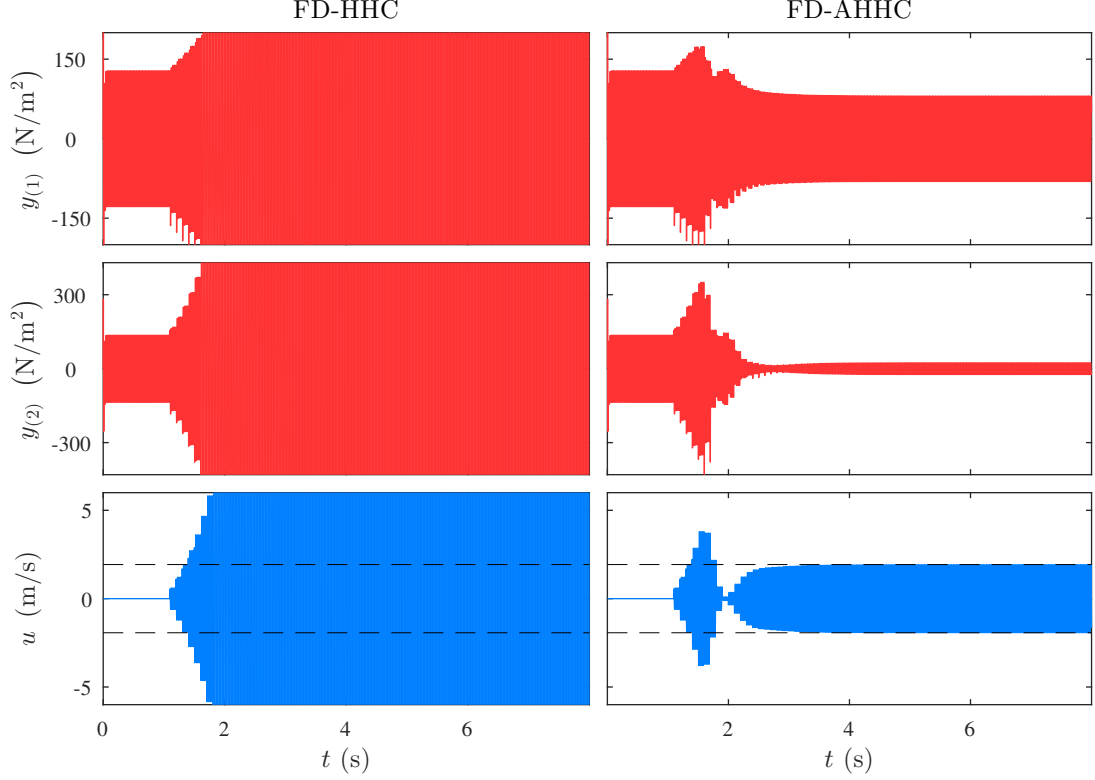


Figure 2.12: FD-HHC and FD-AHHC for a single-input two-output system that does not satisfy (2.14). The response y with FD-HHC diverges, whereas FD-AHHC minimizes $\lim_{k \rightarrow \infty} \|y_k\|$. The dashed lines show $\pm|u_*|$.

It follows from (2.6) that $\hat{y}_{\text{hss}}(u_*) = 0$. Moreover, it follows from (2.6) and (2.8) that

$$\begin{aligned}
J(u_*) &= \frac{1}{2}(u_*^* M_*^* M_* u_* + u_*^* M_*^* d_* + d_*^* M_* u_* + d_*^* d_*) \\
&= \frac{1}{2} \left([-d_*^* (M_* M_*^*)^{-1} M_* + v^* (I_m - M_*^* (M_* M_*^*)^{-1} M_*)] M_*^* M_* u_* \right. \\
&\quad \left. + 2\text{Re} [-d_*^* (M_* M_*^*)^{-1} M_* + v^* (I_m - M_*^* (M_* M_*^*)^{-1} M_*)] M_* d_* + d_*^* d_* \right) \\
&= 0,
\end{aligned}$$

which confirms *ii*). □

Proof of Theorem 2.2. To show *i*), assume $\ell > m$, and define

$$u_* \triangleq -(M_*^* M_*)^{-1} M_*^* d_*.$$

Define $\tilde{u}_k \triangleq u_k - u_*$. Subtracting u_* from both sides of (2.11) and using (2.10) yields

$$\begin{aligned}
\tilde{u}_{k+1} &= \tilde{u}_k - \rho M_e^* y_{k+1} \\
&= \tilde{u}_k - \rho M_e^* (M_* \tilde{u}_k + M_* u_* + d_*),
\end{aligned}$$

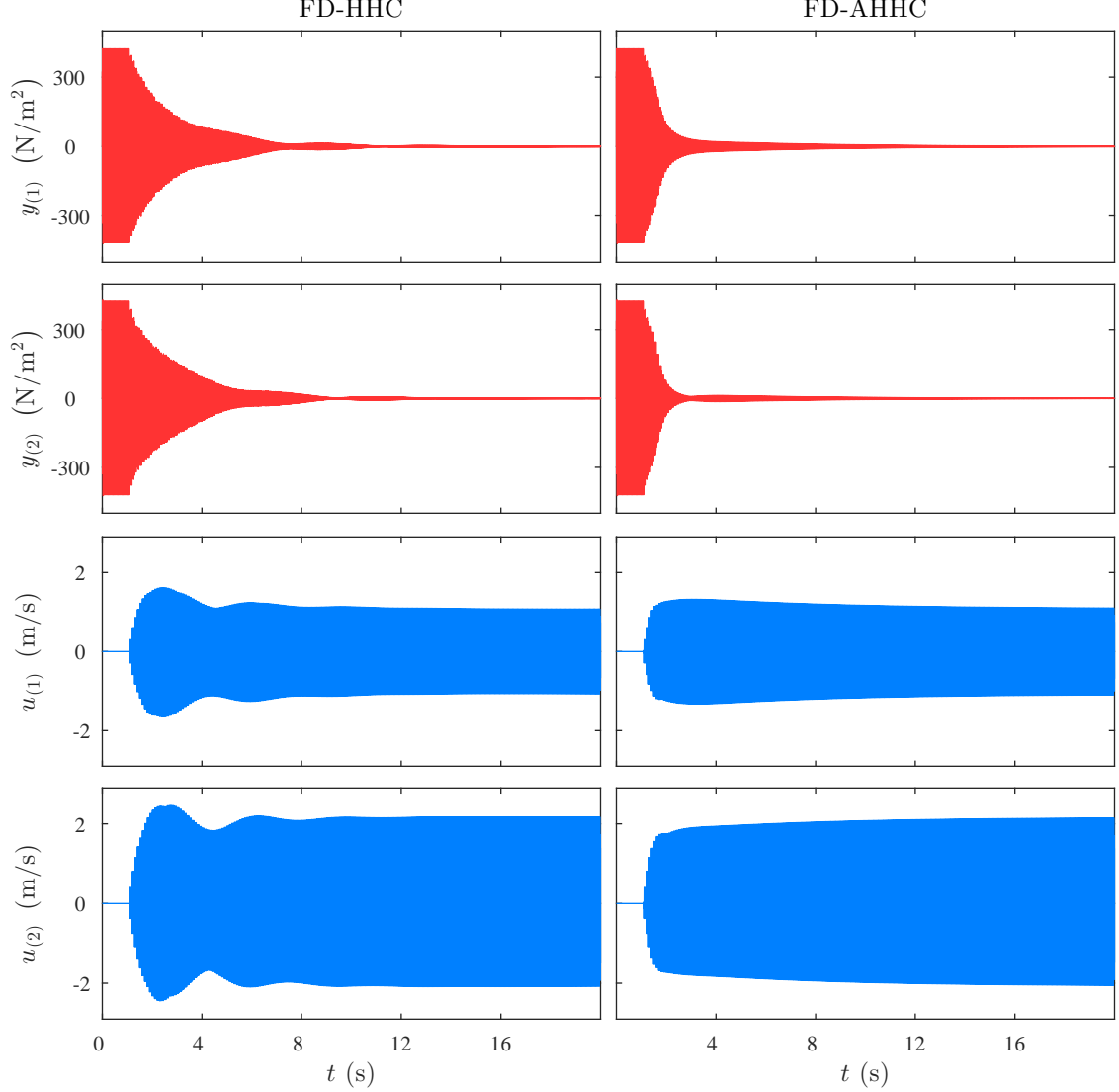


Figure 2.13: FD-HHC and FD-AHHC for a MIMO system that satisfies (2.14) with a 2-tone disturbance. Both FD-HHC and FD-AHHC yield $y(t) \rightarrow 0$ as $t \rightarrow \infty$.

which has the solution

$$\tilde{u}_k = A_1^k \tilde{u}_0 + \sum_{i=0}^{k-1} A_1^i [-\rho M_e^* (M_* u_* + d_*)], \quad (2.34)$$

where $A_1 \triangleq I_m - \rho M_e^* M_*$. Since $\Lambda \subset \text{ORHP}$ and $\ell > m$, it follows that $\text{spec}(M_e^* M_*) \subset \text{ORHP}$. Thus, (2.14) implies that $\text{spec}(\rho M_e^* M_*) \subset \{\lambda \in \mathbb{C} : \text{Re } \lambda \in (0, 2)\}$, which implies that $\text{spec}(A_1) \subset \text{OUD}$. Thus, $\sum_{i=0}^{\infty} A_1^i = (I_m - A_1)^{-1}$, and it follows from (2.34) that $\lim_{k \rightarrow \infty} \tilde{u}_k = (I_m - A_1)^{-1} [-\rho M_e^* (M_* u_* + d_*)] = -u_* - (M_e^* M_*)^{-1} M_e^* d_*$, which implies that $\lim_{k \rightarrow \infty} u_k = -(M_e^* M_*)^{-1} M_e^* d_*$. Therefore, (2.10) implies that $\lim_{k \rightarrow \infty} y_k = \lim_{k \rightarrow \infty} M_* u_k + d_* = [I_\ell - M_* (M_e^* M_*)^{-1} M_e^*] d_*$, which confirms *i*).

To show *ii*) and *iii*), assume $\ell \leq m$. It follows from (2.13) that $y_{k+1} = (I_\ell -$

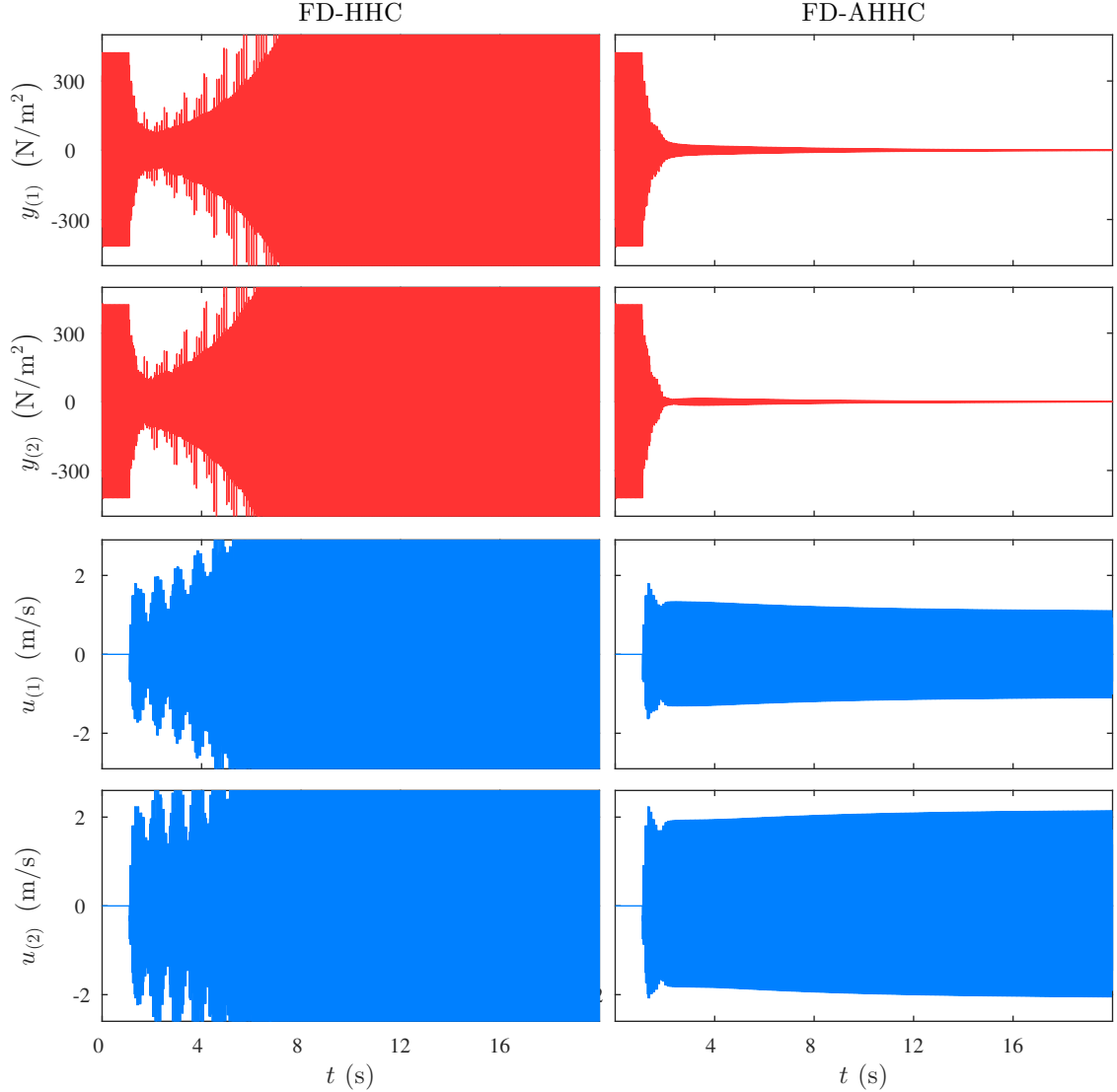


Figure 2.14: FD-HHC and FD-AHHC for a MIMO system that does not satisfy (2.14) with a 2-tone disturbance. The response y with FD-HHC diverges, whereas FD-AHHC yields $y(t) \rightarrow 0$ as $t \rightarrow \infty$.

$\rho M_* M_e^*) y_k$, which has the solution

$$y_k = A_2^{k-1} y_1, \quad (2.35)$$

where $A_2 = I_\ell - \rho M_* M_e^*$. Since $\Lambda \subset \text{ORHP}$ and $\ell \leq m$, it follows that $\text{spec}(M_e^* M_*) \subset \text{ORHP}$. Thus, (2.14) implies that $\text{spec}(\rho M_* M_e^*) \subset \{\lambda \in \mathbb{C} : \text{Re } \lambda \in (0, 2)\}$, which implies that $\text{spec}(A_2) \subset \text{OD}$. Therefore, (2.35) implies that $\lim_{k \rightarrow \infty} y_k = 0$. Next, it follows from (2.11) that

$$u_{k+1} = u_0 - \rho M_e^* \sum_{i=0}^k y_{i+1} \quad (2.36)$$

$$= u_0 - \rho M_e^* \sum_{i=0}^k A_2^i y_1. \quad (2.37)$$

Since $\text{spec}(A_2) \subset \text{OUD}$, it follows that $\sum_{i=0}^{\infty} A_2^i = (I_\ell - A_2)^{-1}$, which combined with (2.36) implies that $\lim_{k \rightarrow \infty} u_{k+1} = u_0 - \rho M_e^* (I_\ell - A_2)^{-1} y_1 = u_0 - M_e^* (M_* M_e^*)^{-1} y_1 = u_0 - M_e^* (M_* M_e^*)^{-1} (M_* u_0 + d_*)$, which confirms *ii*) and *iii*). \square

2.12 Proofs of Proposition 2.1 and Theorems 2.3 and 2.4

Proof of Proposition 2.1. Define $\tilde{M}_k \triangleq M_k - M_*$, and it follows from (2.22) that

$$\tilde{M}_k = \tilde{M}_{k-1} (I_m - \Lambda_k), \quad (2.38)$$

where

$$\Lambda_k \triangleq \frac{\gamma}{\nu_2 + \|M_{k-1}^* y_k\|^2} M_{k-1}^* y_k y_k^* M_{k-1}.$$

Define the Lyapunov-like function $V_M(\tilde{M}_k) \triangleq \|\tilde{M}_k\|_F^2$, and the Lyapunov-like difference $\Delta V_M(k) \triangleq V_M(\tilde{M}_k) - V_M(\tilde{M}_{k-1})$. Evaluating ΔV_M along the trajectories of (2.38) yields

$$\begin{aligned} \Delta V_M(k) &= -\text{tr} \left(\tilde{M}_{k-1}^* \tilde{M}_{k-1} \Lambda_k + \Lambda_k \tilde{M}_{k-1}^* \tilde{M}_{k-1} - \Lambda_k \tilde{M}_{k-1}^* \tilde{M}_{k-1} \Lambda_k \right) \\ &= -\text{tr} \left(2 \tilde{M}_{k-1} \Lambda_k \tilde{M}_{k-1}^* - \tilde{M}_{k-1} \Lambda_k \Lambda_k \tilde{M}_{k-1}^* \right). \end{aligned} \quad (2.39)$$

Next, note that

$$\begin{aligned} \Lambda_k \Lambda_k &= \gamma^2 \frac{M_{k-1}^* y_k y_k^* M_{k-1} M_{k-1}^* y_k y_k^* M_{k-1}}{(\nu_2 + y_k^* M_{k-1} M_{k-1}^* y_k)^2} \\ &= \gamma \frac{y_k^* M_{k-1} M_{k-1}^* y_k}{\nu_2 + y_k^* M_{k-1} M_{k-1}^* y_k} \Lambda_k \\ &\leq \gamma \Lambda_k. \end{aligned} \quad (2.40)$$

Since $\gamma \in (0, 1]$, it follows from (2.39) and (2.40) that

$$\begin{aligned} \Delta V_M(k) &\leq -\text{tr} \left(2 \tilde{M}_{k-1} \Lambda_k \tilde{M}_{k-1}^* - \gamma \tilde{M}_{k-1} \Lambda_k \tilde{M}_{k-1}^* \right) \\ &= -(2 - \gamma) \text{tr} \tilde{M}_{k-1} \Lambda_k \tilde{M}_{k-1}^* \\ &\leq -\frac{\gamma \|\tilde{M}_{k-1} M_{k-1}^* y_k\|^2}{\nu_2 + \|M_{k-1}^* y_k\|^2}, \end{aligned}$$

which confirms (2.23). Since ΔV_M is nonpositive, it follows that for all $k \in \mathbb{N}$, $\|\tilde{M}_k\|_F^2 \leq \|\tilde{M}_0\|_F^2$, which implies that M_k is bounded. \square

Proof of Theorem 2.3. Define $\tilde{M}_k \triangleq M_k - M_*$, $V_M(\tilde{M}_k) \triangleq \|\tilde{M}_k\|_F^2$, and

$\Delta V_M(k) \triangleq V_M(\tilde{M}_k) - V_M(\tilde{M}_{k-1})$. It follows from Proposition 1 that for all $k \in \mathbb{N}$,

$$\Delta V_M(k) \leq -\frac{\gamma \|\tilde{M}_{k-1} M_{k-1}^* y_k\|^2}{\nu_2 + \|M_{k-1}^* y_k\|^2}. \quad (2.41)$$

Next, define $V_y(y_k) \triangleq \|y_k\|^2$ and $\Delta V_y(k) \triangleq V_y(y_{k+1}) - V_y(y_k)$. Evaluating ΔV_y along the trajectories of (2.21) yields

$$\begin{aligned} \Delta V_y(k) &= -\frac{\mu y_k^* M_* M_{k-1}^* y_k}{\nu_1 + \|M_{k-1}\|_F^2} - \frac{\mu y_k^* M_{k-1} M_*^* y_k}{\nu_1 + \|M_{k-1}\|_F^2} + \frac{\mu^2 \|M_* M_{k-1}^* y_k\|^2}{(\nu_1 + \|M_{k-1}\|_F^2)^2} \\ &= -\frac{\mu y_k^* (M_* M_{k-1}^* + M_{k-1} M_*^*) y_k}{\nu_1 + \|M_{k-1}\|_F^2} + \frac{\mu^2 \|M_* M_{k-1}^* y_k\|^2}{(\nu_1 + \|M_{k-1}\|_F^2)^2}. \end{aligned} \quad (2.42)$$

Define the Lyapunov function

$$V(y_k, \tilde{M}_{k-1}) \triangleq \ln\left(1 + \frac{\nu_1}{\nu_2} V_y(y_k)\right) + a V_M(\tilde{M}_{k-1}), \quad (2.43)$$

where $a > 0$ is provided later, and define the Lyapunov difference

$$\Delta V(k) \triangleq V(y_{k+1}, \tilde{M}_k) - V(y_k, \tilde{M}_{k-1}). \quad (2.44)$$

Evaluating $\Delta V(k)$ along the trajectories of (2.21) and (2.22) yields

$$\begin{aligned} \Delta V(k) &= \ln\left[1 + \frac{\nu_1}{\nu_2} (V_y(y_k) + \Delta V_y(k))\right] - \ln\left[1 + \frac{\nu_1}{\nu_2} V_y(y_k)\right] + a \Delta V_M(k) \\ &= \ln\left(1 + \frac{\nu_1 \Delta V_y(k)}{\nu_2 + \nu_1 V_y(y_k)}\right) + a \Delta V_M(k). \end{aligned} \quad (2.45)$$

Since for all $x > 0$, $\ln x \leq x - 1$, (2.45) implies that

$$\Delta V(k) \leq \frac{\nu_1 \Delta V_y(k)}{\nu_2 + \nu_1 V_y(y_k)} + a \Delta V_M(k),$$

and substituting (2.41) yields

$$\begin{aligned} \Delta V(k) &\leq \frac{\nu_1 \Delta V_y(k)}{\nu_2 + \nu_1 V_y(y_k)} - \frac{a \gamma \|\tilde{M}_{k-1} M_{k-1}^* y_k\|^2}{\nu_2 + \|M_{k-1}^* y_k\|^2} \\ &= \frac{\nu_1 \Delta V_y(k)}{\nu_2 + \nu_1 V_y(y_k)} - \frac{a \gamma \|M_{k-1} M_{k-1}^{-1} \tilde{M}_{k-1} M_{k-1}^* y_k\|^2}{\nu_2 + \|M_{k-1}^* y_k\|^2} \\ &\leq \frac{\nu_1 \Delta V_y(k)}{\nu_2 + \nu_1 V_y(y_k)} - \frac{a \gamma \lambda_{\min}(M_{k-1}^* M_{k-1}) \|M_{k-1}^{-1} \tilde{M}_{k-1} M_{k-1}^* y_k\|^2}{\nu_2 + \|M_{k-1}\|_F^2 \|y_k\|^2}. \end{aligned} \quad (2.46)$$

To show *iii*), assume there exist $\varepsilon > 0$ and $k_s \geq 0$ such that for all $k \geq k_s$,

$\lambda_{\min}(M_k^* M_k) \geq \varepsilon$. Thus, it follows from (2.46) that for all $k > k_s$,

$$\begin{aligned}
\Delta V(k) &\leq \frac{\nu_1 \Delta V_y(k)}{\nu_2 + \nu_1 V_y(y_k)} - \frac{a\gamma\varepsilon \|M_{k-1}^{-1} \tilde{M}_{k-1} M_{k-1}^* y_k\|^2}{\nu_2 + \|M_{k-1}\|_{\mathbb{F}}^2 \|y_k\|^2} \\
&\leq \frac{\nu_1 \Delta V_y(k)}{\nu_2 + \nu_1 V_y(y_k)} - \frac{a\gamma\varepsilon y_k^* M_{k-1} (M_{k-1} - M_*)^* M_{k-1}^{-*} M_{k-1}^{-1} (M_{k-1} - M_*) M_{k-1}^* y_k}{\nu_2 + \|M_{k-1}\|_{\mathbb{F}}^2 \|y_k\|^2 + \frac{\nu_2}{\nu_1} \|M_{k-1}\|_{\mathbb{F}}^2 + \nu_1 \|y_k\|^2} \\
&= \frac{\nu_1 \Delta V_y(k)}{\nu_2 + \nu_1 V_y(y_k)} - \frac{a\gamma\varepsilon y_k^* (M_{k-1} - M_{k-1} M_*^* M_{k-1}^{-*}) (M_{k-1}^* - M_{k-1}^{-1} M_* M_{k-1}^*) y_k}{\nu_2 + \|M_{k-1}\|_{\mathbb{F}}^2 \|y_k\|^2 + \frac{\nu_2}{\nu_1} \|M_{k-1}\|_{\mathbb{F}}^2 + \nu_1 \|y_k\|^2} \\
&= \frac{\nu_1 \Delta V_y(k)}{\nu_2 + \nu_1 V_y(y_k)} + \frac{a\nu_1 \gamma \varepsilon y_k^* (M_* M_{k-1}^* + M_{k-1} M_*^*) y_k}{(\nu_2 + \nu_1 \|y_k\|^2)(\nu_1 + \|M_{k-1}\|_{\mathbb{F}}^2)} \\
&\quad - \frac{a\nu_1 \gamma \varepsilon y_k^* (M_{k-1} M_{k-1}^* + M_{k-1} M_*^* M_{k-1}^{-*} M_{k-1}^{-1} M_* M_{k-1}^*) y_k}{(\nu_2 + \nu_1 \|y_k\|^2)(\nu_1 + \|M_{k-1}\|_{\mathbb{F}}^2)}. \tag{2.47}
\end{aligned}$$

Substituting (2.42) into (2.47) yields

$$\begin{aligned}
\Delta V(k) &\leq -\frac{\nu_1 \mu y_k^* (M_* M_{k-1}^* + M_{k-1} M_*^*) y_k}{(\nu_2 + \nu_1 \|y_k\|^2)(\nu_1 + \|M_{k-1}\|_{\mathbb{F}}^2)} + \frac{\nu_1 \mu^2 \|M_* M_{k-1}^* y_k\|^2}{(\nu_2 + \nu_1 \|y_k\|^2)(\nu_1 + \|M_{k-1}\|_{\mathbb{F}}^2)^2} \\
&\quad + \frac{a\nu_1 \gamma \varepsilon y_k^* (M_* M_{k-1}^* + M_{k-1} M_*^*) y_k}{(\nu_2 + \nu_1 \|y_k\|^2)(\nu_1 + \|M_{k-1}\|_{\mathbb{F}}^2)} \\
&\quad - \frac{a\nu_1 \gamma \varepsilon (\|M_{k-1}^* y_k\|^2 + \|M_{k-1}^{-1} M_* M_{k-1}^* y_k\|^2)}{(\nu_2 + \nu_1 \|y_k\|^2)(\nu_1 + \|M_{k-1}\|_{\mathbb{F}}^2)}. \tag{2.48}
\end{aligned}$$

Let $a \triangleq \frac{\mu}{\gamma\varepsilon}$, and it follows from (2.48) that

$$\begin{aligned}
\Delta V(k) &\leq \frac{\nu_1 \mu^2 \|M_* M_{k-1}^* y_k\|^2}{(\nu_2 + \nu_1 \|y_k\|^2)(\nu_1 + \|M_{k-1}\|_{\mathbb{F}}^2)^2} - \frac{\nu_1 \mu (\|M_{k-1}^* y_k\|^2 + \|M_{k-1}^{-1} M_* M_{k-1}^* y_k\|^2)}{(\nu_2 + \nu_1 \|y_k\|^2)(\nu_1 + \|M_{k-1}\|_{\mathbb{F}}^2)} \\
&\leq \frac{\nu_1 \mu^2 \|M_* M_{k-1}^* y_k\|^2}{(\nu_2 + \nu_1 \|y_k\|^2)(\nu_1 + \|M_{k-1}\|_{\mathbb{F}}^2)^2} - \frac{\nu_1 \mu \|M_{k-1}^* y_k\|^2}{(\nu_2 + \nu_1 \|y_k\|^2)(\nu_1 + \|M_{k-1}\|_{\mathbb{F}}^2)} \\
&\quad - \frac{\nu_1 \mu \|M_{k-1}\|_{\mathbb{F}}^2 \|M_{k-1}^{-1} M_* M_{k-1}^* y_k\|^2}{(\nu_2 + \nu_1 \|y_k\|^2)(\nu_1 + \|M_{k-1}\|_{\mathbb{F}}^2)^2} \\
&\leq -\frac{\nu_1 \mu \|M_{k-1}^* y_k\|^2}{(\nu_2 + \nu_1 \|y_k\|^2)(\nu_1 + \|M_{k-1}\|_{\mathbb{F}}^2)} \\
&\leq -\frac{\nu_1 \mu \varepsilon \|y_k\|^2}{(\nu_2 + \nu_1 \|y_k\|^2)(\nu_1 + \|M_{k-1}\|_{\mathbb{F}}^2)}. \tag{2.49}
\end{aligned}$$

Proposition 1 implies that for all $k \in \mathbb{Z}^+$, $\|\tilde{M}_{k-1}\|_{\mathbb{F}} \leq \|\tilde{M}_0\|_{\mathbb{F}}$. Thus, for all $k \in \mathbb{Z}^+$,

$$\|M_{k-1}\|_{\mathbb{F}}^2 = \|\tilde{M}_{k-1} + M_*\|_{\mathbb{F}}^2 \leq (\|\tilde{M}_{k-1}\|_{\mathbb{F}} + \|M_*\|_{\mathbb{F}})^2 \leq (\|\tilde{M}_0\|_{\mathbb{F}} + \|M_*\|_{\mathbb{F}})^2. \tag{2.50}$$

Thus, using (2.50), it follows from (2.49) that

$$\Delta V(k) \leq -\frac{c_1 \|y_k\|^2}{\nu_2 + \nu_1 \|y_k\|^2}, \quad (2.51)$$

where $c_1 \triangleq \frac{\nu_1 \mu \varepsilon}{\nu_1 + (\|\tilde{M}_0\|_{\mathbb{F}} + \|M_*\|_{\mathbb{F}})^2} > 0$. Since $V(y_k, \tilde{M}_{k-1})$ is positive definite, and, for all $k \in \mathbb{N}$, $\Delta V(k)$ is nonpositive, it follows from (2.44) and (2.51) that $0 \leq \lim_{k \rightarrow \infty} \sum_{i=1}^k \frac{c_1 \|y_i\|^2}{\nu_2 + \nu_1 \|y_i\|^2} \leq -\lim_{k \rightarrow \infty} \sum_{i=1}^k \Delta V(i) = V(y_1, \tilde{M}_0) - \lim_{k \rightarrow \infty} V(y_k, \tilde{M}_{k-1}) \leq V(y_1, \tilde{M}_0)$, where the upper and lower bounds imply that all the limits exist. Thus, $\lim_{k \rightarrow \infty} \frac{c_1 \|y_k\|^2}{\nu_2 + \nu_1 \|y_k\|^2} = 0$, which implies that $\lim_{k \rightarrow \infty} y_k = 0$. Furthermore, it follows from (2.10) that $\lim_{k \rightarrow \infty} u_k = \lim_{k \rightarrow \infty} M_*^{-1}(y_{k+1} - d_*) = u_*$, which confirms *iii*).

To show *ii*), note that $\text{rank } M_* = \ell$. Thus, there exist $r > 0$ and $\varepsilon_1 > 0$ such that for all $M \in \mathbb{B}_r(M_*)$, $\lambda_{\min}(M^*M) \geq \varepsilon_1$. Assume that $M_0 \in \mathbb{B}_r(M_*)$, which implies that $(y_1, \tilde{M}_0) \in \mathcal{D} \triangleq \mathbb{C}^\ell \times \mathbb{B}_r(0)$. Since Proposition 1 implies that ΔV_M is nonpositive, it follows that for all $k \in \mathbb{N}$, $(y_{k+1}, \tilde{M}_k) \in \mathcal{D}$, which implies that for all $k \in \mathbb{N}$, $M_k \in \mathbb{B}_r(M_*)$. Therefore, for all $k \in \mathbb{N}$, $\lambda_{\min}(M_k^*M_k) \geq \varepsilon_1$. Thus, *iii*) implies that $\lim_{k \rightarrow \infty} u_k = u_*$ and $\lim_{k \rightarrow \infty} y_k = 0$, which confirms *ii*).

To show *i*), assume that $(y_1, \tilde{M}_0) \in \mathcal{D}$, which implies that for all $k \in \mathbb{N}$,

$$\lambda_{\min}(M_k^*M_k) \geq \varepsilon_1.$$

Thus, it follows from (2.46) that for all $k \in \mathbb{N}$,

$$\Delta V(k) \leq \frac{\nu_1 \Delta V_y(k)}{\nu_2 + \nu_1 V_y(y_k)} - \frac{a\gamma\varepsilon_1 \|M_{k-1}^{-1} \tilde{M}_{k-1} M_{k-1}^* y_k\|^2}{\nu_2 + \|M_{k-1}\|_{\mathbb{F}}^2 \|y_k\|^2}.$$

Next, using the same process as in (2.47)–(2.51) with ε replaced by ε_1 , we obtain $\Delta V(k) \leq -c_1 \|y_k\|^2 / (\nu_2 + \nu_1 \|y_k\|^2)$, which is nonpositive. Thus, the equilibrium $(y_k, M_{k-1}) \equiv (0, M_*)$ is Lyapunov stable. \square

Proof of Theorem 2.4. It follows from part *i*) of Theorem 3 that $(y_k, M_{k-1}) \equiv (0, M_*)$ is a Lyapunov stable equilibrium of (2.21) and (2.22). Moreover, it follows from Proposition 1 that M_k is bounded.

To show convergence of y_k and u_k , let $M_0 \in \mathcal{M} \setminus \{0\}$, and define

$$\varepsilon \triangleq \begin{cases} |M_*|^2, & \text{if } M_0 = M_*, \\ |\text{Im } \tilde{M}_0 M_*^*|^2 / |\tilde{M}_0|^2, & \text{if } M_0 \neq M_*. \end{cases} \quad (2.52)$$

First, assume $M_0 = M_*$, and it follows from Proposition 1 that for all $k \in \mathbb{N}$, $M_k = M_*$. In this case, for all $k \in \mathbb{N}$, $|M_k|^2 = \varepsilon$.

Next, assume $M_0 \neq M_*$. Since $M_0 \in \mathcal{M} \setminus \{0\}$, it follows that, $|\angle M_* - \angle M_0| \neq \pi$, which implies that $|\angle(M_0/M_*)| \neq \pi$. Thus, $\text{Im}(M_0/M_*) \neq 0$, which implies that $\text{Im } \tilde{M}_0 M_*^* = \text{Im}(\tilde{M}_0 M_*^* + M_* M_*^*) = \text{Im } M_0 M_*^* = |M_*|^2 \text{Im} \frac{M_0}{M_*} \neq 0$, and it follows

from (2.52) that $\varepsilon > 0$. Next, it follows from (2.22) that

$$\tilde{M}_k = \left(1 - \frac{\gamma |M_{k-1}|^2 |y_k|^2}{\nu_2 + |M_{k-1}|^2 |y_k|^2}\right) \tilde{M}_{k-1},$$

which has the solution $\tilde{M}_k = \beta_k \tilde{M}_0$, where $\beta_k \triangleq \prod_{i=0}^{k-1} \left(1 - \frac{\gamma |M_i|^2 |y_{i+1}|^2}{\nu_2 + |M_i|^2 |y_{i+1}|^2}\right)$. Thus, for all $k \in \mathbb{Z}^+$, $|M_k|^2 = |\tilde{M}_k + M_*|^2 = |\tilde{M}_0 \beta_k + M_*|^2 = |\tilde{M}_0|^2 \beta_k^2 + 2(\operatorname{Re} \tilde{M}_0 M_*^*) \beta_k + |M_*|^2$. Since $f(x) \triangleq |\tilde{M}_0|^2 x^2 + 2(\operatorname{Re} \tilde{M}_0 M_*^*) x + |M_*|^2$ is quadratic and positive definite in x , it follows that f is minimized at $-(\operatorname{Re} \tilde{M}_0 M_*^*)/|\tilde{M}_0|^2$. Thus, for all $k \in \mathbb{N}$,

$$|M_k|^2 \geq \frac{|M_*|^2 |\tilde{M}_0|^2 - (\operatorname{Re} \tilde{M}_0 M_*^*)^2}{|\tilde{M}_0|^2} = \varepsilon.$$

Thus, for all $k \in \mathbb{N}$, $\lambda_{\min}(M_k^* M_k) = |M_k|^2 \geq \varepsilon$, and it follows from part *ii*) of Theorem 2.3 that $\lim_{k \rightarrow \infty} u_k = u_*$ and $\lim_{k \rightarrow \infty} y_k = 0$. \square

Chapter 3

Time-Domain Adaptive Higher Harmonic Control

We present two time-domain feedback control algorithms for rejection of known-frequency sinusoidal disturbances that act on an asymptotically stable linear time-invariant (LTI) system. The first algorithm is time-domain higher harmonic control (TD-HHC), which is effective for uncertain LTI systems. However, TD-HHC requires an estimate of the control-to-performance transfer function evaluated at the disturbance frequencies. The second algorithm is time-domain adaptive higher harmonic control (TD-AHHC), which is effective for completely unknown LTI systems. We analyze the stability and performance of TD-HHC and TD-AHHC. For both TD-HHC and TD-AHHC, we show that the controller asymptotically rejects the disturbance. We present numerical simulations comparing TD-HHC and TD-AHHC with frequency-domain higher-harmonic control (FD-HHC), which is an existing sinusoidal disturbance rejection method in the frequency domain. We also present results from an active disturbance rejection experiment in an acoustic environment. These experimental results demonstrate the practical effectiveness of both TD-HHC and TD-AHHC.

3.1 Introduction

The problem of sinusoidal disturbance rejection arises in a variety of engineering applications, including active noise cancellation [32], vibration suppression [10, 156], and active rotor balancing [20]. If an accurate model of the system is known, then the internal-model principle [116, 117, 119, 204] can be used to design a feedback controller capable of rejecting sinusoidal disturbances with known frequencies. If an accurate system model is not known, but the open-loop dynamics are asymptotically stable, then adaptive feedforward cancellation can be employed [129–131, 205]. These approaches use a harmonic regressor consisting of sinusoids at the known disturbance frequencies. The control is generated by updating the amplitudes and phases of these sinusoids in a manner that achieves asymptotic disturbance rejection. However, these approaches

require certain model information or assumptions regarding the open-loop system. For single-input single-output (SISO) systems, the only model information required is the sign of the control-to-performance transfer function at the disturbance frequencies. For multi-input multi-output (MIMO) systems, stronger assumptions (e.g., strict positive realness) are typically required. Adaptive feedforward methods for rejecting sinusoids with unknown frequency include [139]. Feedback (rather than feedforward) adaptive control methods are also capable of rejecting sinusoids of known or even unknown frequencies (e.g., [140, 141, 148, 206]); however, these approaches generally rely on some model information (e.g., relative degree) and structural assumptions regarding the system (e.g., minimum phase, or state feedback).

Another approach to sinusoidal disturbance rejection relies on an asymptotically stable linear time-invariant (LTI) system’s harmonic steady-state (HSS) response, that is, the residual sinusoidal response that remains after the transient response decays to zero. This approach was developed independently in [10, 20, 32, 156], and is known variously as convergent control (for active rotor balancing) and higher-harmonic control (for helicopter vibration reduction). In this chapter, we adopt the name frequency-domain higher-harmonic control (FD-HHC).

To explain FD-HHC, consider an LTI system acted on by a sinusoidal disturbance with known frequency ω . The FD-HHC control signal is a sinusoid with frequency ω , but where the amplitude and phase are updated at discrete times. All control computations are performed using discrete Fourier transform (DFT) data. Let $T_s > 0$ denote the FD-HHC update period. Then, at each time step $k \in \mathbb{N}$, the control amplitudes and phases are updated using DFT data, which is computed from a sampling of the performance measurement over the time interval $[(k - 1)T_s, kT_s]$. FD-HHC relies on the key assumption that the update period T_s is sufficiently large relative to the settling time of the system. This assumption ensures that by the end of each time interval between control updates, the closed-loop response approximates the HSS response. If T_s is too small, then the HSS approximation is not accurate, and the closed-loop system can become unstable. In practice, T_s can be increased to achieve closed-loop stability; however, increasing T_s also increases convergence time. In fact, large convergence time is one shortcoming of FD-HHC [81].

To address this shortcoming, we present time-domain higher harmonic control (TD-HHC), which is effective for rejection of known-frequency sinusoids that act on an LTI system with at least as many controls as performance measurements. The main analytic result on TD-HHC shows that the controller asymptotically rejects the disturbance. In contrast to FD-HHC, TD-HHC does not require DFT computations. We present numerical simulations that demonstrate that TD-HHC can be implemented at faster sample rates than FD-HHC without destabilizing the closed-loop system. These faster sample rates can significantly reduce convergence time.

Another potential drawback of FD-HHC is that it requires an estimate of the control-to-performance transfer function evaluated at the disturbance frequency. Note that TD-HHC also requires this estimate. In the SISO case, this estimate must have an angle within 90° of the actual value for closed-loop stability. In the MIMO case, closed-loop stability is ensured provided that the estimate is sufficiently accurate. If there are multiple disturbance frequencies, then estimates are required at each fre-

quency. For certain applications, this transfer function can be difficult to estimate or subject to change. To address uncertainty, adaptive methods based on HSS response have been proposed [81, 157, 158]. However, the methods in [81, 157] require an external excitation signal to ensure stability, and the analysis in [158] is restricted to an averaged system. In Chapter 2, we presented FD-AHHC algorithm with stability properties that do not require external excitation signals. However, FD-AHHC (similar to FD-HHC) is a frequency-domain method and thus may have a large convergence time.

Therefore, we extend TD-HHC to address model uncertainty. The resulting algorithm is time-domain adaptive higher harmonic control (TD-AHHC), which is effective for rejection of known-frequency sinusoids that act on a completely unknown LTI system with at least as many controls as performance measurements. The main analytic result on TD-AHHC shows that the controller asymptotically rejects the disturbance. We also demonstrate the effectiveness of both TD-HHC and TD-AHHC using active disturbance rejection experiments in an acoustic environment. These experiments show that the TD-HHC and TD-AHHC can effectively reject single-tone and multi-tone sinusoidal disturbances acting on unknown MIMO systems.

3.2 Notation

Let \mathbb{F} be either \mathbb{R} or \mathbb{C} . Let $x_{(i)}$ denote the i th element of $x \in \mathbb{F}^n$. Let $\|\cdot\|$ be the 2-norm on \mathbb{F}^n . Next, let A^* denote the complex conjugate transpose of $A \in \mathbb{F}^{m \times n}$, and define $\|A\|_F \triangleq \sqrt{\text{tr } A^*A}$, which is the Frobenius norm of $A \in \mathbb{F}^{m \times n}$. Let $j \in \mathbb{C}$ denote the imaginary number, and let $\angle \lambda$ denote the argument of $\lambda \in \mathbb{C}$ defined on the interval $(-\pi, \pi]$ rad. Let ORHP and OUD denote the open-left-half plane and open unit disk in \mathbb{C} , respectively.

Let $\text{spec}(A) \triangleq \{\lambda \in \mathbb{C} : \det(\lambda I - A) = 0\}$ denote the spectrum of $A \in \mathbb{F}^{n \times n}$. Let $\lambda_{\min}(A)$ denote the minimum eigenvalue of the symmetric positive-semidefinite matrix $A \in \mathbb{F}^{n \times n}$. Let $\sigma_{\max}(A)$ denote the maximum singular value of $A \in \mathbb{F}^{m \times n}$, and let $\text{sprad}(A) \triangleq \max_{\lambda \in \text{spec}(A)} |\lambda|$ denote the spectral radius of $A \in \mathbb{F}^{n \times n}$. The Moore-Penrose generalized inverse [207, Chap. 6.1] of $A \in \mathbb{R}^{m \times n}$ is denoted by $A^+ \in \mathbb{R}^{n \times m}$. Note that if $A \in \mathbb{R}^{m \times n}$ is right invertible (i.e., $\text{rank } A = m$), then $A^+ = A^T(AA^T)^{-1}$.

Define $\mathbb{N} \triangleq \{0, 1, 2, 3, \dots\}$ and $\mathbb{Z}^+ \triangleq \mathbb{N} \setminus \{0\}$. Define the *open ball of radius $r > 0$ centered at $C \in \mathbb{C}^{m \times n}$* by $\mathbb{B}_r(C) \triangleq \{X \in \mathbb{C}^{m \times n} : \|X - C\|_F < r\}$.

3.3 Problem Formulation

Consider the LTI system

$$\dot{x}(t) = Ax(t) + Bu(t) + D_1d(t), \quad (3.1)$$

$$y(t) = Cx(t) + Du(t) + D_2d(t), \quad (3.2)$$

where $t \geq 0$, $x(t) \in \mathbb{R}^n$ is the state, $x(0) = x_0 \in \mathbb{R}^n$ is the initial condition, $u(t) \in \mathbb{R}^m$ is the control, $y(t) \in \mathbb{R}^\ell$ is the measured performance, $d(t) \in \mathbb{R}^{\ell_d}$ is the unmeasured

disturbance, and $A \in \mathbb{R}^{n \times n}$ is asymptotically stable. Define $G_{yu} : \mathbb{C} \rightarrow \mathbb{C}^{\ell \times m}$ and $G_{yd} : \mathbb{C} \rightarrow \mathbb{C}^{\ell \times \ell_d}$ by

$$\begin{aligned} G_{yu}(s) &\triangleq C(sI - A)^{-1}B + D, \\ G_{yd}(s) &\triangleq C(sI - A)^{-1}D_1 + D_2, \end{aligned}$$

which are the transfer functions from u to y , and from d to y . Let $\omega_1, \omega_2, \dots, \omega_q > 0$, and consider the sinusoidal disturbance

$$d(t) = \sum_{i=1}^q d_{c,i} \cos \omega_i t + d_{s,i} \sin \omega_i t, \quad (3.3)$$

where $d_{c,1}, \dots, d_{c,q}, d_{s,1}, \dots, d_{s,q} \in \mathbb{R}^{\ell_d}$.

Our objective is to design a feedback control u that eliminates the effect of the disturbance d on the performance y . We seek to design a control that requires limited (i.e., for TD-HHC) or no (i.e., for TD-AHHC) model information regarding (3.1) and (3.2), and requires knowledge of only the disturbance frequencies $\omega_1, \omega_2, \dots, \omega_q > 0$. Thus, the disturbance amplitudes $d_{c,1}, \dots, d_{c,q}, d_{s,1}, \dots, d_{s,q}$, and the system model A, B, C, D, D_1 , and D_2 are unknown.

Unless otherwise stated, all statements in this chapter that involve the subscript i are for all $i \in Q \triangleq \{1, 2, \dots, q\}$.

In this chapter, we consider a sinusoidal control with frequencies ω_i but where the amplitudes and phases are updated in discrete time. Let $T_s > 0$ be the update period. Then, for each $k \in \mathbb{N}$ and for all $t \in [kT_s, (k+1)T_s)$, the control is

$$u(t) = \sum_{i=1}^q (f_i^T(t) \otimes I_m) u_{i,k}, \quad (3.4)$$

where $u_{i,k} \in \mathbb{R}^{2m}$ is determined from update equations for TD-HHC or TD-AHHC presented in Sections 3.5 and 3.7, respectively. Note that, the control (3.4) is a piecewise-continuous sinusoid.

3.4 Mathematical Preliminaries

We present some assumptions, definitions, and results that we use in this chapter. We make the following assumption:

$$(A3.1) \quad G_{yu}(j\omega_i) \text{ has full row rank, that is, } \text{rank } G_{yu}(j\omega_i) = \ell.$$

Assumption (A3.1) implies that the number of actuators is at least as large as the number of performance measurements, that is, $m \geq \ell$. This assumption is required to ensure that there exists a control u such that the performance y tends to zero asymptotically.

For the moment, assume that $d_{c,i}$, $d_{s,i}$, $G_{yu}(j\omega_i)$, and $G_{yd}(j\omega_i)$ are known. Let $u_{c,i}, u_{s,i} \in \mathbb{R}^m$, and consider the control

$$\begin{aligned} u(t) &= \sum_{i=1}^q u_{c,i} \cos \omega_i t + u_{s,i} \sin \omega_i t \\ &= \sum_{i=1}^q (f_i^T(t) \otimes I_m) \hat{u}_i, \end{aligned} \quad (3.5)$$

where

$$\hat{u}_i \triangleq \begin{bmatrix} u_{c,i} \\ u_{s,i} \end{bmatrix} \in \mathbb{R}^{2m}, \quad f_i(t) \triangleq \begin{bmatrix} \cos \omega_i t \\ \sin \omega_i t \end{bmatrix} \in \mathbb{R}^2.$$

The harmonic steady-state (HSS) performance of (3.1) and (3.2) with disturbance (3.3) and control (3.5) is defined by

$$\begin{aligned} y_{\text{hss}}(t, \hat{u}_1, \dots, \hat{u}_q) &\triangleq \sum_{i=1}^q \operatorname{Re} \left(G_{yu}(j\omega_i)(u_{c,i} - ju_{s,i}) + G_{yd}(j\omega_i)(d_{c,i} - jd_{s,i}) \right) e^{j\omega_i t} \\ &= \sum_{i=1}^q (f_i^T(t) \otimes I_\ell) (H_{i,*} \hat{u}_i + d_{i,*}), \end{aligned} \quad (3.6)$$

where

$$\begin{aligned} H_{i,*} &\triangleq \begin{bmatrix} \operatorname{Re} G_{yu}(j\omega_i) & \operatorname{Im} G_{yu}(j\omega_i) \\ -\operatorname{Im} G_{yu}(j\omega_i) & \operatorname{Re} G_{yu}(j\omega_i) \end{bmatrix} \in \mathbb{R}^{2\ell \times 2m}, \\ d_{i,*} &\triangleq \begin{bmatrix} \operatorname{Re} G_{yd}(j\omega_i) & \operatorname{Im} G_{yd}(j\omega_i) \\ -\operatorname{Im} G_{yd}(j\omega_i) & \operatorname{Re} G_{yd}(j\omega_i) \end{bmatrix} \begin{bmatrix} d_{c,i} \\ d_{s,i} \end{bmatrix} \in \mathbb{R}^{2\ell}. \end{aligned}$$

The HSS performance y_{hss} is the steady-state response of (3.1)–(3.5), that is, $\lim_{t \rightarrow \infty} [y_{\text{hss}}(t, \hat{u}_1, \dots, \hat{u}_q) - y(t)] = 0$. See [207, Chap. 12.12] for details.

Consider the cost function

$$J(\hat{u}_1, \dots, \hat{u}_q) \triangleq \lim_{t \rightarrow \infty} \frac{1}{t} \int_0^t \|y_{\text{hss}}(\tau, \hat{u}_1, \dots, \hat{u}_q)\|^2 d\tau, \quad (3.7)$$

which is the average power of y_{hss} . Substituting (3.6) into (3.7) and integrating yields

$$\begin{aligned} J(\hat{u}_1, \dots, \hat{u}_q) &= \sum_{i=1}^q \sum_{j=1}^q (H_{i,*} \hat{u}_i + d_{i,*})^T \left(\lim_{t \rightarrow \infty} \frac{1}{t} \int_0^t (f_i(\tau) f_j^T(\tau)) \otimes I_\ell d\tau \right) (H_{j,*} \hat{u}_j + d_{j,*}) \\ &= \frac{1}{2} \sum_{i=1}^q \|H_{i,*} \hat{u}_i + d_{i,*}\|^2. \end{aligned}$$

Since (A3.1) implies that $\operatorname{rank} G_{yu}(j\omega_i) = \ell$, it follows that $\operatorname{rank} H_{i,*} = 2\ell$, which implies that $H_{i,*}$ is right invertible. The following result provides an expression for a control that minimizes J .

Theorem 3.1. Assume that (A3.1) is satisfied, and define

$$u_{i,*} \triangleq -H_{i,*}^T (H_{i,*} H_{i,*}^T)^{-1} d_{i,*}.$$

Then, $J(u_{1,*}, \dots, u_{q,*}) = 0$.

Theorem 3.1 provides the ideal control parameter $u_{i,*}$, but $u_{i,*}$ requires knowledge of $H_{i,*}$ and $d_{i,*}$, which are unknown.

For all $\alpha \in \mathbb{Z}^+$, define

$$\Lambda_\alpha \triangleq \begin{bmatrix} 0 & -1 \\ 1 & 0 \end{bmatrix} \otimes I_\alpha \in \mathbb{R}^{2\alpha \times 2\alpha},$$

and define

$$\mathcal{H} \triangleq \left\{ H \in \mathbb{R}^{2\ell \times 2m} : H = \Lambda_\ell^T H \Lambda_m \right\},$$

which is the set of $2\ell \times 2m$ real matrices that have the block structure of $H_{i,*}$.

For each $k \in \mathbb{Z}^+$, define the sampled performance

$$y_k \triangleq y(kT_s).$$

If T_s is sufficiently large relative to the settling time of G_{yu} , then for all $k \in \mathbb{Z}^+$, $y_k \approx y_{\text{hss}}(kT_s, u_{1,k-1}, \dots, u_{q,k-1})$. We make the HSS assumption:

$$(A3.2) \quad y_k = y_{\text{hss}}(kT_s, u_{1,k-1}, \dots, u_{q,k-1}).$$

Assumption (A3.2) is used for stability analyses only. Assumption (A3.2) combined with (3.6) implies that for all $k \in \mathbb{N}$,

$$y_{k+1} = \sum_{i=1}^q (f_{i,k+1}^T \otimes I_\ell) (H_{i,*} u_{i,k} + d_{i,*}), \quad (3.8)$$

where $f_{i,k} \triangleq [\cos k\omega_i T_s \quad \sin k\omega_i T_s]^T \in \mathbb{R}^2$.

For all $\alpha \in \mathbb{Z}^+ \setminus \{1, 2, \dots, 2q-1\}$, define the Vandermonde matrix

$$V_\alpha \triangleq \begin{bmatrix} 1 & e^{-j\omega_1 T_s} & e^{-j2\omega_1 T_s} & \dots & e^{-j(\alpha-1)\omega_1 T_s} \\ 1 & e^{j\omega_1 T_s} & e^{j2\omega_1 T_s} & \dots & e^{j(\alpha-1)\omega_1 T_s} \\ \vdots & \vdots & \vdots & & \vdots \\ 1 & e^{-j\omega_q T_s} & e^{-j2\omega_q T_s} & \dots & e^{-j(\alpha-1)\omega_q T_s} \\ 1 & e^{j\omega_q T_s} & e^{j2\omega_q T_s} & \dots & e^{j(\alpha-1)\omega_q T_s} \end{bmatrix} \in \mathbb{C}^{2q \times \alpha}.$$

The following lemma concerns right invertibility of V_α . The proof follows from [207, Fact 5.16.3].

Lemma 3.1. Assume that the following assumptions are satisfied:

$$(A3.3) \quad \text{For all } j \in Q \setminus \{i\}, e^{j\omega_j T_s} \neq e^{j\omega_i T_s} \text{ and } e^{-j\omega_j T_s} \neq e^{j\omega_i T_s}.$$

$$(A3.4) \quad \angle e^{j\omega_i T_s} \notin \{0, \pi\}.$$

Then, for all $\alpha \geq 2q$, V_α is right invertible.

Assumptions (A3.3) and (A3.4) imply that elements on the second column of V_α are distinct. Moreover, note that Assumption (A3.3) implies that the disturbance frequencies are distinct, and assumption (A3.4) implies that $\omega_i T_s$ is not an integer multiple of π .

Remark. Assumptions (A3.3) and (A3.4) involve disturbance frequencies ω_i and the update period T_s . Since the disturbance frequencies are known, it follows that T_s can be selected to satisfy assumptions (A3.3) and (A3.4).

3.5 Time-Domain Higher Harmonic Control

We present TD-HHC, which relies on knowledge of an estimate of $H_{i,*}$. To derive the TD-HHC update equation for $u_{i,k}$, consider the cost $\mathcal{J}_k : \mathbb{R}^{2m} \times \dots \times \mathbb{R}^{2m} \rightarrow [0, \infty)$ defined by

$$\mathcal{J}_k(\hat{u}_1, \dots, \hat{u}_q) \triangleq \frac{1}{2} \|y_{\text{hss}}((k+1)T_s, \hat{u}_1, \dots, \hat{u}_q)\|^2.$$

It follows from (3.6) that the gradient of \mathcal{J}_k with respect to \hat{u}_i evaluated at $(\hat{u}_1, \dots, \hat{u}_q) = (u_{1,k}, \dots, u_{q,k})$ is

$$\left. \frac{\partial \mathcal{J}_k(\hat{u}_1, \dots, \hat{u}_q)}{\partial \hat{u}_i} \right|_{(\hat{u}_1, \dots, \hat{u}_q) = (u_{1,k}, \dots, u_{q,k})} = H_{i,*}^\top (f_{i,k+1} \otimes I_\ell) y_{\text{hss}}((k+1)T_s, \hat{u}_1, \dots, \hat{u}_q). \quad (3.9)$$

Let $H_{i,e} \in \mathcal{H}$ be an estimate of $H_{i,*}$. Since $H_{i,*}$ is unknown, and y_{hss} is not measurable, we replace $H_{i,*}$ and $y_{\text{hss}}((k+1)T_s, \hat{u}_1, \dots, \hat{u}_q)$ in (3.9) by $H_{i,e}$ and y_{k+1} , respectively, to estimate the gradient. Let $\rho > 0$, and for all $k \in \mathbb{N}$, consider the control

$$u_{i,k+1} = u_{i,k} - \rho H_{i,e}^\top (f_{i,k+1} \otimes I_\ell) y_{k+1}, \quad (3.10)$$

where $u_{i,0} \in \mathbb{R}^{2m}$ is the initial condition. Thus, TD-HHC is given by (3.4) and (3.10). The control architecture is shown in Fig. 3.1.

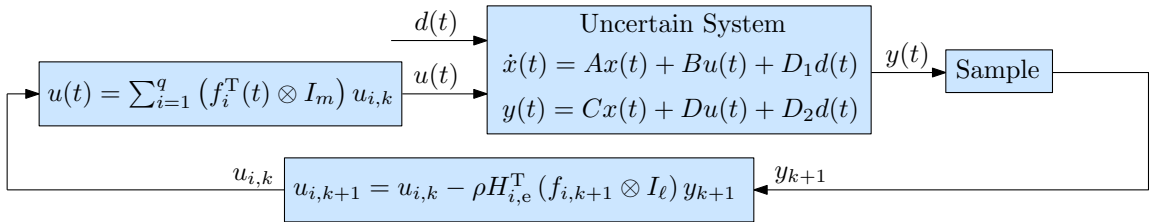


Figure 3.1: Schematic of TD-HHC given by (3.4) and (3.10).

3.6 Stability Analysis of TD-HHC

We analyze the stability properties of the closed-loop system that consists of (3.8) and (3.10). Define

$$G_{i,e} \triangleq \left(\begin{bmatrix} 1 & 0 \end{bmatrix} \otimes I_\ell \right) H_{i,e} \left(\begin{bmatrix} 1 & j \end{bmatrix}^\top \otimes I_m \right) \in \mathbb{C}^{\ell \times m},$$

which is an estimate of $G_{yu}(j\omega_i)$ because $H_{i,e} \in \mathcal{H}$ is an estimate of $H_{i,*}$. For all $\alpha \in \{0, 1, \dots, 2q-1\}$, define

$$R_\alpha \triangleq \operatorname{Re} \sum_{i=1}^q e^{-j\alpha\omega_i T_s} G_{i,*} G_{i,e}^* \in \mathbb{R}^{\ell \times \ell},$$

and define

$$R \triangleq \begin{bmatrix} R_0 & 0 & 0 & \cdots & 0 \\ R_1 & R_0 & 0 & \cdots & 0 \\ \vdots & \vdots & \ddots & \ddots & \vdots \\ R_{2q-2} & R_{2q-3} & \cdots & R_0 & 0 \\ R_{2q-1} & R_{2q-2} & \cdots & R_1 & R_0 \end{bmatrix} \in \mathbb{R}^{2\ell q \times 2\ell q}.$$

Note that R is a block-Toeplitz matrix. For all $k \geq 2q$, define

$$Y_k \triangleq \begin{bmatrix} y_k^\top & y_{k-1}^\top & \cdots & y_{k-2q+1}^\top \end{bmatrix}^\top \in \mathbb{R}^{2\ell q}.$$

The following result provides a time-invariant representation of the closed-loop system (3.8) and (3.10). The proof is in Section 3.12.

Proposition 3.1. Consider the closed-loop system (3.8) and (3.10), where (A3.2)–(A3.4) are satisfied. Then, for all $k \geq 2q$,

$$Y_{k+1} = \begin{bmatrix} \left((V_{2q}^{-1}v)^\top \otimes I_\ell \right) (I_{2\ell q} - \rho R) \\ \hline I_{\ell(2q-1)} \quad 0_{\ell(2q-1) \times \ell} \end{bmatrix} Y_k, \quad (3.11)$$

where $v \triangleq \begin{bmatrix} e^{j\omega_1 T_s} & e^{-j\omega_1 T_s} & \cdots & e^{j\omega_q T_s} & e^{-j\omega_q T_s} \end{bmatrix}^\top \in \mathbb{C}^{2q}$.

To analyze the stability properties of (3.11), which is a time-invariant representation of the closed-loop system (3.8) and (3.10), define the set

$$\Lambda \triangleq \bigcup_{i \in Q} \operatorname{spec} \left(H_{i,*} H_{i,e}^\top \right).$$

The following result provides the stability properties of the closed-loop system (3.8) and (3.10). The proof is in Section 3.13.

Theorem 3.2. Consider the closed-loop system (3.11), where (A3.1)–(A3.4) are satisfied. Let $T_s > 0$ be such that $\frac{\omega_i T_s}{2\pi}$ is a rational number, and define

$$N \triangleq \min \{n \in \mathbb{Z}^+ : \text{for all } i \in Q, n\omega_i T_s / 2\pi \in \mathbb{Z}^+\}.$$

Assume that $\Lambda \subset \text{ORHP}$. Then, there exists $\bar{\rho} \in \left(0, \min_{\lambda \in \Lambda} \frac{4\text{Re } \lambda}{N|\lambda|^2}\right)$ such that for all $\rho \in (0, \bar{\rho}]$, $Y_k \equiv 0$ is a globally asymptotically stable equilibrium of (3.11).

Theorem 3.2 implies that if $\Lambda \subset \text{ORHP}$ and ρ is sufficiently small, then for all $u_{i,0} \in \mathbb{R}^{2m}$, $\lim_{k \rightarrow \infty} y_k = 0$. Note that $\Lambda \subset \text{ORHP}$ if and only if $\bigcup_{i \in Q} \text{spec}(G_{i,*} G_{i,e}^*) \subset \text{ORHP}$. Therefore, $\Lambda \subset \text{ORHP}$ is equivalent to the FD-HHC stability condition in Theorem 2.2. In the SISO case, $\Lambda \subset \text{ORHP}$ if and only if $G_{i,e}$ is within 90° of $G_{i,*}$, that is, $|\angle(G_{i,e}/G_{i,*})| < \pi/2$.

The following result concerns the stability properties of the closed-loop TD-HHC system (3.11) for the single-tone (i.e., $q = 1$) and single-output (i.e., $\ell = 1$) case. The proof is in Section 3.14.

Theorem 3.3. Consider the closed-loop system (3.11), where $q = 1$, $\ell = 1$, and (A3.1)–(A3.4) are satisfied. Assume $\rho > 0$ and $R_0 > 0$. Then, $Y_k \equiv 0$ is a globally asymptotically stable equilibrium of (3.11) if and only if $\rho \in (0, \bar{\rho})$, where

$$\bar{\rho} \triangleq \begin{cases} \rho_1, & \text{if } 2R_0 \cos \omega_1 T_s - R_1 \geq R_0, \\ \min\{\rho_1, \rho_2\}, & \text{if } |2R_0 \cos \omega_1 T_s - R_1| < R_0, \\ \rho_2, & \text{if } 2R_0 \cos \omega_1 T_s - R_1 \leq -R_0, \end{cases}$$

and

$$\rho_1 \triangleq \frac{2(1 + \cos \omega_1 T_s)}{R_0(1 + 2 \cos \omega_1 T_s) - R_1}, \quad \rho_2 \triangleq \frac{2(1 - \cos \omega_1 T_s)}{R_0(1 - 2 \cos \omega_1 T_s) + R_1}.$$

Theorem 3.3 provides the necessary and sufficient condition for global asymptotic stability of the closed-loop system (3.11) for the case, where $q = 1$ and $\ell = 1$. In this case, $R_0 > 0$ if and only if $\Lambda \subset \text{ORHP}$, which is equivalent to the FD-HHC stability condition in Theorem 2.2.

3.7 Time-Domain Adaptive Higher Harmonic Control

We present TD-AHHC, which does not require any information regarding either $d_{i,*}$ or $H_{i,*}$. Let $r \in \mathbb{Z}^+$ be such that $r \geq 2q$, and for all $k \in \mathbb{Z}^+$, define

$$f_k \triangleq \begin{bmatrix} f_{1,k}^T & \cdots & f_{q,k}^T \end{bmatrix}^T \in \mathbb{R}^{2q}, \quad F_k \triangleq \begin{bmatrix} f_k & \cdots & f_{k-r+1} \end{bmatrix} \in \mathbb{R}^{2q \times r}.$$

Note that choice of the parameter r affects the performance of TD-AHHC, which we will discuss in Example 3.4. The following lemma concerns the right-invertibility of F_k , and provides an expression for F_k^+ . The proof is in Section 3.15.

Lemma 3.2. Assume that (A3.3) and (A3.4) are satisfied. Then, for all $k \in \mathbb{N}$, F_k is right invertible, and

$$F_k^+ = F_k^T S_k^T (V_r V_r^T)^{-1} S_k, \quad (3.12)$$

where

$$S_k \triangleq \text{diag}(S_{1,k}, \dots, S_{q,k}) \in \mathbb{C}^{2q \times 2q},$$

and

$$S_{i,k} \triangleq \begin{bmatrix} e^{-jk\omega_i T_s} & je^{-jk\omega_i T_s} \\ e^{jk\omega_i T_s} & -je^{jk\omega_i T_s} \end{bmatrix} \in \mathbb{C}^{2 \times 2}.$$

Remark. Lemma 3.2 provides the expression (3.12) for F_k^+ that can be computed without an online matrix inversion. In particular, $(V_r V_r^T)^{-1}$ can be computed offline and (3.12) can be used to compute F_k^+ . The TD-AHHC algorithm makes use of F_k^+ .

Let $\mu \in (0, 4)$, $\nu_1 > 0$, and $u_{i,0} \in \mathbb{R}^{2m}$. For all $k \in \mathbb{N}$, consider the control

$$u_{i,k+1} = u_{i,k} - \frac{\mu}{\nu_1 + \sum_{i=1}^q \|H_{i,k}\|_F^2} H_{i,k}^T (f_{i,k+1} \otimes I_\ell) y_{k+1}, \quad (3.13)$$

where $H_{i,k} \in \mathbb{R}^{2\ell \times 2m}$ is an estimate of $H_{i,*}$ obtained from the adaptive equations presented below. Note that (3.13) is similar to (3.10) except that the fixed estimate $H_{i,e}$ is replaced by the adaptive estimate $H_{i,k}$, and the fixed step size ρ is replaced by the $H_{i,k}$ -dependent step size $\mu/(\nu_1 + \sum_{i=1}^q \|H_{i,k}\|_F^2)$.

For all $k \geq r$, consider $d_{i,k} : \mathcal{H} \times \dots \times \mathcal{H} \rightarrow \mathbb{R}^{2\ell}$ defined by

$$d_{i,k}(\hat{H}_1, \dots, \hat{H}_q) \triangleq (e_i \otimes I_{2\ell}) \left((F_k^+)^T \otimes I_\ell \right) \begin{bmatrix} y_k - \sum_{j=1}^q (f_{j,k}^T \otimes I_\ell) \hat{H}_j u_{j,k-1} \\ \vdots \\ y_{k-r+1} - \sum_{j=1}^q (f_{j,k-r+1}^T \otimes I_\ell) \hat{H}_j u_{j,k-r} \end{bmatrix}, \quad (3.14)$$

where $e_i \in \mathbb{R}^{1 \times q}$ is the i th row of I_q .

Remark. If (A3.2)–(A3.4) are satisfied, then it follows from Lemma 3.2, (3.8), and (3.14) that for all $k \geq r$,

$$\begin{aligned} d_{i,k}(H_{1,*}, \dots, H_{q,*}) &= (e_i \otimes I_{2\ell}) \left((F_k^+)^T \otimes I_\ell \right) \sum_{j=1}^q \begin{bmatrix} (f_{j,k}^T \otimes I_\ell) d_{j,*} \\ \vdots \\ (f_{j,k-r+1}^T \otimes I_\ell) d_{j,*} \end{bmatrix} \\ &= (e_i \otimes I_{2\ell}) \left((F_k^+)^T \otimes I_\ell \right) (F_k^T \otimes I_\ell) \begin{bmatrix} d_{1,*}^T & \dots & d_{q,*}^T \end{bmatrix}^T \\ &= d_{i,*}, \end{aligned}$$

which implies that $d_{i,k}(\hat{H}_1, \dots, \hat{H}_q)$ is an estimate of $d_{i,*}$.

Next, for all $k > r$, consider $\hat{y}_k : \mathcal{H} \times \dots \times \mathcal{H} \rightarrow \mathbb{R}^\ell$ defined by

$$\hat{y}_k(\hat{H}_1, \dots, \hat{H}_q) \triangleq \sum_{i=1}^q \left(f_{i,k}^\top \otimes I_\ell \right) \left(\hat{H}_i u_{i,k-1} + d_{i,k-1}(\hat{H}_1, \dots, \hat{H}_q) \right). \quad (3.15)$$

If (A3.2)–(A3.4) are satisfied, then it follows from (3.8) and (3.14) that for all $k \geq r$, $\hat{y}_{k+1}(H_{1,*}, \dots, H_{q,*}) = y_{k+1}$. To determine the adaptive equation for $H_{i,k}$, consider the cost $\mathcal{J}_k : \mathcal{H} \times \dots \times \mathcal{H} \rightarrow [0, \infty)$ defined by

$$\begin{aligned} \mathcal{J}_k(\hat{H}_1, \dots, \hat{H}_q) &\triangleq \frac{1}{2} \left\| y_{k+1} - \hat{y}_{k+1}(\hat{H}_1, \dots, \hat{H}_q) \right\|^2 \\ &\quad + \frac{1}{2} \left\| y_{k+1} - \hat{y}_{k+1}(\Lambda_\ell^\top \hat{H}_1 \Lambda_m, \dots, \Lambda_\ell^\top \hat{H}_q \Lambda_m) \right\|^2. \end{aligned}$$

Note that the second term of the cost \mathcal{J}_k is similar to the first term except \hat{H}_i is replaced by $\Lambda_\ell^\top \hat{H}_i \Lambda_m$. If $\hat{H}_i \in \mathcal{H}$, then $\hat{H}_i = \Lambda_\ell^\top \hat{H}_i \Lambda_m$. In this case, the two terms of \mathcal{J}_k are equal. These two terms are included in the cost in order to obtain estimates of $H_{i,*}$ that have the block structure of $H_{i,*}$ (i.e., are contained in \mathcal{H}). If $\hat{H}_i \in \mathcal{H}$, then \mathcal{J}_k can be interpreted as a measure of how well $\hat{y}_{k+1}(\hat{H}_1, \dots, \hat{H}_q)$ approximates the measurement y_{k+1} , which itself is approximately equal to the sampled HSS performance $y_{\text{hss}}((k+1)T_s, u_{1,k-1}, \dots, u_{q,k-1}) = \sum_{i=1}^q (f_{i,k+1}^\top \otimes I_\ell) (H_{i,*} u_{i,k-1} + d_{i,*})$. Thus, if (A3.2)–(A3.4) are satisfied, then $\hat{y}_{k+1}(H_{1,*}, \dots, H_{q,*}) = y_{k+1}$ and $\mathcal{J}_k(H_{1,*}, \dots, H_{q,*}) = 0$, that is, \mathcal{J}_k is minimized by $\hat{H}_i = H_{i,*}$.

Evaluating the gradient of \mathcal{J}_k with respect to \hat{H}_i yields

$$\frac{\partial \mathcal{J}_k(\hat{H}_1, \dots, \hat{H}_q)}{\partial \hat{H}_i} = \Gamma_{i,k}(\hat{H}_1, \dots, \hat{H}_q) + \Lambda_\ell \Gamma_{i,k}(\hat{H}_1, \dots, \hat{H}_q) \Lambda_m^\top,$$

where for all $k \geq r$, $\Gamma_{i,k} : \mathcal{H} \times \dots \times \mathcal{H} \rightarrow \mathbb{R}^{2\ell \times 2m}$ is defined by

$$\begin{aligned} \Gamma_{i,k}(\hat{H}_1, \dots, \hat{H}_q) &\triangleq \text{vec}^{-1} \left(\left(\left[u_{i,k-1} \otimes f_{i,k} \quad \dots \quad u_{i,k-r} \otimes f_{i,k-r+1} \right] F_k^+ f_{k+1} \right) \right. \\ &\quad \left. \otimes \left(y_{k+1} - \hat{y}_{k+1}(\hat{H}_1, \dots, \hat{H}_q) \right) \right) \\ &\quad - (f_{i,k+1} \otimes I_\ell) \left(y_{k+1} - \hat{y}_{k+1}(\hat{H}_1, \dots, \hat{H}_q) \right) u_{i,k}^\top, \end{aligned} \quad (3.16)$$

where $\text{vec}^{-1} : \mathbb{R}^{4\ell m} \rightarrow \mathbb{R}^{2\ell \times 2m}$ is the inverse vec operator, that is, for all $X \in \mathbb{R}^{2\ell \times 2m}$, $\text{vec}^{-1} \text{vec } X = X$.

Let $H_{i,0} \in \mathcal{H}$, and for all $k \in \{1, 2, \dots, r-1\}$, let $H_{i,k} = H_{i,0}$. For all $k \geq r$, consider the update equation

$$H_{i,k} = H_{i,k-1} - \eta_k \left. \frac{\partial \mathcal{J}_k(\hat{H}_1, \dots, \hat{H}_q)}{\partial \hat{H}_i} \right|_{(\hat{H}_1, \dots, \hat{H}_q) = (H_{1,k-1}, \dots, H_{q,k-1})}$$

$$= H_{i,k-1} - \eta_k \left(\Gamma_{i,k}(H_{1,k-1}, \dots, H_{q,k-1}) + \Lambda_\ell \Gamma_{i,k}(H_{1,k-1}, \dots, H_{q,k-1}) \Lambda_m^T \right), \quad (3.17)$$

where

$$\eta_k \triangleq \frac{\gamma}{\nu_2 + \sum_{j=1}^q \left\| \left[u_{i,k-1} \otimes f_{i,k} \quad \dots \quad u_{i,k-r} \otimes f_{i,k-r+1} \right] F_k^+ f_{k+1} - (u_{i,k} \otimes f_{i,k+1}) \right\|^2}, \quad (3.18)$$

where $\gamma \in (0, 1)$ and $\nu_2 > 0$. Thus, TD-AHHC is given by (3.4) and (3.13)–(3.18). The control architecture is shown in Fig. 3.2.

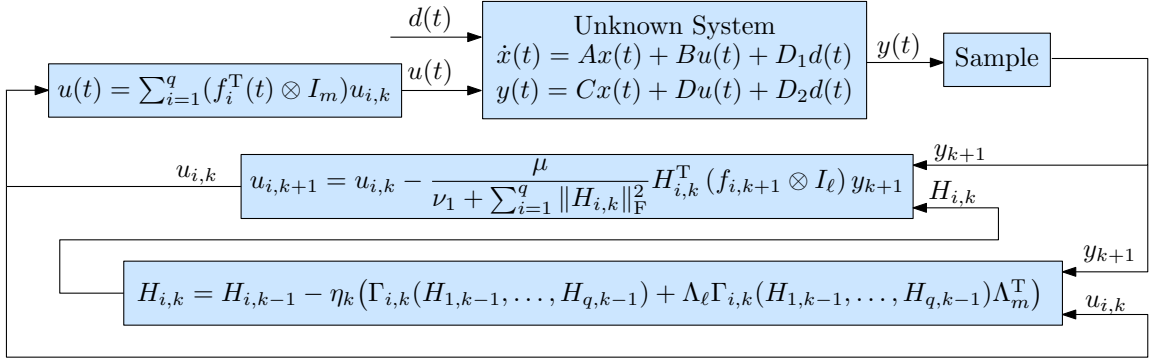


Figure 3.2: Schematic of TD-AHHC given by (3.4) and (3.13)–(3.18).

3.8 Stability Analysis of TD-AHHC

We analyze the stability of the closed-loop system that consists of (3.8) and (3.13)–(3.18). The following result provides properties of (3.17). The proof is in Section 3.16.

Proposition 3.2. Consider the closed-loop system (3.8) and (3.13)–(3.18), where $\gamma \in (0, 1)$, $\nu_2 > 0$, and (A3.1)–(A3.4) are satisfied. Then, for all $u_{i,0} \in \mathbb{R}^{2m}$ and all $H_{i,0} \in \mathcal{H}$, the following statements hold:

i) $H_{i,k}$ is bounded, and for all $k \geq r$,

$$\sum_{i=1}^q \left(\|H_{i,k} - H_{i,*}\|_F^2 - \|H_{i,k-1} - H_{i,*}\|_F^2 \right) \leq -4(1 - \gamma)\eta_k \times \|y_{k+1} - \hat{y}_{k+1}(H_{1,k-1}, \dots, H_{q,k-1})\|^2.$$

ii) $\lim_{k \rightarrow \infty} (H_{i,k} - H_{i,k-1}) = 0$.

Part i) of Proposition 3.2 implies that $\sum_{i=1}^q \|H_{i,k} - H_{i,*}\|_F^2$ is nonincreasing. Note that, except the assumption $m \geq \ell$ implied by (A3.1), Proposition 3.2 does not impose any assumption on the number ℓ of performance measurements, number m of controls, or number q of disturbance frequencies.

For all $k \in \mathbb{N}$, define

$$G_{i,k} \triangleq \left(\begin{bmatrix} 1 & 0 \end{bmatrix} \otimes I_\ell \right) H_{i,k} \left(\begin{bmatrix} 1 & j \end{bmatrix}^\top \otimes I_m \right) \in \mathbb{C}^{\ell \times m},$$

which is an estimate of $G_{yu}(j\omega_i)$ because $H_{i,k} \in \mathcal{H}$ is an estimate of $H_{i,*}$. The following result provides the stability properties of the closed-loop system (3.8) and (3.13)–(3.18) for the case, where $q = 1$ and $m \geq \ell = 1$. The proof is in Appendix 3.16.

Theorem 3.4. Consider the open-loop system (3.8) and the control (3.13)–(3.18), where $q = 1$, $\ell = 1$, and (A3.1)–(A3.4) are satisfied. Let $\mu \in (0, 4)$, $\gamma \in (0, 1)$, $\nu_1 > 0$, $\nu_2 > 0$, $r = 2$, and let $u_{1,0} \in \mathbb{R}^{2m}$ and $H_{1,0} \in \mathcal{H}$. Assume that there exists $k_s \in \mathbb{N}$ and $\varepsilon > 0$ such that for all $k \geq k_s$, $|\text{Im } G_{1,*} G_{1,k}^*| \geq \varepsilon$. Then, $\lim_{k \rightarrow \infty} y_k = 0$.

Theorem 3.4 invokes the assumption that there exist $\varepsilon > 0$ and $k_s \in \mathbb{N}$ such that for all $k \geq k_s$, $|\text{Im } G_{1,*} G_{1,k}^*| \geq \varepsilon$. This assumption, which implies that $|\text{Im } G_{1,*} G_{1,k}^*|$ is asymptotically nonzero, cannot be verified *a priori*. However, simulations suggest that for almost all initial conditions $u_{1,0} \in \mathbb{R}^{2m}$ and $H_{1,0} \in \mathcal{H}$, $|\text{Im } G_{1,*} G_{1,k}^*|$ is asymptotically nonzero, and thus, satisfies $|\text{Im } G_{1,*} G_{1,k}^*| \geq \varepsilon$. In this case, Theorem 3.4 states that the performance y_k globally tends to zero.

3.9 Numerical Examples

We present numerical examples comparing FD-HHC and TD-HHC for rejection of disturbances acting on a two-mass structure. We also present numerical examples that demonstrate and compare the performance of FD-HHC, TD-HHC, and TD-AHHC implemented for active noise cancellation in an acoustic duct.

TD-HHC requires estimates $H_{i,e}$ of $H_{i,*}$ given by

$$H_{i,e} = \begin{bmatrix} \text{Re } G_{i,e} & \text{Im } G_{i,e} \\ -\text{Im } G_{i,e} & \text{Re } G_{i,e} \end{bmatrix} \in \mathbb{C}^{2\ell \times 2m}.$$

Note that FD-HHC also requires estimates $G_{i,e} \in \mathbb{C}^{\ell \times m}$ of $G_{yu}(j\omega_i)$. Similar to the estimates for TD-HHC, the estimates for FD-HHC must be sufficiently accurate to ensure closed-loop stability. See Theorem 2.2 for details. For a SISO system subject to a single-tone disturbance, for both TD-HHC and FD-HHC, the closed-loop is asymptotically stable only if the estimate $G_{1,e}$ is within 90° of $G_{yu}(j\omega_1)$. FD-HHC is a frequency-domain method, and all computations use DFT data. We implement FD-HHC according to (2.11). The DFT is performed using a 1 kHz sampling frequency.

TD-AHHC, in contrast to TD-HHC and FD-HHC, requires no system model information. For TD-AHHC, we let the initial condition $H_{i,0}$ be given by

$$H_{i,0} = \begin{bmatrix} \text{Re } G_{i,0} & \text{Im } G_{i,0} \\ -\text{Im } G_{i,0} & \text{Re } G_{i,0} \end{bmatrix} \in \mathbb{C}^{2\ell \times 2m}, \quad (3.19)$$

where $G_{i,0}$ is specified in each example. For the cases, where we compare FD-HHC and TD-HHC with TD-AHHC, we let $G_{i,e} = G_{i,0}$. For all examples, the control is turned on after 1 s.

Two-Mass Structure

Consider the two-mass structure shown in Fig. 3.3, where u is the control force, d_1 and d_2 are disturbance forces, and ξ_1 and ξ_2 are displacements of masses m_1 and m_2 . We consider the SISO system (3.1), where $x(t) = [\xi_1(t) \ \dot{\xi}_1(t) \ \xi_2(t) \ \dot{\xi}_2(t)]^T$, $d(t) = [d_1(t) \ d_2(t)]^T$, $y = \xi_2$, and

$$A = \begin{bmatrix} 0 & 1 & 0 & 0 \\ \frac{-(k_1+k_2)}{m_1} & \frac{-(c_1+c_2)}{m_1} & \frac{k_2}{m_1} & \frac{c_2}{m_1} \\ 0 & 0 & 0 & 1 \\ \frac{k_2}{m_2} & \frac{c_2}{m_2} & \frac{-(k_2+k_3)}{m_2} & \frac{-(c_2+c_3)}{m_2} \end{bmatrix}, \quad B = \begin{bmatrix} 0 \\ \frac{1}{m_1} \\ 0 \\ 0 \end{bmatrix}, \quad D_1 = \begin{bmatrix} 0 & 0 \\ \frac{1}{m_1} & 0 \\ 0 & 0 \\ 0 & \frac{1}{m_2} \end{bmatrix},$$

where $m_1 = 2$ kg, $m_2 = 1$ kg, $c_1 = 60$ kg/s, $c_2 = 50$ kg/s, $c_3 = 40$ kg/s, $k_1 = 300$ N/m, $k_2 = 200$ N/m and $k_3 = 400$ N/m. The initial condition is $x(0) = 0$.

We compare FD-HHC and TD-HHC for initial estimates $G_{1,e}$ that satisfy the FD-HHC and TD-HHC stability conditions, that is, $G_{1,e}$ is within 90° of $G_{yu}(j\omega_1)$. For each comparison, we select the gain ρ , and the update period T_s that yield the fastest convergence time for each algorithm. For both FD-HHC and TD-HHC, we let $u_{1,0} = 0$.

Example 3.1. Let $d_1 = 10 \cos \omega_1 t$ and $d_2 = 10 \sin \omega_1 t$, where $\omega_1 = 4\pi$ rad/s. For both FD-HHC and TD-HHC, let $G_{1,e} = e^{j\frac{\pi}{6}} G_{yu}(j\omega_1)$, which is 30° away from $G_{yu}(j\omega_1)$. For FD-HHC, we select $\rho = 1.90 \times 10^6$ and $T_s = 0.5$ s, and for TD-HHC, we select $\rho = 2.98 \times 10^6$ and $T_s = 0.1$ s. Figure 3.4 shows y and u for FD-HHC and TD-HHC.

Both FD-HHC and TD-HHC yield asymptotic disturbance rejection. The convergence time is improved with TD-HHC relative to FD-HHC. In this case, the *settling time* of the system, that is, the time it takes the unit step response to reach and stay within $\pm 2\%$ of its final value, is approximately 0.3 s, which is smaller than the period

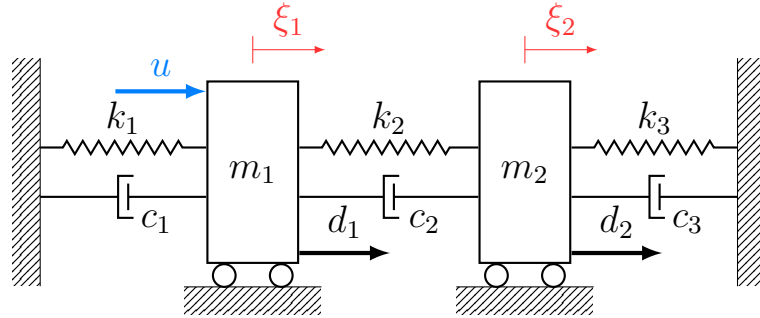


Figure 3.3: The two-mass structure used in Examples 3.1 and 3.2.

of disturbance (i.e., $2\pi/\omega_1 = 0.5$ s). Numerical simulations suggest that, in general, if the settling time of the system is smaller than the period of the disturbance, then TD-HHC yields faster convergence than FD-HHC. The faster convergence of TD-HHC can be explained by the fact that TD-HHC is a time-domain method, and thus TD-HHC does not rely on batch data processing (i.e., DFT).

The convergence time of FD-HHC and TD-HHC also depends on the estimate $G_{1,e}$. Let $G_{1,e} = e^{j\frac{\pi}{3}}G_{yu}(j\omega_1)$, which is 60° away from $G_{yu}(j\omega_1)$. In this case, for FD-HHC, we select $\rho = 1.47 \times 10^6$ and $T_s = 0.5$ s, and for TD-HHC, we select $\rho = 3.25 \times 10^6$ and $T_s = 0.1$ s. Figure 3.5 shows y and u for FD-HHC and TD-HHC.

Both FD-HHC and TD-HHC yield asymptotic disturbance rejection. In this case, the convergence time is significantly improved with TD-HHC relative to FD-HHC. Numerical simulations suggest that for the cases, where the settling time of the system is smaller than the period of the disturbance, TD-HHC yields faster convergence than FD-HHC as the angle difference between $G_{1,e}$ and $G_{yu}(j\omega_1)$ (i.e., $|\angle G_{1,e} - \angle G_{yu}(j\omega_1)|$) increases. \triangle

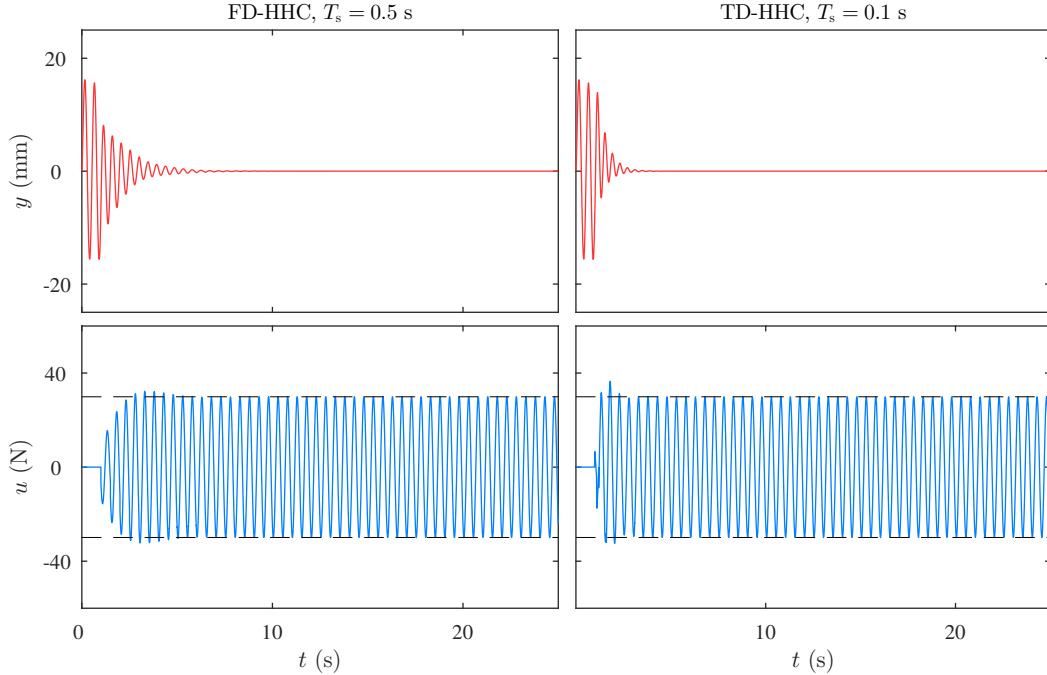


Figure 3.4: For a SISO system with a settling time smaller than the period of disturbance, and where $G_{1,e}$ is 30° away from $G_{yu}(j\omega_1)$, both FD-HHC and TD-HHC yield $y(t) \rightarrow 0$ as $t \rightarrow \infty$. However, the convergence time is improved with TD-HHC relative to FD-HHC. The dashed lines show $\pm\|u_{1,*}\|$.

Example 3.2. We revisit Example 3.1 but with a disturbance that has a smaller period than the settling time of the system. Specifically, we let $\omega_1 = 20\pi$ rad/s. In this case, the settling time of the system is approximately 0.5 s, which is larger than the period of disturbance (i.e., $2\pi/\omega_1 = 0.1$ s). For both FD-HHC and TD-HHC, we let $G_{1,e} = e^{j\frac{\pi}{6}}G_{yu}(j\omega_1)$, which is 30° away from $G_{yu}(j\omega_1)$. For FD-HHC, we select

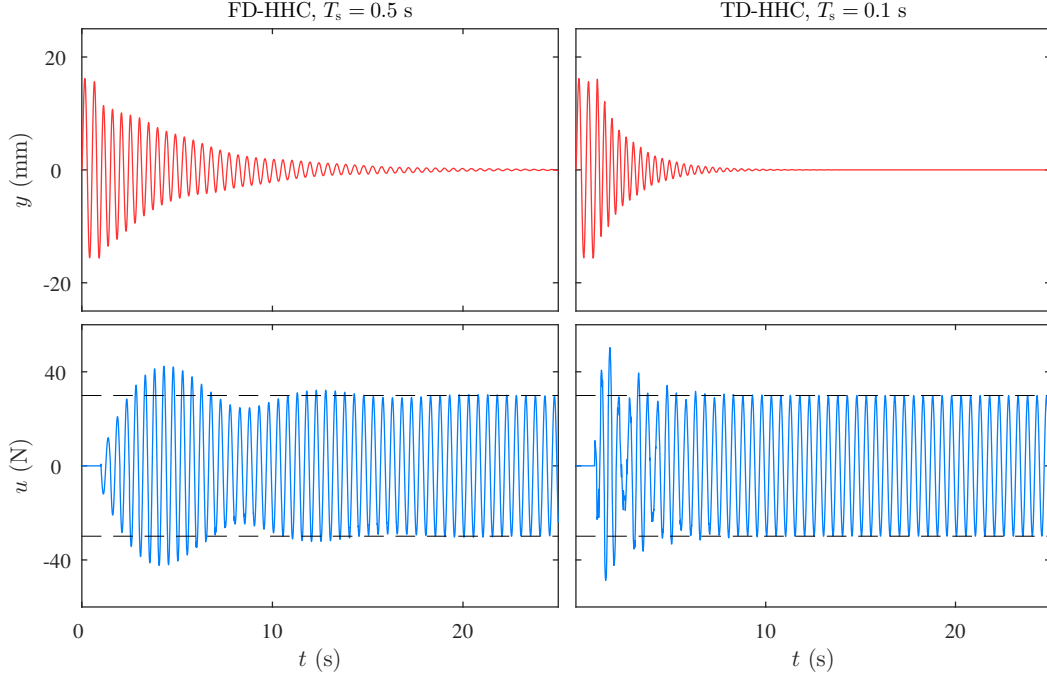


Figure 3.5: For a SISO system with a settling time smaller than the period of disturbance, and where $G_{1,e}$ is 60° away from $G_{yu}(\mathcal{J}\omega_1)$, both FD-HHC and TD-HHC yield $y(t) \rightarrow 0$ as $t \rightarrow \infty$. However, the convergence time is significantly improved with TD-HHC relative to FD-HHC. The dashed lines show $\pm\|u_{1,*}\|$.

$\rho = 3.46 \times 10^8$ and $T_s = 0.1$ s, and for TD-HHC, we select $\rho = 9.15 \times 10^7$ and $T_s = 0.03$ s. Figure 3.6 shows y and u for FD-HHC and TD-HHC. Both FD-HHC and TD-HHC yield asymptotic disturbance rejection with approximately the same convergence rate.

To investigate the effects of estimate $G_{1,e}$ on convergence time, we let $G_{1,0} = e^{\mathcal{J}\frac{\pi}{3}}G_{yu}(\mathcal{J}\omega_1)$, which is 60° away from $G_{yu}(\mathcal{J}\omega_1)$. In this case, for FD-HHC, we select $\rho = 1.77 \times 10^8$ and $T_s = 0.1$ s, and for TD-HHC, we select $\rho = 5.78 \times 10^7$ and $T_s = 0.03$ s. Figure 3.7 shows y and u for FD-HHC and TD-HHC. Similar to the previous case, both FD-HHC and TD-HHC yield asymptotic disturbance rejection with approximately the same convergence rate. Numerical simulations suggest that, in general, if the settling time of the system is larger than the period of the disturbance, then TD-HHC and FD-HHC that are tuned for fastest convergence, yield approximately the same convergence time, regardless of the angle difference between $G_{1,e}$ and $G_{yu}(\mathcal{J}\omega_1)$. \triangle

Acoustic Duct

Consider the acoustic duct of length $L = 2$ m shown in Fig. 3.8. A disturbance speaker is at $\xi_d = 0.95$ m, while two control speakers are at $\xi_{\psi_1} = 0.4$ m and $\xi_{\psi_2} = 1.25$ m. All speakers have cross-sectional area $A_s = 0.0025$ m². The equation for the

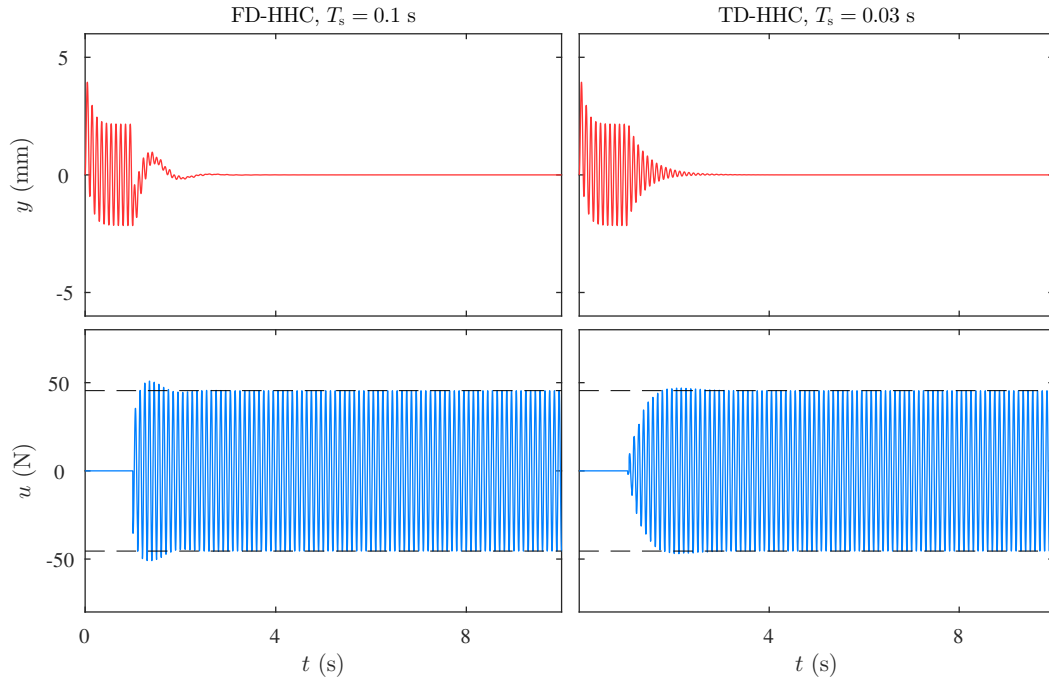


Figure 3.6: For a SISO system with a settling time larger than the period of disturbance, and where $G_{1,e}$ is 30° away from $G_{yu}(j\omega_1)$, both FD-HHC and TD-HHC yield $y(t) \rightarrow 0$ as $t \rightarrow \infty$, with approximately the same convergence time. The dashed lines show $\pm\|u_{1,*}\|$.

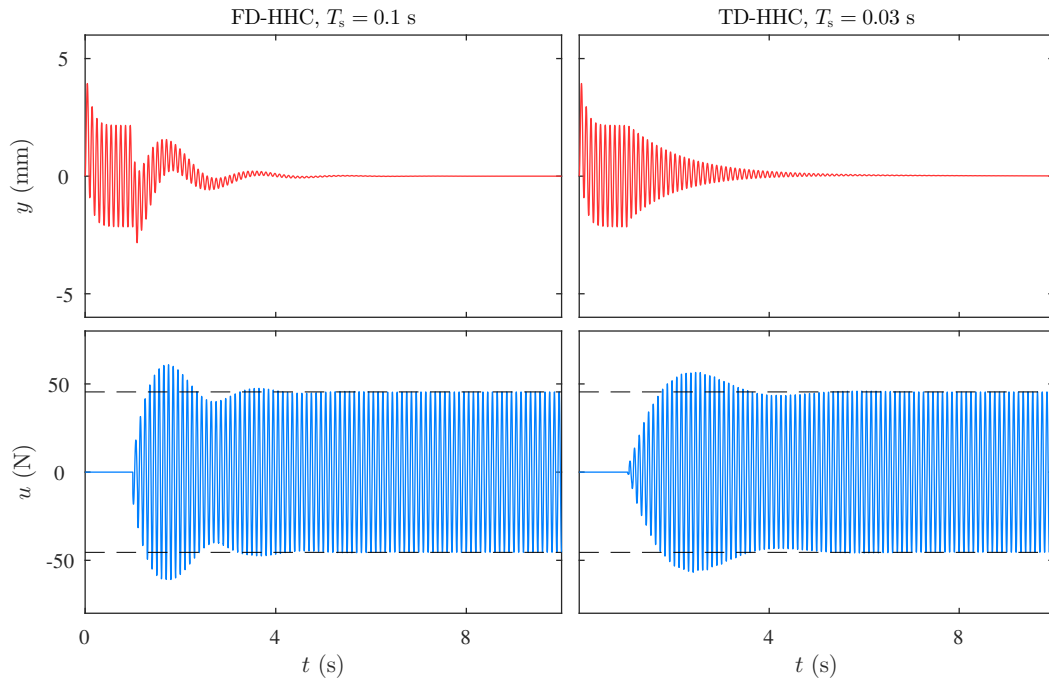


Figure 3.7: For a SISO system with a settling time larger than the period of disturbance, and where $G_{1,e}$ is 60° away from $G_{yu}(j\omega_1)$, both FD-HHC and TD-HHC yield $y(t) \rightarrow 0$ as $t \rightarrow \infty$, with approximately the same convergence time. The dashed lines show $\pm\|u_{1,*}\|$.

acoustic duct is

$$\frac{1}{c^2} \frac{\partial^2 p(\xi, t)}{\partial t^2} = \frac{\partial^2 p(\xi, t)}{\partial \xi^2} + \rho_0 \dot{\psi}_1(t) \delta(\xi - \xi_{\psi_1}) + \rho_0 \dot{\psi}_2(t) \delta(\xi - \xi_{\psi_2}) + \rho_0 \dot{d}(t) \delta(\xi - \xi_d),$$

where $p(\xi, t)$ is the acoustic pressure, δ is the Dirac delta, $c = 343$ m/s is the phase speed of the acoustic wave, ψ_1 and ψ_2 are the speaker cone velocities of the control speakers, d is the speaker cone velocity of the disturbance speaker, and $\rho_0 = 1.21$ kg/m³. See [203] for more details.

Using separation of variables and retaining s modes, $p(\xi, t)$ is approximated by $p(\xi, t) = \sum_{i=0}^s q_i(t) V_i(\xi)$, where for $i = 1, \dots, s$, $V_i(\xi) \triangleq c\sqrt{2/L} \sin i\pi\xi/L$, and q_i satisfies (3.1), where

$$x(t) = \begin{bmatrix} \int_0^t q_1(\sigma) d\sigma & q_1(t) & \cdots & \int_0^t q_s(\sigma) d\sigma & q_s(t) \end{bmatrix}^T, \\ A = \text{diag} \left(\begin{bmatrix} 0 & 1 \\ -\omega_{n_1}^2 & -2\zeta_1 \omega_{n_1} \end{bmatrix}, \dots, \begin{bmatrix} 0 & 1 \\ -\omega_{n_s}^2 & -2\zeta_s \omega_{n_s} \end{bmatrix} \right), \\ B = \frac{\rho_0}{A_s} \begin{bmatrix} 0 & V_1(\xi_{\psi_1}) & \cdots & 0 & V_s(\xi_{\psi_1}) \\ 0 & V_1(\xi_{\psi_2}) & \cdots & 0 & V_s(\xi_{\psi_2}) \end{bmatrix}^T, \quad D_1 = \frac{\rho_0}{A_s} \begin{bmatrix} 0 & V_1(\xi_d) & \cdots & 0 & V_s(\xi_d) \end{bmatrix}^T,$$

and for $i = 1, \dots, s$, $\omega_{n_i} \triangleq i\pi c/L$, and $\zeta_i = 0.2$.

Two feedback microphones are in the duct at $\xi_{\phi_1} = 0.3$ m and $\xi_{\phi_2} = 1.7$ m, and they measure the acoustic pressures $\phi_1(t) = p(\xi_{\phi_1}, t)$ and $\phi_2(t) = p(\xi_{\phi_2}, t)$, respectively. Thus, for $i = 1, 2$, $\phi_i(t) = C_i x(t)$, where $C_i = \frac{\rho_0}{A_s} [0 \quad V_1(\xi_{\phi_i}) \quad \cdots \quad 0 \quad V_s(\xi_{\phi_i})]$. For all examples, $s = 5$, and $x(0) = 0$. and $G_{i,0}$ is specified in each example. The following examples consider the acoustic duct with different control speaker and feedback microphone configurations. Let $\omega_1 = 200\pi$ rad/s and $\omega_2 = 300\pi$ rad/s.

Example 3.3. Consider the SISO system, where we let $\psi_1 = u$, $y = \phi_1$, $\psi_2 = 0$, and $d = 10 \sin \omega_1 t + 10 \cos \omega_1 t$. First, consider the case where $G_{1,0}$ satisfies FD-HHC and TD-HHC stability condition, that is, $G_{1,0}$ within 90° of $G_{yu}(j\omega_1)$. Specifically, let

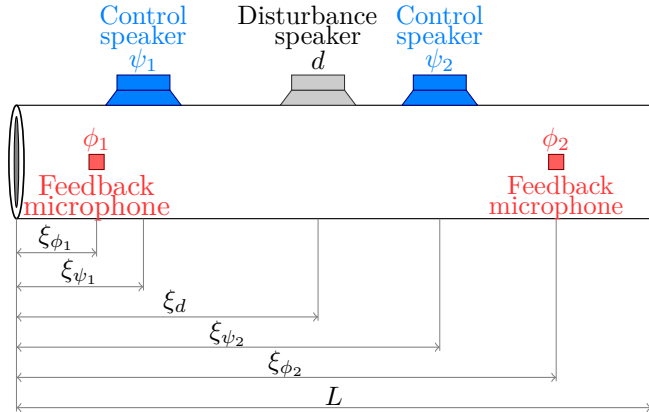


Figure 3.8: The acoustic duct used in Examples 3.3–3.5.

$G_{1,0} = e^{j\frac{\pi}{8}}G_{yu}(j\omega_1)$, which is 30° away from $G_{yu}(j\omega_1)$. For FD-HHC, we let $T_s = 0.01$ s and $\rho = 1.58 \times 10^{-5}$; for TD-HHC, we let $T_s = 0.011$ s and $\rho = 4.28 \times 10^{-5}$; and for TD-AHHC, we let $T_s = 0.011$ s, $r = 2$, $\mu = 1.5$, $\gamma = 0.5$, and $\nu_1 = \nu_2 = 10^{-3}$. Figure 3.9 shows the response y and control u for FD-HHC, TD-HHC and TD-AHHC. In this case FD-HHC, TD-HHC, and TD-AHHC yield asymptotic disturbance rejection with approximately the same convergence time.

Next, consider the case where $G_{1,0}$ is within 90° of $G_{yu}(j\omega_1)$ but has a larger angle difference with $G_{yu}(j\omega_1)$ than the previous case. Specifically, we let $G_{1,0} = e^{j0.47\pi}G_{yu}(j\omega_1)$, which is 85° away from $G_{yu}(j\omega_1)$. For FD-HHC, we let $T_s = 0.01$ s and $\rho = 9.48 \times 10^{-6}$; for TD-HHC, we let $T_s = 0.011$ s and $\rho = 9.72 \times 10^{-5}$; and for TD-AHHC, we let $T_s = 0.011$ s, $r = 2$, $\mu = 1.5$, $\gamma = 0.5$, and $\nu_1 = \nu_2 = 10^{-3}$. Figure 3.10 shows the response y and control u for FD-HHC, TD-HHC and TD-AHHC. In this case FD-HHC, TD-HHC, and TD-AHHC yield asymptotic disturbance rejection; however, the convergence time with TD-AHHC is smaller than convergence time with FD-HHC and TD-HHC.

Next, consider the case where $G_{1,0}$ does not satisfy FD-HHC and TD-HHC stability condition, that is, $G_{1,0}$ is not within 90° of $G_{yu}(j\omega_1)$. Specifically, we let $G_{1,0} = e^{j\frac{2\pi}{3}}G_{yu}(j\omega_1)$, which is 120° away from $G_{yu}(j\omega_1)$. For FD-HHC, we let $T_s = 0.01$ s and $\rho = 1.58 \times 10^{-5}$; for TD-HHC, we let $T_s = 0.011$ s and $\rho = 4.28 \times 10^{-5}$; and for TD-AHHC, we let $T_s = 0.011$ s, $r = 2$, $\mu = 0.08$, $\gamma = 0.08$, and $\nu_1 = \nu_2 = 10^{-3}$. Figure 3.11 shows the response y and control u for FD-HHC, TD-HHC and TD-AHHC. In this case, the response y with FD-HHC and TD-HHC diverge, whereas the response y with TD-AHHC converges to zero. Figure 3.12 shows the trajectory of the estimate $G_{1,k}$, which moves toward $G_{yu}(j\omega_1)$. The behavior of the estimate $G_{1,k}$ is in accordance with the statement of Proposition 3.2. \triangle

Example 3.4. Consider the SISO system, where we let $\psi_1 = u$, $\psi_2 = 0$, $d = 10 \sin \omega_1 t + 10 \cos \omega_1 t$, and $y = \phi_1 + v$, where v is a zero-mean Gaussian white noise with intensity $1 \text{ kN}^2/\text{m}^4$. Let $G_{1,0} = 5e^{j\frac{2\pi}{3}}G_{yu}(j\omega_1)$. We implement TD-AHHC for two different values of r . Let $T_s = 0.011$ s, $\mu = 0.06$, $\gamma = 0.2$, and $\nu_1 = \nu_2 = 10^{-3}$. The left-hand side of Fig. 3.13 shows the response y and control u for TD-AHHC with $r = 2$, whereas the right-hand side of Fig. 3.13 shows the response y and control u for TD-AHHC with $r = 10$. For both cases, TD-AHHC yields near-zero steady-state performance as $t \rightarrow \infty$; however, the transient response and the convergence time are improved with $r = 10$. \triangle

Example 3.5. Consider the MIMO ($m = 2$ and $\ell = 2$) system where we let $[\psi_1 \ \psi_2]^T = u$, $y = [\phi_1 \ \phi_2]^T$, and $d = 10 \sin \omega_1 t + 10 \cos \omega_2 t$, which is a two-tone disturbance. First, consider the case where $G_{i,0}$ are such that the TD-HHC stability condition is satisfied, that is $\Lambda \subset \text{ORHP}$. Specifically, we let $G_{i,0} = e^{j\frac{\pi}{3}}G_{yu}(j\omega_i)$. Figure 3.14 shows the response y and the control u for TD-HHC and TD-AHHC. Both TD-HHC and TD-AHHC yield asymptotic disturbance rejection.

Next, consider the case where $G_{i,0} = e^{2j\frac{\pi}{3}}G_{yu}(j\omega_i)$, which does not satisfy the TD-HHC stability condition, that is, $\Lambda \not\subset \text{ORHP}$. Figure 3.15 shows the response y and

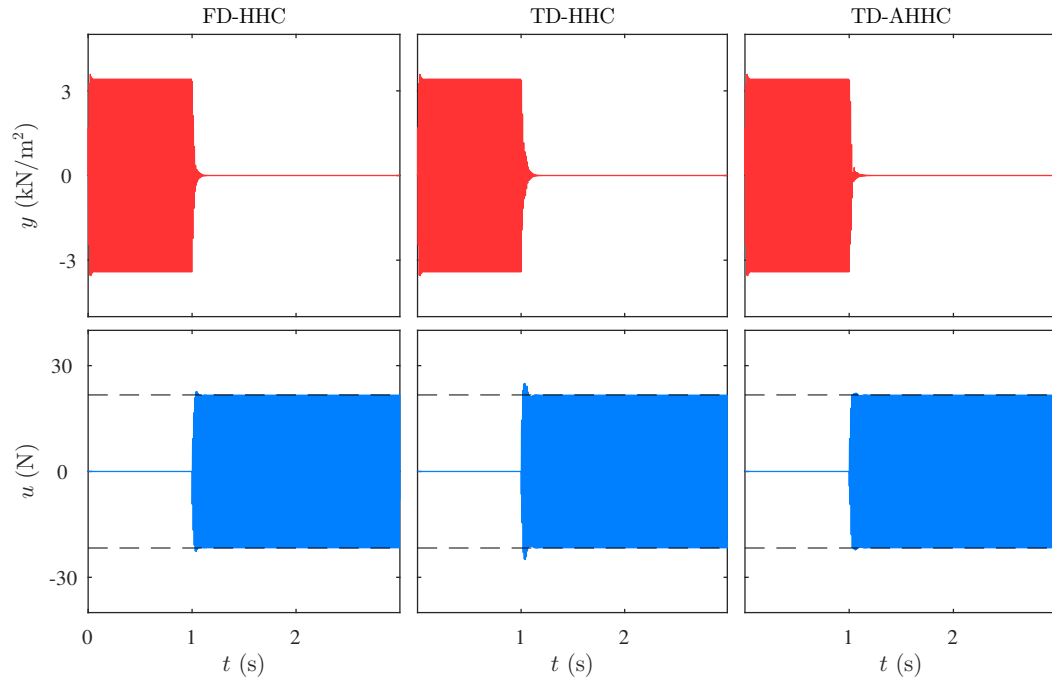


Figure 3.9: For a SISO system, where $G_{1,0}$ is 30° away from $G_{yu}(j\omega_1)$, FD-HHC, TD-HHC, and TD-AHHC yield $y(t) \rightarrow 0$ as $t \rightarrow \infty$, with approximately the same convergence time. The dashed lines show $\pm \|u_{1,*}\|$.

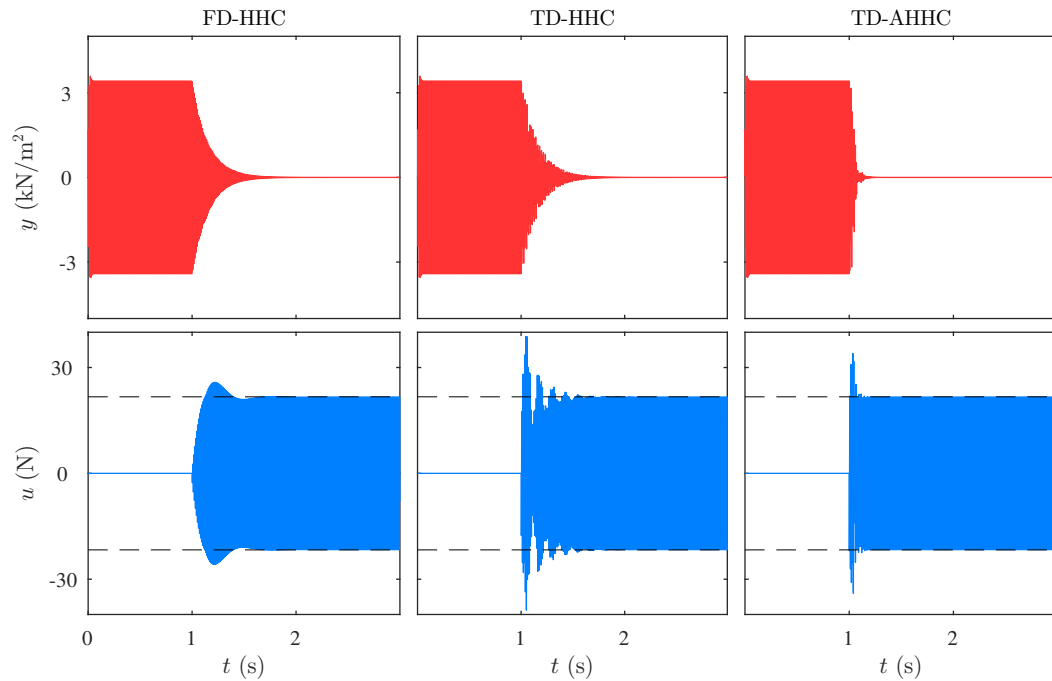


Figure 3.10: For a SISO system, where $G_{1,0}$ is 85° away from $G_{yu}(j\omega_1)$, FD-HHC, TD-HHC, and TD-AHHC yield $y(t) \rightarrow 0$ as $t \rightarrow \infty$; however, the convergence time with TD-AHHC is smaller than the convergence time with FD-HHC and TD-HHC. The dashed lines show $\pm \|u_{1,*}\|$.

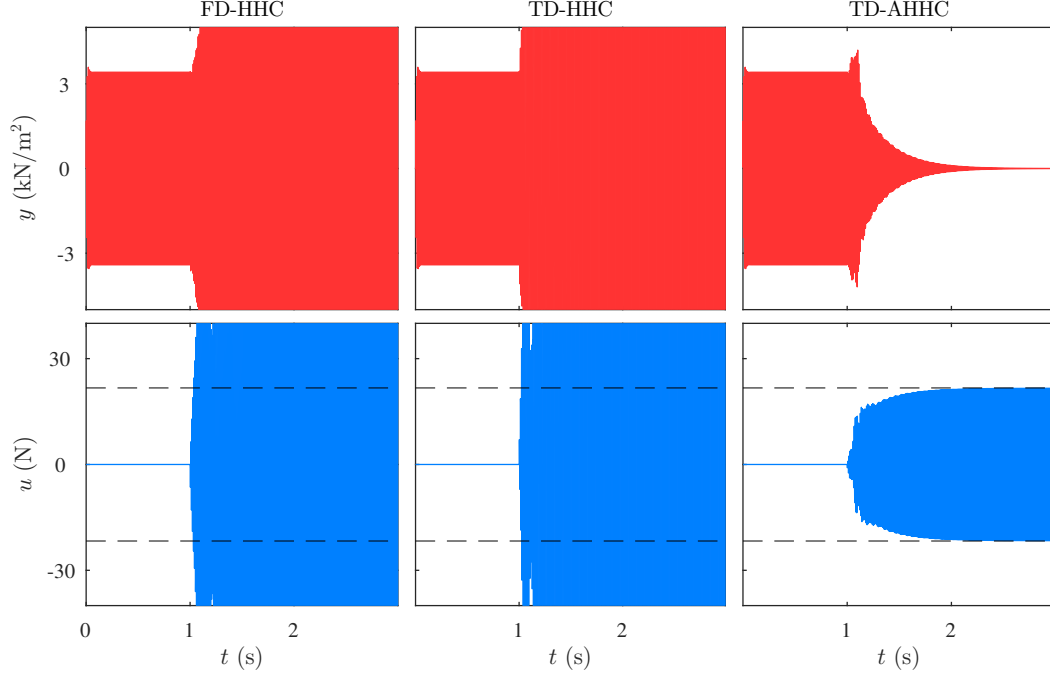


Figure 3.11: For a SISO system, where $G_{1,0}$ is not within 90° of $G_{yu}(j\omega)$, the response y with both FD-HHC and TD-HHC diverges, whereas TD-AHHC yields $y(t) \rightarrow 0$ as $t \rightarrow \infty$. The dashed lines show $\pm ||u_{1,*}||$.

control u for TD-HHC and TD-AHHC. In this case, the response y with TD-HHC diverges, whereas the response y with TD-AHHC converges to zero. \triangle

3.10 Results from Active Noise Control Experiments

We present results from an active noise control experiment to demonstrate TD-HHC and TD-AHHC. Figure 3.16 is a photograph of the experimental setup, and Fig. 3.17 shows a schematic of the experimental setup, where n_1 and n_2 are the horizontal and vertical axes of a fixed Cartesian frame. Disturbance speakers are located at $(-0.20, 0)$ m and $(0.20, 0)$ m, and these speakers generate disturbances d_1 and d_2 . Control speakers are located at $(-0.35, -0.25)$ m and $(0.35, -0.25)$ m, and these speakers generate control inputs ψ_1 and ψ_2 , which are determined by TD-HHC or TD-AHHC. Microphones are located at $(-0.03, -0.25)$ m and $(0.20, -0.30)$ m, and these microphones measure the pressures ξ_1 and ξ_2 , which are used as the measured performance y .

Measurement signals from the microphones are amplified by a SM Pro Audio PR8E microphone preamplifier. The four speakers are M-Audio AV42 2-way 4-in monitor speakers. The two microphones are Audio2000 1064BL vocal microphones. The controller is implemented on a dSPACE DS1103 controller board. Note that, we do not use any knowledge of the characteristics or locations of the experimental components to implement TD-HHC or TD-AHHC.

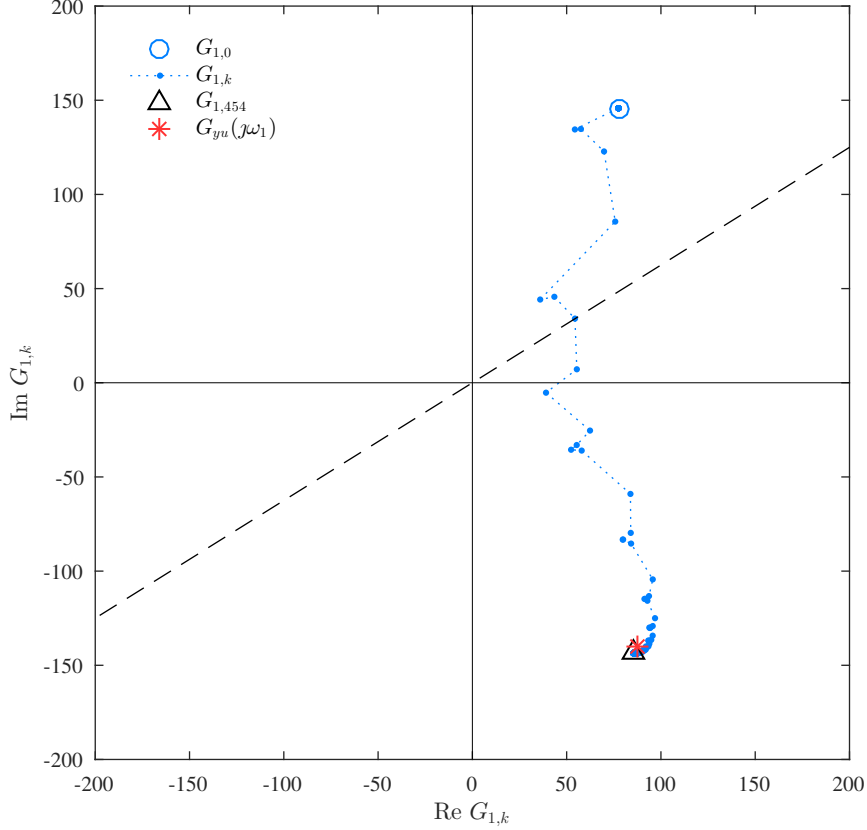


Figure 3.12: Trajectory of $G_{1,k}$ with TD-AHHC for a SISO system where $|\angle(G_{1,0}/G_{yu}(j\omega_i))| > \frac{\pi}{2}$. The dashed line shows the locus of G such that $|\angle(G/G_{yu}(j\omega_i))| = \frac{\pi}{2}$, which is FD-HCC and TD-HHC stability boundary for selection of $G_{1,e}$. Selecting $G_{1,e} = G_{1,0}$ from the upper region, where $|\angle(G_{1,e}/G_{yu}(j\omega_i))| > \frac{\pi}{2}$, results in an unstable response with FD-HCC and TD-HHC, whereas TD-AHHC moves the initial condition $G_{1,0}$ towards $G_{yu}(j\omega_1)$ and yields asymptotic disturbance rejection.

For all experiments, the controller is turned on at 5 s, $T_s = 0.05$ s, $u_{i,0} = 0$, $H_{i,e} = H_{i,0}$, and $H_{i,0}$ is given by (3.19), where $G_{i,0} \in \mathbb{C}^{\ell \times m}$. The initial condition $G_{i,0}$, and the gains ρ , μ and γ are specified in each experiment. For TD-AHHC, we let $\nu_1 = \nu_2 = 10^{-5}$. Let $u_m > 0$ be the maximum allowable magnitude for each control input. For all control speakers, $u_m = 447$ mV. Let $\omega_1 = 200\pi$ rad/s and $\omega_2 = 300\pi$ rad/s.

Experiment 3.1. Consider the SISO system, where $\psi_1 = u$, $\psi_2 = 0$, $y = \xi_1$, $d_1(t) = 0.15 \sin \omega_1 t$, and $d_2(t) = 0.15 \cos \omega_1 t$. Let $\rho = 1.4 \times 10^{-6}$, and $\mu = \gamma = 0.2$. We examine two initial conditions $G_{1,0}$, which have angles that are 180° apart. The 180° difference guarantees that one of the initial conditions satisfies the TD-HHC stability condition (i.e., $G_{1,0}$ is within 90° of $G_{yu}(j\omega_1)$), whereas the other initial condition does not satisfy the TD-HHC stability condition.

First, we let $G_{1,0} = -1.46 + j7.75$. Figure 3.18 shows y and u with TD-HHC and TD-AHHC. Both TD-HHC and TD-AHHC yield asymptotic disturbance rejection; however, the convergence time is improved with TD-AHHC.

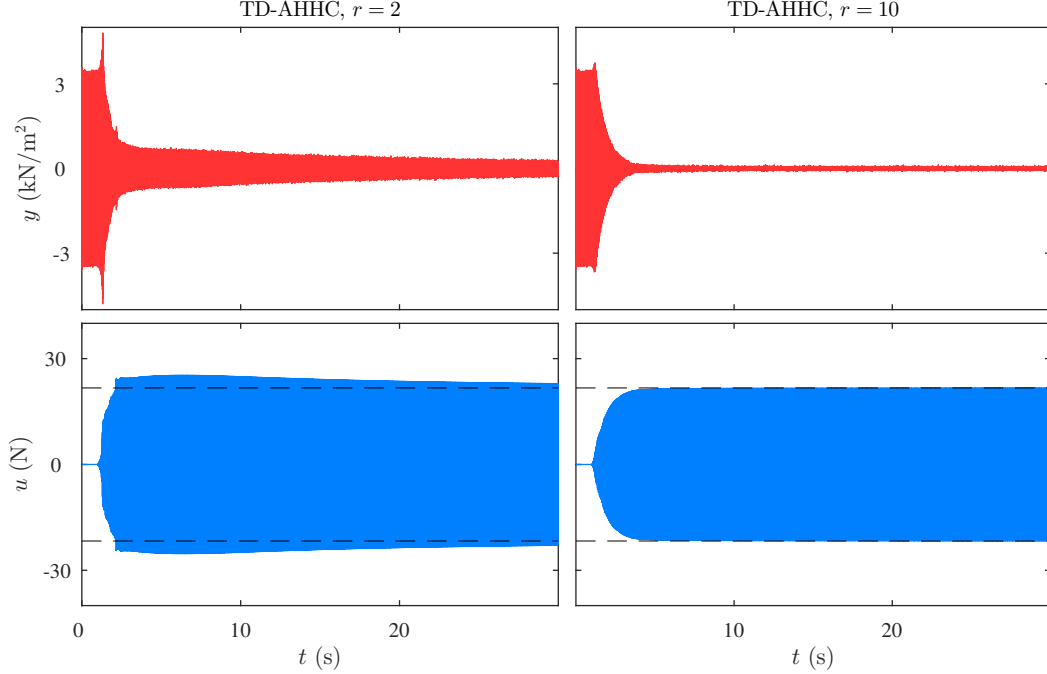


Figure 3.13: For a SISO system subject to measurement noise, TD-AHHC yields asymptotic disturbance rejection. Increasing the parameter r can improve the transient performance and the convergence time. The dashed lines show $\pm\|u_{1,*}\|$.

Next, we let $G_{1,0} = 1.46 - j7.75$. Figure 3.19 shows y and u with TD-HHC and TD-AHHC. The response y with TD-HHC diverges, while TD-AHHC yields asymptotic disturbance rejection. This suggests that the initial condition $G_{1,0} = 1.46 - j7.75$ does not satisfy the TD-HHC stability condition, whereas the initial condition $G_{1,0} = -1.46 + j7.75$ for the first case does satisfy the TD-HHC stability condition. \triangle

The following experiment investigates the robustness of TD-HHC and TD-AHHC to changes in the system dynamics. Specifically, the location of the control speaker changes during the experiment. TD-HHC is robust to sufficiently small changes, while TD-AHHC can adapt to all changes that happen in the location of the control speaker.

Experiment 3.2. Consider the SISO system, where $\psi_1 = u$, $\psi_2 = 0$, $y = \xi_1$, $d_1(t) = 0.15 \sin \omega_1 t$, and $d_2(t) = 0.15 \cos \omega_1 t$. Let $G_{1,0} = -1.46 + j7.75$, $\rho = 6 \times 10^{-7}$, $\mu = \gamma = 0.05$. Figures 3.20 and 3.21 show y and u with TD-HHC and TD-AHHC, respectively. Both TD-HHC and TD-AHHC yield disturbance attenuation after the control is turned on. At approximately $t = 20$ s, the location of control speaker is changed from $(-0.35, -0.25)$ m to $(-0.20, -0.25)$ m. Both controllers adapt to this change and yield disturbance attenuation. At approximately $t = 35$ s, the location of control speaker is again changed from $(-0.20, -0.25)$ m to $(-0.40, -0.37)$ m. TD-HHC cannot adapt to the second change, and the response y with TD-HHC diverges. However, TD-AHHC adapts to the second change as well as the first one, and yields disturbance attenuation. \triangle

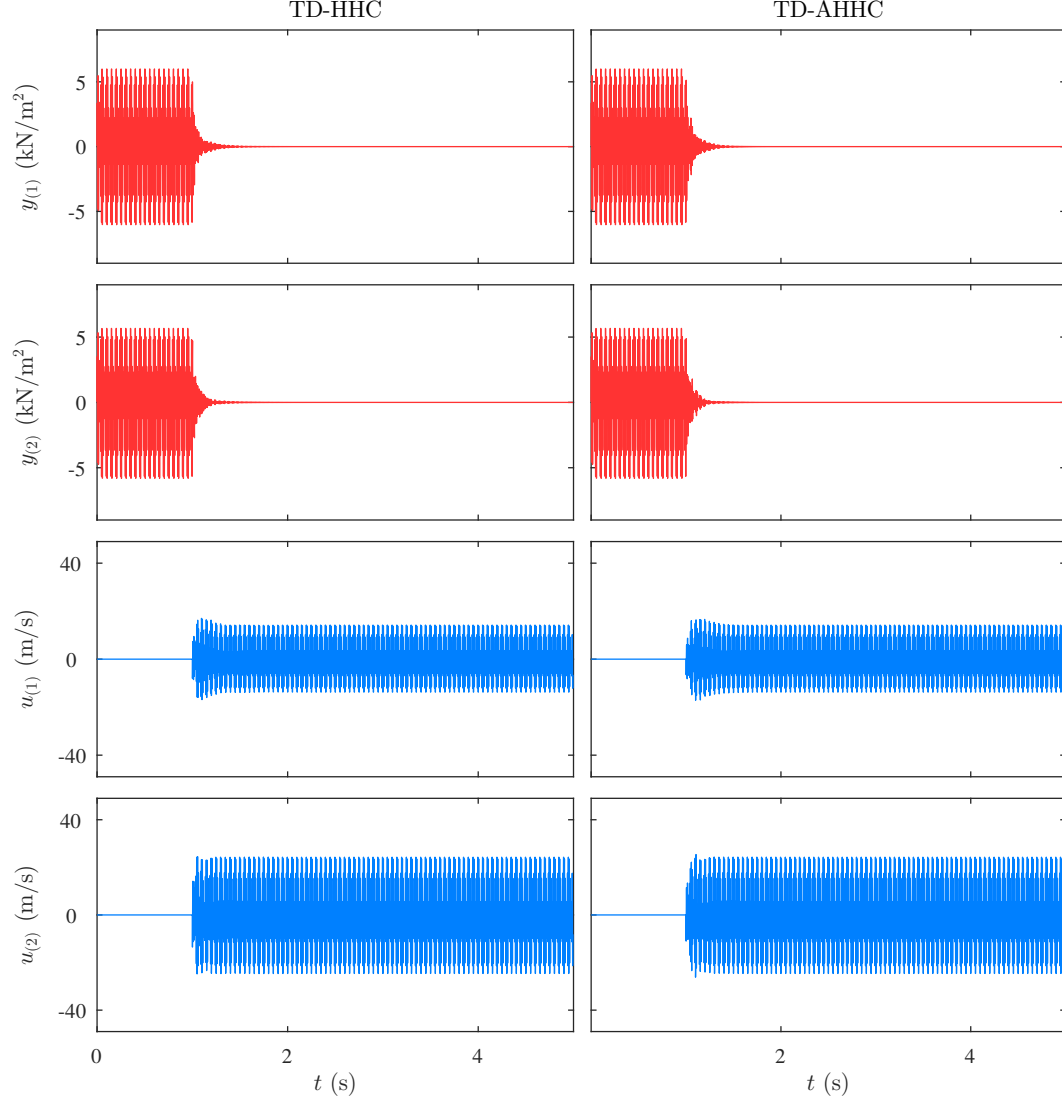


Figure 3.14: For a MIMO system subject to a multi-tone disturbance, where $G_{i,0}$ satisfies the condition $\Lambda \subset \text{ORHP}$, both TD-HHC and TD-AHHC yield $y(t) \rightarrow 0$ as $t \rightarrow \infty$.

The following experiment demonstrates that the choice of initial condition $G_{1,0}$ and gains ρ, μ , and γ affects the transient response of system with TD-HHC and TD-AHHC, and can cause actuator saturation.

Experiment 3.3. We reconsider the SISO system used in Experiment 3.1, but we let $d_1(t) = 0.28 \sin \omega_1 t$, and $d_2(t) = 0.28 \cos \omega_1 t$, and we use different initial condition and gains to implement TD-HHC and TD-AHHC. Specifically, we let $G_{1,0} = -5.73 + j5.41$, $\rho = 2.5 \times 10^{-6}$, $\mu = 0.25$, and $\gamma = 0.05$. Figure 3.22 shows y and u with TD-HHC and TD-AHHC. At multiple instances, the magnitude of $u_{1,k}$ determined by TD-HHC and TD-AHHC exceeds u_m , which saturates the control speaker. However, in this case, both TD-HHC and TD-AHHC yield near-zero steady-state performance. \triangle

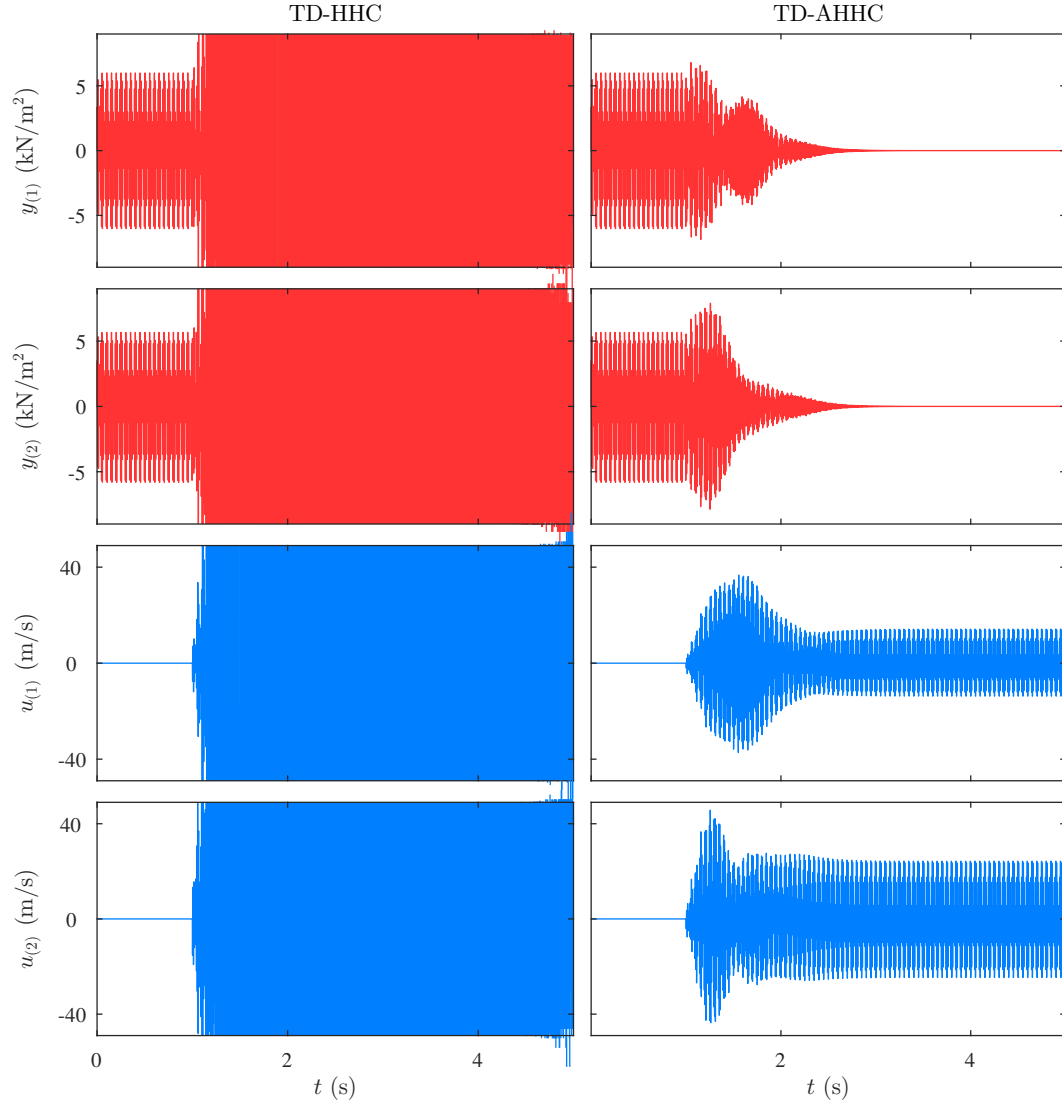


Figure 3.15: For a MIMO system subject to a multi-tone disturbance, where $G_{i,0}$ does not satisfy the condition $\Lambda \subset \text{ORHP}$, the response y with TD-HHC diverges, whereas TD-AHHC yields $y(t) \rightarrow 0$ as $t \rightarrow \infty$.

Experiment 3.3 demonstrates that the choice of initial condition $G_{i,0}$, and gains ρ , μ , and γ can cause actuator saturation. In Fig. 3.22, both TD-HHC and TD-AHHC yield near-zero steady-state performance despite actuator saturation during the transient. However, the following experiment demonstrates that actuator saturation can prevent disturbance rejection even if zero steady-state performance is achievable (i.e., $\|u_{i,*}\| < u_m$).

Experiment 3.4. We reconsider Experiment 3.3, but with we use different initial condition and gains to implement TD-AHHC. Specifically, we let $G_{1,0} = -5.73 + j5.41$, $\rho = 2.5 \times 10^{-6}$, $\mu = 0.25$, and $\gamma = 0.05$. Figure 3.23 shows y and u with TD-AHHC. At approximately $t = 9$ s, the magnitude of u exceeds u_m , which saturates the control speaker. In this case, TD-AHHC does not yield near-zero steady-state performance.

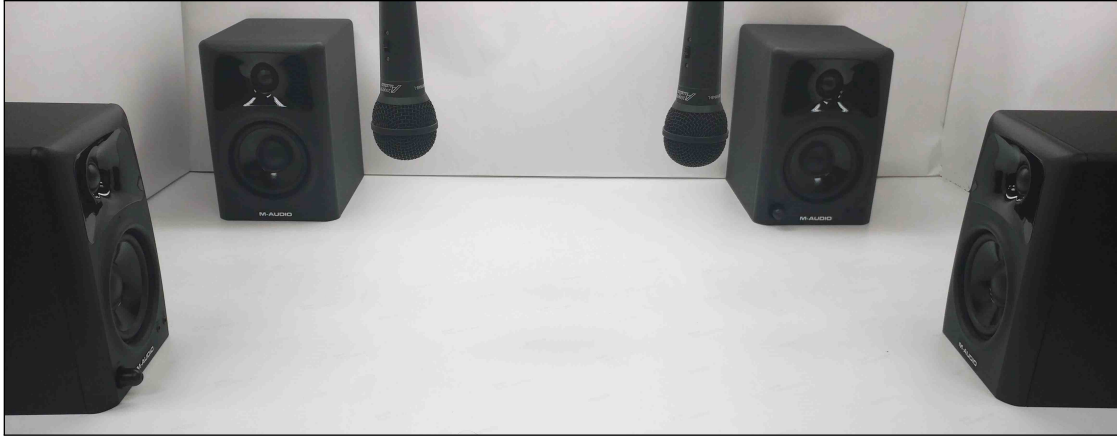


Figure 3.16: Photograph of the experimental setup.

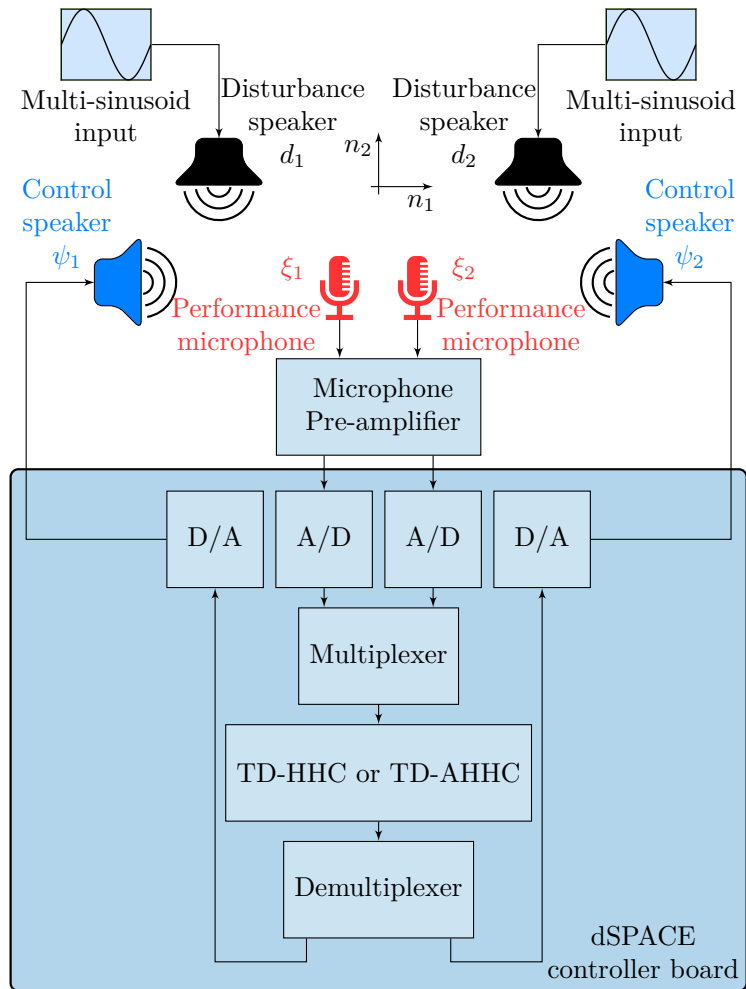


Figure 3.17: Schematic of the experimental setup.

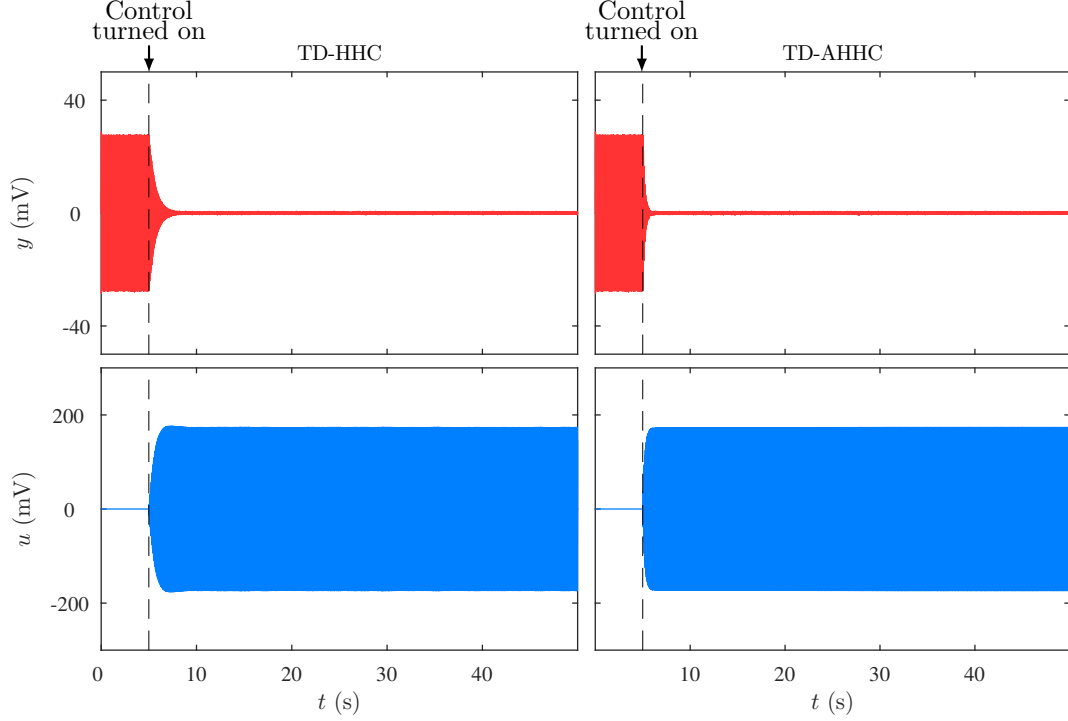


Figure 3.18: For a SISO system, and for a given $G_{1,0}$, both TD-HHC and TD-AHHC yield near-zero steady-state performance, which suggests that $G_{1,0}$ is within 90° of $G_{yu}(j\omega_1)$.

In this case, note that Experiment 3.3 implies that perfect asymptotic disturbance rejection is possible because $\|u_{1,*}\| < u_m$. However, the transient response causes actuator saturation, which prevents $u_{1,k}$ from converging to $u_{1,*}$. \triangle

Experiment 3.4 demonstrates that actuator saturation can prevent disturbance rejection, even if disturbance rejection is achievable (i.e., $\|u_{1,*}\| < u_m$). To address this shortcoming, we present a modified version of TD-AHHC. Specifically, we present a modification to the update equation for $u_{i,k}$.

For all $k \in \mathbb{N}$, consider the update equations for $u_{i,k}$ given by

$$u_{i,k+1} = \begin{cases} \frac{\theta_{i,k+1}}{\alpha_{k+1}} u_m, & \text{if } \alpha_{k+1} > u_m, \\ \theta_{i,k+1}, & \text{otherwise,} \end{cases} \quad (3.20)$$

where for all $k \in \mathbb{N}$,

$$\theta_{i,k+1} \triangleq u_{i,k} - \frac{\mu}{\nu_1 + \sum_{i=1}^q \|H_{i,k}\|_F^2} H_{i,k}^T (f_{i,k+1} \otimes I_\ell) y_{k+1}, \quad (3.21)$$

$$\alpha_{k+1} \triangleq \max_{j \in \{1, \dots, m\}} \sum_{i=1}^q \|E_j \theta_{i,k+1}\|, \quad (3.22)$$

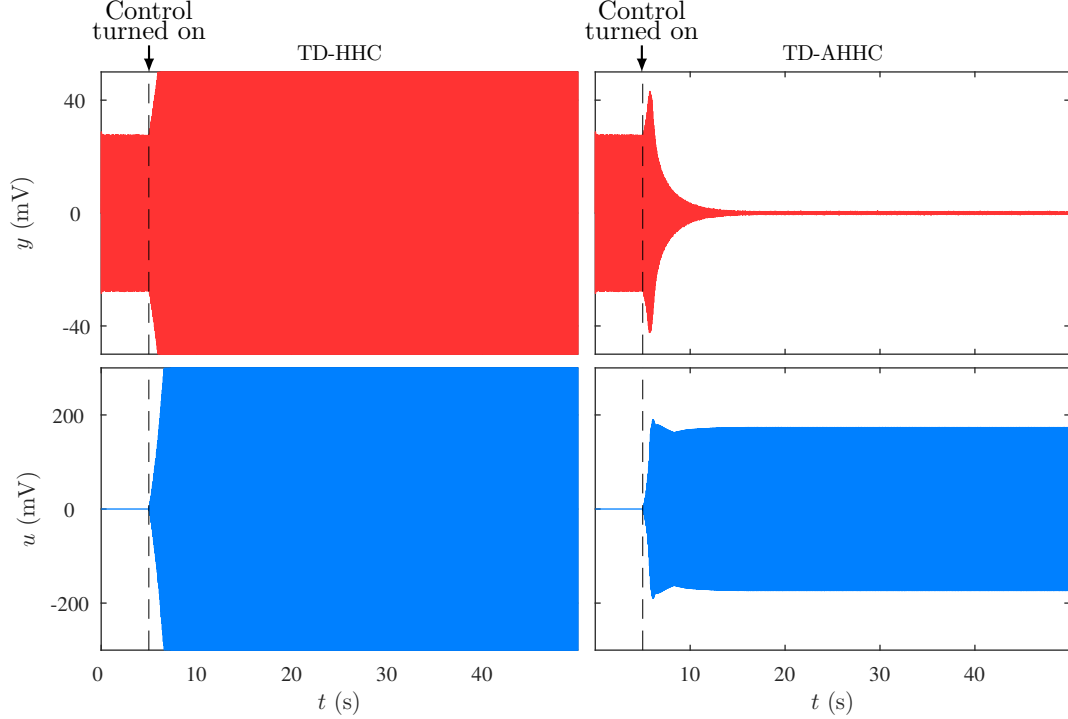


Figure 3.19: For the same SISO system as in Fig. 3.18, but with an initial condition $G_{1,0}$ that is 180° from the initial condition used to obtain Fig. 3.18, the response y with TD-HHC diverges, which suggests that $G_{1,0}$ is not within 90° of $G_{yu}(\omega_1)$. In contrast, TD-AHHC yields near-zero steady-state performance.

and for all $j \in \{1, 2, \dots, m\}$,

$$E_j \triangleq \begin{bmatrix} e_j & 0_{1 \times m} \\ 0_{1 \times m} & e_j \end{bmatrix} \in \mathbb{R}^{2 \times 2m}, \quad (3.23)$$

where $e_j \in \mathbb{R}^{1 \times m}$ denotes the j th row of I_m . Thus, the modified TD-AHHC is given by (3.4) and (3.14)–(3.18), and (3.20)–(3.23).

Experiment 3.5. We revisit Experiment 3.4 with modified TD-AHHC. Figure 3.24 shows y and u with modified TD-AHHC. In contrast to the results with TD-AHHC (i.e., shown in Fig. 3.23), modified TD-AHHC yields near-zero steady-state performance. \triangle

Numerical simulations suggest that modified TD-AHHC can improve the transient response and the convergence rate. We also present a modified version of TD-HHC. Similar to the modified TD-AHHC, we present a modification to the $u_{i,k}$ update equation of TD-HHC.

For all $k \in \mathbb{N}$, define

$$\theta_{i,k+1} \triangleq u_{i,k} - \rho H_{i,e}^T (f_{i,k+1} \otimes I_\ell) y_{k+1}. \quad (3.24)$$

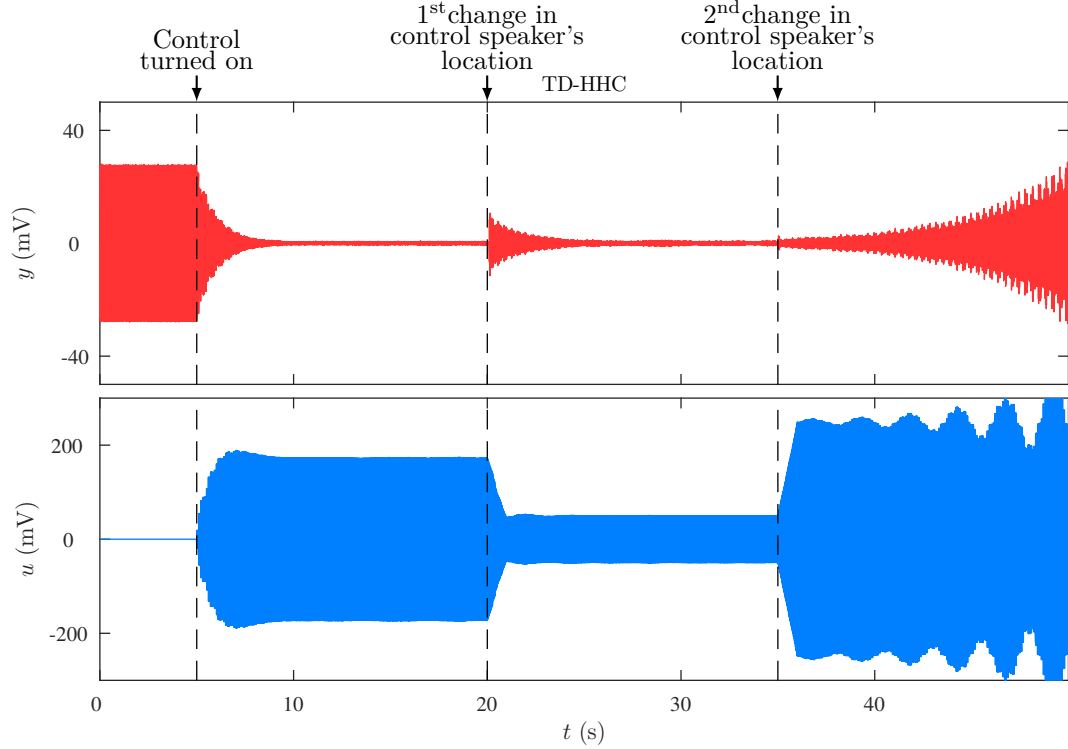


Figure 3.20: TD-HHC can accommodate sufficiently small changes in control speaker location, and yields disturbance attenuation. If the changes in control speaker location are not sufficiently small, TD-HHC does not achieve disturbance attenuation.

Then, modified TD-HHC is given by (3.4), (3.20), and (3.22)–(3.24). Note that, for both modified TD-HHC and modified TD-AHHC, it follows from (3.4), (3.20), and (3.22) that

$$\begin{aligned}
 \max_{t \in [kT_s, (k+1)T_s)} u_{(j)}(t) &\leq \sum_{i=1}^q \|E_j u_{i,k}\| \\
 &= \begin{cases} \frac{\sum_{i=1}^q \|E_j \theta_{i,k}\|}{\alpha_k} u_m, & \text{if } \alpha_k > u_m, \\ \sum_{i=1}^q \|E_j \theta_{i,k}\|, & \text{otherwise} \end{cases} \\
 &< u_m.
 \end{aligned}$$

Therefore, the maximum value of each channel of control at each time step (i.e., $\max_{t \in [kT_s, (k+1)T_s)} u_{(j)}(t)$) is less than u_m with both modified algorithms. Thus, both modified TD-HHC and modified TD-AHHC guarantee that the controls do not saturate.

Experiment 3.6. We revisit Experiment 3.3 with modified TD-HHC and modified TD-AHHC. Figure 3.25 shows y and u with modified TD-HHC and modified TD-AHHC. The transient response and the convergence time are improved compared to the results of Experiment 3.3 shown in Fig. 3.22. In fact, numerical simulations

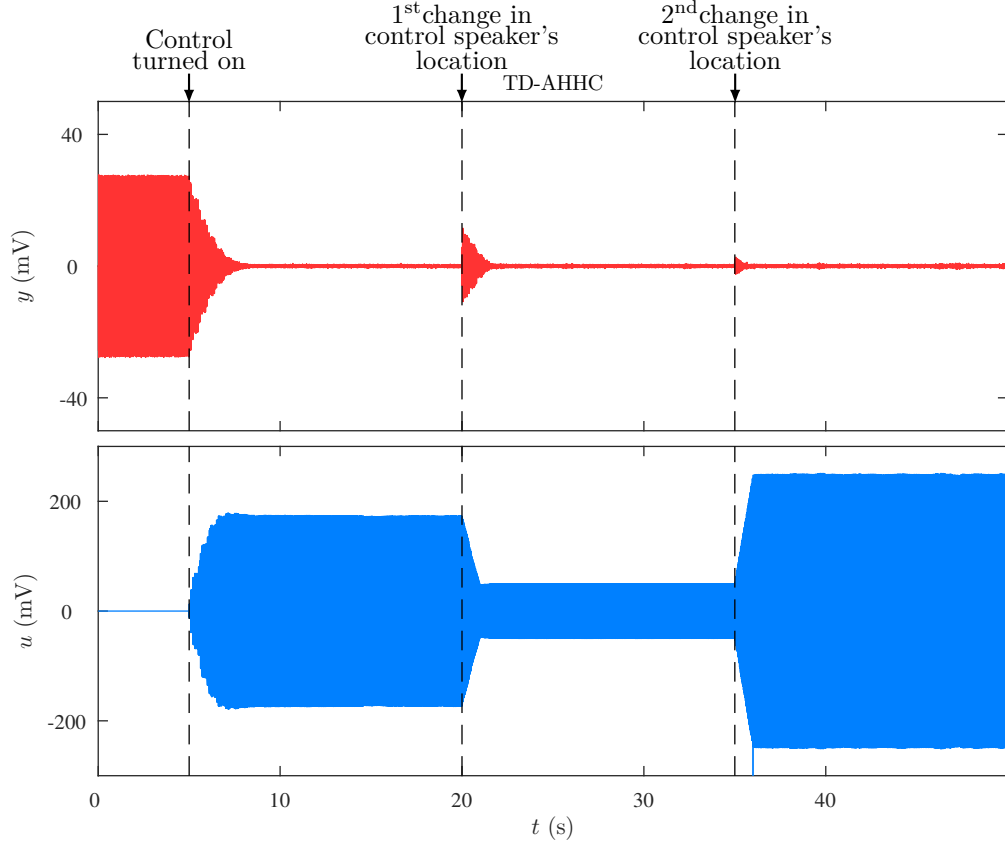


Figure 3.21: TD-AHHC adapts to changes in control speaker location, and yields disturbance attenuation.

suggest that modified TD-HHC and modified TD-AHHC improve transient response and convergence time in general. \triangle

In the following experiment, we use TD-HHC and TD-AHHC to reject a two-tone disturbance acting on a MIMO system.

Experiment 3.7. Consider the MIMO system, where $y = [\xi_1 \ \xi_2]^T$ and $[\psi_1 \ \psi_2]^T = u$. The two-tone disturbances are $d_1(t) = 0.2 \cos \omega_1 t + 0.2 \sin \omega_2 t$ and $d_2(t) = 0.15 \cos \omega_1 t + 0.15 \sin \omega_2 t$. Let $\rho =$, $\mu =$, and $\gamma =$. First, we let $G_{1,0} = G_{2,0} = \bar{G}$, where

$$\bar{G} = \begin{bmatrix} 0.42 + j0.07 & 0.35 + j0.02 \\ -0.05 + j0.02 & 0.68 + j0.09 \end{bmatrix}.$$

Figure 3.26 shows that both TD-HHC and TD-AHHC yield asymptotic disturbance rejection, which suggest that the initial conditions $G_{1,0}$ and $G_{2,0}$ satisfy the TD-HHC stability condition. Next, we let $G_{1,0} = G_{2,0} = -\bar{G}$. Figure 3.27 shows that the response y with TD-HHC diverges, while TD-AHHC yields asymptotic disturbance rejection. This suggests that the initial conditions $G_{1,0} = G_{2,0} = -\bar{G}$ do not satisfy the TD-HHC stability condition. \triangle

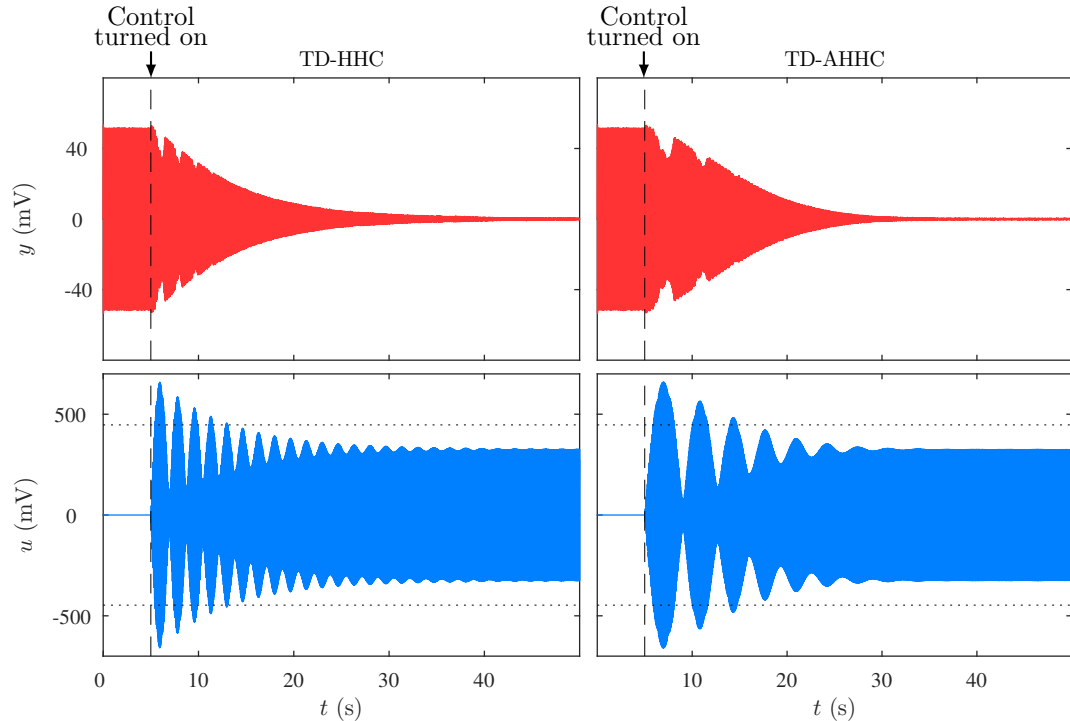


Figure 3.22: TD-HHC and TD-AHHC can cause actuator saturation during the transient. However, in this case, both TD-HHC and TD-AHHC yield near-zero steady-state performance. The dotted lines show $\pm u_m$

3.11 Conclusions

We presented TD-HHC and TD-AHHC which are new adaptive controllers in time domain that are effective for rejecting sinusoidal disturbances with known frequencies that act on an asymptotically stable MIMO LTI system.

TD-HHC is effective for uncertain LTI systems, and requires an estimate of the control-to-performance transfer function evaluated at the disturbance frequencies. However, TD-AHHC is effective for completely unknown LTI systems. We analyzed the stability and performance of TD-HHC and TD-AHHC. For both TD-HHC and TD-AHHC, we showed that the controller asymptotically rejects the disturbance.

We presented numerical simulations comparing TD-HHC and TD-AHHC with FD-HHC, which is an existing sinusoidal disturbance rejection method in the frequency domain. We also presented results from an active disturbance rejection experiment in an acoustic environment. These experimental results demonstrated the practical effectiveness of both TD-HHC and TD-AHHC.

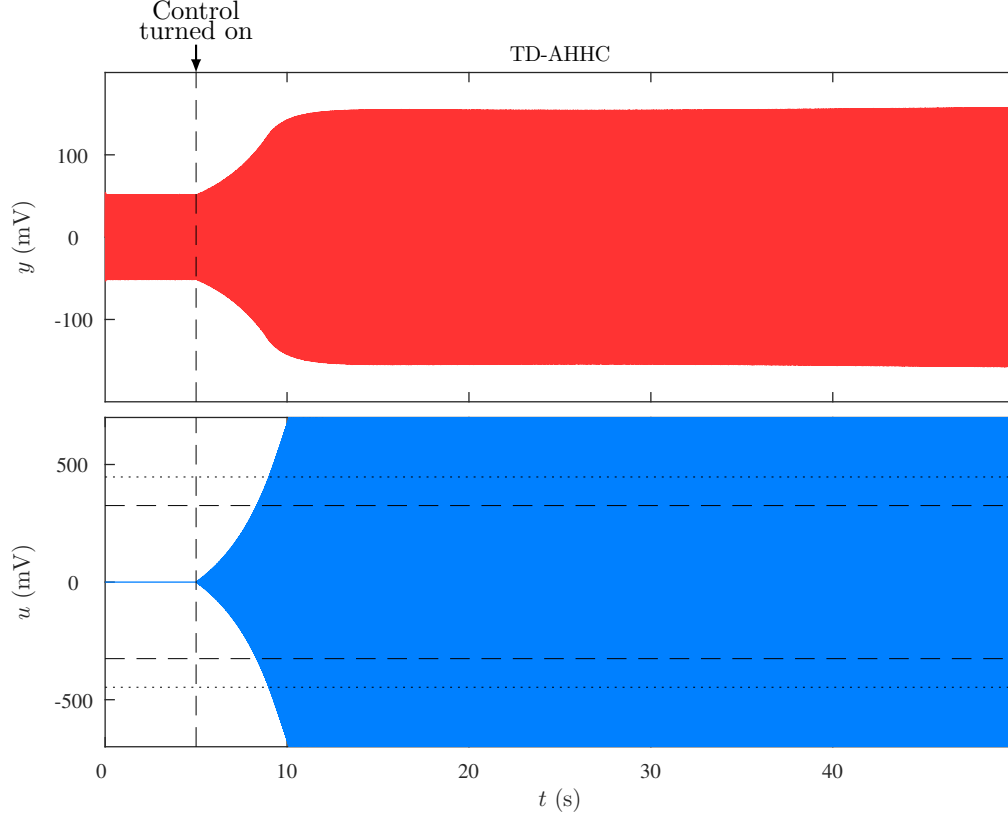


Figure 3.23: TD-AHHC causes actuator saturation during the transient. Perfect asymptotic disturbance rejection is not achieved even though $\|u_{1,*}\| < \|u_m\|$. The dotted lines show $\pm u_m$, and the dashed lines show $\pm \|u_{1,*}\|$.

3.12 Proof of Proposition 3.1

Proof. For all $k \in \mathbb{Z}^+$, define $\bar{y}_{i,k} \in \mathbb{R}^{2\ell}$ by $\bar{y}_{i,k} \triangleq H_{i,*}u_{i,k-1} + d_{i,*}$, and it follows that for all $k \in \mathbb{Z}^+$,

$$\bar{y}_{i,k+1} - \bar{y}_{i,k} = H_{i,*}(u_{i,k} - u_{i,k-1}). \quad (3.25)$$

Multiplying (3.10) by $H_{i,*}$ and using (3.25) implies that for all $k \in \mathbb{Z}^+$,

$$\bar{y}_{i,k+1} = \bar{y}_{i,k} - \rho H_{i,*} H_{i,e}^T (f_{i,k} \otimes I_\ell) y_k. \quad (3.26)$$

For all $k \in \mathbb{Z}^+$, define

$$\bar{Y}_k \triangleq [\bar{y}_{1,k}^T \ \cdots \ \bar{y}_{q,k}^T]^T \in \mathbb{R}^{2\ell q}, \quad f_k \triangleq [f_{1,k}^T \ \cdots \ f_{q,k}^T]^T \in \mathbb{R}^{2q},$$

and using (3.26), it follows that

$$\bar{Y}_{k+1} = \bar{Y}_k - \rho \mathcal{D}_H (f_k \otimes I_\ell) y_k, \quad (3.27)$$

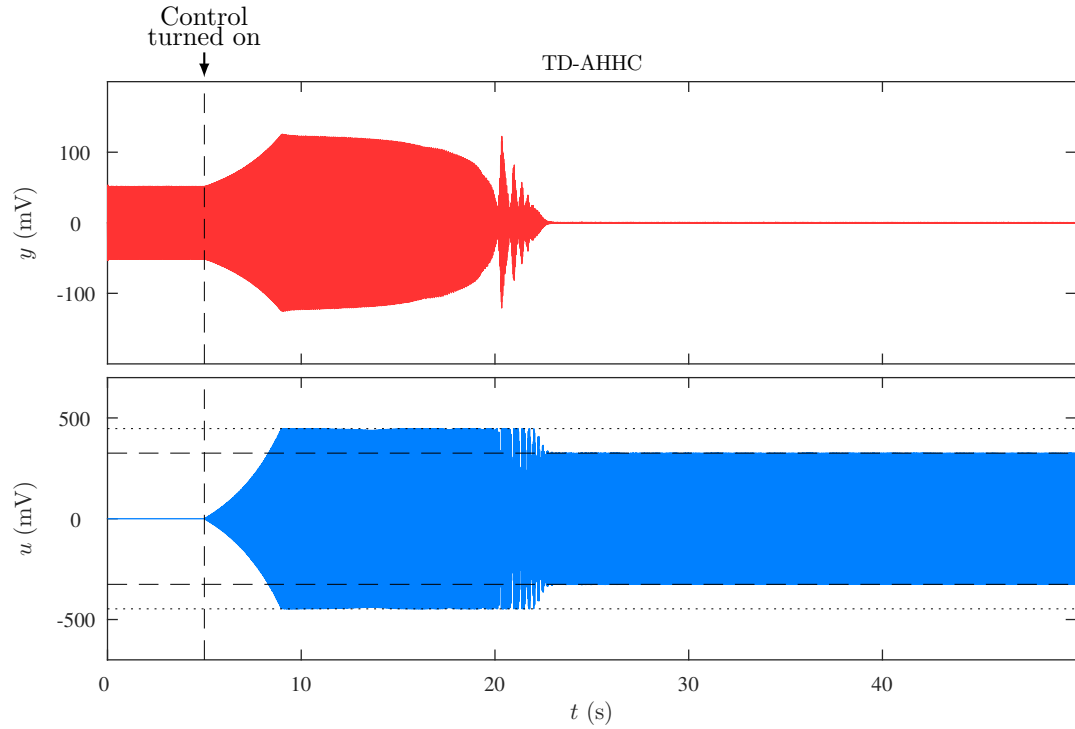


Figure 3.24: Modified TD-AHHC yields near-zero steady-state performance despite actuator saturation. The dotted lines show $\pm u_m$, and the dashed lines show $\pm \|u_{1,*}\|$.

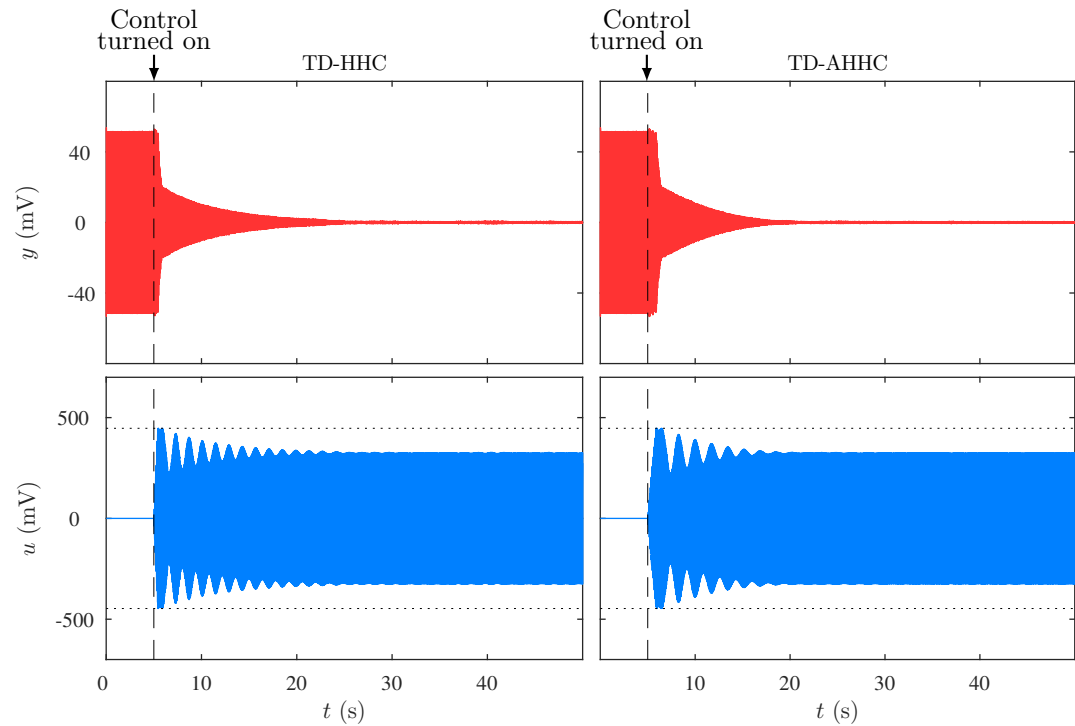


Figure 3.25: For the same SISO system used to obtain Fig. 3.22, modified TD-HHC and modified TD-AHHC improve the transient response and convergence rate. The dotted lines show $\pm u_m$

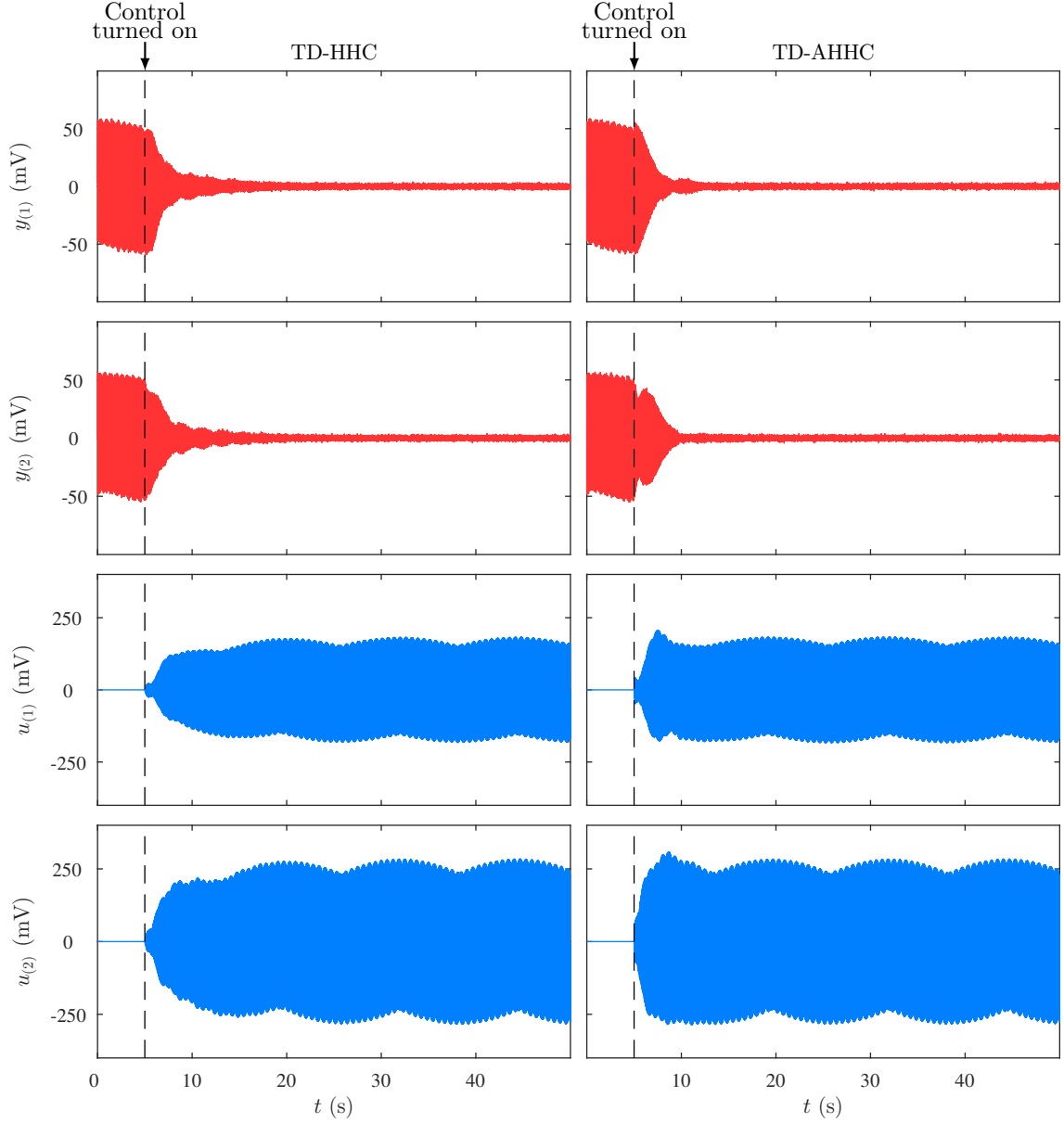


Figure 3.26: For a MIMO system subject to a two-tone disturbance, and for given $G_{1,0}$ and $G_{2,0}$, both TD-HHC and TD-AHHC yield asymptotic disturbance rejection.

where

$$\mathcal{D}_H \triangleq \text{diag}(H_{1,*}H_{1,e}^T, \dots, H_{q,*}H_{q,e}^T) \in \mathbb{R}^{2\ell q \times 2\ell q}.$$

Note that, it follows from (3.27) that for all $k \in \mathbb{Z}^+$, and all $\alpha \in \{0, 1, \dots, k-1\}$,

$$\bar{Y}_{k+1} = \bar{Y}_{k-\alpha} - \rho \mathcal{D}_H \sum_{s=0}^{\alpha} (f_{k-s} \otimes I_\ell) y_{k-s}. \quad (3.28)$$

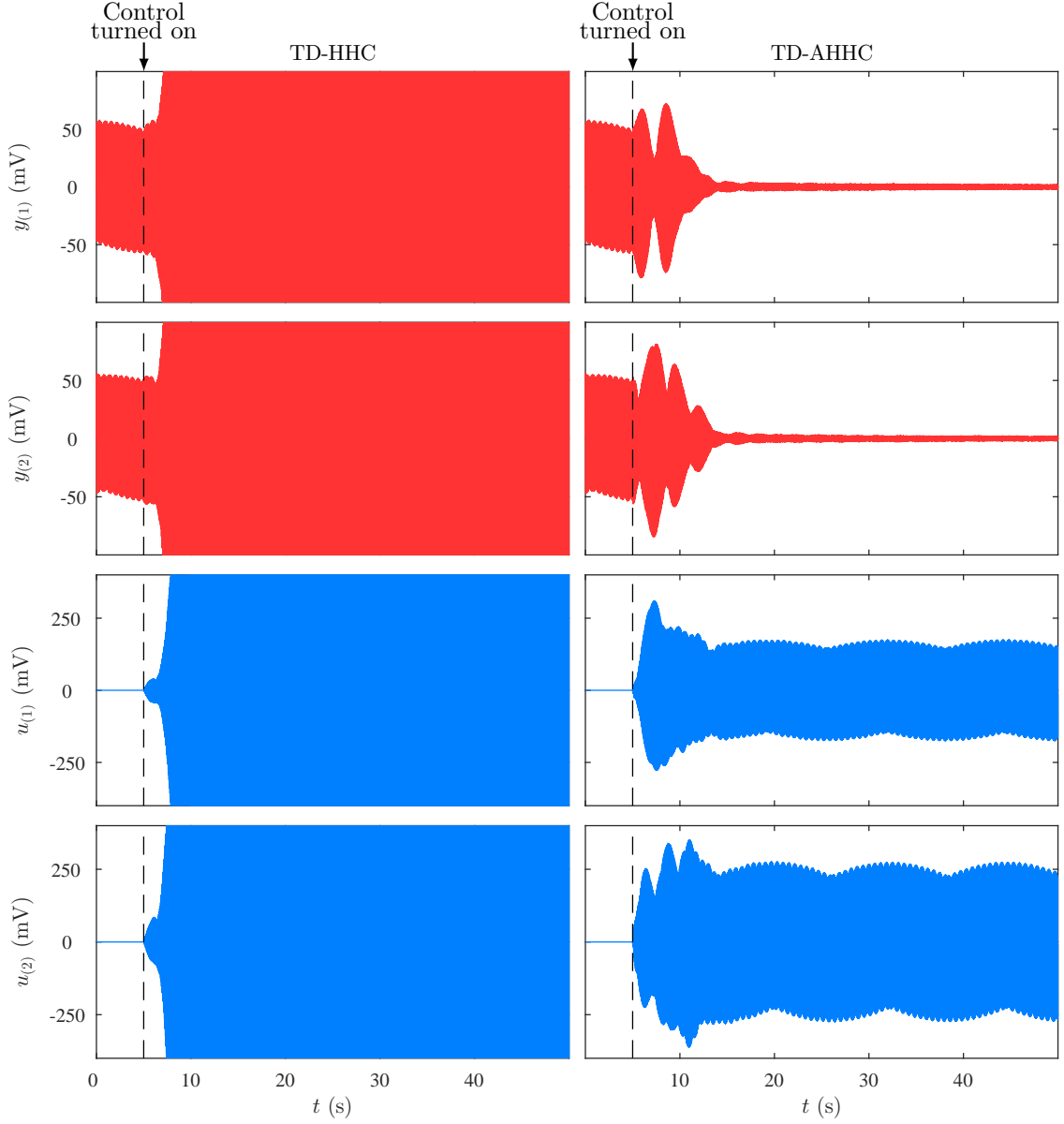


Figure 3.27: For the same MIMO system as in Fig. 3.26, but with initial conditions $G_{1,0}$ and $G_{2,0}$ that are negative of those initial conditions used to obtain Fig. 3.26, the response y with TD-HHC diverges, while TD-AHHC yields near-zero steady-state performance.

Multiplying (3.28) by $f_{k-\alpha}^T \otimes I_\ell$, using (3.8), and using Lemma 3.3 in Section 3.17 yield that for all $k \in \mathbb{Z}^+$, and all $\alpha \in \{0, 1, \dots, k-1\}$,

$$\begin{aligned}
(f_{k-\alpha}^T \otimes I_\ell) \bar{Y}_{k+1} &= y_{k-\alpha} - \rho (f_{k-\alpha}^T \otimes I_\ell) \mathcal{D}_H \sum_{s=0}^{\alpha} (f_{k-s} \otimes I_\ell) y_{k-s} \\
&= y_{k-\alpha} - \rho \operatorname{Re} \sum_{s=0}^{\alpha} \left(\sum_{i=1}^q e^{j(s-\alpha)\omega_i T_s} G_{i,*} G_{i,e}^* \right) y_{k-s}. \tag{3.29}
\end{aligned}$$

Considering (3.29) for each $k \geq 2q$ and all $\alpha \in \{0, 1, \dots, k-1\}$, and stacking up yield that for all $k \geq 2q$,

$$(F_k^T \otimes I_\ell) \bar{Y}_{k+1} = (I_{2\ell q} - \rho R) Y_k \quad (3.30)$$

where for all $k \geq 2q$,

$$F_k \triangleq \begin{bmatrix} f_k & \cdots & f_{k-2q+1} \end{bmatrix} \in \mathbb{R}^{2q \times 2q}.$$

Since (A3.3) and (A3.4) are satisfied, it follows from Lemma 3.2 in Section 3.7 that F_k is invertible, and for all $k \geq 2q$,

$$F_k^{-1} = V^{-1} S_k,$$

where

$$S_{i,k} \triangleq \begin{bmatrix} e^{-jk\omega_i T_s} & j e^{-jk\omega_i T_s} \\ e^{jk\omega_i T_s} & -j e^{jk\omega_i T_s} \end{bmatrix} \in \mathbb{C}^{2 \times 2}, \quad S_k \triangleq \text{diag}(S_{1,k}, \dots, S_{q,k}) \in \mathbb{C}^{2q \times 2q}.$$

Thus, multiplying (3.30) by $(f_{k+1}^T F_k^{-T}) \otimes I_\ell$, and using (3.8) yield that for all $k \geq 2q$,

$$\begin{aligned} y_{k+1} &= \left((f_{k+1}^T S_k^T V^{-T}) \otimes I_\ell \right) (I_{2\ell q} - \rho R) Y_k \\ &= \left((v V^{-T}) \otimes I_\ell \right) (I_{2\ell q} - \rho R) Y_k, \end{aligned}$$

which implies (3.11). □

3.13 Proof of Theorem 3.2

Proof. Let $u_{i,0} \in \mathbb{R}^{2m}$. For all $k \in \mathbb{Z}^+$, define $\bar{y}_{i,k} \in \mathbb{R}^{2\ell}$ by $\bar{y}_{i,k} \triangleq H_{i,*} u_{i,k-1} + d_{i,*}$, and it follows that for all $k \in \mathbb{Z}^+$,

$$\bar{y}_{i,k+1} - \bar{y}_{i,k} = H_{i,*} (u_{i,k} - u_{i,k-1}). \quad (3.31)$$

Multiplying (3.10) by $H_{i,*}$ and using (3.31) implies that for all $k \in \mathbb{Z}^+$,

$$\bar{y}_{i,k+1} = \bar{y}_{i,k} - \rho H_{i,*} H_{i,e}^T (f_{i,k} \otimes I_\ell) y_k. \quad (3.32)$$

For all $k \in \mathbb{Z}^+$, define

$$\bar{Y}_k \triangleq \begin{bmatrix} \bar{y}_{1,k}^T & \cdots & \bar{y}_{q,k}^T \end{bmatrix}^T \in \mathbb{R}^{2\ell q}.$$

Since (A3.3) is satisfied, using (3.8), it follows from (3.32) that

$$\bar{Y}_{k+1} = A_k \bar{Y}_k, \quad (3.33)$$

where for all $k \in \mathbb{Z}^+$,

$$A_k \triangleq I_{2\ell q} - \rho \mathcal{D}_H \Omega_k \in \mathbb{R}^{2\ell q \times 2\ell q},$$

and

$$\begin{aligned} \mathcal{D}_H &\triangleq \text{diag}(H_{1,*} H_{1,e}^T, \dots, H_{q,*} H_{q,e}^T) \in \mathbb{R}^{2\ell q \times 2\ell q}, \\ \Omega_k &\triangleq (f_k f_k^T) \otimes I_\ell \in \mathbb{R}^{2\ell q \times 2\ell q}, \quad f_k \triangleq \begin{bmatrix} f_{1,k}^T & \cdots & f_{q,k}^T \end{bmatrix}^T \in \mathbb{R}^{2q}. \end{aligned}$$

Note that since $\omega_i T_s / 2\pi$ is a rational number, it follows that N exist. For all $k \in \mathbb{Z}^+$, define

$$\Phi_k \triangleq A_{k+N-1} A_{k+N-2} \cdots A_k,$$

and it follows from direct calculations that

$$\Phi_1 = I_{2\ell q} - \rho \mathcal{D}_H \sum_{j=1}^N \Omega_j + \sum_{j=2}^N \sum_{1 \leq s_1 < s_2 < \cdots < s_j \leq N} (-\rho)^j \mathcal{D}_H \Omega_{s_j} \cdots \mathcal{D}_H \Omega_{s_2} \mathcal{D}_H \Omega_{s_1}. \quad (3.34)$$

Moreover, note that for all $i_1, i_2 \in Q$,

$$\begin{aligned} \sum_{j=1}^N (\cos j\omega_{i_1} T_s) (\cos j\omega_{i_2} T_s) &= \sum_{j=1}^N (\sin j\omega_{i_1} T_s) (\sin j\omega_{i_2} T_s) = \begin{cases} 0, & \text{if } i_1 \neq i_2, \\ \frac{N}{2}, & \text{if } i_1 = i_2, \end{cases} \\ \sum_{j=1}^N (\cos j\omega_{i_1} T_s) (\sin j\omega_{i_2} T_s) &= 0, \end{aligned}$$

which imply that for all $i_1, i_2 \in Q$,

$$\sum_{j=1}^N f_{i_1,k} f_{i_2,k}^T = \begin{cases} 0, & \text{if } i_1 \neq i_2, \\ \frac{N}{2} I_2, & \text{if } i_1 = i_2. \end{cases} \quad (3.35)$$

Using (3.35), it follows that

$$\begin{aligned} \sum_{j=1}^N \Omega_j &= \sum_{j=1}^N (f_j f_j^T) \otimes I_\ell \\ &= \sum_{j=1}^N \begin{bmatrix} f_{1,j} f_{1,j}^T & \cdots & f_{1,j} f_{q,j}^T \\ \vdots & \ddots & \vdots \\ f_{q,j} f_{1,j}^T & \cdots & f_{q,j} f_{q,j}^T \end{bmatrix} \\ &= \frac{N}{2} I_{2\ell q}. \end{aligned} \quad (3.36)$$

Substituting (3.36) into (3.34) yields

$$\Phi_1 = I_{2\ell q} - \frac{\rho N}{2} \mathcal{D}_H + \sum_{j=2}^N \sum_{1 \leq s_1 < s_2 < \dots < s_j \leq N} (-\rho)^j \mathcal{D}_H \Omega_{s_j} \cdots \mathcal{D}_H \Omega_{s_2} \mathcal{D}_H \Omega_{s_1}. \quad (3.37)$$

Note that for all $k \in \mathbb{N}$, $\sigma_{\max}(\Omega_k) = \sigma_{\max}(f_k f_k^T) = \sigma_{\max}(f_k^T f_k) = q$. Moreover, note that for all $X, Y \in \mathbb{R}^{n \times n}$, $\text{sprad}(X + Y) \leq \sigma_{\max}(X + Y) \leq \sigma_{\max}(X) + \sigma_{\max}(Y)$, and $\sigma_{\max}(XY) \leq \sigma_{\max}(X) \sigma_{\max}(Y)$ [207, Fact 5.12.2]. Thus, it follows from (3.37) that

$$\begin{aligned} \text{sprad}(\Phi_1) &\leq \sigma_{\max}\left(I_{2\ell q} - \frac{\rho N}{2} \mathcal{D}_H\right) + \sigma_{\max}(S) \\ &\leq \sigma_{\max}\left(I_{2\ell q} - \frac{\rho N}{2} \mathcal{D}_H\right) \\ &\quad + \sum_{j=2}^N \rho^j \sigma_{\max}^j(\mathcal{D}_H) \sum_{1 \leq s_1 < s_2 < \dots < s_j \leq N} \sigma_{\max}(\Omega_{s_j}) \cdots \sigma_{\max}(\Omega_{s_2}) \sigma_{\max}(\Omega_{s_1}) \\ &\leq \sigma_{\max}\left(I_{2\ell q} - \frac{\rho N}{2} \mathcal{D}_H\right) + \sum_{j=2}^N \rho^j (\sigma_{\max}(\mathcal{D}_H))^j \frac{N! q^j}{(N-j)!}. \end{aligned} \quad (3.38)$$

Moreover, note that

$$\text{spec}(\mathcal{D}_H) = \bigcup_{i \in Q} \text{spec}(H_{i,*} H_{i,e}^T) = \Lambda.$$

Since $\Lambda \subset \text{ORHP}$ and $\rho \in (0, \min_{\lambda \in \Lambda} \frac{4\text{Re } \lambda}{N|\lambda|^2})$, it follows that $\max_{\lambda \in \Lambda} |1 - \rho N \lambda / 2| < 1$, which implies that $\text{spec}(I_{2\ell q} - \frac{\rho N}{2} \mathcal{D}_H) \subset \text{OUD}$. Moreover, note that for all $\varepsilon > 0$, there exists $\bar{\rho} > 0$ such that $\sum_{j=2}^N \bar{\rho}^j (\sigma_{\max}(\mathcal{D}_H))^j \frac{N! q^j}{(N-j)!} < \varepsilon$. Thus, using (3.38), it follows that there exists $\bar{\rho} \in (0, \min_{\lambda \in \Lambda} \frac{4\text{Re } \lambda}{N|\lambda|^2})$ such that for all $\rho \in (0, \bar{\rho}]$,

$$\text{sprad}(\Phi_1) < 1. \quad (3.39)$$

Next, note that since $N/N_i \in \mathbb{Z}^+$, it follows that for all $k \in \mathbb{Z}^+$, $\Omega_k = \Omega_{k+N}$. Thus, it follows that for all $k \in \mathbb{Z}^+$, $A_{k+N} = A_k$ and $\Phi_k = \Phi_{k+N}$, which together with (3.33) imply that for all $k, i \in \mathbb{Z}^+$,

$$\bar{Y}_{k+iN} = \Phi_k^i \bar{Y}_k. \quad (3.40)$$

Let $j \in \mathbb{Z}^+ \setminus \{1\}$, and it follows that there exist $\alpha \in \mathbb{N}$ and $\beta \in \mathbb{Z}^+$ such that $j = 1 + \beta + \alpha N$. Thus, since for all $k \in \mathbb{Z}^+$, $A_{k+N} = A_k$, and for all $X, Y \in \mathbb{R}^{n \times n}$, $\text{spec}(XY) = \text{spec}(YX)$, it follows that for all $j \in \mathbb{Z}^+ \setminus \{1\}$,

$$\begin{aligned} \text{spec}(\Phi_j) &= \text{spec}(A_{j+N-1} A_{j+N-2} \cdots A_{j+N-\beta} A_{j+N-\beta-1} \cdots A_j) \\ &= \text{spec}(A_{j-1} A_{j-2} \cdots A_{j-\beta} A_{j-\beta-1} \cdots A_j) \\ &= \text{spec}(A_{j-\beta-1} A_{j-\beta-2} \cdots A_j A_{j-1} \cdots A_{j-\beta}) \end{aligned}$$

$$\begin{aligned}
&= \text{spec}(A_{N+\alpha N} A_{N+\alpha N-1} \cdots A_{1+\beta+\alpha N} A_{\beta+\alpha N} \cdots A_{1+\alpha N}) \\
&= \text{spec}(A_N A_{N-1} \cdots A_{1+\beta} A_\beta \cdots A_1) \\
&= \text{spec}(\Phi_1).
\end{aligned} \tag{3.41}$$

Therefore, using (3.39) and (3.41), it follows from (3.40) that $\lim_{k \rightarrow \infty} \bar{Y}_k = 0$, which together with (3.8) yield that $\lim_{k \rightarrow \infty} Y_k = 0$. Therefore, since (A3.2)–(A3.4) are satisfied, it follows from (3.11) that

$$\text{sprad} \left(\begin{bmatrix} \left((V^{-1}v)^T \otimes I_\ell \right) (I_{2\ell q} - \rho R) \\ \hline I_{\ell(2q-1)} \quad 0_{\ell(2q-1) \times \ell} \end{bmatrix} \right) < 1,$$

which implies that $Y_k \equiv 0$ is a globally asymptotically stable equilibrium of (3.11). \square

3.14 Proof of Theorem 3.3

Proof. Let $u_{i,0} \in \mathbb{R}^{2m}$, $\ell = 1, q = 1$, and $R_0 > 0$. Since (A3.2)–(A3.4) are satisfied, Proposition 3.1 implies that for all $k \in \mathbb{Z}^+$,

$$\begin{aligned}
y_{k+2} &= (V^{-1}v)^T \begin{bmatrix} 1 - \rho R_0 & 0 \\ -\rho R_1 & 1 - \rho R_0 \end{bmatrix} \begin{bmatrix} y_{k+1} \\ y_k \end{bmatrix} \\
&= \begin{bmatrix} 2 \cos \omega_1 T_s & -1 \end{bmatrix} \begin{bmatrix} 1 - \rho R_0 & 0 \\ -\rho R_1 & 1 - \rho R_0 \end{bmatrix} \begin{bmatrix} y_{k+1} \\ y_k \end{bmatrix},
\end{aligned}$$

which implies that for all $k \in \mathbb{Z}^+$,

$$y_{k+2} + a_1 y_{k+1} + a_0 y_k = 0, \tag{3.42}$$

where

$$a_1 \triangleq 2(\rho R_0 - 1) \cos \omega_1 T_s - \rho R_1 \in \mathbb{R}, \quad a_0 \triangleq 1 - \rho R_0 \in \mathbb{R}.$$

To show that $Y_k \equiv 0$ is a globally asymptotically stable equilibrium of (3.11), let $\rho \in (0, \bar{\rho})$, and it follows that $\rho < 2/R_0$, which implies that $|a_0| < 1$. Moreover, since $R_0 > 0$ and $\rho \in (0, \bar{\rho})$, it follows from direct calculations that

$$2 \cos \omega_1 T_s - 2 + \rho R_0 < \rho(2R_0 \cos \omega_1 T_s - R_1) < 2 \cos \omega_1 T_s + 2 - \rho R_0, \tag{3.43}$$

which implies that $|a_1| < 1 + a_0$. Therefore, since $|a_0| < 1$ and $|a_1| < 1 + a_0$, it follows from [207, Fact 11.20.1] that $y_k \equiv 0$ is a globally asymptotically stable equilibrium of (3.42), and thus, $Y_k \equiv 0$ is a globally asymptotically stable equilibrium of (3.11).

Conversely, assume that $Y_k \equiv 0$ is a globally asymptotically stable equilibrium of (3.11), which implies that $y_k \equiv 0$ is a globally asymptotically stable equilibrium of (3.42). Thus, it follows from [207, Fact 11.20.1] that $|a_0| < 1$ and $|a_1| < 1 + a_0$. Note that $|a_0| < 1$ implies $\rho < 2/R_0$, and $|a_1| < 1 + a_0$ implies (3.43). In addition, note

that $\bar{\rho} < 2/R_0$. Moreover, since $\rho > 0$ and $R_0 > 0$, (3.43) implies that $\rho \in (0, \bar{\rho})$. Thus, since $|a_0| < 1$ and $|a_1| < 1 + a_0$, it follows that $\rho \in (0, \bar{\rho})$. \square

3.15 Proof of Lemma 3.2

Proof. Note that it follows from direct calculations that for all $k \in \mathbb{N}$,

$$V_r = S_k F_k. \quad (3.44)$$

Assume that (A3.3) and (A3.4) are satisfied, and it follows from Lemma 3.1 that V_r is right invertible. Moreover, note that since for all $k \in \mathbb{N}$, $\det S_{i,k} = -2j$, it follows that for all $k \in \mathbb{N}$, S_k is nonsingular. Therefore, it follows from (3.44) that for all $k \in \mathbb{N}$, F_k is right invertible, and $F_k^+ = F_k^T (F_k F_k^T)^{-1} = F_k^T S_k^T (V_r V_r^T)^{-1} S_k$. \square

3.16 Proofs of Proposition 3.2 and Theorem 3.4

For all $k \in \mathbb{N}$, define $\tilde{H}_{i,k} \triangleq H_{i,k} - H_{i,*}$. Subtracting $H_{i,*}$ from both sides of (3.17), and using (3.16) yields that for all $k \geq r$,

$$\tilde{H}_{i,k} = \tilde{H}_{i,k-1} - \eta_k \left(\Gamma_{i,k} + \Lambda_\ell \Gamma_{i,k} \Lambda_m^T \right), \quad (3.45)$$

where the argument $(H_{1,k-1}, \dots, H_{q,k-1})$ of $\Gamma_{i,k}(H_{1,k-1}, \dots, H_{q,k-1})$ is dropped for brevity. Define the function

$$V_H(\tilde{H}_{1,k}, \dots, \tilde{H}_{q,k}) \triangleq \sum_{i=1}^q \|\tilde{H}_{i,k}\|_{\mathbb{F}}^2,$$

and the difference

$$\Delta V_H(k) \triangleq V_H(\tilde{H}_{1,k}, \dots, \tilde{H}_{q,k}) - V_H(\tilde{H}_{1,k-1}, \dots, \tilde{H}_{q,k-1}). \quad (3.46)$$

Evaluating ΔV_H along the trajectories of (3.45) yields that for all $k \geq r$,

$$\begin{aligned} \Delta V_H(k) &= -\eta_k \operatorname{tr} \sum_{i=1}^q \left(2\tilde{H}_{i,k-1}^T \left(\Gamma_{i,k} + \Lambda_\ell \Gamma_{i,k} \Lambda_m^T \right) - \eta_k \left(\Gamma_{i,k} + \Lambda_\ell \Gamma_{i,k} \Lambda_m^T \right)^T \right. \\ &\quad \left. \times \left(\Gamma_{i,k} + \Lambda_\ell \Gamma_{i,k} \Lambda_m^T \right) \right) \\ &= -\eta_k \operatorname{tr} \sum_{i=1}^q \left(2\tilde{H}_{i,k-1}^T \Gamma_{i,k} + 2\Lambda_m^T \tilde{H}_{i,k+r-1}^T \Lambda_\ell \Gamma_{i,k} \right. \\ &\quad \left. - \eta_k \left(\Gamma_{i,k}^T \Gamma_{i,k} + \Lambda_m^T \Lambda_m \Gamma_{i,k}^T \Lambda_\ell^T \Lambda_\ell \Gamma_{i,k} + 2\Lambda_m^T \Gamma_{i,k}^T \Lambda_\ell \Gamma_{i,k} \right) \right). \end{aligned} \quad (3.47)$$

Note that since $H_{i,0} \in \mathcal{H}$, it follows from (3.17) that for all $k \in \mathbb{Z}^+$, $\tilde{H}_{i,k} \in \mathcal{H}$, that is, $\Lambda_\ell^T \tilde{H}_{i,k} \Lambda_m = \tilde{H}_{i,k}$. Moreover, for all $j \in \mathbb{Z}^+$, $\Lambda_j^T \Lambda_j = I_{2j}$. Therefore, it follows from

(3.47) that for all $k \geq r$,

$$\begin{aligned}\Delta V_H(k) &= -2\eta_k \text{tr} \sum_{i=1}^q \left(2\tilde{H}_{i,k-1}^\top \Gamma_{i,k} - \eta_k \left(\Gamma_{i,k}^\top \Gamma_{i,k} + \Gamma_{i,k}^\top \Lambda_\ell \Gamma_{i,k} \Lambda_m^\top \right) \right) \\ &= -4\eta_k \text{tr} \sum_{i=1}^q \left(\tilde{H}_{i,k-1}^\top \Gamma_{i,k} - \eta_k \Gamma_{i,k}^\top \Gamma_{i,k} \right),\end{aligned}\tag{3.48}$$

where the last equality follows since $\text{tr} \bar{A}\bar{B}\bar{C}\bar{D} = (\text{vec } \bar{A})^\top (\bar{B} \otimes \bar{D}^\top) \text{vec } \bar{C}^\top$. For all $k \geq r$, define

$$\varepsilon_k \triangleq y_{k+1} - \hat{y}_{k+1}(H_{1,k-1}, \dots, H_{q,k-1}),$$

and it follows from (3.16) that

$$\Gamma_{i,k} = \text{vec}^{-1} \left(\left(\left[u_{i,k-1} \otimes f_{i,k} \quad \cdots \quad u_{i,k-r} \otimes f_{i,k-r+1} \right] F_k^+ f_{k+1} - (u_{i,k} \otimes f_{i,k+1}) \right) \otimes \varepsilon_k \right).\tag{3.49}$$

Therefore, using (3.49), it follows from (3.48) that for all $k \geq r$,

$$\begin{aligned}\Delta V_H(k) &= -4\eta_k \text{tr} \sum_{i=1}^q \left(\tilde{H}_{i,k-1}^\top \Gamma_{i,k} - \eta_k \Gamma_{i,k}^\top \Gamma_{i,k} \right) \\ &= -4\eta_k \sum_{i=1}^q (\text{vec } \tilde{H}_{i,k-1})^\top \left(\left(\left[u_{i,k-1} \otimes f_{i,k} \quad \cdots \quad u_{i,k-r} \otimes f_{i,k-r+1} \right] F_k^+ f_{k+1} \right. \right. \\ &\quad \left. \left. - (u_{i,k} \otimes f_{i,k+1}) \right) \otimes \varepsilon_k \right) \\ &\quad + 4\eta_k^2 \|\varepsilon_k\|^2 \sum_{i=1}^q \left\| \left[u_{i,k-1} \otimes f_{i,k} \quad \cdots \quad u_{i,k-r} \otimes f_{i,k-r+1} \right] F_k^+ f_{k+1} \right. \\ &\quad \left. - (u_{i,k} \otimes f_{i,k+1}) \right\|^2 \\ &= -4\eta_k \sum_{i=1}^q (\text{vec } \tilde{H}_{i,k-1})^\top \left(\left(\left[u_{i,k-1} \otimes f_{i,k} \quad \cdots \quad u_{i,k-r} \otimes f_{i,k-r+1} \right] F_k^+ f_{k+1} \right. \right. \\ &\quad \left. \left. - (u_{i,k} \otimes f_{i,k+1}) \right) \otimes I_\ell \right) \varepsilon_k \\ &\quad + 4\eta_k^2 \|\varepsilon_k\|^2 \sum_{i=1}^q \left\| \left[u_{i,k-1} \otimes f_{i,k} \quad \cdots \quad u_{i,k-r} \otimes f_{i,k-r+1} \right] F_k^+ f_{k+1} \right. \\ &\quad \left. - (u_{i,k} \otimes f_{i,k+1}) \right\|^2,\end{aligned}\tag{3.50}$$

Moreover, note that it follows from (3.8), (3.14), and (3.15) that for all $k \geq r$,

$$\begin{aligned}\varepsilon_k &= - \sum_{i=1}^q \left(f_{i,k+1}^\top \otimes I_\ell \right) \left(\tilde{H}_{i,k-1} u_{i,k} + d_{i,k}(H_{1,k-1}, \dots, H_{q,k-1}) - d_{i,*} \right) \\ &= - \sum_{i=1}^q \left(f_{i,k+1}^\top \otimes I_\ell \right)\end{aligned}$$

$$\begin{aligned}
& \times \left(\tilde{H}_{i,k-1} u_{i,k} - (e_i \otimes I_{2\ell}) \left((F_k^+)^T \otimes I_\ell \right) \begin{bmatrix} \sum_{j=1}^q (f_{j,k}^T \otimes I_\ell) \tilde{H}_{j,k-1} u_{j,k-1} \\ \vdots \\ \sum_{j=1}^q (f_{j,k-r+1}^T \otimes I_\ell) \tilde{H}_{j,k-1} u_{j,k-r} \end{bmatrix} \right) \\
&= - \sum_{i=1}^q (u_{i,k}^T \otimes f_{i,k+1}^T \otimes I_\ell) \text{vec } \tilde{H}_{i,k-1} + f_{k+1}^T \left((F_k^+)^T \otimes I_\ell \right) \\
& \quad \times \left[u_{i,k-1} \otimes f_{i,k} \quad \cdots \quad u_{i,k-r} \otimes f_{i,k-r+1} \right]^T \text{vec } \tilde{H}_{i,k-1} \\
&= - \sum_{i=1}^q \left(\left((u_{i,k} \otimes f_{i,k+1}) - \left[u_{i,k-1} \otimes f_{i,k} \quad \cdots \quad u_{i,k-r} \otimes f_{i,k-r+1} \right] F_k^+ f_{k+1} \right)^T \otimes I_\ell \right) \\
& \quad \times \text{vec } \tilde{H}_{i,k-1}. \tag{3.51}
\end{aligned}$$

Using (3.51) and (3.18), it follows from (3.50) that for all $k \geq r$,

$$\begin{aligned}
\Delta V_H(k) &= -4\eta_k \|\varepsilon_k\|^2 \left(1 - \eta_k \sum_{i=1}^q \left\| \left[u_{i,k-1} \otimes f_{i,k} \quad \cdots \quad u_{i,k-r} \otimes f_{i,k-r+1} \right] F_k^+ f_{k+1} \right. \right. \\
& \quad \left. \left. - (u_{i,k} \otimes f_{i,k+1}) \right\|^2 \right) \\
&\leq -4\eta_k \|\varepsilon_k\|^2 (1 - \gamma). \tag{3.52}
\end{aligned}$$

Proof of Proposition 3.2. To show *i*), note that (3.52) implies that for all $k \geq r$, $\Delta V_H(k) \leq 0$. Since, in addition, for all $k \in \{1, 2, \dots, r-1\}$, $H_{i,k} = H_{i,0}$, it follows that for all $k \in \mathbb{Z}^+$, $\sum_{i=1}^q \|\tilde{H}_{i,k}\|_F^2 \leq \sum_{i=1}^q \|\tilde{H}_{i,0}\|_F^2$, which implies that $H_{i,k}$ is bounded, which together with (3.52) confirms *i*).

To show *ii*), note that since $V_H(\tilde{H}_{1,k}, \dots, \tilde{H}_{q,k})$ is positive definite, and for all $k \in \mathbb{Z}^+$, $\Delta V_H(k)$ is nonpositive, it follows from (3.46) and (3.52) that

$$\begin{aligned}
0 &\leq \lim_{k \rightarrow \infty} \sum_{j=1}^k 2(2 - \gamma) \eta_j \|\varepsilon_j\|^2 \\
&\leq \lim_{k \rightarrow \infty} \sum_{j=1}^k \Delta V_H(j) \\
&= V_H(\tilde{H}_{1,0}, \dots, \tilde{H}_{q,0}) - \lim_{k \rightarrow \infty} V_H(\tilde{H}_{1,k}, \dots, \tilde{H}_{q,k}) \\
&\leq V_H(\tilde{H}_{1,0}, \dots, \tilde{H}_{q,0}),
\end{aligned}$$

where the upper and lower bounds imply that all the limits exist. Thus,

$$\lim_{k \rightarrow \infty} \eta_k \|\varepsilon_k\|^2 = 0. \tag{3.53}$$

Since (3.18) implies that

$$\eta_k \left\| \left[u_{i,k-1} \otimes f_{i,k} \quad \cdots \quad u_{i,k-r} \otimes f_{i,k-r+1} \right] F_k^+ f_{k+1} - (u_{i,k} \otimes f_{i,k+1}) \right\|^2$$

is bounded, it follows from (3.53) that

$$\lim_{k \rightarrow \infty} \eta_k^2 \|\varepsilon_k\|^2 \left\| \left[u_{i,k-1} \otimes f_{i,k} \quad \cdots \quad u_{i,k-r} \otimes f_{i,k-r+1} \right] F_k^+ f_{k+1} - (u_{i,k} \otimes f_{i,k+1}) \right\|^2 = 0. \quad (3.54)$$

Moreover, note that (3.49) implies that

$$\begin{aligned} \eta_k^2 \|\Gamma_{i,k}\|_{\mathbb{F}}^2 &= \eta_k^2 (\text{vec } \Gamma_{i,k})^{\text{T}} (\text{vec } \Gamma_{i,k}) \\ &= \eta_k^2 \|\varepsilon_k\|^2 \left\| \left[u_{i,k-1} \otimes f_{i,k} \quad \cdots \quad u_{i,k-r} \otimes f_{i,k-r+1} \right] F_k^+ f_{k+1} - (u_{i,k} \otimes f_{i,k+1}) \right\|^2, \end{aligned} \quad (3.55)$$

which together with (3.54) imply that $\lim_{k \rightarrow \infty} \eta_k \Gamma_{i,k} = 0$. Thus, it follows from (3.17) that $\lim_{k \rightarrow \infty} (H_{i,k} - H_{i,k-1}) = 0$, which confirms *ii*). \square

Proof of Theorem 3.4. Assume $q = 1$, $\ell = 1$, and $r = 2$. It follows from direct calculations that

$$F_k^+ f_{k+1} = \begin{bmatrix} 2 \cos \theta & -1 \end{bmatrix}^{\text{T}}, \quad (3.56)$$

where $\theta \triangleq \omega_1 T_s$. Substituting (3.56) into (3.18) and (3.51), and using (3.52) yields that for all $k \geq 2$,

$$\begin{aligned} \Delta V_H(k) &\leq \frac{-4\gamma(1-\gamma)}{\nu_2 + \|u_{1,k} \otimes f_{k+1} - 2(\cos \theta)u_{1,k-1} \otimes f_k + u_{1,k-2} \otimes f_{k-1}\|^2} \\ &\quad \times \left((u_{1,k} \otimes f_{k+1} - 2(\cos \theta)u_{1,k-1} \otimes f_k + u_{1,k-2} \otimes f_{k-1})^{\text{T}} \text{vec } \tilde{H}_{1,k-1} \right)^2. \end{aligned} \quad (3.57)$$

Note that it follows from direct calculations that for all $k \in \mathbb{Z}^+$,

$$f_{k+1} + f_{k-1} = 2(\cos \theta)f_k. \quad (3.58)$$

Substituting (3.58) into (3.57), using (3.13), and using Lemma 3.3 yields that for all $k \geq 2$,

$$\begin{aligned} \Delta V_H(k) &\leq \frac{-4\gamma(1-\gamma)}{\nu_2 + \|(u_{1,k} - u_{1,k-1}) \otimes f_{k+1} + (u_{1,k-2} - u_{1,k-1}) \otimes f_{k-1}\|^2} \\ &\quad \times \left(((u_{1,k} - u_{1,k-1}) \otimes f_{k+1} + (u_{1,k-2} - u_{1,k-1}) \otimes f_{k-1})^{\text{T}} \text{vec } \tilde{H}_{1,k-1} \right)^2 \\ &= \frac{-4\gamma(1-\gamma) \left(f_{k+1}^{\text{T}} \tilde{H}_{1,k}(u_{1,k} - u_{1,k-1}) + f_{k-1}^{\text{T}} \tilde{H}_{1,k-1}(u_{1,k-2} - u_{1,k-1}) \right)^2}{\nu_2 + \left\| (f_{k+1}^{\text{T}} \otimes I_m)(u_{1,k} - u_{1,k-1}) + (f_{k-1}^{\text{T}} \otimes I_m)(u_{1,k-2} - u_{1,k-1}) \right\|^2} \\ &= \frac{-4\gamma(1-\gamma) \left(\xi_{k-1} f_{k+1}^{\text{T}} \tilde{H}_{1,k-1} H_{1,k-1}^{\text{T}} f_k y_k - \xi_{k-2} f_{k-1}^{\text{T}} \tilde{H}_{1,k-1} H_{1,k-2}^{\text{T}} f_{k-1} y_{k-1} \right)^2}{\nu_2 + \left\| (f_{k+1}^{\text{T}} \otimes I_m)(\xi_{k-1} H_{1,k-1}^{\text{T}} f_k y_k) - (f_{k-1}^{\text{T}} \otimes I_m)(\xi_{k-2} H_{1,k-2}^{\text{T}} f_{k-1} y_{k-1}) \right\|^2} \end{aligned}$$

$$= \frac{-4\gamma(1-\gamma)\left(\xi_{k-1}\operatorname{Re} e^{j\theta}\tilde{G}_{1,k-1}G_{1,k-1}^*y_k - \xi_{k-2}\operatorname{Re} \tilde{G}_{1,k-1}G_{1,k-2}^*y_{k-1}\right)^2}{\nu_2 + \left\|\xi_{k-1}\operatorname{Re} e^{j\theta}G_{1,k-1}^*y_k - \xi_{k-2}\operatorname{Re} G_{1,k-2}^*y_{k-1}\right\|^2}, \quad (3.59)$$

where for all $k \in \mathbb{N}$,

$$\xi_k \triangleq \frac{\mu}{\nu_1 + \|H_{1,k}\|_{\mathbb{F}}^2}. \quad (3.60)$$

Next, let $u_{1,0} \in \mathbb{R}^{2m}$, and for all $k \in \mathbb{N}$, define $\bar{y}_{k+1} \triangleq H_{1,*}u_{1,k} + d_{1,*}$. It follows that for all $k \in \mathbb{Z}^+$,

$$\bar{y}_{k+1} - \bar{y}_k = H_{1,*}(u_{1,k} - u_{1,k-1}). \quad (3.61)$$

Multiplying (3.13) by $H_{1,*}$ and using (3.61) implies that for all $k \in \mathbb{Z}^+$,

$$\bar{y}_{k+1} = \bar{y}_k - \xi_{k-1}H_{1,*}H_{1,k-1}^T f_{1,k}y_k. \quad (3.62)$$

Multiplying (3.62) by $f_{1,k}^T$, using (3.8), and using Lemma 3.3 in Appendix 3.17 yield

$$\begin{aligned} f_{1,k}^T \bar{y}_{k+1} &= y_k - \xi_{k-1}f_{1,k}^T H_{1,*}H_{1,k-1}^T f_{1,k}y_k \\ &= y_k - \xi_{k-1}\operatorname{Re} G_{1,*}G_{1,k-1}^*y_k. \end{aligned} \quad (3.63)$$

Similarly, multiplying (3.62) by $f_{1,k+1}^T$, using (3.8), and using Lemma 3.3 in Section 3.17 yield

$$\begin{aligned} y_{k+1} &= f_{1,k+1}^T \bar{y}_k - \xi_{k-1}f_{1,k+1}^T H_{1,*}H_{1,k-1}^T f_{1,k}y_k \\ &= f_{1,k+1}^T \bar{y}_k - \xi_{k-1}\operatorname{Re} e^{j\theta}G_{1,*}G_{1,k-1}^*y_k, \end{aligned}$$

which implies that

$$f_{1,k+2}^T \bar{y}_{k+1} = y_{k+2} + \xi_k \operatorname{Re} e^{j\theta}G_{1,*}G_{1,k}^*y_{k+1}. \quad (3.64)$$

Therefore, adding (3.63) and (3.64), and using (3.8) and (3.58) yield that for all $k \in \mathbb{Z}^+$,

$$2(\cos \theta)y_{k+1} = y_k - \xi_{k-1}\operatorname{Re} G_{1,*}G_{1,k-1}^*y_k + y_{k+2} + \xi_k \operatorname{Re} e^{j\theta}G_{1,*}G_{1,k}^*y_{k+1},$$

which implies

$$y_{k+2} + \left(\xi_k \operatorname{Re} e^{j\theta}G_{1,*}G_{1,k}^* - 2\cos \theta\right)y_{k+1} + \left(1 - \xi_{k-1}\operatorname{Re} G_{1,*}G_{1,k-1}^*\right)y_k = 0. \quad (3.65)$$

Define the partial Lyapunov function

$$V_y(y_k, y_{k-1}) \triangleq \left|e^{j\theta}y_k - y_{k-1}\right|^2, \quad (3.66)$$

and define the difference

$$\Delta V_y(k) \triangleq V_y(y_{k+1}, y_k) - V_y(y_k, y_{k-1}). \quad (3.67)$$

Evaluating $\Delta V_y(k)$ along the trajectories of (3.65) yields

$$\begin{aligned} \Delta V_y(k) &= -\left(2(\cos \theta)\xi_{k-1}\operatorname{Re} e^{j\theta}G_{1,*}G_{1,k-1}^* - \xi_{k-1}^2(\operatorname{Re} e^{j\theta}G_{1,*}G_{1,k-1}^*)^2\right)y_k^2 \\ &\quad - \left(2\xi_{k-2}\operatorname{Re} G_{1,*}G_{1,k-2}^* - \xi_{k-2}^2(\operatorname{Re} G_{1,*}G_{1,k-2}^*)^2\right)y_{k-1}^2 \\ &\quad + 2\left((\cos \theta)\xi_{k-2}\operatorname{Re} G_{1,*}G_{1,k-2}^* - \xi_{k-1}\operatorname{Re} e^{j\theta}G_{1,*}G_{1,k-1}^*\right. \\ &\quad \left.\times (\xi_{k-2}\operatorname{Re} G_{1,*}G_{1,k-2}^* - 1)\right)y_k y_{k-1}. \end{aligned} \quad (3.68)$$

Define the Lyapunov function

$$V(y_k, y_{k-1}, \tilde{H}_{1,k-1}) \triangleq \ln(1 + aV_y(y_k, y_{k-1})) + bV_H(\tilde{H}_{1,k-1}), \quad (3.69)$$

where $a, b > 0$ are provided later, and define the Lyapunov difference

$$\begin{aligned} \Delta V(k) &\triangleq V(y_{k+1}, y_k, \tilde{H}_{1,k}) - V(y_k, y_{k-1}, \tilde{H}_{1,k-1}) \\ &= \ln(1 + a(V_y(y_k, y_{k-1}) + \Delta V_y(k))) - \ln(1 + aV_y(y_k, y_{k-1})) + b\Delta V_H(k) \\ &= \ln\left(1 + \frac{a\Delta V_y(k)}{1 + aV_y(y_k, y_{k-1})}\right) + b\Delta V_H(k). \end{aligned} \quad (3.70)$$

Since for all $x > 0$, $\ln x \leq x - 1$, it follows from (3.70) that

$$\Delta V(k) \leq \frac{a\Delta V_y(k)}{1 + aV_y(y_k, y_{k-1})} + b\Delta V_H(k). \quad (3.71)$$

Evaluating $\Delta V(k)$ along the trajectories of (3.65) and (3.45), and substituting (3.59) and (3.66) yield that for all $k \geq 2$,

$$\begin{aligned} \Delta V(k) &\leq \frac{a\Delta V_y(k)}{1 + a|e^{j\theta}y_k - y_{k-1}|^2} \\ &\quad - \frac{4b\gamma(1 - \gamma)\left(\xi_{k-1}\operatorname{Re} e^{j\theta}\tilde{G}_{1,k-1}G_{1,k-1}^*y_k - \xi_{k-2}\operatorname{Re} \tilde{G}_{1,k-1}G_{1,k-2}^*y_{k-1}\right)^2}{\nu_2 + \left\|\xi_{k-1}\operatorname{Re} e^{j\theta}G_{1,k-1}^*y_k - \xi_{k-2}\operatorname{Re} G_{1,k-2}^*y_{k-1}\right\|^2} \\ &= \frac{a\Delta V_y(k)}{1 + a\begin{bmatrix} y_k & y_{k-1} \end{bmatrix}C_1\begin{bmatrix} y_k & y_{k-1} \end{bmatrix}^\top} \\ &\quad - \frac{4b\gamma(1 - \gamma)\left(\xi_{k-1}\operatorname{Re} e^{j\theta}\tilde{G}_{1,k-1}G_{1,k-1}^*y_k - \xi_{k-2}\operatorname{Re} \tilde{G}_{1,k-1}G_{1,k-2}^*y_{k-1}\right)^2}{\nu_2 + \begin{bmatrix} y_k & y_{k-1} \end{bmatrix}C_{2,k}\begin{bmatrix} y_k & y_{k-1} \end{bmatrix}^\top}, \end{aligned} \quad (3.72)$$

where $C_1 \triangleq \begin{bmatrix} 1 & -\cos\theta \\ -\cos\theta & 1 \end{bmatrix} \in \mathbb{R}^{2 \times 2}$, and

$$C_{2,k} \triangleq \begin{bmatrix} \xi_{k-1}^2 \|\operatorname{Re} e^{j\theta} G_{1,k-1}^*\|^2 & -\xi_{k-1} \xi_{k-2} (\operatorname{Re} G_{1,k-2}^*)^\top (\operatorname{Re} e^{j\theta} G_{1,k-1}^*) \\ -\xi_{k-1} \xi_{k-2} (\operatorname{Re} e^{j\theta} G_{1,k-1}^*)^\top (\operatorname{Re} G_{1,k-2}^*) & \xi_{k-2}^2 \|\operatorname{Re} G_{1,k-2}^*\|^2 \end{bmatrix} \in \mathbb{R}^{2 \times 2}.$$

Since (A3.4) is satisfied, it follows that $\cos\theta \neq 1$, and thus, C_1 is symmetric positive definite. Moreover, note that for all $G_{1,k-2}, G_{1,k-1} \in \mathbb{C}^{1,m}$, $C_{2,k}$ is symmetric positive semidefinite. Thus, it follows from (3.72) that for all $k \geq 2$,

$$\begin{aligned} \Delta V(k) &\leq \frac{a\nu_2 \Delta V_y(k)}{\nu_2 + a\nu_2 \begin{bmatrix} y_k & y_{k-1} \end{bmatrix} C_1 \begin{bmatrix} y_k & y_{k-1} \end{bmatrix}^\top} \\ &\quad - \frac{4b\gamma(1-\gamma) \left(\xi_{k-1} \operatorname{Re} e^{j\theta} \tilde{G}_{1,k-1} G_{1,k-1}^* y_k - \xi_{k-2} \operatorname{Re} \tilde{G}_{1,k-1} G_{1,k-2}^* y_{k-1} \right)^2}{\nu_2 + \begin{bmatrix} y_k & y_{k-1} \end{bmatrix} C_1^{\frac{1}{2}} C_1^{-\frac{1}{2}} C_{2,k} C_1^{-\frac{1}{2}} C_1^{\frac{1}{2}} \begin{bmatrix} y_k & y_{k-1} \end{bmatrix}^\top} \\ &\leq \frac{a\nu_2 \Delta V_y(k)}{\nu_2 + a\nu_2 \begin{bmatrix} y_k & y_{k-1} \end{bmatrix} C_1 \begin{bmatrix} y_k & y_{k-1} \end{bmatrix}^\top} \\ &\quad - \frac{4b\gamma(1-\gamma) \left(\xi_{k-1} \operatorname{Re} e^{j\theta} \tilde{G}_{1,k-1} G_{1,k-1}^* y_k - \xi_{k-2} \operatorname{Re} \tilde{G}_{1,k-1} G_{1,k-2}^* y_{k-1} \right)^2}{\nu_2 + \lambda_m \begin{bmatrix} y_k & y_{k-1} \end{bmatrix} C_1 \begin{bmatrix} y_k & y_{k-1} \end{bmatrix}^\top}, \end{aligned} \tag{3.73}$$

where

$$\lambda_m \triangleq \sup_{k \in \mathbb{N}} \lambda_{\max} \left(C_1^{-\frac{1}{2}} C_{2,k} C_1^{-\frac{1}{2}} \right),$$

which exits since part *i*) of Proposition 3.2 implies that $G_{1,k}$ is bounded.

Next, let $a \triangleq \lambda_m / \nu_2$, and substituting (3.68) into (3.73) yields that for all $k \geq 2$,

$$\begin{aligned} \Delta V(k) &\leq - \frac{a\nu_2 \left(2(\cos\theta) \xi_{k-1} \operatorname{Re} e^{j\theta} G_{1,*} G_{1,k-1}^* - \xi_{k-1}^2 (\operatorname{Re} e^{j\theta} G_{1,*} G_{1,k-1}^*)^2 \right) y_k^2}{\nu_2 + a\nu_2 \begin{bmatrix} y_k & y_{k-1} \end{bmatrix} C_1 \begin{bmatrix} y_k & y_{k-1} \end{bmatrix}^\top} \\ &\quad - \frac{a\nu_2 \left(2\xi_{k-2} \operatorname{Re} G_{1,*} G_{1,k-2}^* - \xi_{k-2}^2 (\operatorname{Re} G_{1,*} G_{1,k-2}^*)^2 \right) y_{k-1}^2}{\nu_2 + a\nu_2 \begin{bmatrix} y_k & y_{k-1} \end{bmatrix} C_1 \begin{bmatrix} y_k & y_{k-1} \end{bmatrix}^\top} \\ &\quad + \frac{2a\nu_2 y_k y_{k-1}}{\nu_2 + a\nu_2 \begin{bmatrix} y_k & y_{k-1} \end{bmatrix} C_1 \begin{bmatrix} y_k & y_{k-1} \end{bmatrix}^\top} \\ &\quad \times \left((\cos\theta) \xi_{k-2} \operatorname{Re} G_{1,*} G_{1,k-2}^* - \xi_{k-1} \operatorname{Re} e^{j\theta} G_{1,*} G_{1,k-1}^* (\xi_{k-2} \operatorname{Re} G_{1,*} G_{1,k-2}^* - 1) \right) \\ &\quad - \frac{4b\gamma(1-\gamma) \left(\xi_{k-1} \operatorname{Re} e^{j\theta} \tilde{G}_{1,k-1} G_{1,k-1}^* y_k - \xi_{k-2} \operatorname{Re} \tilde{G}_{1,k-1} G_{1,k-2}^* y_{k-1} \right)^2}{\nu_2 + a\nu_2 \begin{bmatrix} y_k & y_{k-1} \end{bmatrix} C_1 \begin{bmatrix} y_k & y_{k-1} \end{bmatrix}^\top} \end{aligned}$$

$$= -\frac{\begin{bmatrix} y_k & y_{k-1} \end{bmatrix} (P_k + \Delta_k) \begin{bmatrix} y_k & y_{k-1} \end{bmatrix}^T}{\nu_2 + a\nu_2 \begin{bmatrix} y_k & y_{k-1} \end{bmatrix} C_1 \begin{bmatrix} y_k & y_{k-1} \end{bmatrix}^T}, \quad (3.74)$$

where

$$P_k \triangleq \begin{bmatrix} \phi_k & -\chi_k \\ -\chi_k & \psi_k \end{bmatrix} \in \mathbb{R}^{2 \times 2}, \quad \Delta_k \triangleq \begin{bmatrix} 0 & \delta_{\chi,k} \\ \delta_{\chi,k} & \delta_{\psi,k} \end{bmatrix},$$

and

$$\begin{aligned} \phi_k &\triangleq a\nu_2 \left(2(\cos \theta) \xi_{k-1} \operatorname{Re} e^{j\theta} G_{1,*} G_{1,k-1}^* - \xi_{k-1}^2 (\operatorname{Re} e^{j\theta} G_{1,*} G_{1,k-1}^*)^2 \right) \\ &\quad + 4b\gamma(1-\gamma) \xi_{k-1}^2 (\operatorname{Re} e^{j\theta} \tilde{G}_{1,k-1} G_{1,k-1}^*)^2 \in \mathbb{R}, \\ \psi_k &\triangleq a\nu_2 \left(2\xi_{k-1} \operatorname{Re} G_{1,*} G_{1,k-1}^* - \xi_{k-1}^2 (\operatorname{Re} G_{1,*} G_{1,k-1}^*)^2 \right) \\ &\quad + 4b\gamma(1-\gamma) \xi_{k-1}^2 (\operatorname{Re} \tilde{G}_{1,k-1} G_{1,k-1}^*)^2 \in \mathbb{R}, \\ \chi_k &\triangleq a\nu_2 \left((\cos \theta) \xi_{k-1} \operatorname{Re} G_{1,*} G_{1,k-1}^* - \xi_{k-1} \operatorname{Re} e^{j\theta} G_{1,*} G_{1,k-1}^* (\xi_{k-1} \operatorname{Re} G_{1,*} G_{1,k-1}^* - 1) \right) \\ &\quad + 4b\gamma(1-\gamma) \xi_{k-1}^2 (\operatorname{Re} e^{j\theta} \tilde{G}_{1,k-1} G_{1,k-1}^*) (\operatorname{Re} \tilde{G}_{1,k-1} G_{1,k-1}^*) \in \mathbb{R}, \\ \delta_{\psi,k} &\triangleq a\nu_2 \left[2(\xi_{k-2} - \xi_{k-1}) \operatorname{Re} G_{1,*} G_{1,k-2}^* + 2\xi_{k-2} \operatorname{Re} G_{1,*} (G_{1,k-2} - G_{1,k-1})^* \right. \\ &\quad \left. - (\xi_{k-2}^2 - \xi_{k-1}^2) (\operatorname{Re} G_{1,*} G_{1,k-2}^*)^2 - \xi_{k-2}^2 \left((\operatorname{Re} G_{1,*} G_{1,k-2}^*)^2 \right. \right. \\ &\quad \left. \left. - (\operatorname{Re} G_{1,*} G_{1,k-1}^*)^2 \right) \right] + 4b\gamma(1-\gamma) \left[(\xi_{k-2}^2 - \xi_{k-1}^2) (\operatorname{Re} \tilde{G}_{1,k-1} G_{1,k-2}^*)^2 \right. \\ &\quad \left. + \xi_{k-2}^2 \left((\operatorname{Re} \tilde{G}_{1,k-1} G_{1,k-2}^*)^2 - (\operatorname{Re} \tilde{G}_{1,k-1} G_{1,k-1}^*)^2 \right) \right] \in \mathbb{R}, \\ \delta_{\chi,k} &\triangleq a\nu_2 \left[(\cos \theta) (\xi_{k-2} - \xi_{k-1}) \operatorname{Re} G_{1,*} G_{1,k-2}^* + (\cos \theta) \xi_{k-2} \operatorname{Re} G_{1,*} (G_{1,k-2} - G_{1,k-1})^* \right. \\ &\quad \left. - \xi_{k-1} \operatorname{Re} e^{j\theta} G_{1,*} G_{1,k-1}^* \left((\xi_{k-2} - \xi_{k-1}) \operatorname{Re} G_{1,*} G_{1,k-2}^* \right. \right. \\ &\quad \left. \left. + \xi_{k-2} \operatorname{Re} G_{1,*} (G_{1,k-2} - G_{1,k-1})^* \right) \right] \\ &\quad + 4b\gamma(1-\gamma) \left[\xi_{k-1} (\xi_{k-2} - \xi_{k-1}) (\operatorname{Re} e^{j\theta} \tilde{G}_{1,k-1} G_{1,k-1}^*) (\operatorname{Re} \tilde{G}_{1,k-1} G_{1,k-2}^*) \right. \\ &\quad \left. + \xi_{k-1} \xi_{k-2} (\operatorname{Re} e^{j\theta} \tilde{G}_{1,k-1} G_{1,k-1}^*) (\operatorname{Re} e^{j\theta} \tilde{G}_{1,k-1} (G_{1,k-2} - G_{1,k-1})^*) \right] \in \mathbb{R}. \end{aligned}$$

Next, define

$$c_0 \triangleq \sup_{k \in \mathbb{Z}^+} \left(2 - \xi_{k-1} \|G_{1,k-1}\|_{\mathbb{F}}^2 \right), \quad c_1 \triangleq \sup_{k \in \mathbb{Z}^+} \left(\xi_{k-1} \|G_{k-1}\|_{\mathbb{F}}^2 - 1 \right)^2,$$

$$c_2 \triangleq \inf_{k \in \mathbb{Z}^+} \left(\xi_{k-1}^3 \|G_{1,k-1}\|_{\mathbb{F}}^2 \left(2 - \xi_{k-1} \|G_{1,k-1}\|_{\mathbb{F}}^2 \right) \right),$$

$$c_3 \triangleq \inf_{k \in \mathbb{Z}^+} \left(\xi_{k-1} \|G_{1,k-1}\|_{\mathbb{F}}^2 \left(2 - \xi_{k-1} \|G_{1,k-1}\|_{\mathbb{F}}^2 \right) \right),$$

which exist since part *i*) of Proposition 3.2 implies that $G_{1,k}$ is bounded. Note that since $\|H_{1,k}\|_{\mathbb{F}}^2 = 2\|G_{1,k}\|_{\mathbb{F}}^2$ and $\mu \in (0, 4)$, (3.60) implies that for all $k \in \mathbb{Z}^+$,

$$0 \leq \xi_{k-1} \|G_{1,k-1}\|_{\mathbb{F}}^2 < 2, \quad (3.75)$$

which implies that $c_0 > 0$ and $1 > c_1 > 0$. Assume that there exists $\varepsilon > 0$ and $k_s \in \mathbb{N}$ such that for all $k \geq k_s$, $|\operatorname{Im} G_{1,*}^* G_{1,k}| \geq \varepsilon$, which implies that there exists $\varepsilon_1 > 0$ such that for all $k > k_s$, $\|G_{1,k-1}\|_{\mathbb{F}}^2 \geq \varepsilon_1$. Thus, using (3.75), it follows that for all $k > k_s$, $c_2 > 0$.

Next, let $b \triangleq \frac{1}{\gamma(1-\gamma)} \max\left\{ a\nu_2, \sqrt{a\nu_2 c_1 / c_2}, \frac{a\nu_2}{c_3} \right\}$. Note that for all $k \in \mathbb{Z}^+$,

$$\operatorname{Re} e^{j\theta} G_{1,*} G_{1,k-1}^* = (\cos \theta) \|G_{1,k-1}\|_{\mathbb{F}}^2 - \operatorname{Re} e^{j\theta} \tilde{G}_{1,k-1} G_{1,k-1}^*. \quad (3.76)$$

Using (3.76), it follows that for all $k > k_s$,

$$\begin{aligned} \phi_k &= (4b\gamma(1-\gamma) - a\nu_2) \xi_{k-1}^2 \left(\operatorname{Re} e^{j\theta} \tilde{G}_{1,k-1} G_{1,k-1}^* \right)^2 \\ &\quad + 2a\nu_2 (\cos \theta) \xi_{k-1} \left(\xi_{k-1} \|G_{k-1}\|_{\mathbb{F}}^2 - 1 \right) \left(\operatorname{Re} e^{j\theta} \tilde{G}_{1,k-1} G_{1,k-1}^* \right) \\ &\quad + a\nu_2 \xi_{k-1} (\cos \theta)^2 \|G_{1,k-1}\|_{\mathbb{F}}^2 \left(2 - \xi_{k-1} \|G_{1,k-1}\|_{\mathbb{F}}^2 \right) \\ &= (4b\gamma(1-\gamma) - a\nu_2) \xi_{k-1}^2 \left(\operatorname{Re} e^{j\theta} \tilde{G}_{1,k-1} G_{1,k-1}^* + \frac{a\nu_2 (\cos \theta) (\xi_{k-1} \|G_{k-1}\|_{\mathbb{F}}^2 - 1)}{(4b\gamma(1-\gamma) - a\nu_2) \xi_{k-1}} \right)^2 \\ &\quad + a\nu_2 \xi_{k-1} (\cos \theta)^2 \|G_{1,k-1}\|_{\mathbb{F}}^2 \left(2 - \xi_{k-1} \|G_{1,k-1}\|_{\mathbb{F}}^2 \right) \\ &\quad - \frac{a^2 \nu_2^2 (\cos \theta)^2 (\xi_{k-1} \|G_{k-1}\|_{\mathbb{F}}^2 - 1)^2}{16b^2 \gamma^2 (1-\gamma)^2 \xi_{k-1}^2} \\ &\geq a\nu_2 \xi_{k-1} (\cos \theta)^2 \|G_{1,k-1}\|_{\mathbb{F}}^2 \left(2 - \xi_{k-1} \|G_{1,k-1}\|_{\mathbb{F}}^2 \right) - \frac{a^2 \nu_2^2 (\cos \theta)^2 (\xi_{k-1} \|G_{k-1}\|_{\mathbb{F}}^2 - 1)^2}{16b^2 \gamma^2 (1-\gamma)^2 \xi_{k-1}^2} \\ &= \frac{a\nu_2 (\cos \theta)^2}{16b^2 \gamma^2 (1-\gamma)^2 \xi_{k-1}^2} \\ &\quad \times \left(16b^2 \gamma^2 (1-\gamma)^2 \xi_{k-1}^3 \|G_{1,k-1}\|_{\mathbb{F}}^2 \left(2 - \xi_{k-1} \|G_{1,k-1}\|_{\mathbb{F}}^2 \right) - a\nu_2 \left(\xi_{k-1} \|G_{k-1}\|_{\mathbb{F}}^2 - 1 \right)^2 \right) \\ &\geq \frac{a\nu_2 (\cos \theta)^2 (16b^2 \gamma^2 (1-\gamma)^2 c_2 - a\nu_2 c_1)}{16b^2 \gamma^2 (1-\gamma)^2 \xi_{k-1}^2}. \end{aligned} \quad (3.77)$$

Note that (3.60) implies that for all $k \in \mathbb{N}$, $0 < \xi_k \leq \mu/\nu_1$. Thus, since $\cos \theta \neq 0$ and $b > \frac{\sqrt{a\nu_2 c_1 / c_2}}{4\gamma(1-\gamma)}$, it follows from (3.77) that for all $k > k_s$,

$$\phi_k \geq \frac{a\nu_2 \nu_1^2 (\cos \theta)^2 (16b^2 \gamma^2 (1-\gamma)^2 c_2 - a\nu_2 c_1)}{16b^2 \gamma^2 (1-\gamma)^2 \mu^2}$$

$$> 0. \quad (3.78)$$

Similarly, using (3.76), it follows that for all $k > k_s$,

$$\begin{aligned}
\psi_k &= (4b\gamma(1-\gamma) - a\nu_2)\xi_{k-2}^2 \left(\operatorname{Re} \tilde{G}_{1,k-2} G_{1,k-2}^* \right)^2 + 2a\nu_2 \xi_{k-2} \left(\xi_{k-2} \|G_{k-2}\|_{\mathbb{F}}^2 - 1 \right) \\
&\quad \times \left(\operatorname{Re} \tilde{G}_{1,k-2} G_{1,k-2}^* \right) + a\nu_2 \xi_{k-2} \|G_{1,k-2}\|_{\mathbb{F}}^2 \left(2 - \xi_{k-2} \|G_{1,k-2}\|_{\mathbb{F}}^2 \right) \\
&= (4b\gamma(1-\gamma) - a\nu_2)\xi_{k-2}^2 \left(\operatorname{Re} \tilde{G}_{1,k-2} G_{1,k-2}^* + \frac{a\nu_2(\xi_{k-2} \|G_{k-2}\|_{\mathbb{F}}^2 - 1)}{(4b\gamma(1-\gamma) - a\nu_2)\xi_{k-2}} \right)^2 \\
&\quad + a\nu_2 \xi_{k-2} \|G_{1,k-2}\|_{\mathbb{F}}^2 \left(2 - \xi_{k-2} \|G_{1,k-2}\|_{\mathbb{F}}^2 \right) - \frac{a^2 \nu_2^2 (\xi_{k-2} \|G_{k-2}\|_{\mathbb{F}}^2 - 1)^2}{16b^2 \gamma^2 (1-\gamma)^2 \xi_{k-2}^2} \\
&\geq a\nu_2 \xi_{k-2} \|G_{1,k-2}\|_{\mathbb{F}}^2 \left(2 - \xi_{k-2} \|G_{1,k-2}\|_{\mathbb{F}}^2 \right) - \frac{a^2 \nu_2^2 (\xi_{k-2} \|G_{k-2}\|_{\mathbb{F}}^2 - 1)^2}{16b^2 \gamma^2 (1-\gamma)^2 \xi_{k-2}^2} \\
&= \frac{a\nu_2 \left(16b^2 \gamma^2 (1-\gamma)^2 \xi_{k-2}^3 \|G_{1,k-2}\|_{\mathbb{F}}^2 \left(2 - \xi_{k-2} \|G_{1,k-2}\|_{\mathbb{F}}^2 \right) - a\nu_2 (\xi_{k-2} \|G_{k-2}\|_{\mathbb{F}}^2 - 1)^2 \right)}{16b^2 \gamma^2 (1-\gamma)^2 \xi_{k-2}^2} \\
&\geq \frac{a\nu_2 (16b^2 \gamma^2 (1-\gamma)^2 c_2 - a\nu_2 c_1)}{16b^2 \gamma^2 (1-\gamma)^2 \xi_{k-1}^2}. \quad (3.79)
\end{aligned}$$

Note that (3.60) implies that for all $k \in \mathbb{N}$, $0 < \xi_k \leq \mu/\nu_1$. Thus, since $\cos \theta \neq 0$ and $b > \frac{\sqrt{a\nu_2 c_1/c_2}}{4\gamma(1-\gamma)}$, it follows from (3.79) that for all $k > k_s$,

$$\begin{aligned}
\psi_k &\geq \frac{a\nu_2 \nu_1^2 (16b^2 \gamma^2 (1-\gamma)^2 c_2 - a\nu_2 c_1)}{16b^2 \gamma^2 (1-\gamma)^2 \mu^2} \\
&> 0. \quad (3.80)
\end{aligned}$$

Moreover, note that for all $k > k_s$,

$$\begin{aligned}
\det P_k &= \phi_k \psi_k - \chi_k^2 \\
&= a\nu_2 \xi_{k-1}^2 \left(4b\gamma(1-\gamma)\xi_k \|G_{1,k-1}\|_{\mathbb{F}}^2 \left(2 - \xi_{k-1} \|G_{1,k-1}\|_{\mathbb{F}}^2 \right) - a\nu_2 \right) \\
&\quad \times \left((\cos \theta) \operatorname{Re} G_{1,*} G_{1,k-1}^* - \operatorname{Re} e^{j\theta} G_{1,*} G_{1,k-1}^* \right)^2 \\
&\geq a\nu_2 \xi_{k-1}^2 (4b\gamma(1-\gamma)c_3 - a\nu_2) \left((\cos \theta) \operatorname{Re} G_{1,*} G_{1,k-1}^* - \operatorname{Re} e^{j\theta} G_{1,*} G_{1,k-1}^* \right)^2 \\
&= a\nu_2 \xi_{k-1}^2 (4b\gamma(1-\gamma)c_3 - a\nu_2) (\sin \theta)^2 \left(\operatorname{Im} G_{1,*} G_{1,k-1}^* \right)^2. \quad (3.81)
\end{aligned}$$

Define

$$c_4 \triangleq \inf_{k \in \mathbb{N}} \xi_k^2,$$

which exists since part *i*) of Proposition 3.2 implies that $G_{1,k}$ is bounded. Thus, since

$b > \frac{a\nu_2}{4c_3\gamma(1-\gamma)}$, it follows from (3.81) that

$$\begin{aligned} \det P_k &\geq a\nu_2c_4(4b\gamma(1-\gamma)c_3 - a\nu_2)(\sin\theta)^2\varepsilon^2 \\ &> 0. \end{aligned} \quad (3.82)$$

Therefore, (3.78), (3.80), and (3.82) imply that for all $k > k_s$, P_k is symmetric positive definite.

Thus, it follows from (3.74) that for all $k > k_s$,

$$\Delta V(k) \leq -\frac{(\lambda_0 - \|\Delta_k\|_F) \left\| \begin{bmatrix} y_k & y_{k-1} \end{bmatrix}^T \right\|^2}{\nu_2 + a\nu_2 \begin{bmatrix} y_k & y_{k-1} \end{bmatrix} C_1 \begin{bmatrix} y_k & y_{k-1} \end{bmatrix}^T}, \quad (3.83)$$

where $\lambda_0 \triangleq \inf_{k \in \mathbb{N}} \lambda_{\min}(P_k)$. Next, note that it follows from (3.60) that for all $k \in \mathbb{Z}^+ \setminus \{1\}$,

$$\xi_{k-2} - \xi_{k-1} = -\frac{\xi_{k-1}^2 (G_{1,k-1} - G_{1,k-2})(G_{1,k-1} + G_{1,k-2})}{(\mu - \xi_{k-1}(G_{1,k-1} + G_{1,k-2}))}. \quad (3.84)$$

Since part *i*) of Proposition 3.2 implies that $G_{1,k}$ is bounded, using (3.84) it follows that there exists $M > 0$, such that for all $k \in \mathbb{Z}^+ \setminus \{1\}$,

$$\begin{aligned} \|\Delta_k\|_F &= \sqrt{\delta_{\psi,k}^2 + 2\delta_{\chi,k}^2} \\ &\leq M \|G_{1,k-1} - G_{1,k-2}\|_F. \end{aligned} \quad (3.85)$$

Note that part *ii*) of Proposition 3.2 implies that $\lim_{k \rightarrow \infty} \|G_{1,k-1} - G_{1,k-2}\|_F = 0$, which implies that there exists $k_0 \in \mathbb{Z}^+$ such that for all $k > k_0$, $\|G_{1,k-1} - G_{1,k-2}\|_F \leq \lambda_0/2$. Since, in addition, $\lambda_{\min}(C_1) = \min\{1 + \cos\theta, 1 - \cos\theta\} \geq 1 - |\cos\theta| > 0$, it follows from (3.83) that for all $k > k_1 \triangleq \max\{k_0, k_s\}$,

$$\Delta V(k) \leq -\frac{\lambda_0 \left\| \begin{bmatrix} y_k & y_{k-1} \end{bmatrix}^T \right\|^2}{2\nu_2 + 2a\nu_2(1 - |\cos\theta|) \left\| \begin{bmatrix} y_k & y_{k-1} \end{bmatrix}^T \right\|^2}, \quad (3.86)$$

Since, in addition, $V(y_k, y_{k+1}, \tilde{H}_{1,k})$ is positive definite, it follows from (3.70) and (3.86) that

$$\begin{aligned} 0 &\leq \lim_{k \rightarrow \infty} \sum_{j=k_1}^k \frac{\lambda_0 \left\| \begin{bmatrix} y_j & y_{j-1} \end{bmatrix}^T \right\|^2}{2\nu_2 + 2a\nu_2(1 - |\cos\theta|) \left\| \begin{bmatrix} y_k & y_{k-1} \end{bmatrix}^T \right\|^2} \\ &\leq -\lim_{k \rightarrow \infty} \sum_{j=k_1}^k \Delta V(j) \end{aligned}$$

$$\begin{aligned}
&\leq V(y_{k_1+1}, y_{k_1}, \tilde{H}_{1,k_1}) - \lim_{k \rightarrow \infty} V(y_{k+1}, y_k, \tilde{H}_{1,k}) \\
&\leq V(y_{k_s+1}, y_{k_s}, \tilde{H}_{1,k_s}),
\end{aligned} \tag{3.87}$$

where the upper and lower bounds imply that all the limits exist. Thus,

$$\lim_{k \rightarrow \infty} \frac{\left\| \begin{bmatrix} y_k & y_{k-1} \end{bmatrix}^T \right\|^2}{2\nu_2 + 2a\nu_2(1 - |\cos \theta|) \left\| \begin{bmatrix} y_k & y_{k-1} \end{bmatrix}^T \right\|^2} = 0, \tag{3.88}$$

which implies that $\lim_{k \rightarrow \infty} y_k = 0$. \square

3.17 Lemma 3.3 used in proof of Theorems 3.3 and 3.4

Lemma 3.3. Let $\bar{G}_1, \bar{G}_2 \in \mathbb{C}^{\ell \times m}$, and define

$$\bar{H}_1 \triangleq \begin{bmatrix} \operatorname{Re} \bar{G}_1 & \operatorname{Im} \bar{G}_1 \\ -\operatorname{Im} \bar{G}_1 & \operatorname{Re} \bar{G}_1 \end{bmatrix}, \quad \bar{H}_2 \triangleq \begin{bmatrix} \operatorname{Re} \bar{G}_2 & \operatorname{Im} \bar{G}_2 \\ -\operatorname{Im} \bar{G}_2 & \operatorname{Re} \bar{G}_2 \end{bmatrix}.$$

Then, for all $k \in \mathbb{N}$,

$$\begin{aligned}
(f_{i,k}^T \otimes I_\ell) \bar{H}_1 \bar{H}_2^T (f_{i,k} \otimes I_\ell) &= \operatorname{Re} \bar{G}_1 \bar{G}_2^*, \\
(f_{i,k+1}^T \otimes I_\ell) \bar{H}_1 \bar{H}_2^T (f_{i,k} \otimes I_\ell) &= \operatorname{Re} e^{j\omega_i T_s} \bar{G}_1 \bar{G}_2^*.
\end{aligned}$$

Proof. The proof follows from direct calculations. \square

Chapter 4

Frequency-Domain Adaptive Harmonic Control

In this chapter, we present frequency-domain adaptive harmonic control (FD-AHC) algorithm that addresses the problem of rejecting sinusoids with known frequencies that act on a completely unknown asymptotically stable linear time-invariant system. We analyze the stability and closed-loop performance of FD-AHC for multi-input multi-output systems with at least as many controls as performance measurements. We show that the closed-loop system is Lyapunov stable and that the adaptive controller asymptotically rejects the disturbances. We also present numerical simulations comparing FD-AHC with the existing sinusoidal disturbance rejection approach FD-HHC. The result of this chapter appears in [196, 197].

4.1 Introduction

Sinusoidal disturbance rejection is a fundamental control objective, which arises in a wide variety of applications, including active noise cancellation [33], helicopter vibration suppression [10], active rotor balancing [20], and vibration reduction in spacecraft [59].

For an accurately modeled linear time-invariant (LTI) system, the internal-model principle can be used to design a feedback controller capable of rejecting sinusoidal disturbances of known frequencies [115–117, 119]. In this case, disturbance rejection is accomplished by incorporating copies of the disturbance dynamics in the feedback loop. For sinusoids with unknown frequencies, a model-based disturbance observer can be implemented [121–125].

If, on the other hand, an accurate model of the system is not available, but the open-loop dynamics are asymptotically stable, then adaptive feedforward cancellation can be used to accomplish disturbance rejection [129–135]. These approaches use a harmonic regressor consisting of sinusoids at the known disturbance frequencies. The control is generated by updating the amplitudes and phases of these sinusoids in a manner that achieves asymptotic disturbance rejection. Adaptive feedforward

approaches require certain model information or assumptions regarding the open-loop transfer function. In the simplest case where the system is single-input single-output (SISO), the only required model information is the sign of the control-to-performance transfer function at the disturbance frequencies. However, if the system is multi-input multi-output (MIMO), then stronger assumptions (e.g., strict positive realness, a nominal system model, or upper bounds on uncertainties) are invoked. Feedback (rather than feedforward) adaptive control methods are also capable of rejecting sinusoids of known or even unknown frequencies (e.g., [139–146]); however, these approaches generally rely on some model information (e.g., relative degree) and structural assumptions regarding the system (e.g., minimum phase, or state feedback).

The filtered-X least-mean-squares algorithm is an approach from the digital signal processing literature [152, 153]. Filtered-X can be used in cases where the disturbance frequencies are uncertain or unknown; however, filtered-X relies on a model of the control-to-performance transfer function (referred to as the secondary path in the noise control literature). If this model is inaccurate, then filtered-X can destabilize the closed loop [33]. To reduce the required model information, algorithms have been proposed which incorporate real-time identifiers [154, 155]. However, these methods require injection of white-noise excitation to ensure convergence of the parameter identifier.

Another approach to sinusoidal disturbance rejection takes advantage of an asymptotically stable LTI system’s harmonic steady-state (HSS) response, that is, the sinusoidal response that remains after the system’s transient response decays to zero. This HSS approach was developed independently in several research communities, specifically, i) active sound and vibration control [32], ii) helicopter vibration reduction [10, 156], and iii) active rotor balancing [20]. For active rotor balancing, this approach is called convergent control, whereas for helicopter vibration reduction, the approach is known as higher harmonic control. In this chapter, we refer to the approach as frequency-domain higher harmonic control (FD-HHC).

To discuss FD-HHC control further, let G_{yu} denote the control-to-performance transfer function, and assume that there is a single known disturbance frequency ω . Then, FD-HHC requires an estimate of $G_{yu}(j\omega)$, that is, an estimate of the transfer function evaluated at the disturbance frequency. In the SISO case, FD-HHC stabilizes the closed-loop if the estimate of $G_{yu}(j\omega)$, which is a single complex number, has an angle within 90° of $\angle G_{yu}(j\omega)$. In the MIMO case, closed-loop stability is ensured if the estimate of $G_{yu}(j\omega)$ is sufficiently accurate. If there are multiple disturbance frequencies, then estimates are required at each frequency.

For certain applications $G_{yu}(j\omega)$ can be difficult to estimate or subject to change. For example, a helicopter’s structural dynamics may vary depending on payload. To address this uncertainty, online estimation methods have been combined with HSS control [81, 157, 158]. For example, a recursive-least-squares identifier is used in [81, 157] to estimate $G_{yu}(j\omega)$ in real time; however, an external excitation signal is required to ensure stability.

In this chapter, we present a new frequency-domain adaptive harmonic control (FD-AHC) algorithm, which is effective for rejecting sinusoids with known frequencies that act on a completely unknown MIMO LTI system. We analyze the stability

and closed-loop performance of FD-AHC for MIMO systems with at least as many controls as performance measurements. We provide conditions such that the measured performance tends to zero, that is, the disturbance is asymptotically rejected. In contrast to FD-HHC [10, 20, 32, 156] and other existing adaptive feedforward methods [129–135], FD-AHC requires no model information.

The new FD-AHC algorithm presented in this chapter is a frequency-domain method, meaning that all computations use discrete Fourier transform (DFT) data rather than time-domain data. The FD-AHC algorithm (including DFT) is demonstrated on a numerical simulation of an acoustic duct.

4.2 Notation

Let \mathbb{F} be either \mathbb{R} or \mathbb{C} . Let $x_{(i)}$ denote the i th element of $x \in \mathbb{F}^n$, and let $A_{(i,j)}$ denote the element in row i and column j of $A \in \mathbb{F}^{m \times n}$. Let $\|\cdot\|$ be the 2-norm on \mathbb{F}^n . Next, let A^* denote the complex conjugate transpose of $A \in \mathbb{F}^{m \times n}$, and define $\|A\|_{\mathbb{F}} \triangleq \sqrt{\text{tr } A^*A}$, which is the Frobenius norm of $A \in \mathbb{F}^{m \times n}$.

Let $\text{spec}(A) \triangleq \{\lambda \in \mathbb{C} : \det(\lambda I - A) = 0\}$ denote the spectrum of $A \in \mathbb{F}^{n \times n}$. Let $\lambda_{\min}(A)$ and $\lambda_{\max}(A)$ denote the minimum and maximum eigenvalues, respectively, of the Hermitian positive-semidefinite matrix $A \in \mathbb{F}^{n \times n}$. Let $\angle \lambda$ denote the argument of $\lambda \in \mathbb{C}$ defined on the interval $(-\pi, \pi]$ rad. Let OLHP, ORHP, OUD, and CUD denote the open-left-half plane, open-right-half plane, open unit disk, and closed unit disk in \mathbb{C} , respectively.

Define $\mathbb{N} \triangleq \{0, 1, 2, \dots\}$ and $\mathbb{Z}^+ \triangleq \mathbb{N} \setminus \{0\}$. Define the *open ball of radius $r > 0$ centered at $C \in \mathbb{C}^{m \times n}$* by $\mathbb{B}_r(C) \triangleq \{X \in \mathbb{C}^{m \times n} : \|X - C\|_{\mathbb{F}} < r\}$.

4.3 Problem Formulation

Consider the LTI system

$$\dot{x}(t) = Ax(t) + Bu(t) + D_1d(t), \quad (4.1)$$

$$y(t) = Cx(t) + Du(t) + D_2d(t), \quad (4.2)$$

where $t \geq 0$, $x(t) \in \mathbb{R}^n$ is the state, $x(0) = x_0 \in \mathbb{R}^n$ is the initial condition, $u(t) \in \mathbb{R}^m$ is the control, $y(t) \in \mathbb{R}^\ell$ is the measured performance, $d(t) \in \mathbb{R}^p$ is the unmeasured disturbance, and $A \in \mathbb{R}^{n \times n}$ is asymptotically stable. Define the transfer functions $G_{yu} : \mathbb{C} \rightarrow \mathbb{C}^{\ell \times m}$ and $G_{yd} : \mathbb{C} \rightarrow \mathbb{C}^{\ell \times p}$ by $G_{yu}(s) \triangleq C(sI - A)^{-1}B + D$ and $G_{yd}(s) \triangleq C(sI - A)^{-1}D_1 + D_2$.

Let $\omega_1, \omega_2, \dots, \omega_q > 0$, and consider the tonal disturbance

$$d(t) = \sum_{i=1}^q d_{c,i} \cos \omega_i t + d_{s,i} \sin \omega_i t, \quad (4.3)$$

where $d_{c,1}, \dots, d_{c,q}, d_{s,1}, \dots, d_{s,q} \in \mathbb{R}^p$ determine the disturbance amplitude and phase at each frequency.

The objective is to design a control u that reduces or even eliminates the effect of the disturbance d on the performance y . We seek a control that relies on no model information regarding the system (4.1) and (4.2), and requires knowledge of only the disturbance frequencies $\omega_1, \dots, \omega_q$. Thus, the disturbance amplitudes $d_{c,i}$ and $d_{s,i}$, and the system (4.1) and (4.2) are completely unknown.

We first focus on the case where d is the single-tone disturbance

$$d(t) = d_c \cos \omega t + d_s \sin \omega t.$$

However, the adaptive controller presented in this chapter generalizes to the case, where d consists of multiple tones. We discuss the extension to multiple tones in Section 4.6.

For the moment, assume that G_{yu} , G_{yd} , d_c , and d_s are known. In this case, consider the harmonic control

$$u(t) = u_c \cos \omega t + u_s \sin \omega t, \quad (4.4)$$

where $u_c, u_s \in \mathbb{R}^m$. Define $\hat{u} \triangleq u_c - ju_s$, which is the DFT at frequency ω obtained from a sampling of u . In addition, define

$$\begin{aligned} M_* &\triangleq G_{yu}(j\omega) \in \mathbb{C}^{\ell \times m}, \\ d_* &\triangleq G_{yd}(j\omega)(d_c - jd_s) \in \mathbb{C}^{\ell}. \end{aligned}$$

Then, the harmonic steady-state (HSS) performance of (4.1) and (4.2) with control (4.4) is

$$\begin{aligned} y_{\text{hss}}(t, \hat{u}) &\triangleq \text{Re} \left[\left(G_{yu}(j\omega) \hat{u} + G_{yd}(j\omega)(d_c - jd_s) \right) e^{j\omega t} \right] \\ &= \text{Re} (M_* \hat{u} + d_*) \cos \omega t - \text{Im} (M_* \hat{u} + d_*) \sin \omega t. \end{aligned} \quad (4.5)$$

The HSS performance y_{hss} is the steady-state output y of (4.1) and (4.2) with control (4.4), that is, $\lim_{t \rightarrow \infty} [y_{\text{hss}}(t) - y(t)] = 0$ [201, Chap. 12.12]. Define

$$\hat{y}_{\text{hss}}(\hat{u}) \triangleq M_* \hat{u} + d_*, \quad (4.6)$$

which is the DFT at frequency ω obtained from a sampling of y_{hss} . Consider the cost function

$$J(\hat{u}) \triangleq \lim_{t \rightarrow \infty} \frac{1}{t} \int_0^t \|y_{\text{hss}}(\tau, \hat{u})\|^2 d\tau, \quad (4.7)$$

which is the average power of y_{hss} . Using (4.5) and (4.6), it follows that

$$\begin{aligned} J(\hat{u}) &= \lim_{t \rightarrow \infty} \frac{1}{t} \int_0^t \|\text{Re} \hat{y}_{\text{hss}}(\hat{u}) \cos \omega \tau - \text{Im} \hat{y}_{\text{hss}}(\hat{u}) \sin \omega \tau\|^2 d\tau \\ &= \begin{bmatrix} \text{Re} \hat{y}_{\text{hss}}(\hat{u}) \\ \text{Im} \hat{y}_{\text{hss}}(\hat{u}) \end{bmatrix}^T \left(\lim_{t \rightarrow \infty} \frac{1}{t} \int_0^t \begin{bmatrix} \cos^2 \omega \tau & -(\cos \omega \tau)(\sin \omega \tau) \\ -(\cos \omega \tau)(\sin \omega \tau) & \sin^2 \omega \tau \end{bmatrix} d\tau \right) \end{aligned}$$

$$\begin{aligned}
& \times \begin{bmatrix} \operatorname{Re} \hat{y}_{\text{hss}}(\hat{u}) \\ \operatorname{Im} \hat{y}_{\text{hss}}(\hat{u}) \end{bmatrix} \\
& = \frac{1}{2} \hat{y}_{\text{hss}}^*(\hat{u}) \hat{y}_{\text{hss}}(\hat{u}).
\end{aligned} \tag{4.8}$$

The following result provides an expression for a control $\bar{u} = u_*$ that minimizes J . See Theorem 2.1 for details.

Theorem 4.1. Consider the cost function (4.7), and assume that $\operatorname{rank} M_* = \min\{m, \ell\}$. Define $u_* \triangleq -M_*^*(M_*M_*^*)^{-1}d_*$. Then, $\hat{y}_{\text{hss}}(u_*) = 0$, and $J(u_*) = 0$.

Theorem 4.1 provides an expression for a control u_* that minimizes J , but u_* requires knowledge of M_* and d_* .

In this chapter, we consider a sinusoidal control with frequency ω but where the amplitude and phase are updated in discrete time. Let $T_s > 0$ be the update period, and for each $k \in \mathbb{N}$, let $u_k \in \mathbb{C}^m$ contain information regarding the control amplitude and phase, which is determined from control update equations presented later. Then, for each $k \in \mathbb{N}$ and for all $t \in [kT_s, (k+1)T_s)$, the control is

$$u(t) = \operatorname{Re} u_k \cos \omega t - \operatorname{Im} u_k \sin \omega t. \tag{4.9}$$

For each $k \in \mathbb{Z}^+$, let $y_k \in \mathbb{C}^\ell$ denote DFT at frequency ω of the sequence obtained by sampling y on the interval $[(k-1)T_s, kT_s)$. If T_s is sufficiently large relative to the settling time of G_{yu} , then for all $k \in \mathbb{N}$, $y_{k+1} \approx \hat{y}_{\text{hss}}(u_k)$. For the remainder of this chapter, we assume that for all $k \in \mathbb{N}$, $y_{k+1} = \hat{y}_{\text{hss}}(u_k)$. In this case, (4.6) implies that for all $k \in \mathbb{N}$,

$$y_{k+1} = M_* u_k + d_*. \tag{4.10}$$

The HSS assumption $y_{k+1} = \hat{y}_{\text{hss}}(u_k)$ is used for stability analyses only. For the remainder of this chapter, we also assume that $\operatorname{rank} M_* = \min\{\ell, m\}$, which is a technical assumption that depends on sensor and actuator placement.

4.4 Frequency-Domain Adaptive Harmonic Control

We now develop a new frequency-domain adaptive harmonic control (FD-AHC), that does not require any information regarding M_* or d_* . For all $k \in \mathbb{N}$, u_k is given by

$$u_k \triangleq -M_k^+ d_k, \tag{4.11}$$

where $d_k \in \mathbb{C}^\ell$ and $M_k \in \mathbb{C}^{\ell \times m}$ are adaptive parameters that are determined from update equations presented below.

Consider the cost function $\mathcal{J}_k : \mathbb{C}^\ell \times \mathbb{C}^{\ell \times m} \rightarrow [0, \infty)$ defined by

$$\mathcal{J}_k(\bar{d}, \bar{M}) \triangleq \frac{1}{2} \left\| \bar{M} u_k + \bar{d} - y_{k+1} \right\|^2.$$

Note that \mathcal{J}_k can be interpreted as a measure of how well $\bar{M}u_k + \bar{d}$ approximates the performance y_{k+1} , which itself is approximately equal to the HSS performance $\hat{y}_{\text{hss}}(u_k) = M_*u_k + d_*$.

To determine the update equations, we define the gradients of \mathcal{J}_k with respect to \bar{d} and \bar{M} evaluated at $\bar{d} = d_k$ and $\bar{M} = M_k$, which are given by

$$\begin{aligned}\delta_k &\triangleq \left(\frac{\partial \mathcal{J}_k}{\partial \bar{d}} \bigg|_{(\bar{d}, \bar{M})=(d_k, M_k)} \right)^{\text{T}} \\ &= M_k u_k + d_k - y_{k+1},\end{aligned}\tag{4.12}$$

$$\begin{aligned}\Gamma_k &\triangleq \left(\frac{\partial \mathcal{J}_k}{\partial \bar{M}} \bigg|_{(\bar{d}, \bar{M})=(d_k, M_k)} \right)^{\text{T}} \\ &= (M_k u_k + d_k - y_{k+1}) u_k^*.\end{aligned}\tag{4.13}$$

Let $\mu > 0$, $\gamma > 0$, and $\nu \geq 0$. Then, for all $k \in \mathbb{N}$, the update equations are

$$d_{k+1} = d_k - \mu \eta_k \delta_k,\tag{4.14}$$

$$M_{k+1} = M_k - \gamma \eta_k \Gamma_k,\tag{4.15}$$

where

$$\eta_k \triangleq \frac{1}{\nu + \|u_k\|^2}.\tag{4.16}$$

The initial conditions for (4.14) and (4.15) are $d_0 \in \mathbb{C}^\ell$ and $M_0 \in \mathbb{C}^{\ell \times m}$.

Thus, FD-AHC is given by (4.9)–(4.16). The control architecture is shown in Fig. 4.1.

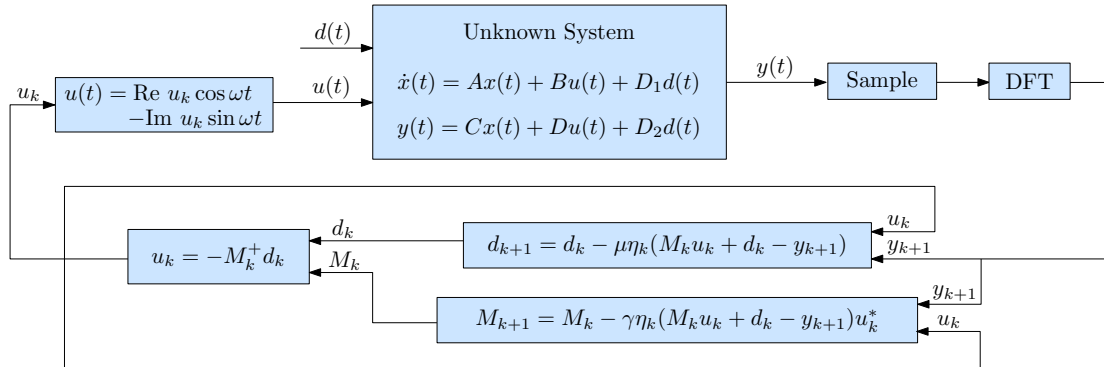


Figure 4.1: Schematic of FD-AHC given by (4.9)–(4.16).

4.5 FD-AHC Stability Analysis

Let $\alpha > \gamma/2 + \mu/(2\nu)$, and define the estimation errors

$$\tilde{d}_k \triangleq d_k - \alpha d_*, \quad \tilde{M}_k \triangleq M_k - \alpha M_*.$$

Then, subtracting αd_* from both sides of (4.14) and substituting (4.10)–(4.12), and (4.16) yields

$$\tilde{d}_{k+1} = \tilde{d}_k + \frac{\mu}{\nu + \|M_k^+ d_k\|^2} \left[\tilde{M}_k M_k^+ d_k - \tilde{d}_k + (1 - \alpha) y_{k+1} \right]. \quad (4.17)$$

Similarly, subtracting αM_* from both sides of (4.15) and substituting (4.10), (4.11), (4.13), and (4.16) yields

$$\tilde{M}_{k+1} = \tilde{M}_k + \frac{\gamma}{\nu + \|M_k^+ d_k\|^2} \left[\tilde{M}_k M_k^+ d_k - \tilde{d}_k + (1 - \alpha) y_{k+1} \right] (M_k^+ d_k)^*. \quad (4.18)$$

The following theorem is the main analytic result of this chapter and provides the stability properties of the closed-loop system (4.10), (4.17), and (4.18). The proof is in Section 4.9.

Theorem 4.2. Consider the closed-loop system (4.10), (4.17), and (4.18), which consists of (4.10)–(4.16), where $\nu > 0$, $\mu > 0$, and $\gamma > 0$. Then, for all $\alpha > \gamma/2 + \mu/(2\nu)$, the following statements hold:

- i)* $(\tilde{d}_k, \tilde{M}_k) \equiv 0$ is a Lyapunov stable equilibrium of (4.10), (4.17), and (4.18).
- ii)* There exists $r > 0$ such that for all $\tilde{d}_0 \in \mathbb{B}_r(0)$ and all $\tilde{M}_0 \in \mathcal{H} \cap \mathbb{B}_r(0)$, d_k , M_k , and u_k are bounded and $\lim_{k \rightarrow \infty} y_k = 0$.
- iii)* Let $d_0 \in \mathbb{R}^\ell$, and let $M_0 \in \mathbb{C}^{\ell \times m}$. Assume that there exists $k_s \in \mathbb{N}$ and $\varepsilon > 0$ such that for all $k \geq k_s$, $\lambda_{\min}(M_k M_k^*) > \varepsilon$. Then, d_k , M_k , and u_k are bounded, and $\lim_{k \rightarrow \infty} y_k = 0$.

Part *i)* of Theorem 4.2 states that the equilibria of the closed-loop system (4.10), (4.17), and (4.18) are Lyapunov stable, and part *ii)* guarantees local convergence of the performance y_k to zero. Part *iii)* provides a sufficient condition for global boundedness of d_k , M_k , and u_k , as well as global convergence of the performance y_k to zero. Specifically, part *iii)* invokes the assumption that there exist $k_s \in \mathbb{N}$ and $\varepsilon > 0$ such that for all $k \geq k_s$, $\lambda_{\min}(M_k M_k^*) > \varepsilon$. This assumption, which implies that M_k is asymptotically full row rank, cannot be verified *a priori*. However, the assumption $\lambda_{\min}(M_k M_k^*) > \varepsilon$, for some arbitrarily small $\varepsilon > 0$, can be verified at each time step. If the condition $\lambda_{\min}(M_k M_k^*) > \varepsilon$ is violated on a time step, then M_k can be perturbed to ensure $\lambda_{\min}(M_k M_k^*) > \varepsilon$. However, analyzing the stability of such a perturbation is an open problem. Nevertheless, simulations and experiments suggest that for almost all initial conditions $d_0 \in \mathbb{R}^\ell$ and $M_0 \in \mathbb{C}^{\ell \times m}$, M_k is asymptotically

full row rank, and thus, satisfies $\lambda_{\min}(M_k M_k^*) > \varepsilon$. In this case, part *iii*) states that the performance y_k globally tends to zero.

Notably, Theorem 4.2 does not impose upper bounds on the gains μ and γ . Thus, FD-AHC can be implemented with arbitrarily large gains, which can improve convergence time.

4.6 FD-AHC for Multi-Tone Disturbances

In this section, we extend FD-AHC to address the multi-tone disturbance (4.3). For the moment, assume that G_{yu} , G_{yd} , $d_{c,1}, \dots, d_{c,q}$, and $d_{s,1}, \dots, d_{s,q}$ are known, and consider the harmonic control

$$u(t) = \sum_{i=1}^q u_{c,i} \cos \omega_i t + u_{s,i} \sin \omega_i t, \quad (4.19)$$

where $u_{c,1}, \dots, u_{c,q}, u_{s,1}, \dots, u_{s,q} \in \mathbb{C}^m$. For $i = 1, \dots, q$, define $\hat{u}_i \triangleq u_{c,i} - j u_{s,i}$, which is the DFT at frequency ω_i obtained from a sampling of u . In addition, for $i = 1, \dots, q$, define

$$\begin{aligned} M_{*,i} &\triangleq G_{yu}(j\omega_i) \in \mathbb{C}^{\ell \times m}, \\ d_{*,i} &\triangleq G_{yd}(j\omega_i)(d_{c,i} - j d_{s,i}) \in \mathbb{C}^{\ell}. \end{aligned}$$

Then, the HSS performance of (4.1) and (4.2) with control (4.19) and disturbance (4.3) is

$$\begin{aligned} y_{m,\text{hss}}(t, \hat{u}_1, \dots, \hat{u}_q) &\triangleq \sum_{i=1}^q \text{Re} \left[\left(G_{yu}(j\omega_i) \hat{u}_i + G_{yd}(j\omega_i)(d_{c,i} - j d_{s,i}) \right) e^{j\omega_i t} \right] \\ &= \sum_{i=1}^q \text{Re} (M_{*,i} \hat{u}_i + d_{*,i}) \cos \omega_i t - \text{Im} (M_{*,i} \hat{u}_i + d_{*,i}) \sin \omega_i t, \quad (4.20) \end{aligned}$$

which is the multi-tone generalization of (4.5). For $i = 1, \dots, q$, define

$$\hat{y}_{\text{hss},i}(\hat{u}_i) \triangleq M_{*,i} \hat{u}_i + d_{*,i}, \quad (4.21)$$

which is DFT at frequency ω_i obtained from a sampling of $y_{m,\text{hss}}$. Consider the cost function

$$J_m(\hat{u}_1, \dots, \hat{u}_q) \triangleq \lim_{t \rightarrow \infty} \frac{1}{t} \int_0^t \|y_{m,\text{hss}}(\tau, \hat{u}_1, \dots, \hat{u}_q)\|^2 d\tau. \quad (4.22)$$

Using (4.20) and (4.21), it follows that

$$J_m(\hat{u}_1, \dots, \hat{u}_q) = \lim_{t \rightarrow \infty} \frac{1}{t} \int_0^t \left\| \sum_{i=1}^q \left[\text{Re} \hat{y}_{\text{hss},i}(\hat{u}_i) \right] \cos \omega_i \tau - \left[\text{Im} \hat{y}_{\text{hss},i}(\hat{u}_i) \right] \sin \omega_i \tau \right\|^2 d\tau$$

$$\begin{aligned}
&= \frac{1}{2} \sum_{i=1}^q \hat{y}_{\text{hss},i}^*(\hat{u}_i) \hat{y}_{\text{hss},i}(\hat{u}_i) \\
&= \sum_{i=1}^q \lim_{t \rightarrow \infty} \frac{1}{t} \int_0^t \|y_{\text{hss},i}(\tau, \hat{u}_i)\|^2 d\tau,
\end{aligned}$$

where for $i = 1, \dots, q$, the steady-state response at frequency ω_i is given by

$$y_{\text{hss},i}(t, \hat{u}_i) \triangleq \text{Re}(M_{*,i}\hat{u}_i + d_{*,i}) \cos \omega_i t - \text{Im}(M_{*,i}\hat{u}_i + d_{*,i}) \sin \omega_i t,$$

Thus, if for each $i = 1, \dots, q$, the average power $\lim_{t \rightarrow \infty} \frac{1}{t} \int_0^t \|y_{\text{hss},i}(\tau, \hat{u}_i)\|^2 d\tau$ at frequency ω_i is minimized, then the average power (4.22) is minimized. For $i = 1, 2, \dots, q$, the ideal control is

$$u_{*,i} \triangleq -M_{*,i}^+ d_{*,*}.$$

Therefore, we can use q copies of the FD-AHC algorithm (4.11)–(4.16)—one at each disturbance frequency.

For $i = 1, \dots, q$, let $y_{i,k} \in \mathbb{C}^\ell$ denote the DFT at frequency ω_i of the sequence obtained by sampling y on the interval $[(k-1)T_s, kT_s)$. For each $k \in \mathbb{N}$ and for all $t \in [kT_s, (k+1)T_s)$, the control is

$$u(t) = \sum_{i=1}^q \text{Re } u_{i,k} \cos \omega_i t - \text{Im } u_{i,k} \sin \omega_i t, \quad (4.23)$$

where for all $i = 1, \dots, q$,

$$u_{i,k} \triangleq -M_{i,k}^+ d_{i,k}, \quad (4.24)$$

and

$$d_{i,k} \triangleq d_{i,k} - \mu_i \eta_{i,k} (M_{i,k} u_{i,k} + d_{i,k} - y_{i,k+1}), \quad (4.25)$$

$$M_{i,k+1} \triangleq M_{i,k} - \gamma_i \eta_{i,k} (M_{i,k} u_{i,k} + d_{i,k} - y_{i,k+1}) u_{i,k}^*, \quad (4.26)$$

where $\mu_i > 0$, $\gamma_i > 0$, $\nu_i > 0$, and $d_{i,0} \in \mathbb{C}^\ell$ and $M_{i,0} \in \mathbb{C}^{\ell \times m}$ are the initial conditions, and

$$\eta_{i,k} \triangleq \frac{1}{\nu_i + \|u_{i,k}\|^2}. \quad (4.27)$$

Thus, FD-AHC for multi-tone disturbance is given by (4.23)–(4.27). If T_s is sufficiently large relative to the settling time of G_{yu} , then for $i = 1, \dots, q$, and for all $k \in \mathbb{N}$, $y_{i,k+1} \approx \hat{y}_{\text{hss},i}(u_{i,k})$. We assume that for $i = 1, \dots, q$, and for all $k \in \mathbb{N}$, $y_{i,k+1} = \hat{y}_{\text{hss},i}(u_{i,k})$. In this case, (4.21) implies that for all $k \in \mathbb{N}$,

$$y_{i,k+1} = M_{*,i} u_{i,k} + d_{*,i}. \quad (4.28)$$

For all $i \in \{1, 2, \dots, q\}$, let $\alpha_i > \gamma_i/2 + \mu_i/\nu_i$, and define the estimation errors

$$\tilde{d}_{i,k} \triangleq d_{i,k} - \alpha_i d_{*,i}, \quad \tilde{M}_{i,k} \triangleq M_{i,k} - \alpha M_{*,i}.$$

Then, similar to derivation of (4.17) and (4.18), it follows from (4.24)–(4.28) that

$$\begin{aligned} \tilde{d}_{i,k+1} &= \tilde{d}_{i,k} + \frac{\mu_i}{\nu_i + \|M_{i,k}^+ d_{i,k}\|^2} \left[(1 - \alpha_i) y_{i,k+1} + (\tilde{M}_{i,k} M_{i,k}^+ d_{i,k} - \tilde{d}_{i,k}) \right], \\ \tilde{M}_{i,k+1} &= \tilde{M}_{i,k} + \frac{\gamma_i}{\nu_i + \|M_{i,k}^+ d_{i,k}\|^2} \left[(1 - \alpha_i) y_{i,k+1} + (\tilde{M}_{i,k} M_{i,k}^+ d_{i,k} - \tilde{d}_{i,k}) \right] (M_{i,k}^+ d_{i,k})^*. \end{aligned} \quad (4.29)$$

$$(4.30)$$

The following result is a corollary of Theorem 4.2 and provides the stability properties of the closed-loop system (4.28)–(4.30) with multi-tone disturbance.

Corollary 4.1. For $i = 1, \dots, q$, consider the closed-loop system (4.28)–(4.30), which consists of the open-loop system (4.28) and the control (4.24)–(4.27), where $\mu_i > 0$, $\gamma_i > 0$, $\nu_i > 0$, and where $m \geq \ell$. Then, for all $\alpha_i > \gamma_i/2 + \mu_i/\nu_i$, the following statements hold:

- i) $(\tilde{d}_{i,k}, \tilde{M}_{i,k}) \equiv 0$ is a uniformly Lyapunov stable equilibrium of (4.10), (4.17), and (4.18).
- ii) There exists $r > 0$ such that for all $\tilde{d}_{i,0} \in \mathbb{B}_r(0)$ and all $\tilde{M}_{i,0} \in \mathbb{B}_r(0)$, $d_{i,k}$, $M_{i,k}$, and $u_{i,k}$ are bounded and $\lim_{k \rightarrow \infty} y_{i,k} = 0$.
- iii) Let $d_{i,0} \in \mathbb{R}^\ell$, and let $M_{i,0} \in \mathbb{C}^{\ell \times m}$. Assume that there exists $k_s \in \mathbb{N}$ and $\varepsilon > 0$ such that for all $k \geq k_s$, $\lambda_{\min}(M_{i,k} M_{i,k}^*) > \varepsilon$. Then, $d_{i,k}$, $M_{i,k}$, and $u_{i,k}$ are bounded, and $\lim_{k \rightarrow \infty} y_{i,k} = 0$.

4.7 Numerical Examples

Consider the two-mass structure shown in Fig. 4.2, where ψ_1 and ψ_2 are control forces, and d_1 and d_2 are disturbance forces. The equations of motion are given by (4.1), where

$$A = \begin{bmatrix} 0 & 1 & 0 & 0 \\ \frac{-(k_1+k_2)}{m_1} & \frac{-(c_1+c_2)}{m_1} & \frac{k_2}{m_1} & \frac{c_2}{m_1} \\ 0 & 0 & 0 & 1 \\ \frac{k_2}{m_2} & \frac{c_2}{m_2} & \frac{-(k_2+k_3)}{m_2} & \frac{-(c_2+c_3)}{m_2} \end{bmatrix}, \quad B = \begin{bmatrix} 0 & 0 \\ \frac{1}{m_1} & 0 \\ 0 & 0 \\ 0 & \frac{1}{m_2} \end{bmatrix}, \quad D_1 = B, \quad (4.31)$$

$$x(t) = \begin{bmatrix} \xi_1(t) \\ \dot{\xi}_1(t) \\ \xi_2(t) \\ \dot{\xi}_2(t) \end{bmatrix}, \quad u(t) = \begin{bmatrix} \psi_1(t) \\ \psi_2(t) \end{bmatrix}, \quad d(t) = \begin{bmatrix} d_1(t) \\ d_2(t) \end{bmatrix}. \quad (4.32)$$

Let $m_1 = 2$ kg, $m_2 = 1$ kg, $c_1 = 60$ kg/s, $c_2 = 50$ kg/s, $c_3 = 40$ kg/s, $k_1 = 300$ N/m, $k_2 = 200$ N/m, and $k_3 = 400$ N/m. For all examples, $\nu = 1$. The initial conditions are $x(0) = 0$, $d_{i,0} = 0$. The initial condition $M_{i,0}$, the update period T_s , and the gains μ_i and γ_i are specified in each example.

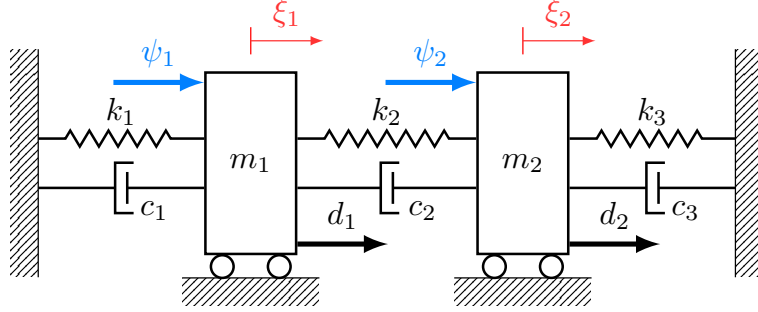


Figure 4.2: Two-mass structure used in Examples 4.1–4.3.

In the following examples, we compare FD-HHC to FD-AHC. FD-HHC requires an estimate of $G_{yu}(j\omega_i)$, and the estimate must be sufficiently accurate to ensure closed-loop stability. See Theorem 2.2 for details. In the SISO case, the closed-loop FD-HHC system is asymptotically stable only if the estimate of $M_{*,i}$ is within 90° of $M_{*,i}$. In contrast, FD-AHC does not require a sufficiently accurate estimate of $M_{*,i}$. To compare FD-HHC and FD-AHC, we set the FD-HHC estimate of $M_{*,i}$ equal to the FD-AHC initial condition $M_{i,0}$, which, in most applications, is the best *a priori* estimate of $M_{*,i}$.

We implement FD-HHC according to (2.11). FD-HHC is a frequency-domain method, and all computations use DFT data. The DFT is performed using a 1 kHz sampling frequency. We select the FD-HHC gain $\rho = 4.4 \times 10^5$, which was determined through numerical experimentation to yield the fastest convergence rate.

Example 4.1. Consider the SISO system (4.1) and (4.31)–(4.32), where $y = \xi_1$, $\psi_1 = u$, $\psi_2 = 0$, $d_1 = 0$, and $d_2(t) = 10 \cos \omega_1 t + 10 \sin \omega_1 t$, where $\omega_1 = 8\pi$ rad/s. Let $\mu = \gamma = 1$. We consider the case where $M_{1,0}$ satisfies the FD-HHC stability condition, that is, $M_{1,0}$ is within 90° of $M_{*,1}$. Specifically, $M_{1,0} = 5e^{j\frac{5\pi}{12}} M_{*,1}$.

Both FD-HHC and FD-AHC are updated with update period 0.25 s, which was determined through numerical experimentation to yield the fastest convergence time. Figure 4.3 shows y and u for FD-HHC and FD-AHC. The control is turned on after 1 s. Both FD-HHC and FD-AHC yield asymptotic disturbance rejection. However, the convergence time is improved significantly with FD-AHC relative to FD-HHC. \triangle

Example 4.2. We reconsider Example 4.1 but with an initial estimate $M_{1,0}$ that does not satisfy FD-HHC stability condition, that is, $M_{1,0}$ is not within 90° of $M_{*,1}$. Specifically, $M_{1,0} = 5e^{j\frac{2\pi}{3}} M_{*,1}$. The control is turned on after 1 s. Figure 4.4 shows y and u for FD-HHC and FD-AHC. In this case, y with FD-HHC diverges because the

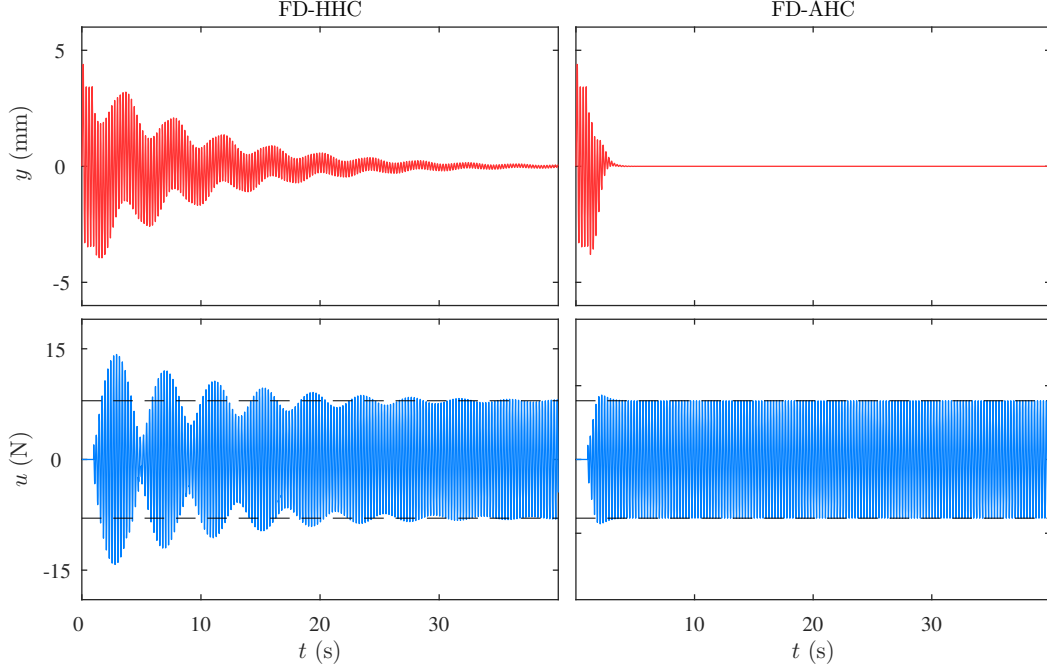


Figure 4.3: For a SISO system, where $M_{1,0}$ is within 90° of $M_{*,1}$, both FD-HHC and FD-AHC yield $y(t) \rightarrow 0$ as $t \rightarrow \infty$. The dashed lines show $\pm\|u_{*,1}\|$.

estimate $M_{1,0}$ is not sufficiently accurate. In contrast, y with FD-AHC converges to zero. \triangle

Example 4.3. Consider the MIMO system (4.1) and (4.31)–(4.32), where $y = [\xi_1 \ \xi_2]^T$ and $[\psi_1 \ \psi_2]^T = u$. The two-tone disturbances are $d_1(t) = 5 \cos \omega_1 t + 7 \sin \omega_2 t$ and $d_2(t) = 6 \cos \omega_1 t + 9 \sin \omega_2 t$, where $\omega_1 = 8\pi$ rad/s and $\omega_2 = 4\pi$ rad/s. We let $M_{1,0} = 5e^{j\frac{5\pi}{3}} M_{*,1}$, $M_{2,0} = 5e^{j\frac{3\pi}{2}} M_{*,2}$, $T_s = 0.5$ s, and $\mu_1 = \mu_2 = \gamma_1 = \gamma_2 = 2$. Figure 4.5 shows y and u with FD-AHC. The control is turned on after 1 s. FD-AHC yields asymptotic disturbance rejection. \triangle

4.8 Conclusions

We presented FD-AHC algorithm for rejection of known-frequency sinusoids that act on a completely unknown MIMO LTI system with at least as many controls as performance measurements. The main analytic result shows that the closed-loop system is Lyapunov stable and that the closed-loop performance tends to zero asymptotically. Numerical simulations suggest that FD-AHC can be implemented with larger gains than FD-HHC. These larger gains tend to reduce convergence time of FD-AHC relative to that of FD-HHC.

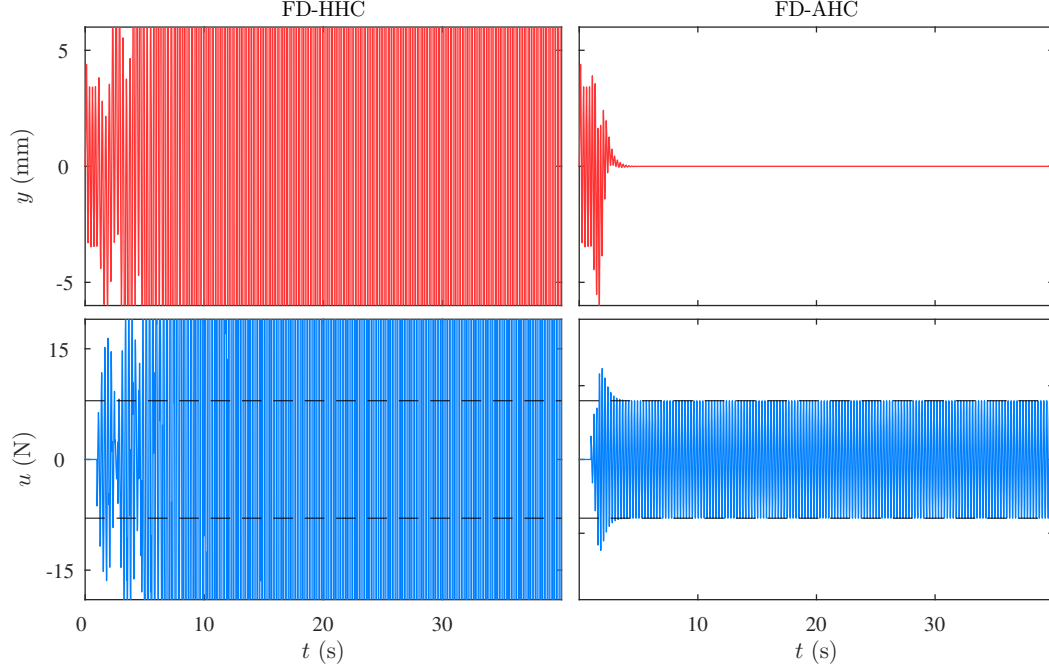


Figure 4.4: For a SISO system, where $M_{1,0}$ is not within 90° of $M_{*,1}$, y with FD-HHC diverges, whereas FD-AHC yields $y(t) \rightarrow 0$ as $t \rightarrow \infty$. The dashed lines show $\pm\|u_{*,1}\|$.

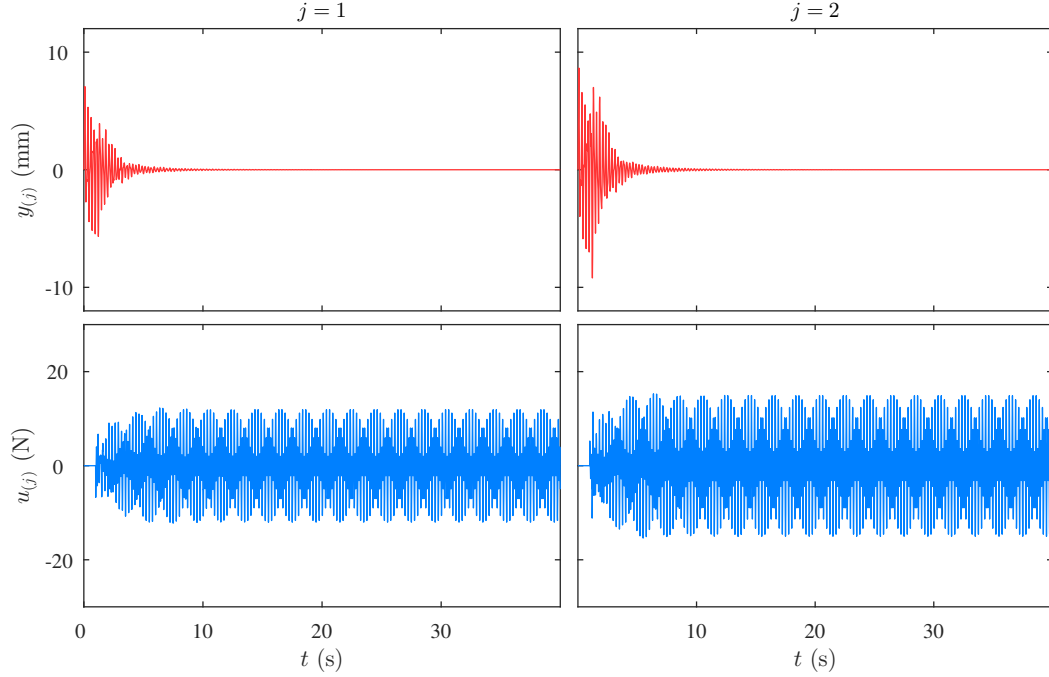


Figure 4.5: For a MIMO system with a two-tone disturbance, FD-AHC yields $y(t) \rightarrow 0$ as $t \rightarrow \infty$.

4.9 Proof of Theorem 4.2

Let $\alpha > \gamma/2 + \mu/(2\nu)$. For all $k \in \mathbb{N}$, define

$$\hat{y}_{k+1} \triangleq (1 - \alpha)y_{k+1} + \tilde{M}_k M_k^+ d_k - \tilde{d}_k. \quad (4.33)$$

Substituting (4.16) and (4.33) into (4.17) and (4.18) yields

$$\tilde{d}_{k+1} = \tilde{d}_k + \mu\eta_k\hat{y}_{k+1}, \quad (4.34)$$

$$\tilde{M}_{k+1} = \tilde{M}_k + \gamma\eta_k\hat{y}_{k+1}u_k^*. \quad (4.35)$$

Define the partial Lyapunov function

$$V_d(\tilde{d}_k) \triangleq \|\tilde{d}_k\|^2,$$

and the difference

$$\Delta V_d(k) \triangleq V_d(\tilde{d}_{k+1}) - V_d(\tilde{d}_k).$$

Evaluating ΔV_d along the trajectories of (4.34) yields

$$\Delta V_d(k) = 2\mu\eta_k\tilde{d}_k^*\hat{y}_{k+1} + \mu^2\eta_k^2\|\hat{y}_{k+1}\|^2. \quad (4.36)$$

Define the partial Lyapunov function

$$V_M(\tilde{M}_k) \triangleq \|\tilde{M}_k\|_{\mathbb{F}}^2,$$

and the difference

$$\Delta V_M(k) \triangleq V_M(\tilde{M}_{1,k+1}) - V_M(\tilde{M}_{1,k}).$$

Evaluating ΔV_M along (4.35) yields

$$\Delta V_M(k) = 2\gamma\eta_k u_k^* \tilde{M}_k^* \hat{y}_{k+1} + \gamma^2 \eta_k^2 \|u_k\|^2 \|\hat{y}_{k+1}\|^2. \quad (4.37)$$

Define the Lyapunov function

$$V(\tilde{d}_k, \tilde{M}_k) \triangleq \frac{1}{\mu} V_d(\tilde{d}_k) + \frac{1}{\gamma} V_M(\tilde{M}_k), \quad (4.38)$$

and define the Lyapunov difference

$$\begin{aligned} \Delta V(k) &\triangleq V(\tilde{d}_{k+1}, \tilde{M}_{k+1}) - V(\tilde{d}_k, \tilde{M}_k) \\ &= \frac{1}{\mu} \Delta V_d(k) + \frac{1}{\gamma} \Delta V_M(k). \end{aligned} \quad (4.39)$$

Substituting (4.36) and (4.37) into (4.39) yields

$$\Delta V(k) = \eta_k^2 \left[(\mu + \gamma \|u_k\|^2) \|\hat{y}_{k+1}\|^2 + \frac{2}{\eta_k} (\tilde{M}_k u_k + \tilde{d}_k)^* \hat{y}_{k+1} \right]. \quad (4.40)$$

Then, substituting (4.33) into (4.40) yields

$$\Delta V(k) = -\eta_k (2 - \mu\eta_k - \gamma\eta_k \|u_k\|^2) \|\hat{y}_{k+1}\|^2 - 2\eta_k (\alpha - 1) y_{k+1}^* \hat{y}_{k+1}. \quad (4.41)$$

To show *iii*), assume that there exists $k_s \in \mathbb{N}$ and $\varepsilon > 0$ such that for all $k \geq k_s$, $\lambda_{\min}(M_k M_k^*) > \varepsilon$. Thus, for all $k \geq k_s$, $M_k M_k^+ = I_\ell$, and it follows from (4.11), (4.10), and (4.33) that for all $k \geq k_s$,

$$\begin{aligned}\hat{y}_{k+1} &= y_{k+1} + M_k M_k^+ d_k - d_k \\ &= y_{k+1}.\end{aligned}\tag{4.42}$$

Substituting (4.16) and (4.42) into (4.41) implies that for all $k \geq k_s$,

$$\begin{aligned}\Delta V(k) &= -\eta_k \left[2 - \mu\eta_k - \gamma\eta_k \|u_k\|^2 + 2(\alpha - 1) \right] \|y_{k+1}\|^2 \\ &\leq -\eta_k \left(2\alpha - \frac{\mu}{\nu} - \gamma \right) \|y_{k+1}\|^2 \\ &= -\eta_k c_1 \|y_{k+1}\|^2,\end{aligned}\tag{4.43}$$

where $c_1 \triangleq 2\alpha - \mu/\nu - \gamma$ is positive because $\alpha > \gamma/2 + \mu/(2\nu)$. Thus, (4.43) implies that for all $k \geq k_s$, $\Delta V(k)$ is nonpositive. Therefore, it follows that $V(\tilde{d}_k, \tilde{M}_k)$ is bounded. Since, in addition, V is radially unbounded, it follows that \tilde{d}_k and \tilde{M}_k are bounded. Thus, d_k and M_k are bounded. Since M_k is bounded and for all $k \geq k_s$, $\lambda_{\min}(M_k M_k^*) > \varepsilon$, it follows that for all $k \geq k_s$, $(M_k M_k^*)^{-1}$ exists and is bounded. Thus, for all $k \geq k_s$, $u_k = -M_k^* (M_k M_k^*)^{-1} d_k$. Since M_k , $(M_k M_k^*)^{-1}$, and d_k are bounded, it follows that u_k is bounded. Thus, (4.16) and (4.43) imply that for all $k \geq k_s$,

$$\Delta V(k) \leq -c_2 \|y_{k+1}\|^2,\tag{4.44}$$

where

$$c_2 \triangleq \frac{4c_1}{\nu + \sup_{k \in \mathbb{N}} \|u_k\|^2} > 0.$$

Moreover, since $V(\tilde{d}_k, \tilde{M}_k)$ is positive definite, and $\Delta V(k)$ is nonpositive, it follows from (4.39) and (4.44) that

$$\begin{aligned}0 &\leq \lim_{k \rightarrow \infty} \sum_{j=k_s}^k c_2 \|y_{j+1}\|^2 \\ &\leq - \lim_{k \rightarrow \infty} \sum_{j=k_s}^k \Delta V(j) \\ &\leq V(\tilde{d}_{k_s}, \tilde{M}_{k_s}) - \lim_{k \rightarrow \infty} V(\tilde{d}_{k+1}, \tilde{M}_{k+1}) \\ &\leq V(\tilde{d}_{k_s}, \tilde{M}_{k_s}),\end{aligned}$$

where the upper and lower bounds imply that all the limits exist. Thus, $\lim_{k \rightarrow \infty} y_k = 0$, which confirms *iii*).

To show *i*) and *ii*), note that since $\text{rank } M_* = \ell$, it follows that there exist $r_1 > 0$ and $\varepsilon_1 > 0$ such that for all $M \in \mathbb{B}_{r_1}(\alpha M_*)$, $\lambda_{\min}(MM^*) > \varepsilon_1$. Let $r \in (0, \sqrt{r_1^2 \mu / (\mu + \gamma)})$, and let $\tilde{d}_0 \in \mathbb{B}_r(0)$ and $\tilde{M}_0 \in \mathbb{B}_r(0)$. Assume for contradiction

that there exists $k_1 \in \mathbb{Z}^+$ such that $\tilde{M}_{k_1} \notin \mathbb{B}_{r_1}(0)$ and for all $k \in \mathcal{K} \triangleq \{0, 1, \dots, k_1-1\}$, $\tilde{M}_k \in \mathbb{B}_{r_1}(0)$. Since for all $k \in \mathcal{K}$, $M_k \in \mathbb{B}_{r_1}(0)$, it follows that for all $k \in \mathcal{K}$, $\lambda_{\min}(M_k M_k^*) > \varepsilon_1$. Thus, using the same process as (4.42)–(4.44) with ε replaced by ε_1 yields that for all $k \in \mathcal{K}$, $\Delta V(k) \leq 0$. Therefore, it follows from (4.39) that

$$\begin{aligned}
0 &\leq - \sum_{i=0}^{k_1-1} \Delta V(i) \\
&= V(\tilde{d}_0, \tilde{M}_0) - V(\tilde{d}_{k_1}, \tilde{M}_{k_1}) \\
&= \frac{1}{\mu} (\|\tilde{d}_0\|^2 - \|\tilde{d}_{k_1}\|^2) + \frac{1}{\gamma} \left(\|\tilde{M}_0\|_{\text{F}}^2 - \|\tilde{M}_{k_1}\|_{\text{F}}^2 \right) \\
&\leq \frac{1}{\mu} \|\tilde{d}_0\|^2 + \frac{1}{\gamma} (\|\tilde{M}_0\|_{\text{F}}^2 - \|\tilde{M}_{k_1}\|_{\text{F}}^2) \\
&\leq \frac{r^2}{\mu} + \frac{r^2 - r_1^2}{\gamma} \\
&< \frac{1}{\mu} \left(\frac{r_1^2 \mu}{\mu + \gamma} \right) + \frac{1}{\gamma} \left(\frac{r_1^2 \mu}{\mu + \gamma} - r_1^2 \right) \\
&= 0,
\end{aligned}$$

which is a contradiction. Thus, for all $k \in \mathbb{N}$, $\tilde{M}_k \in \mathbb{B}_{r_1}(0)$, which implies that $M_k \in \mathbb{B}_{r_1}(\alpha M_*)$. Therefore, for all $k \in \mathbb{N}$, $\lambda_{\min}(M_k M_k^*) > \varepsilon_1$, and it follows from *iii*) that d_k , M_k , and u_k are bounded, and $\lim_{k \rightarrow \infty} y_k = 0$, which confirms *ii*).

Since for all $k \in \mathbb{N}$, $\lambda_{\min}(M_k M_k^*) > \varepsilon_1$, using the same process as (4.42)–(4.44), with ε replaced by ε_1 , it follows that for all $k \in \mathbb{N}$, $\Delta V(k) \leq 0$. Thus, the equilibrium $(\tilde{d}_k, \tilde{M}_k) \equiv 0$ is uniformly Lyapunov stable [208, Thm. 13.11], which confirms *i*).

Chapter 5

Time-Domain Adaptive Harmonic Control

In this chapter, we present a sampled-data adaptive harmonic control algorithm that rejects sinusoids with known frequencies that act on a completely unknown asymptotically stable linear time-invariant system. We analyze the stability and closed-loop performance for systems with at least as many controls as performance measurements. We show that the closed-loop system is uniformly Lyapunov stable and that the adaptive controller asymptotically rejects the disturbances. We present numerical simulations comparing the new sampled-data adaptive controller with an existing sinusoidal disturbance rejection approach (i.e., higher-harmonic control). We also present results from an active disturbance rejection experiment in an acoustic environment. These experimental results demonstrate the practical effectiveness of the adaptive harmonic controller. The result of this chapter appears in [198, 199].

5.1 Introduction

The problem of sinusoidal disturbance rejection arises in a variety of engineering applications, including active noise cancellation [32, 42], vibration suppression [10, 156], and active rotor balancing [20, 21]. If an accurate model of the system is known, then the internal-model principle [116–120] can be used to design a feedback controller capable of rejecting sinusoidal disturbances with known frequencies. Model-based disturbance observers can be used in the case where the disturbance frequencies are uncertain [126–128].

If an accurate system model is not known, but the open-loop dynamics are asymptotically stable, then adaptive feedforward cancellation can be employed [129–131, 133, 134, 136–138]. However, these approaches require certain model information or assumptions regarding the open-loop system. For single-input single-output (SISO) systems, the only model information required is the sign of the control-to-performance transfer function at the disturbance frequencies. For multi-input multi-output (MIMO) systems, stronger assumptions (e.g., strict positive realness,

a nominal system model, upper bounds on uncertainties) are typically required. Adaptive feedforward methods for rejecting sinusoids with unknown frequency include [139, 204].

Feedback (instead of feedforward) adaptive control methods can also be implemented for rejecting sinusoidal disturbances of known or even unknown frequencies [140, 141, 146–151]; however, these methods generally require some model information (e.g., relative degree) and structural assumptions regarding the system (e.g., minimum phase, or state feedback).

Another approach to sinusoidal disturbance rejection relies on an asymptotically stable linear time-invariant (LTI) system’s harmonic steady-state (HSS) response, that is, the residual sinusoidal response that remains after the transient response decays to zero. This approach was developed independently in [10, 20, 32, 156], and is known variously as convergent control (for active rotor balancing) and higher-harmonic control (for helicopter vibration reduction). In this chapter, we use the name frequency-domain higher-harmonic control (FD-HHC).

To explain FD-HHC, consider an LTI system that is acted on by a sinusoidal disturbance with known frequency ω . The FD-HHC control signal is a sinusoid with frequency ω , but where the amplitude and phase are updated at discrete times. All control computations are performed using discrete Fourier transform (DFT) data. Let $T_s > 0$ denote the FD-HHC update period. Then, at each time step $k \in \mathbb{N}$, the control amplitude and phase are updated using DFT data, which are computed from a sampling of the performance measurement over the time interval $[(k-1)T_s, kT_s)$. FD-HHC relies on the key assumption that the update period T_s is sufficiently large relative to the settling time of the system. This assumption ensures that by the end of each time interval between control updates, the closed-loop response approximates the HSS response. If T_s is too small, then the HSS approximation is not accurate, and the closed-loop system can become unstable. In practice, T_s can be increased to achieve closed-loop stability; however, increasing T_s also increases convergence time. In fact, large convergence time is one shortcoming of FD-HHC [81].

Another potential drawback of FD-HHC is that it requires an estimate of the control-to-performance transfer function evaluated at the disturbance frequency. In the SISO case, this estimate must have an angle within 90° of the actual value for closed-loop stability. The closed-loop stability conditions for the MIMO case are given in Theorem 2.2. If there are multiple disturbance frequencies, then estimates of the control-to-performance transfer function are required at each frequency. For certain applications, this transfer function can be difficult to estimate or subject to change. To address uncertainty, adaptive HHC methods have been proposed [81, 157, 158]. However, the methods in [81, 157] require an external excitation signal to ensure stability, and the analysis in [158] is restricted to an averaged system. In Chapter 2, we presented a frequency-domain adaptive higher harmonic control (FD-AHHC) algorithm with stability properties that do not require external excitation signals. However, the algorithm in Chapter 2 (similar to FD-HHC) is a frequency-domain method and thus may have a large convergence time.

In this chapter, we present a new time-domain adaptive harmonic control (TD-AHC) method for rejection of known-frequency sinusoids that act on a completely

unknown LTI system with at least as many controls as performance measurements. The main analytic result shows that the closed-loop system is uniformly Lyapunov stable and that the adaptive controller asymptotically rejects the disturbances. In contrast to FD-HHC and FD-AHHC presented in Chapter 2, the controller in this chapter is a time-domain method that does not require DFT computations. We present numerical simulations demonstrating that the new sampled-data adaptive controller can be implemented with larger gains or with faster sample rates than FD-HHC without destabilizing the closed-loop system. These larger gains or faster sample rates can significantly reduce convergence time as demonstrated in Section VI. We also present an experimental demonstration of active disturbance rejection in an acoustic environment. These active noise control experiments show that the adaptive harmonic controller can effectively reject single-tone and multi-tone sinusoidal disturbances acting on unknown MIMO systems.

5.2 Notation

Let $x_{(i)}$ denote the i th element of $x \in \mathbb{R}^m$. Let $\|\cdot\|$ be the 2-norm on \mathbb{R}^m . The Frobenius norm of $A \in \mathbb{R}^{\ell \times m}$ is defined by $\|A\|_F \triangleq \sqrt{\text{tr } A^T A}$. Define the *open ball of radius $r > 0$ centered at $A \in \mathbb{C}^{\ell \times m}$* by $\mathbb{B}_r(A) \triangleq \{X \in \mathbb{C}^{\ell \times m} : \|X - A\|_F < r\}$.

The Moore-Penrose generalized inverse [201, Chap. 6.1] of $A \in \mathbb{R}^{\ell \times m}$ is denoted by $A^+ \in \mathbb{R}^{m \times \ell}$. Note that if $A \in \mathbb{R}^{\ell \times m}$ is right invertible (i.e., $\text{rank } A = \ell$), then $A^+ = A^T(AA^T)^{-1}$. Let $\lambda_{\min}(A)$ denote the minimum eigenvalue of the symmetric positive-semidefinite matrix $A \in \mathbb{R}^{\ell \times \ell}$.

Define $\mathbb{N} \triangleq \{0, 1, 2, 3, \dots\}$ and $\mathbb{Z}^+ \triangleq \mathbb{N} \setminus \{0\}$.

5.3 Problem Formulation

Consider the LTI system

$$\dot{x}(t) = Ax(t) + Bu(t) + D_1d(t), \quad (5.1)$$

$$y(t) = Cx(t) + Du(t) + D_2d(t), \quad (5.2)$$

where $t \geq 0$, $x(t) \in \mathbb{R}^n$ is the state, $x(0) = x_0 \in \mathbb{R}^n$ is the initial condition, $u(t) \in \mathbb{R}^m$ is the control, $y(t) \in \mathbb{R}^\ell$ is the measured performance, $d(t) \in \mathbb{R}^{\ell_d}$ is the unmeasured disturbance, and $A \in \mathbb{R}^{n \times n}$ is asymptotically stable. Define $G_{yu} : \mathbb{C} \rightarrow \mathbb{C}^{\ell \times m}$ and $G_{yd} : \mathbb{C} \rightarrow \mathbb{C}^{\ell \times \ell_d}$ by

$$G_{yu}(s) \triangleq C(sI - A)^{-1}B + D,$$

$$G_{yd}(s) \triangleq C(sI - A)^{-1}D_1 + D_2,$$

which are the transfer functions from the control u and the disturbance d to the performance y . Let $\omega_1, \omega_2, \dots, \omega_q > 0$, and consider the sinusoidal disturbance

$$d(t) = \sum_{i=1}^q d_{c,i} \cos \omega_i t + d_{s,i} \sin \omega_i t, \quad (5.3)$$

where $d_{c,1}, \dots, d_{c,q}, d_{s,1}, \dots, d_{s,q} \in \mathbb{R}^{\ell d}$.

Our objective is to design a feedback control u that eliminates the effect of the disturbance d on the performance y . We seek to design a control that requires no model information regarding (5.1) and (5.2). We make the following assumptions:

$$(A5.1) \text{ For all } i = 1, \dots, q, \text{ rank } G_{yu}(j\omega_i) = \ell.$$

$$(A5.2) \text{ } \omega_1, \dots, \omega_q \text{ are known.}$$

Assumption (A5.1) implies that the number of actuators is at least as large as the number of performance measurements, that is, $m \geq \ell$. This assumption is required to ensure that there exists a control such that the performance y tends to zero asymptotically. Assumption (A5.2) implies that the disturbance frequencies ω_i are known; however, the disturbance amplitudes $d_{c,i}$ and $d_{s,i}$, and the system model A, B, C, D, D_1 , and D_2 are completely unknown.

Unless otherwise stated, all statements in this chapter that involve the subscript i are for all $i \in Q \triangleq \{1, 2, \dots, q\}$.

For the moment, assume that $d_{c,i}$, $d_{s,i}$, $G_{yu}(j\omega_i)$, and $G_{yd}(j\omega_i)$ are known. Let $u_{c,i}, u_{s,i} \in \mathbb{R}^m$, and consider the control

$$\begin{aligned} u(t) &= \sum_{i=1}^q u_{c,i} \cos \omega_i t + u_{s,i} \sin \omega_i t \\ &= \sum_{i=1}^q \left(f_i^T(t) \otimes I_m \right) \hat{u}_i, \end{aligned} \quad (5.4)$$

where \otimes is the Kronecker product, and

$$\hat{u}_i \triangleq \begin{bmatrix} u_{c,i} \\ u_{s,i} \end{bmatrix} \in \mathbb{R}^{2m}, \quad f_i(t) \triangleq \begin{bmatrix} \cos \omega_i t \\ \sin \omega_i t \end{bmatrix} \in \mathbb{R}^2.$$

The harmonic steady-state (HSS) performance of (5.1) and (5.2) with disturbance (5.3) and control (5.4) is defined by

$$\begin{aligned} y_{\text{hss}}(t, \hat{u}_1, \dots, \hat{u}_q) &\triangleq \sum_{i=1}^q \text{Re} \left(G_{yu}(j\omega_i)(u_{c,i} - j u_{s,i}) \right. \\ &\quad \left. + G_{yd}(j\omega_i)(d_{c,i} - j d_{s,i}) \right) e^{j\omega_i t} \\ &= \sum_{i=1}^q \left(f_i^T(t) \otimes I_\ell \right) (H_{i,*} \hat{u}_i + d_{i,*}), \end{aligned} \quad (5.5)$$

where

$$\begin{aligned} H_{i,*} &\triangleq \begin{bmatrix} \text{Re } G_{yu}(j\omega_i) & \text{Im } G_{yu}(j\omega_i) \\ -\text{Im } G_{yu}(j\omega_i) & \text{Re } G_{yu}(j\omega_i) \end{bmatrix} \in \mathbb{R}^{2\ell \times 2m}, \\ d_{i,*} &\triangleq \begin{bmatrix} \text{Re } G_{yd}(j\omega_i) & \text{Im } G_{yd}(j\omega_i) \\ -\text{Im } G_{yd}(j\omega_i) & \text{Re } G_{yd}(j\omega_i) \end{bmatrix} \begin{bmatrix} d_{c,i} \\ d_{s,i} \end{bmatrix} \in \mathbb{R}^{2\ell}. \end{aligned}$$

The HSS performance y_{hss} is the steady-state response of (5.1)–(5.4), that is, $\lim_{t \rightarrow \infty} [y_{\text{hss}}(t, \hat{u}_1, \dots, \hat{u}_q) - y(t)] = 0$. See [201, Chap. 12.12] for details.

Consider the cost function

$$J(\hat{u}_1, \dots, \hat{u}_q) \triangleq \lim_{t \rightarrow \infty} \frac{1}{t} \int_0^t \|y_{\text{hss}}(\tau, \hat{u}_1, \dots, \hat{u}_q)\|^2 d\tau, \quad (5.6)$$

which is the average power of y_{hss} . Substituting (5.5) into (5.6) and integrating yields

$$\begin{aligned} J(\hat{u}_1, \dots, \hat{u}_q) &= \sum_{i=1}^q \sum_{j=1}^q (H_{i,*} \hat{u}_i + d_{i,*})^T \\ &\quad \times \left(\lim_{t \rightarrow \infty} \frac{1}{t} \int_0^t f_i(\tau) f_j^T(\tau) \otimes I_\ell d\tau \right) \\ &\quad \times (H_{j,*} \hat{u}_j + d_{j,*}) \\ &= \frac{1}{2} \sum_{i=1}^q \|H_{i,*} \hat{u}_i + d_{i,*}\|^2. \end{aligned}$$

Since (A5.1) implies that $\text{rank } G_{yu}(j\omega_i) = \ell$, it follows that $\text{rank } H_{i,*} = 2\ell$, which implies that $H_{i,*}$ is right invertible. The following result provides an expression for a control that minimizes J . The proof is similar to the proof of Theorem 2.1.

Theorem 5.1. Assume (A5.1) holds, and for all $i \in Q$, define

$$u_{i,*} \triangleq -H_{i,*}^T (H_{i,*} H_{i,*}^T)^{-1} d_{i,*}.$$

Then, $J(u_{1,*}, \dots, u_{q,*}) = 0$.

Theorem 5.1 provides ideal control parameters $u_{i,*}$, but $u_{i,*}$ requires knowledge of $H_{i,*}$ and $d_{i,*}$, which are unknown.

In this chapter, we consider a sinusoidal control with frequencies $\omega_1, \dots, \omega_q$ but where the amplitudes and phases are updated in discrete time. Let $T_s > 0$ be the update period. Then, for each $k \in \mathbb{N}$ and for all $t \in [kT_s, (k+1)T_s)$, the control is

$$u(t) = \sum_{i=1}^q (f_i^T(t) \otimes I_m) u_{i,k}, \quad (5.7)$$

where $u_{i,k} \in \mathbb{R}^{2m}$ is determined from update equations presented in the next section. Thus, the control (5.7) is a piecewise-continuous sinusoid. If T_s is sufficiently large relative to the settling time of G_{yu} , then for all $k \in \mathbb{Z}^+$, $y(kT_s) \approx y_{\text{hss}}(kT_s, u_{1,k-1}, \dots, u_{q,k-1})$. For the stability analysis in Section 5.5, we invoke the HSS assumption that $y(kT_s) = y_{\text{hss}}(kT_s, u_{1,k-1}, \dots, u_{q,k-1})$; however, this assumption is used for analysis only.

5.4 Time-Domain Adaptive Harmonic Control

We present time-domain adaptive harmonic control (TD-AHC), which does not require any information regarding either $d_{i,*}$ or $H_{i,*}$. For all $j \in \mathbb{Z}^+$, define

$$\Lambda_j \triangleq \begin{bmatrix} 0 & -1 \\ 1 & 0 \end{bmatrix} \otimes I_j \in \mathbb{R}^{2j \times 2j},$$

and consider

$$\mathcal{H} \triangleq \left\{ H \in \mathbb{R}^{2\ell \times 2m} : H = \Lambda_\ell^\top H \Lambda_m \right\},$$

which is the set of $2\ell \times 2m$ real matrices that have the block structure of $H_{i,*}$. For each $k \in \mathbb{N}$, define the sampled data

$$\begin{aligned} y_k &\triangleq y(kT_s) \in \mathbb{R}^\ell, \\ \phi_{i,k} &\triangleq f_i(kT_s) \otimes I_\ell \in \mathbb{R}^{2\ell \times \ell}, \end{aligned}$$

and consider the cost function $\mathcal{J}_k : \mathbb{R}^{2\ell} \times \dots \times \mathbb{R}^{2\ell} \times \mathcal{H} \times \dots \times \mathcal{H} \rightarrow [0, \infty)$ defined by

$$\begin{aligned} \mathcal{J}_k(\hat{d}_1, \dots, \hat{d}_q, \hat{H}_1, \dots, \hat{H}_q) &\triangleq \frac{1}{2} \left\| y_{k+1} - \sum_{j=1}^q \phi_{j,k+1}^\top (\hat{H}_j u_{j,k} + \hat{d}_j) \right\|^2 \\ &\quad + \frac{1}{2} \left\| y_{k+1} - \sum_{j=1}^q \phi_{j,k+1}^\top (\Lambda_\ell^\top \hat{H}_j \Lambda_m u_{j,k} + \hat{d}_j) \right\|^2. \end{aligned}$$

Note that the second term of the cost \mathcal{J}_k is similar to the first term except \hat{H}_i is replaced by $\Lambda_\ell^\top \hat{H}_i \Lambda_m$. If $\hat{H}_i \in \mathcal{H}$, then $\hat{H}_i = \Lambda_\ell^\top \hat{H}_i \Lambda_m$. In this case, the two terms of \mathcal{J}_k are equal. These two terms are included in the cost in order to obtain estimates of $H_{i,*}$ that have the block structure of the $H_{i,*}$ (i.e., are contained in \mathcal{H}). If $\hat{H}_i \in \mathcal{H}$, then \mathcal{J}_k can be interpreted as a measure of how well $\sum_{j=1}^q \phi_{j,k+1}^\top (\hat{H}_j u_{j,k} + \hat{d}_j)$ approximates the measurement y_{k+1} , which itself is approximately equal to the sampled HSS performance $y_{\text{hss}}((k+1)T_s, u_{1,k}, \dots, u_{q,k}) = \sum_{j=1}^q \phi_{j,k+1}^\top (H_{j,*} u_{j,k} + d_{j,*})$. Thus, if the HSS assumption $y_k = y_{\text{hss}}(kT_s, u_{1,k-1}, \dots, u_{q,k-1})$ is satisfied, then $\mathcal{J}_k(d_{1,*}, \dots, d_{q,*}, H_{1,*}, \dots, H_{q,*}) = 0$, that is, \mathcal{J}_k is minimized by $\hat{d}_i = d_{i,*}$ and $\hat{H}_i = H_{i,*}$.

For all $k \in \mathbb{N}$, let $d_{i,k} \in \mathbb{R}^{2\ell}$ and $H_{i,k} \in \mathcal{H}$ be estimates of $d_{i,*}$ and $H_{i,*}$, which are determined from update equations. To obtain these update equations, we define the gradients of \mathcal{J}_k with respect to each \hat{d}_i and \hat{H}_i evaluated at $\hat{d}_i = d_{i,k}$ and $\hat{H}_i = H_{i,k}$, which are given by

$$\begin{aligned} \delta_{i,k} &\triangleq \left(\frac{\partial \mathcal{J}_k}{\partial \hat{d}_i} \Big|_{(\hat{d}_j, \hat{H}_j) = (d_{j,k}, H_{j,k}) \text{ for all } j \in Q} \right)^\top \\ &= -2\phi_{i,k+1} \left[y_{k+1} - \sum_{j=1}^q \phi_{j,k+1}^\top (H_{j,k} u_{j,k} + d_{j,k}) \right], \end{aligned} \quad (5.8)$$

$$\begin{aligned}
\Gamma_{i,k} &\triangleq \left(\frac{\partial \mathcal{J}_k}{\partial \hat{H}_i} \bigg|_{(\hat{d}_j, \hat{H}_j) = (d_{j,k}, H_{j,k}) \text{ for all } j \in Q} \right)^T \\
&= -\phi_{i,k+1} \left[y_{k+1} - \sum_{j=1}^q \phi_{j,k+1}^T (H_{j,k} u_{j,k} + d_{j,k}) \right] u_{i,k}^T \\
&\quad - \Lambda_\ell \phi_{i,k+1} \left[y_{k+1} - \sum_{j=1}^q \phi_{j,k+1}^T (H_{j,k} u_{j,k} + d_{j,k}) \right] u_{i,k}^T \Lambda_m^T. \tag{5.9}
\end{aligned}$$

Then, for all $k \in \mathbb{N}$, the update equations are

$$d_{i,k+1} = d_{i,k} - \gamma_d \eta_k \delta_{i,k}, \tag{5.10}$$

$$H_{i,k+1} = H_{i,k} - \gamma_H \eta_k \Gamma_{i,k}, \tag{5.11}$$

where $\nu > 0, \gamma_d > 0, \gamma_H > 0$, and

$$\eta_k \triangleq \frac{1}{\nu + \sum_{j=1}^q \|u_{j,k}\|^2}. \tag{5.12}$$

The initial conditions for (5.10) and (5.11) are $d_{i,0} \in \mathbb{R}^{2\ell}$ and $H_{i,0} \in \mathcal{H}$. Note that for all $H_{i,0} \in \mathcal{H}$, it follows from (5.9), (5.11), and (5.12) that for all $k \in \mathbb{N}$, $H_{i,k} \in \mathcal{H}$. Thus, the update equation (5.11) for $H_{i,k}$ preserves the block structure of $H_{i,*}$.

For all $k \in \mathbb{N}$, $u_{i,k}$ is calculated using the estimates $d_{i,k}$ and $H_{i,k}$. Specifically, for all $k \in \mathbb{N}$,

$$u_{i,k} = -H_{i,k}^+ d_{i,k}. \tag{5.13}$$

Thus, the adaptive controller is given by (5.7)–(5.13). The control architecture is shown in Fig. 5.1. If $d_{i,k} \equiv d_{i,*}$ and $H_{i,k} = H_{i,*}$, then Theorem 5.1 and (5.13) imply that $u_{i,k} = u_{i,*}$.

The update equations (5.8)–(5.12) are normalized gradients derived from the cost \mathcal{J}_k . See [209, 210] for more details on normalized gradient algorithms. The normalization η_k and gains γ_d and γ_H are obtained from the stability analysis in the next section.

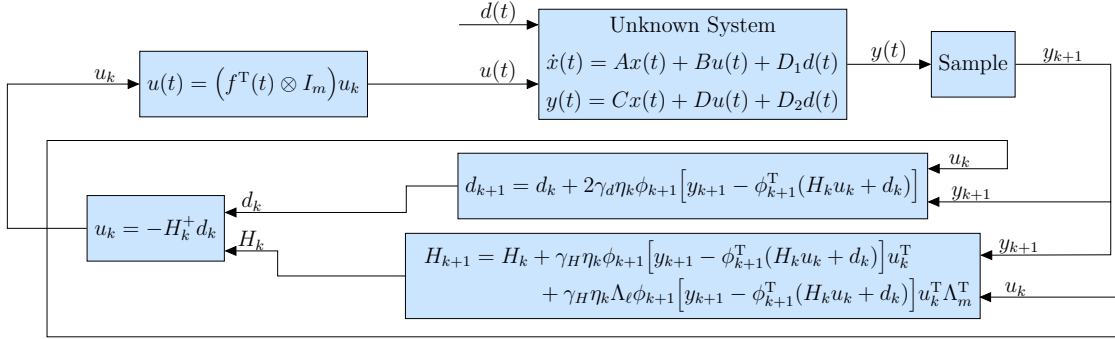


Figure 5.1: Schematic of TD-AHC given by (5.7)–(5.13).

5.5 Stability Analysis

To analyze the stability of the closed-loop system, we make the HSS assumption:

$$(A5.3) \text{ For all } k \in \mathbb{Z}^+, y_k = y_{\text{hss}}(kT_s, u_{1,k-1}, \dots, u_{q,k-1}).$$

Assumption (A5.3) combined with (5.5) and (5.13) implies that

$$y_{k+1} = \sum_{j=1}^q \phi_{j,k+1}^T (d_{j,*} - H_{j,*} H_{j,k}^+ d_{j,k}). \quad (5.14)$$

Let $\alpha > \gamma_H/2 + q\gamma_d/\nu$, and define the estimation errors

$$\tilde{d}_{i,k} \triangleq d_{i,k} - \alpha d_{i,*}, \quad \tilde{H}_{i,k} \triangleq H_{i,k} - \alpha H_{i,*}.$$

Then, subtracting $\alpha d_{i,*}$ from both sides of (5.10) and substituting (5.8) and (5.12)–(5.14) yields

$$\begin{aligned} \tilde{d}_{i,k+1} &= \tilde{d}_{i,k} + \frac{2\gamma_d}{\nu + \sum_{j=1}^q \|H_{j,k}^+ d_{j,k}\|^2} \\ &\quad \times \phi_{i,k+1} \left[(1 - \alpha)y_{k+1} + \sum_{j=1}^q \phi_{j,k+1}^T (\tilde{H}_{j,k} H_{j,k}^+ d_{j,k} - \tilde{d}_{j,k}) \right]. \end{aligned} \quad (5.15)$$

Similarly, subtracting $\alpha H_{i,*}$ from both sides of (5.11) and substituting (5.9) and (5.12)–(5.14) yields

$$\begin{aligned} \tilde{H}_{i,k+1} &= \tilde{H}_{i,k} + \frac{\gamma_H}{\nu + \sum_{j=1}^q \|H_{j,k}^+ d_{j,k}\|^2} \\ &\quad \times \left[\phi_{i,k+1} \left[(1 - \alpha)y_{k+1} + \sum_{j=1}^q \phi_{j,k+1}^T (\tilde{H}_{j,k} H_{j,k}^+ d_{j,k} - \tilde{d}_{j,k}) \right] (H_{i,k}^+ d_{i,k})^T \right. \\ &\quad \left. + \Lambda_\ell \phi_{i,k+1} \left[(1 - \alpha)y_{k+1} + \sum_{j=1}^q \phi_{j,k+1}^T (\tilde{H}_{j,k} H_{j,k}^+ d_{j,k} - \tilde{d}_{j,k}) \right] (H_{i,k}^+ d_{i,k})^T \Lambda_m^T \right]. \end{aligned} \quad (5.16)$$

The following theorem is the main analytic result of this chapter and provides the stability properties of the closed-loop system (5.14)–(5.16). The proof is in Section 5.9.

Theorem 5.2. Consider the closed-loop system (5.14)–(5.16), which consists of (5.8)–(5.14), where $\nu > 0$, $\gamma_d > 0$, and $\gamma_H > 0$, and where (A5.1)–(A5.3) are satisfied. Then, for all $\alpha > \gamma_H/2 + q\gamma_d/\nu$, the following statements hold:

- i*) $(\tilde{d}_{1,k}, \dots, \tilde{d}_{q,k}, \tilde{H}_{1,k}, \dots, \tilde{H}_{q,k}) \equiv 0$ is a uniformly Lyapunov stable equilibrium of (5.14)–(5.16).
- ii*) There exists $r > 0$ such that for all $\tilde{d}_{1,0}, \dots, \tilde{d}_{q,0} \in \mathbb{B}_r(0)$ and all $\tilde{H}_{1,0}, \dots, \tilde{H}_{q,0} \in \mathcal{H} \cap \mathbb{B}_r(0)$, $d_{i,k}$, $H_{i,k}$, and $u_{i,k}$ are bounded and $\lim_{k \rightarrow \infty} y_k = 0$.

iii) Let $d_{1,0}, \dots, d_{q,0} \in \mathbb{R}^\ell$, and let $H_{1,0}, \dots, H_{q,0} \in \mathcal{H}$. Assume that there exists $k_s \in \mathbb{N}$ and $\varepsilon > 0$ such that for all $k \geq k_s$, $\lambda_{\min}(H_{i,k}H_{i,k}^T) > \varepsilon$. Then, $d_{i,k}$, $H_{i,k}$, and $u_{i,k}$ are bounded, and $\lim_{k \rightarrow \infty} y_k = 0$.

Part *i*) of Theorem 5.2 states that the equilibria of the closed-loop system (5.14)–(5.16) are uniformly Lyapunov stable, and part *ii*) guarantees local convergence of the performance y_k to zero. Part *iii*) provides a sufficient condition for global boundedness of $d_{i,k}$, $H_{i,k}$, and $u_{i,k}$, as well as global convergence of the performance y_k to zero. Specifically, part *iii*) invokes the assumption that there exist $k_s \in \mathbb{N}$ and $\varepsilon > 0$ such that for all $k \geq k_s$, $\lambda_{\min}(H_{i,k}H_{i,k}^T) > \varepsilon$. This assumption, which implies that $H_{i,k}$ is asymptotically full row rank, cannot be verified *a priori*. However, the assumption $\lambda_{\min}(H_{i,k}H_{i,k}^T) > \varepsilon$, for some arbitrarily small $\varepsilon > 0$, can be verified at each time step. If the condition $\lambda_{\min}(H_{i,k}H_{i,k}^T) > \varepsilon$ is violated on a time step, then $H_{i,k}$ can be perturbed to ensure $\lambda_{\min}(H_{i,k}H_{i,k}^T) > \varepsilon$. However, analyzing the stability of such a perturbation is an open problem. Nevertheless, simulations and experiments suggest that for almost all initial conditions $d_{i,0} \in \mathbb{R}^{2\ell}$ and $H_{i,0} \in \mathcal{H}$, $H_{i,k}$ is asymptotically full row rank, and thus, satisfies $\lambda_{\min}(H_{i,k}H_{i,k}^T) > \varepsilon$. In this case, part *iii*) states that the performance y_k globally tends to zero.

Notably, Theorem 5.2 does not impose upper bounds on the gains γ_d and γ_H . Thus, TD-AHC can be implemented with arbitrarily large gains, which can improve convergence time as demonstrated in the simulations and experiments in the following two sections.

5.6 Numerical Examples Comparing TD-AHC To FD-HHC

Consider the two-mass structure shown in Fig. 5.2, where ψ_1 and ψ_2 are control forces, and d_1 and d_2 are disturbance forces. The equations of motion are given by (5.1), where

$$A = \begin{bmatrix} 0 & 1 & 0 & 0 \\ \frac{-(k_1+k_2)}{m_1} & \frac{-(c_1+c_2)}{m_1} & \frac{k_2}{m_1} & \frac{c_2}{m_1} \\ 0 & 0 & 0 & 1 \\ \frac{k_2}{m_2} & \frac{c_2}{m_2} & \frac{-(k_2+k_3)}{m_2} & \frac{-(c_2+c_3)}{m_2} \end{bmatrix}, \quad (5.17)$$

$$B = \begin{bmatrix} 0 & 0 \\ \frac{1}{m_1} & 0 \\ 0 & 0 \\ 0 & \frac{1}{m_2} \end{bmatrix}, \quad D_1 = B, \quad (5.18)$$

$$x(t) = \begin{bmatrix} \xi_1(t) \\ \dot{\xi}_1(t) \\ \xi_2(t) \\ \dot{\xi}_2(t) \end{bmatrix}, \quad u(t) = \begin{bmatrix} \psi_1(t) \\ \psi_2(t) \end{bmatrix}, \quad d(t) = \begin{bmatrix} d_1(t) \\ d_2(t) \end{bmatrix}. \quad (5.19)$$

Let $m_1 = 2$ kg, $m_2 = 1$ kg, $c_1 = 60$ kg/s, $c_2 = 50$ kg/s, $c_3 = 40$ kg/s, $k_1 = 300$ N/m, $k_2 = 200$ N/m, and $k_3 = 400$ N/m. For all examples, $\nu = 1$. The initial

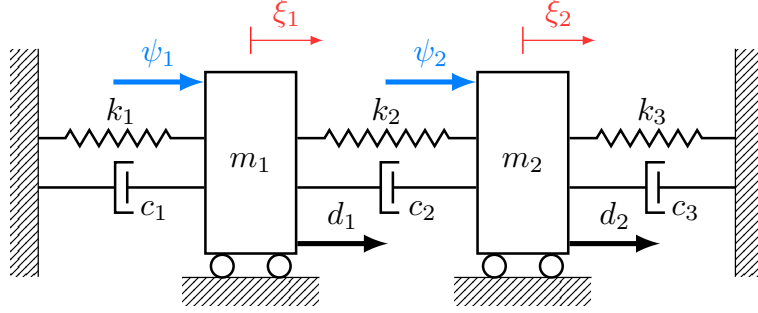


Figure 5.2: Two-mass structure used in Examples 5.1–5.5.

conditions are $x(0) = 0$, $d_{i,0} = 0$, and

$$H_{i,0} = \begin{bmatrix} \operatorname{Re} G_{i,0} & \operatorname{Im} G_{i,0} \\ -\operatorname{Im} G_{i,0} & \operatorname{Re} G_{i,0} \end{bmatrix}, \quad (5.20)$$

where $G_{i,0} \in \mathbb{C}^{\ell \times m}$. The initial condition $G_{i,0}$, the update period T_s , and the gains γ_d and γ_H are specified in each example.

In the following examples, we compare FD-HHC to TD-AHC, which is given by (5.7)–(5.13). FD-HHC requires an estimate of $G_{yu}(j\omega_i)$, and the estimate must be sufficiently accurate to ensure closed-loop stability. See Theorem 2.2 for details. In the SISO case, the closed-loop FD-HHC system is asymptotically stable only if the estimate of $G_{yu}(j\omega_i)$ is within 90° of $G_{yu}(j\omega_i)$. In contrast, TD-AHC does not require a sufficiently accurate estimate of $G_{yu}(j\omega_i)$. To compare FD-HHC and TD-AHC, we set the FD-HHC estimate of $G_{yu}(j\omega_i)$ equal to the TD-AHC initial condition $G_{i,0}$, which, in most applications, is the best *a priori* estimate of $G_{yu}(j\omega_i)$.

We implement FD-HHC according to (2.11). FD-HHC is a frequency-domain method, and all computations use DFT data. The DFT is performed using a 1 kHz sampling frequency. We select the FD-HHC gain $\rho = 4 \times 10^5$, which was determined through numerical experimentation to yield the fastest convergence rate.

Example 5.1. Consider the SISO system (5.1) and (5.17)–(5.19), where $y = \xi_1$, $\psi_1 = u$, $\psi_2 = 0$, $d_1 = 0$, and $d_2(t) = 10 \cos \omega_1 t + 10 \sin \omega_1 t$, where $\omega_1 = 9\pi$ rad/s. Let $\gamma_d = \gamma_H = 0.2$. We consider the case where $G_{1,0}$ satisfies the FD-HHC stability condition, that is, $G_{1,0}$ is within 90° of $G_{yu}(j\omega_1)$. Specifically, $G_{1,0} = 5e^{j\frac{5\pi}{12}} G_{yu}(j\omega_1)$.

FD-HHC is updated with update period 0.25 s, which was determined through numerical experimentation to yield the fastest convergence time. First, we compare FD-HHC to TD-AHC with the same update period (i.e., $T_s = 0.25$). Figure 5.3 shows y and u for FD-HHC and TD-AHC. The control is turned on after 1 s. Both FD-HHC and TD-AHC yield asymptotic disturbance rejection. However, the convergence time is improved slightly with TD-AHC relative to FD-HHC.

FD-HHC cannot be implemented with a larger gain ρ without causing instability. In contrast, TD-AHC can be implemented with larger gains γ_d and γ_H . The left-hand side of Fig. 5.4 shows y and u with TD-AHC, where $T_s = 0.25$ s and $\gamma_d = \gamma_H = 2$. TD-

AHC yields asymptotic disturbance rejection, and the convergence time is improved relative to the best case with FD-HHC, which is shown in Fig. 5.3.

TD-AHC can also be implemented with a smaller update period T_s if the gains γ_d and γ_H are reduced to ensure that the control $u_{i,k}$ does not change too much from one update to the next, and thus, the HSS approximation is valid. In contrast, FD-HHC cannot be implemented with a smaller update period than $T_s = 0.25$ s without causing instability. The right-hand side of Fig. 5.4 shows y and u with TD-AHC, where $T_s = 0.001$ s and $\gamma_d = \gamma_H = 0.004$. TD-AHC yields asymptotic disturbance rejection, and the convergence time is improved relative to the best case with FD-HHC, which is shown in Fig. 5.3. \triangle

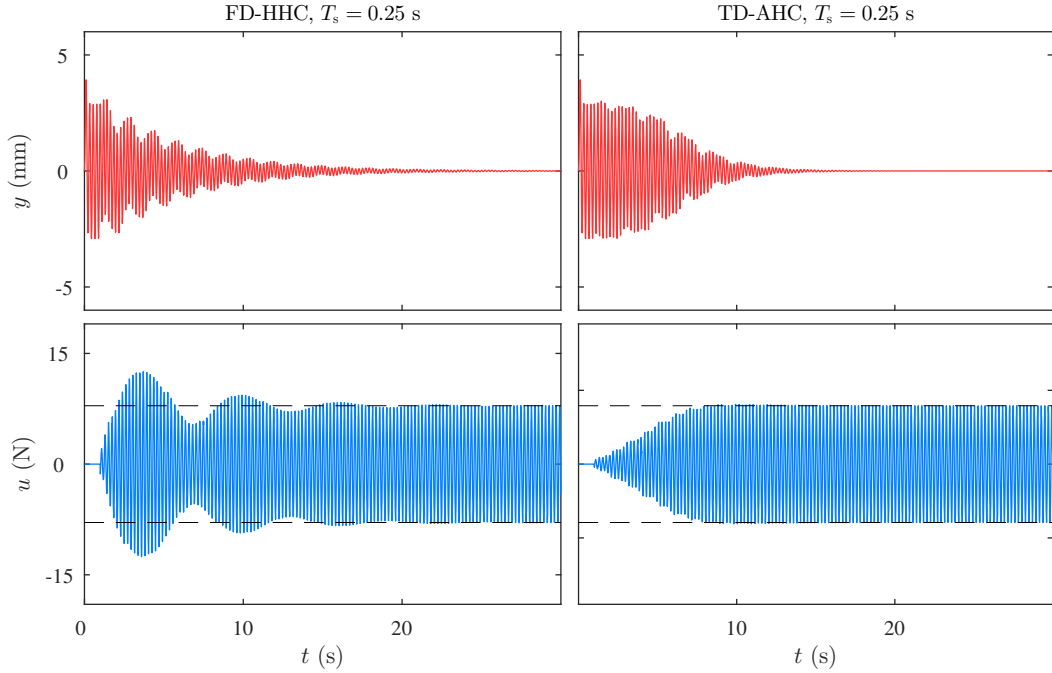


Figure 5.3: For a SISO system, where $G_{1,0}$ is within 90° of $G_{yu}(j\omega_1)$, both FD-HHC and TD-AHC yield $y(t) \rightarrow 0$ as $t \rightarrow \infty$. The dashed lines show $\pm\|u_{1,*}\|$.

Example 5.2. We reconsider Example 1 but with an initial estimate $G_{1,0}$ that does not satisfy FD-HHC stability condition, that is, $G_{1,0}$ is not within 90° of $G_{yu}(j\omega_1)$. Specifically, $G_{1,0} = 5e^{j\frac{2\pi}{3}}G_{yu}(j\omega_1)$. TD-AHC is implemented with $T_s = 0.01$ s and $\gamma_d = \gamma_H = 0.04$. The control is turned on after 1 s. Figure 5.5 shows y and u for FD-HHC and TD-AHC. In this case, y with FD-HHC diverges because the estimate $G_{1,0}$ is not sufficiently accurate. In contrast, y with TD-AHC converges to zero. \triangle

Example 5.3. Consider the SISO system (5.1) and (5.17)–(5.19), where $y = \xi_1 + v$, and v is a zero-mean Gaussian white noise with intensity 10^{-9} mm². We let $\psi_1 = u$, $\psi_2 = 0$, $d_1 = 0$, and $d_2(t) = -30 \cos \omega_1 t + 30 \sin \omega_1 t$, where $\omega_1 = 23.3$ rad/s is a natural frequency of the two-mass system. Let $G_{1,0} = 10e^{j\frac{\pi}{4}}G_{yu}(j\omega_1)$, $T_s = 0.1$ s,

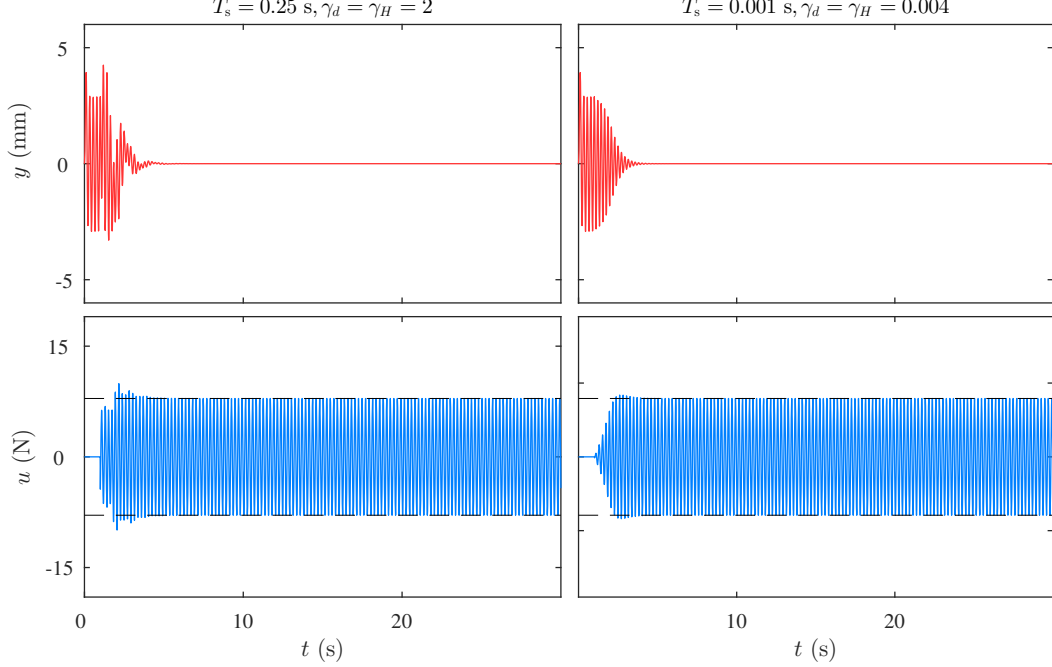


Figure 5.4: TD-AHC can be implemented with larger gains γ_d and γ_H , or with a smaller update period T_s if the gains γ_d and γ_H are reduced to ensure that the HSS approximation is valid. The dashed lines show $\pm\|u_{1,*}\|$.

and $\gamma_d = \gamma_H = 0.9$. Figure 5.6 shows y , u , $d_{1,k}$, and $H_{1,k}$ with TD-AHC. The control is turned on after 1 s. TD-AHC yields near-zero steady-state performance. Note that the noise v does not cause drift in adaptive parameters $d_{1,k}$ and $H_{1,k}$. In fact, numerical testing suggests that noise does not cause parameter drift in general.

Theorem 5.2 shows that there exists a continuum of uniformly Lyapunov stable equilibria, where $-H_{i,k}^+ d_{i,k} = u_{i,*}$. Thus, $d_{i,k}$ and $H_{i,k}$ need not converge to $d_{i,*}$ and $H_{i,*}$ in order to achieve asymptotic disturbance rejection. Figure 5.6 shows that in this example $d_{1,k}$ and $H_{1,k}$ do not converge to $d_{1,*}$ and $H_{1,*}$. The choice of gains γ_d and γ_H , and initial conditions $d_{i,0}$ and $H_{i,0}$ impacts the steady-state values of $d_{i,k}$ and $H_{i,k}$, as well as the transient behavior. As discussed in Example 1, increasing the gains γ_d and γ_H tends to improve convergence time. \triangle

Example 5.4. Consider the SISO system (5.1) and (5.17)–(5.19), where $y = \xi_1$, $\psi_1 = u$, $\psi_2 = 0$. We consider a case, where the disturbance frequency is time-varying. Specifically, we let $d_1 = 0$ and $d_2(t) = 20 \cos \int_0^t \omega_1(\tau) d\tau + 20 \sin \int_0^t \omega_1(\tau) d\tau$, where for all $t \geq 0$, $\omega_1(t) = 2\pi(4 - 3 \cos 0.2t)$ rad/s. Let $G_{1,0} = 10e^{j\frac{\pi}{4}} G_{yu}(j8\pi)$, $T_s = 0.001$ s, and $\gamma_d = \gamma_H = 0.005$. Figure 5.7 shows y and u with TD-AHC. The control is turned on after 1 s. TD-AHC yields asymptotic disturbance rejection. In fact, numerical testing suggests that TD-AHC is effective for rejection of disturbances with time-varying frequency if the time variation is known, and the rate of change of the frequency is sufficiently small. \triangle

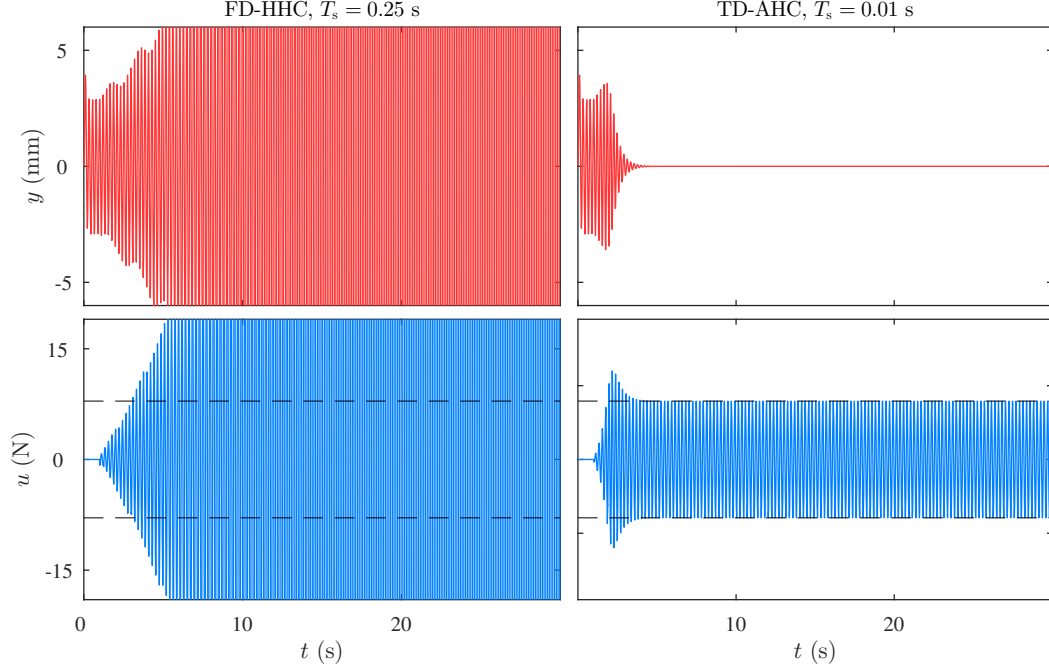


Figure 5.5: For a SISO system, where $G_{1,0}$ is not within 90° of $G_{yu}(j\omega_1)$, y with FD-HHC diverges, whereas TD-AHC yields $y(t) \rightarrow 0$ as $t \rightarrow \infty$. The dashed lines show $\pm\|u_{1,*}\|$.

Example 5.5. Consider the MIMO system (5.1) and (5.17)–(5.19), where $y = [\xi_1 \ \xi_2]^T$ and $[\psi_1 \ \psi_2]^T = u$. The two-tone disturbances are $d_1(t) = 5 \cos \omega_1 t + 7 \sin \omega_2 t$ and $d_2(t) = 6 \cos \omega_1 t + 9 \sin \omega_2 t$, where $\omega_1 = 8\pi$ rad/s and $\omega_2 = 5\pi$ rad/s. We let $G_{1,0} = 5e^{j\frac{5\pi}{3}} G_{yu}(j\omega_1)$, $G_{2,0} = 5e^{j\frac{3\pi}{2}} G_{yu}(j\omega_2)$, $T_s = 0.1$ s, and $\gamma_d = \gamma_H = 0.9$. Figure 5.8 shows y and u with TD-AHC. The control is turned on after 1 s. TD-AHC yields asymptotic disturbance rejection. \triangle

5.7 Results From Active Noise Control Experiments

We present results from an active noise control experiment to demonstrate TD-AHC. Figure 5.9 is a photograph of the experimental setup, and Fig. 10 shows a schematic of the experimental setup, where n_1 and n_2 are the horizontal and vertical axes of a fixed Cartesian frame. Disturbance speakers are located at $(-0.15, 0)$ m and $(0.15, 0)$ m, and these speakers generate disturbances d_1 and d_2 . Control speakers are located at $(-0.30, -0.27)$ m and $(0.30, -0.27)$ m, and these speakers generate control inputs ψ_1 and ψ_2 , which are determined by TD-AHC. Microphones are located at $(-0.03, -0.27)$ m and $(0.20, -0.27)$ m, and these microphones measure the pressures ξ_1 and ξ_2 , which are used as the measured performance y .

Measurement signals from the microphones are amplified by a SM Pro Audio PR8E microphone preamplifier. The four speakers are M-Audio AV42 2-way 4-in monitor speakers. The two microphones are Audio2000 1064BL vocal microphones. The controller is implemented on a dSPACE DS1103 controller board. Note that no system information is required to implement TD-AHC. Thus, we do not use any

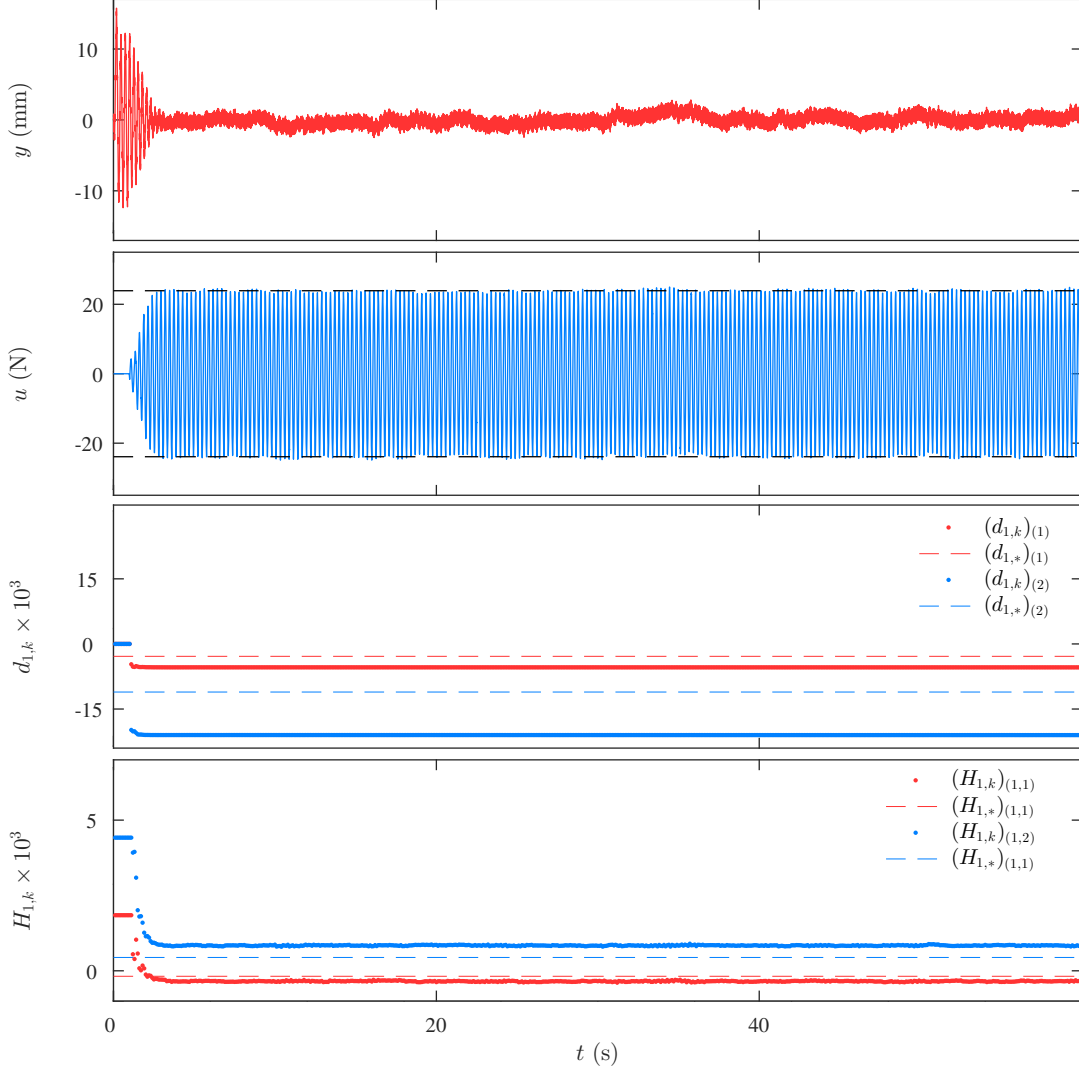


Figure 5.6: For a SISO system subject to measurement noise, TD-AHC yields near-zero steady-state performance. The noise v does not cause drift in $d_{1,k}$ or $H_{1,k}$.

knowledge of the characteristics or locations of the experimental components to implement TD-AHC.

For all experiments, the controller is turned on at 5 s, $T_s = 0.05$ s, $\nu = 1$, $d_{i,0} = 0$, and $H_{i,0}$ is given by (5.20), where $G_{i,0} \in \mathbb{C}^{\ell \times m}$ is specified in each experiment. The gains γ_d and γ_H are specified in each experiment. Let $u_m > 0$ be the maximum allowable magnitude for each control input. For all control speakers, $u_m = 447$ mV. Let $\omega_1 = 206\pi$ rad/s and $\omega_2 = 362\pi$ rad/s.

Experiment 5.1. Consider the SISO system, where $\psi_1 = u$, $\psi_2 = 0$, $y = \xi_1$, $d_1(t) = 0.2 \sin \omega_1 t$, and $d_2(t) = 0.2 \cos \omega_1 t$. Let $\gamma_d = 0.01$ and $\gamma_H = 0.5$. We examine two initial conditions $G_{1,0}$, which have angles that are 180° apart. The 180° difference guarantees that one of the initial conditions satisfies the FD-HHC stability condition (i.e., $G_{1,0}$ is within 90° of $G_{yu}(j\omega_1)$), whereas the other initial condition does not

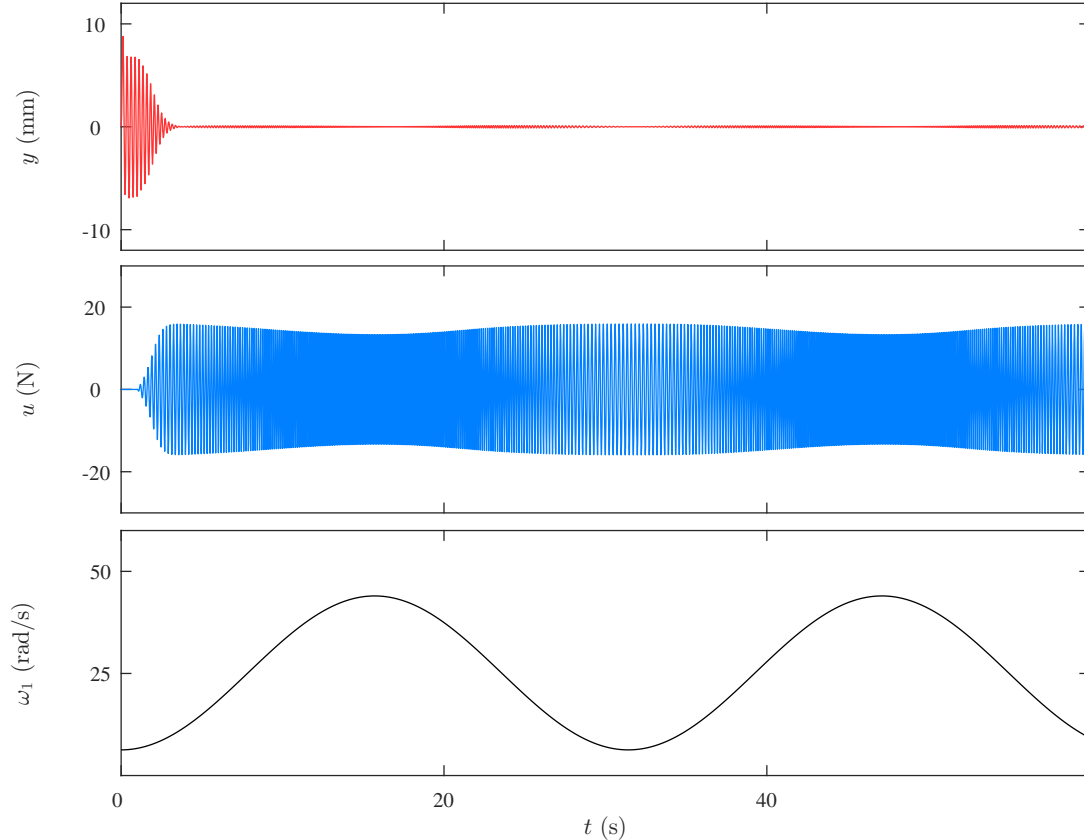


Figure 5.7: For a SISO system subject to a sinusoidal disturbance with time-varying frequency, TD-AHC can yield disturbance rejection if the time variation is known, and the rate of change of the disturbance frequency is sufficiently small.

satisfy the FD-HHC stability condition.

First, we let $G_{1,0} = -0.056 + j0.254$. Figure 5.11 shows that TD-AHC yields asymptotic disturbance rejection. After TD-AHC is turned on, the amplitude of the performance y decreases monotonically and reaches a near-zero steady-state value.

Next, we let $G_{1,0} = 0.056 - j0.254$. Figure 5.12 shows that TD-AHC yields asymptotic disturbance rejection. However, the transient response and the convergence time are degraded compared to the previous case where $G_{1,0} = -0.056 + j0.254$. In particular, the amplitude of the performance y initially grows before it decreases to the near-zero steady-state value. This suggests that the initial condition $G_{1,0} = 0.056 - j0.254$ for the second case does not satisfy the FD-HHC stability condition, whereas the initial condition $G_{1,0} = -0.056 + j0.254$ for the first case does satisfy the FD-HHC stability condition. \triangle

The gains γ_d and γ_H used in Experiment 1 can be increased to yield faster convergence rates. However, increasing γ_d and γ_H can cause actuator saturation (i.e., the magnitude of the control input u determined by TD-AHC can become larger than u_m). The following experiment demonstrates the effects of increasing γ_d and γ_H .

Experiment 5.2. We revisit the two cases in Experiment 5.1 but with larger

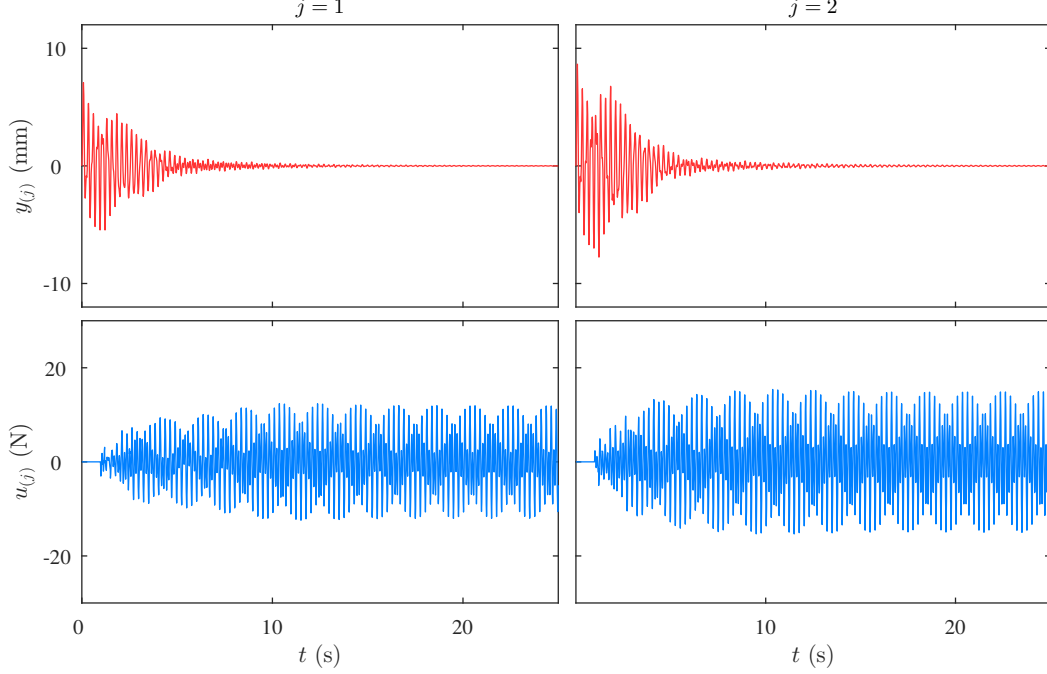


Figure 5.8: For a MIMO system with a two-tone disturbance, TD-AHC yields $y(t) \rightarrow 0$ as $t \rightarrow \infty$.

gains, specifically, $\gamma_d = 0.1$ and $\gamma_H = 1.9$. Figure 5.13 shows y and u , where $G_{1,0} = -0.056 + j0.254$. In this case, TD-AHC yields near-zero steady-state performance, and the convergence time is improved relative to the case with $\gamma_d = 0.01$ and $\gamma_H = 0.5$, which is shown in Fig. 5.11.

Figure 5.14 shows y and u , where $G_{1,0} = 0.056 - j0.254$. At approximately $t = 7$ s, the magnitude of $u_{1,k}$ determined by TD-AHC exceeds u_m , which saturates the control speaker. However, TD-AHC yields near-zero steady-state performance. \triangle

Experiment 2 demonstrates that increasing gains γ_d and γ_H can cause actuator saturation. In Fig. 5.14, TD-AHC yields near-zero steady-state performance despite actuator saturation during the transient. However, the following experiment demonstrates that actuator saturation can degrade TD-AHC performance even if zero steady-state performance is achievable (i.e., $\|u_{i,*}\| < u_m$).

Experiment 5.3. Consider the SISO system, where $\psi_1 = u$, $\psi_2 = 0$, $y = \xi_1$, $d_1(t) = 0.15 \sin \omega_1 t$, and $d_2(t) = 0.15 \cos \omega_1 t$. Let $\gamma_d = 0.1$, $\gamma_H = 1.9$, and $G_{1,0} = -0.021 + j0.092$. Figure 5.15 shows y and u with TD-AHC. At approximately $t = 6$ s, the magnitude of u exceeds u_m , which saturates the control speaker. In this case, TD-AHC does not yield near-zero steady-state performance. Note that perfect asymptotic disturbance rejection is possible because $\|u_{1,*}\| < u_m$. However, the transient response causes the actuator to saturate, and in this case, saturation prevents $u_{1,k}$ from converging to $u_{1,*}$. \triangle

Experiment 3 demonstrates that actuator saturation can prevent perfect asymptotic disturbance rejection even if perfect asymptotic disturbance rejection is achievable (i.e., $\|u_{i,*}\| < u_m$). To address this shortcoming, we present a modified version

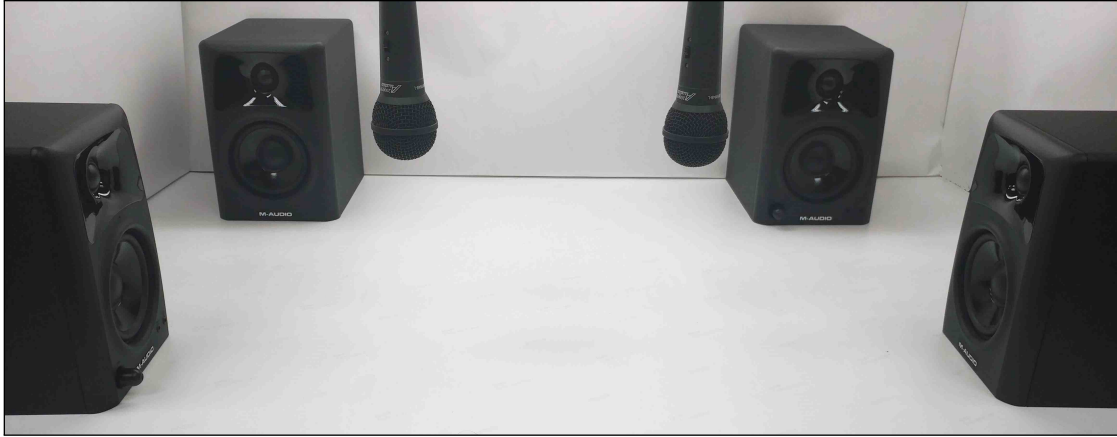


Figure 5.9: Photograph of the experimental setup.

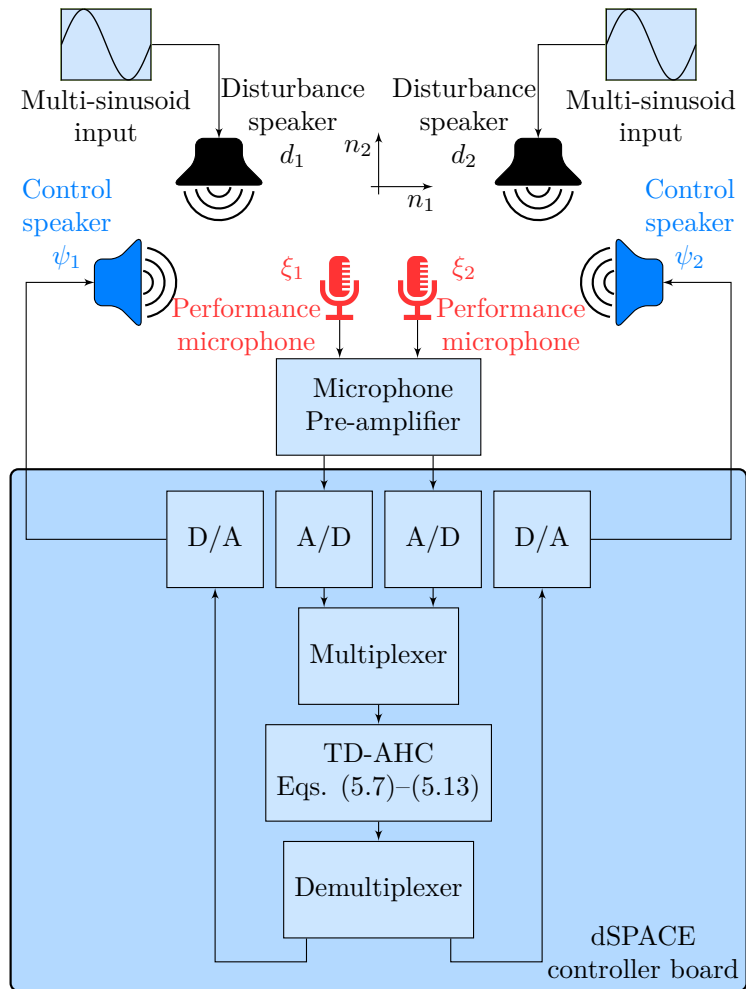


Figure 5.10: Schematic of the experimental setup.

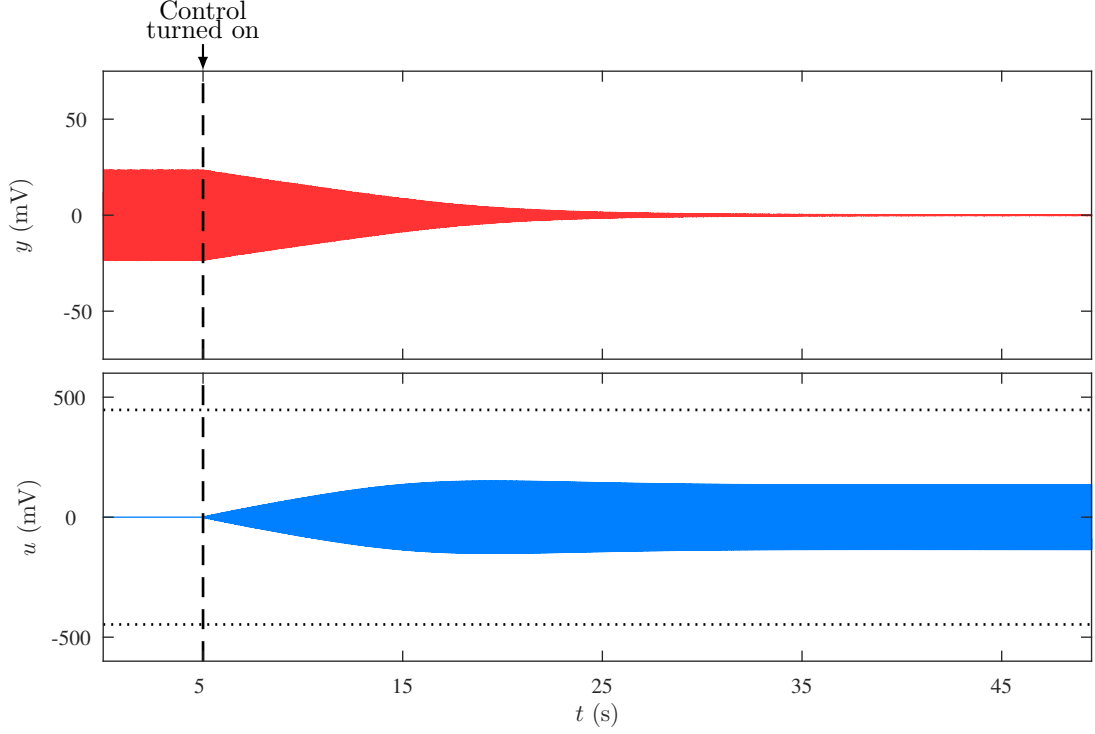


Figure 5.11: TD-AHC yields near-zero steady-state performance. After TD-AHC is turned on, the amplitude of y decreases monotonically, which suggests that $G_{1,0}$ satisfies the FD-HHC stability condition (i.e., $G_{1,0}$ is within 90° of $G_{yu}(j\omega_1)$). The dotted lines show $\pm u_m$.

of TD-AHC. Specifically, we present a modification to the update equations for $d_{i,k}$ and $H_{i,k}$.

For $j = 1, \dots, m$, let $e_j \in \mathbb{R}^{1 \times m}$ be the j th row of I_m , and define

$$E_j \triangleq \begin{bmatrix} e_j & 0_{1 \times m} \\ 0_{1 \times m} & e_j \end{bmatrix} \in \mathbb{R}^{2 \times 2m}. \quad (5.21)$$

Let $\varepsilon > 0$ be an arbitrarily small tolerance for the minimum eigenvalue of $H_{i,k} H_{i,k}^\top$. Then, for all $k \in \mathbb{N}$, the update equations for $H_{i,k}$ and $d_{i,k}$ are

$$H_{i,k+1} = \begin{cases} U_{i,k+1} \Lambda_{i,k+1} V_{i,k+1}, & \text{if } \lambda_{\min}(\bar{H}_{i,k+1} \bar{H}_{i,k+1}^\top) < \varepsilon, \\ \bar{H}_{i,k+1}, & \text{otherwise,} \end{cases} \quad (5.22)$$

$$d_{i,k+1} = \begin{cases} \alpha_{i,k+1} \bar{d}_{i,k+1}, & \text{if } \max_{j \in \{1, \dots, m\}} \|E_j H_{i,k+1}^+ \bar{d}_{i,k+1}\| > u_m, \\ \bar{d}_{i,k+1}, & \text{otherwise,} \end{cases} \quad (5.23)$$

where

$$\bar{H}_{i,k+1} \triangleq H_{i,k} - \gamma_H \eta_k \Gamma_{i,k}, \quad (5.24)$$

$$\bar{d}_{i,k+1} \triangleq d_{i,k} - \gamma_d \eta_k \delta_{i,k}, \quad (5.25)$$

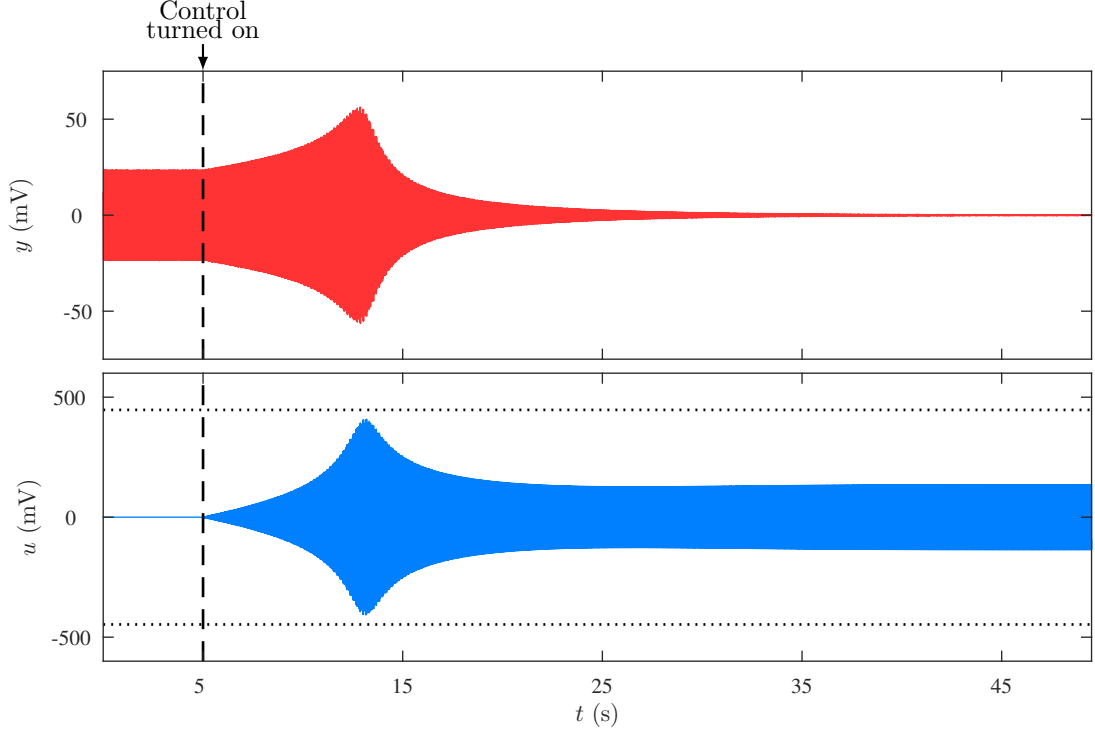


Figure 5.12: TD-AHC yields near-zero steady-state performance for the same SISO system as in Fig. 5.11 but with an initial condition $G_{1,0}$ that is 180° from the initial condition used to obtain Fig. 5.11. After TD-AHC is turned on, the amplitude of y initially grows, which suggests that $G_{1,0}$ does not satisfy the FD-HHC stability condition (i.e., $G_{1,0}$ is not within 90° of $G_{yu}(j\omega_1)$). The dotted lines show $\pm u_m$.

$$\alpha_{i,k+1} \triangleq \frac{u_m \sqrt{\lambda_{\min}(H_{i,k+1} H_{i,k+1}^T)}}{\|\bar{d}_{i,k+1}\|}, \quad (5.26)$$

and $U_{i,k+1} \in \mathbb{R}^{2\ell \times 2\ell}$ and $V_{i,k+1} \in \mathbb{R}^{2m \times 2m}$ are unitary matrices such that

$$\bar{H}_{i,k+1} = U_{i,k+1} \bar{\Lambda}_{i,k+1} V_{i,k+1}, \quad (5.27)$$

where $\bar{\Lambda}_{i,k+1} \in \mathbb{R}^{2\ell \times 2m}$ is given by

$$\bar{\Lambda}_{i,k+1} \triangleq \begin{bmatrix} \sigma_{1,k+1} & & 0 & \vdots \\ & \ddots & & \vdots \\ 0 & & \sigma_{2\ell,k+1} & \vdots \\ & & & 0_{2\ell \times (2m-2\ell)} \end{bmatrix}, \quad (5.28)$$

and $\sigma_{1,k+1}, \dots, \sigma_{2\ell,k+1}$ are the singular values of $\bar{H}_{i,k+1}$, and where

$$\Lambda_{i,k+1} \triangleq \begin{bmatrix} \Sigma_{i,k+1} & 0_{2\ell \times (2m-2\ell)} \end{bmatrix} \in \mathbb{R}^{2\ell \times 2m}, \quad (5.29)$$

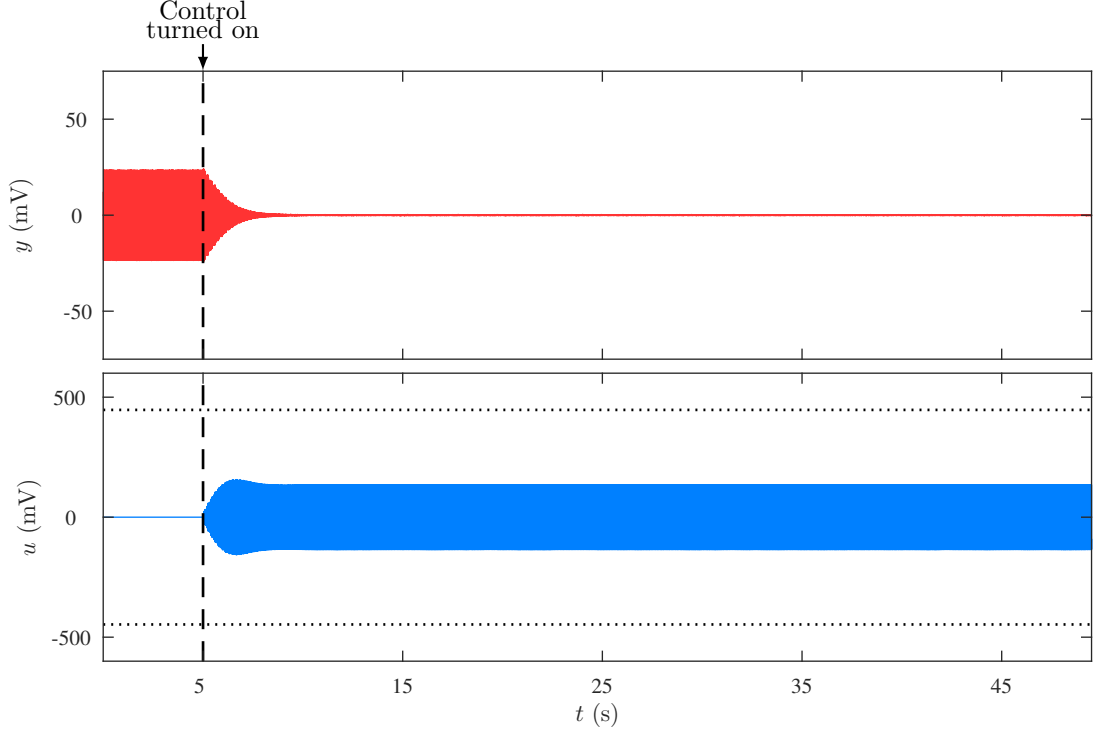


Figure 5.13: With increased gains γ_d and γ_H , TD-AHC yields near-zero steady-state performance, and the convergence rate is faster than that in Fig. 5.11. The dotted lines show $\pm u_m$.

and

$$\Sigma_{i,k+1} \triangleq \begin{bmatrix} \max\{\sigma_{1,k+1}, \sqrt{\varepsilon}\} & & 0 \\ & \ddots & \\ 0 & & \max\{\sigma_{2\ell,k+1}, \sqrt{\varepsilon}\} \end{bmatrix}. \quad (5.30)$$

Thus, the modified TD-AHC is given by (5.7)–(5.9), (5.12), (5.13), and (5.21)–(5.30). Note that, in the SISO case, singular value decomposition required for modified TD-AHC can be performed analytically. In the MIMO case, we use a coordinate-rotation digital-computer algorithm to perform the singular value decomposition. See [211] for more details.

The condition $\max_{j \in \{1, \dots, m\}} \|E_j H_{i,k}^+ \bar{d}_{i,k}\| > u_m$ in (5.23) implies that $\|H_{i,k}^+ \bar{d}_{i,k}\| > u_m$. It follows from (5.13), (5.22), (5.23), and (5.26) that for all $k \in \mathbb{Z}^+$ and all $j \in \{1, \dots, m\}$,

$$\begin{aligned} \|E_j u_{i,k}\| &= \|E_j H_{i,k}^+ d_{i,k}\| \\ &\leq \begin{cases} \frac{\alpha_{i,k} \|\bar{d}_{i,k}\|}{\sqrt{\lambda_{\min}(H_{i,k} H_{i,k}^T)}}, & \text{if } \max_{j \in \{1, \dots, m\}} \|E_j H_{i,k}^+ \bar{d}_{i,k}\| > u_m, \\ u_m, & \text{otherwise} \end{cases} \\ &= u_m. \end{aligned} \quad (5.31)$$

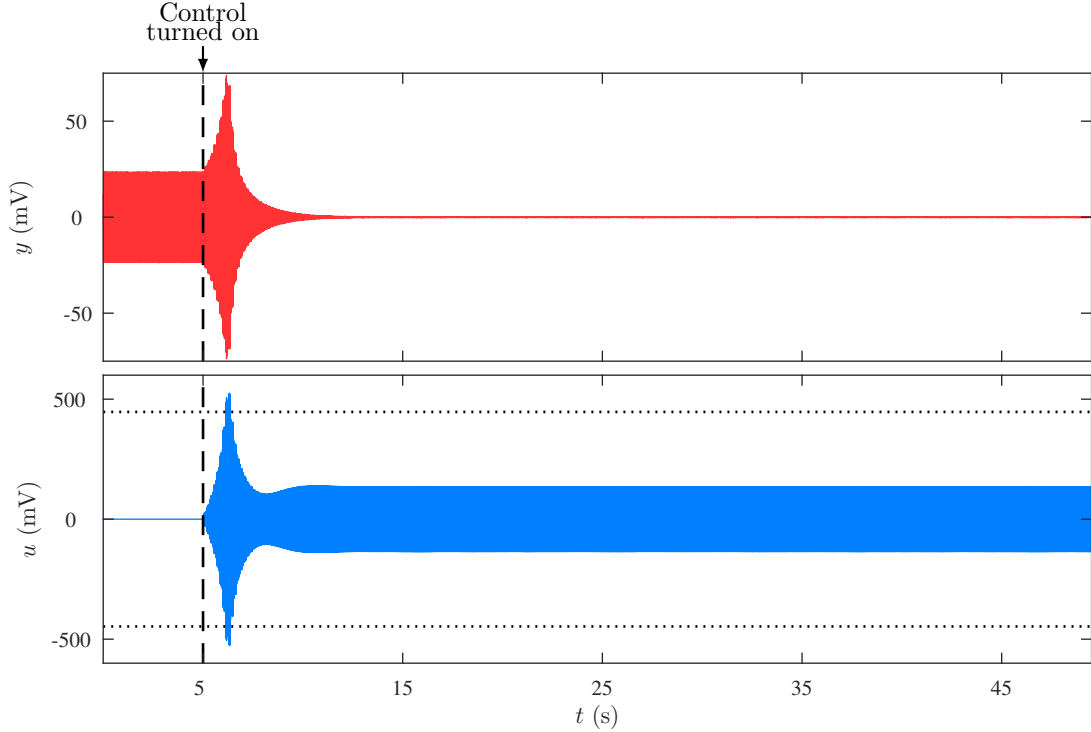


Figure 5.14: With increased gains γ_d and γ_H , TD-AHC causes actuator saturation during the transient. However, in this case, TD-AHC yields near-zero steady-state performance. The dotted lines show $\pm u_m$.

Therefore, the magnitude of each channel of the control (i.e., $\|E_j u_{i,k}\|$) is less than u_m , which implies that the modified TD-AHC guarantees that the controls do not saturate.

Experiment 5.4. We revisit Experiment 5.3 using modified TD-AHC. We let $\varepsilon = 0.1$. Figure 5.16 shows y and u with modified TD-AHC. In contrast to the results with TD-AHC (shown in Fig. 5.15), modified TD-AHC yields near-zero steady-state performance. \triangle

The following experiment demonstrates the robustness of TD-AHC to changes in the system dynamics. Specifically, the location of the control speaker changes during the experiment, and TD-AHC adapts to the changes.

Experiment 5.5. Consider the SISO system, where $\psi_1 = u$, $\psi_2 = 0$, $y = \xi_1$, $d_1(t) = 0.01 \sin \omega_1 t$, and $d_2(t) = 0.01 \cos \omega_1 t$. Let $G_{1,0} = 0.0622 - j0.4478$, $\gamma_d = 0.9$, and $\gamma_H = 1.9$. Figure 5.17 shows y and u with modified TD-AHC. The controller yields disturbance attenuation. At approximately $t = 19$ s, the location of control speaker is changed from $(-0.30, -0.27)$ m to $(-0.15, -0.27)$ m. The controller adapts to the change and yields disturbance attenuation. At approximately $t = 33$ s, the location of control speaker is changed from $(-0.15, -0.27)$ m to $(-0.40, -0.40)$ m. The controller adapts to the second change and yields disturbance attenuation. \triangle

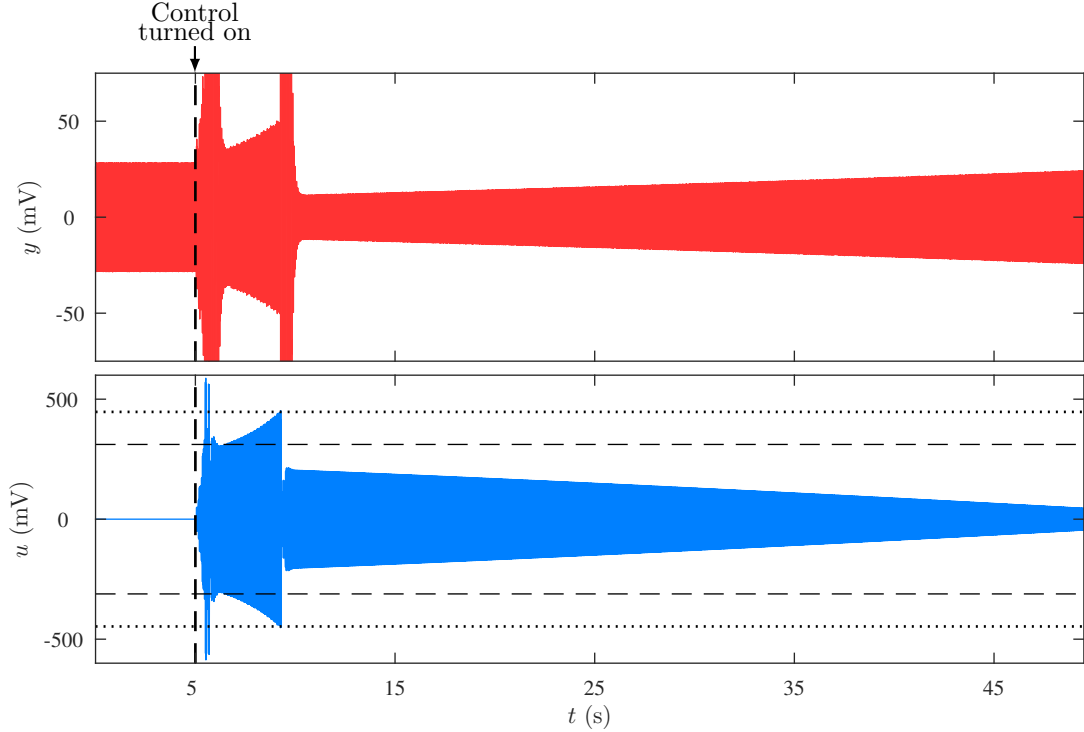


Figure 5.15: TD-AHC causes actuator saturation during the transient. Perfect asymptotic disturbance rejection is not achieved even though $\|u_{1,*}\| < u_m$. The dotted lines show $\pm u_m$, and the dashed lines show $\pm \|u_{1,*}\|$.

The following experiment demonstrates a case, where the disturbance frequency is not known accurately.

Experiment 5.6. Consider the SISO system, where $\psi_1 = u$, $\psi_2 = 0$, $y = \xi_1$, $d_1(t) = 0.01 \sin \omega_1 t$, and $d_2(t) = 0.01 \cos \omega_1 t$. Let $G_{1,0} = 0.0622 - j0.4478$, $\gamma_d = 0.9$, and $\gamma_H = 1.9$. We let the frequency of the control differ from the disturbance frequency. Specifically, we use $1.001\omega_1$ as the frequency of the control (5.7). Figure 5.18 shows y and u with modified TD-AHC. The controller yields disturbance attenuation. At approximately $t = 180$ s the performance grows; however, the performance diminishes by approximately $t = 190$ s. The growing and diminishing of the performance is due to the difference between the frequencies of disturbance and control, and is repeated over time. If the difference between the frequencies of disturbance and control is not sufficiently small, then TD-AHC does not yield disturbance attenuation. However, [212] shows that adaptive feedforward methods are not generally effective for sinusoidal disturbance rejection if the difference between frequencies of disturbance and control is not sufficiently small. \triangle

In the following experiment, we use modified TD-AHC to reject a two-tone disturbance acting on a MIMO system.

Experiment 5.7. Consider the MIMO system, where $y = [\xi_1 \ \xi_2]^T$ and $[\psi_1 \ \psi_2]^T = u$. The two-tone disturbances are $d_1(t) = 0.011 \cos \omega_1 t + 0.012 \sin \omega_2 t$ and $d_2(t) =$

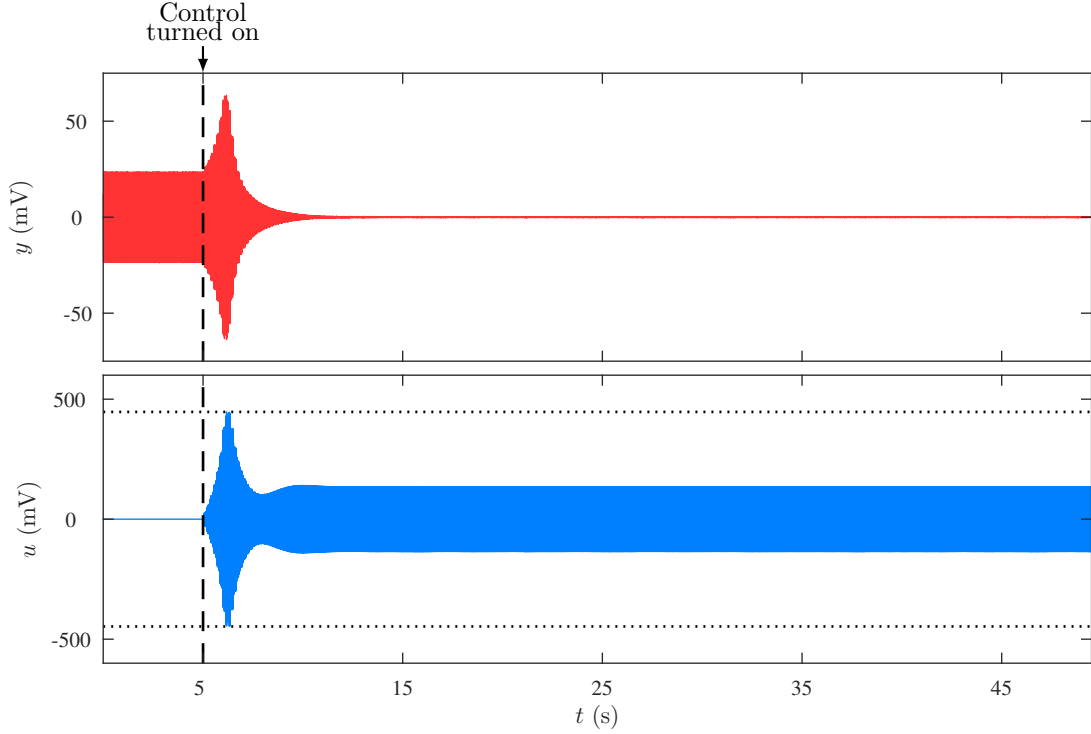


Figure 5.16: Modified TD-AHC yields near-zero steady-state performance despite actuator saturation. The dotted lines show $\pm u_m$, and the dashed lines show $\pm \|u_{1,*}\|$.

$0.015 \cos \omega_1 t + 0.010 \sin \omega_2 t$. Let $\gamma_d = 10^{-4}$, $\gamma_H = 0.01$, and

$$G_{1,0} = G_{2,0} = \begin{bmatrix} 0.1475 + j0.0715 & 0.0357 + j0.0205 \\ -0.0003 + j0.0242 & 0.0561 + j0.1419 \end{bmatrix}.$$

Figure 5.19 shows that modified TD-AHC yields asymptotic disturbance rejection. \triangle

5.8 Conclusions

We presented a sampled-data adaptive harmonic controller for rejection of known-frequency sinusoids that act on a completely unknown MIMO LTI system with at least as many controls as performance measurements. The main analytic result shows that the closed-loop system is uniformly Lyapunov stable and that the closed-loop performance tends to zero asymptotically. In contrast to FD-HHC, the adaptive controller in this chapter is a time-domain method and does not require DFT computations. Numerical simulations suggest that the new sampled-data adaptive harmonic controller can be implemented with larger gains or with faster sample rate than FD-HHC. These larger gains or faster sample rate tend to reduce convergence time of TD-AHC relative to that of FD-HHC. We also presented results from active noise control experiments, which validate the practical effectiveness of TD-AHC.

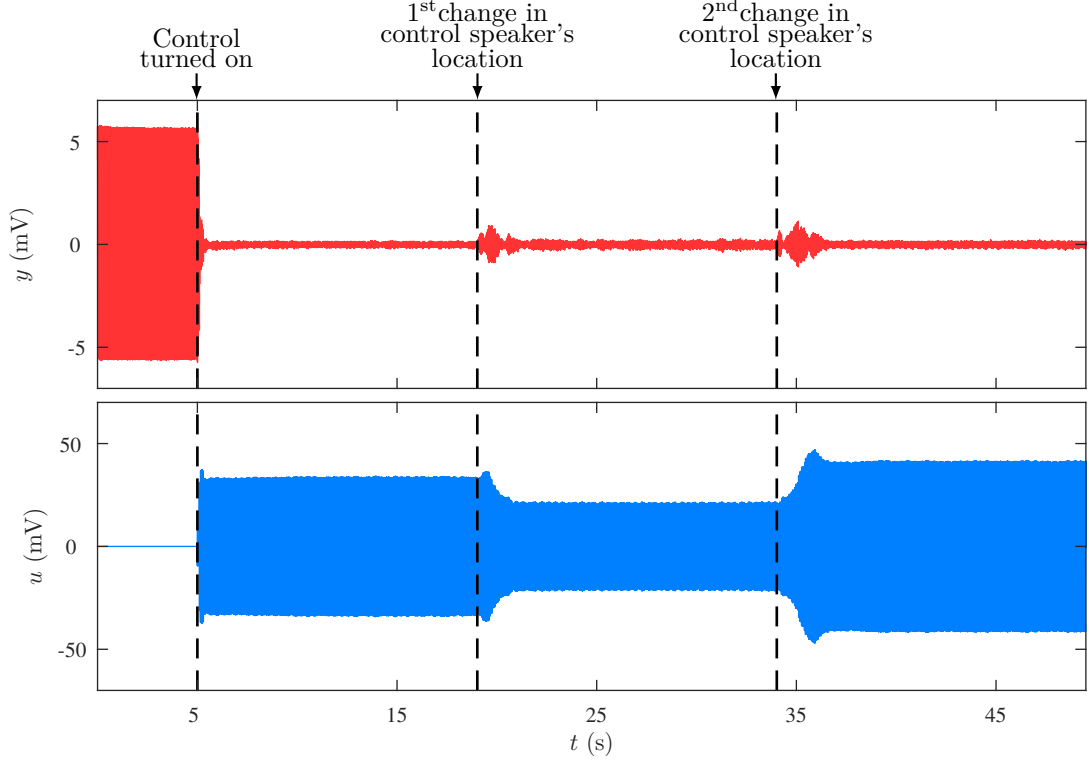


Figure 5.17: Modified TD-AHC adapts to changes in control speaker location, and yields disturbance attenuation.

5.9 Proof of Theorem 5.2

Let $\alpha > \gamma_H/2 + q\gamma_d/\nu$. For all $k \in \mathbb{N}$, define

$$\hat{y}_{k+1} \triangleq (1 - \alpha)y_{k+1} + \sum_{j=1}^q \phi_{j,k+1}^T \left(\tilde{H}_{j,k} H_{j,k}^+ d_{j,k} - \tilde{d}_{j,k} \right). \quad (5.32)$$

Substituting (5.12) and (5.32) into (5.15) and (5.16) yields

$$\tilde{d}_{i,k+1} = \tilde{d}_{i,k} + 2\gamma_d \eta_k \phi_{i,k+1} \hat{y}_{k+1}, \quad (5.33)$$

$$\tilde{H}_{i,k+1} = \tilde{H}_{i,k} + \gamma_H \eta_k \phi_{i,k+1} \hat{y}_{k+1} u_{i,k}^T + \gamma_H \eta_k \Lambda_\ell \phi_{i,k+1} \hat{y}_{k+1} u_{i,k}^T \Lambda_m^T. \quad (5.34)$$

Define the partial Lyapunov function

$$V_d(\tilde{d}_{1,k}, \dots, \tilde{d}_{q,k}) \triangleq \sum_{j=1}^q \|\tilde{d}_{j,k}\|^2,$$

and the difference

$$\Delta V_d(k) \triangleq V_d(\tilde{d}_{1,k+1}, \dots, \tilde{d}_{q,k+1}) - V_d(\tilde{d}_{1,k}, \dots, \tilde{d}_{q,k}).$$

Since for all $k \in \mathbb{N}$, $\phi_{i,k}^T \phi_{i,k} = I_\ell$, evaluating ΔV_d along the trajectories of (5.33) yields

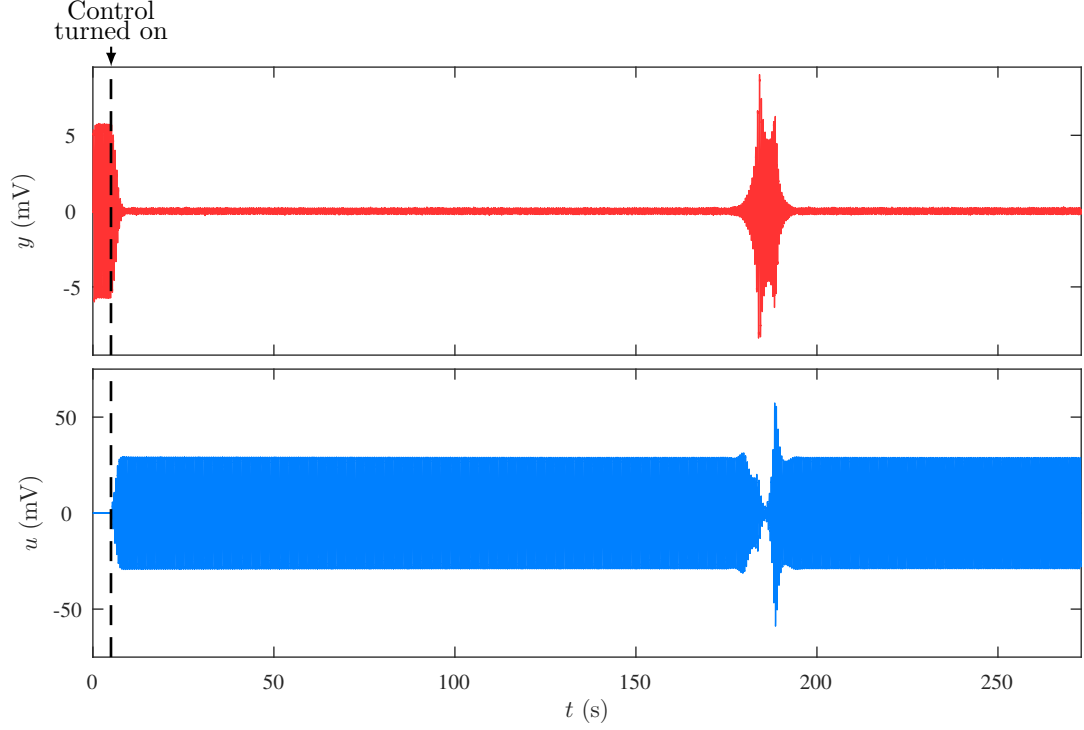


Figure 5.18: For a SISO system, where the disturbance frequency is not known accurately, modified TD-AHC can yield disturbance attenuation if the frequency of the control is sufficiently close to the disturbance frequency.

$$\Delta V_d(k) = 4q\gamma_d^2\eta_k^2\|\hat{y}_{k+1}\|^2 + 4\gamma_d\eta_k \sum_{j=1}^q \tilde{d}_{j,k}^T \phi_{j,k+1} \hat{y}_{k+1}. \quad (5.35)$$

Define the partial Lyapunov function

$$V_H(\tilde{H}_{1,k}, \dots, \tilde{H}_{q,k}) \triangleq \sum_{j=1}^q \|\tilde{H}_{j,k}\|_F^2,$$

and the difference

$$\Delta V_H(k) \triangleq V_H(\tilde{H}_{1,k+1}, \dots, \tilde{H}_{q,k+1}) - V_H(\tilde{H}_{1,k}, \dots, \tilde{H}_{q,k}).$$

Evaluating ΔV_H along (5.34) yields

$$\begin{aligned} \Delta V_H(k) = & \sum_{j=1}^q \text{tr} \left[2\gamma_H\eta_k \tilde{H}_{j,k}^T \phi_{j,k+1} \hat{y}_{k+1} u_{j,k}^T + 2\gamma_H\eta_k \tilde{H}_{j,k}^T \Lambda_\ell \phi_{j,k+1} \hat{y}_{k+1} u_{j,k}^T \Lambda_m^T \right. \\ & + \gamma_H^2 \eta_k^2 u_{j,k}^T u_{j,k} \hat{y}_{k+1}^T \phi_{j,k+1}^T \phi_{j,k+1} \hat{y}_{k+1} + \gamma_H^2 \eta_k^2 u_{j,k}^T \Lambda_m^T \Lambda_m u_{j,k} \hat{y}_{k+1}^T \\ & \times \phi_{j,k+1}^T \Lambda_\ell^T \Lambda_\ell \phi_{j,k+1} \hat{y}_{k+1} \\ & \left. + 2\gamma_H^2 \eta_k^2 u_{j,k} \hat{y}_{k+1}^T \phi_{j,k+1}^T \Lambda_\ell \phi_{j,k+1} \hat{y}_{k+1} u_{j,k}^T \Lambda_m^T \right]. \quad (5.36) \end{aligned}$$

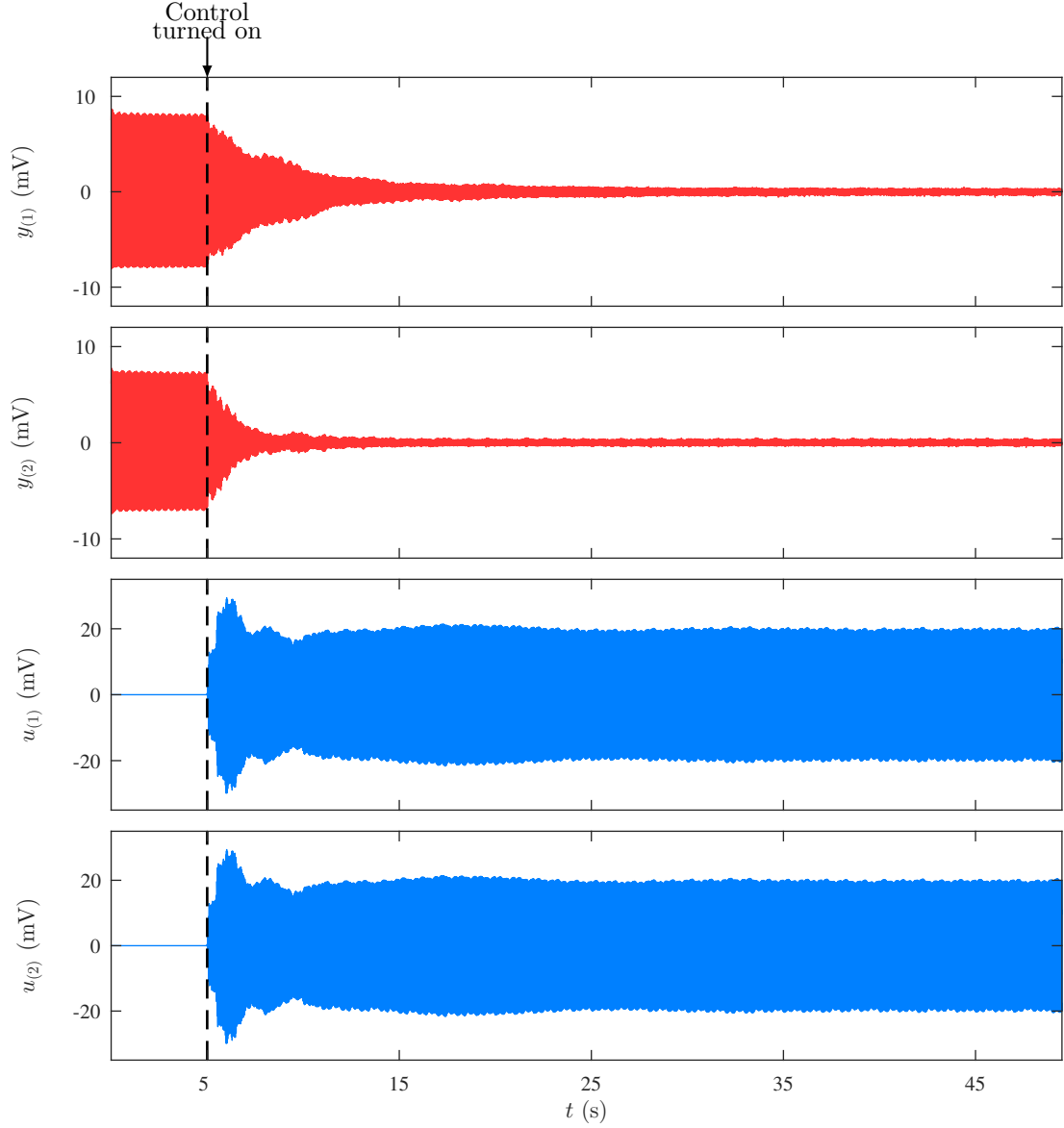


Figure 5.19: For a MIMO system with a two-tone disturbance, modified TD-AHC yields asymptotic disturbance rejection.

Note that $\Lambda_m^T \Lambda_m = I_{2m}$ and $\Lambda_\ell^T \Lambda_\ell = I_{2\ell}$, and for all $k \in \mathbb{N}$, $\phi_{i,k}^T \phi_{i,k} = I_\ell$ and $\phi_{i,k+1}^T \Lambda_\ell \phi_{i,k+1} = 0$. Thus, it follows from (5.36) that

$$\begin{aligned} \Delta V_H(k) = & \sum_{j=1}^q \text{tr} \left[2\gamma_H \eta_k \tilde{H}_{j,k}^T \phi_{j,k+1} \hat{y}_{k+1} u_{j,k}^T + 2\gamma_H \eta_k \Lambda_m^T \tilde{H}_{j,k}^T \Lambda_\ell \phi_{j,k+1} \hat{y}_{k+1} u_{j,k}^T \right] \\ & + 2\gamma_H^2 \eta_k^2 \|u_{j,k}\|^2 \|\hat{y}_{k+1}\|^2. \end{aligned} \quad (5.37)$$

Since $\tilde{H}_{i,0} \in \mathcal{H}$, it follows from (5.34) that for all $k \in \mathbb{Z}^+$, $\tilde{H}_{i,k} \in \mathcal{H}$. Thus, $\Lambda_m^T \tilde{H}_{i,k}^T \Lambda_\ell =$

$\tilde{H}_{i,k}^T$, and (5.37) implies that

$$\Delta V_H(k) = 4\gamma_H\eta_k \sum_{j=1}^q u_{j,k}^T \tilde{H}_{j,k}^T \phi_{j,k+1} \hat{y}_{k+1} + 2\gamma_H^2 \eta_k^2 \|u_{j,k}\|^2 \|\hat{y}_{k+1}\|^2. \quad (5.38)$$

Define the Lyapunov function

$$V(\tilde{d}_{1,k}, \dots, \tilde{d}_{q,k}, \tilde{H}_{1,k}, \dots, \tilde{H}_{q,k}) \triangleq \frac{V_d(\tilde{d}_{1,k}, \dots, \tilde{d}_{q,k})}{\gamma_d} + \frac{V_H(\tilde{H}_{1,k}, \dots, \tilde{H}_{q,k})}{\gamma_H}, \quad (5.39)$$

and define the Lyapunov difference

$$\begin{aligned} \Delta V(k) &\triangleq V(\tilde{d}_{1,k+1}, \dots, \tilde{d}_{q,k+1}, \tilde{H}_{1,k+1}, \dots, \tilde{H}_{q,k+1}) - V(\tilde{d}_{1,k}, \dots, \tilde{d}_{q,k}, \tilde{H}_{1,k}, \dots, \tilde{H}_{q,k}) \\ &= \frac{1}{\gamma_d} \Delta V_d(k) + \frac{1}{\gamma_H} \Delta V_H(k). \end{aligned} \quad (5.40)$$

Substituting (5.35) and (5.38) into (5.40) yields

$$\Delta V(k) = 4\eta_k^2 \left[\left(q\gamma_d + \frac{\gamma_H}{2} \sum_{j=1}^q \|u_{j,k}\|^2 \right) \|\hat{y}_{k+1}\|^2 + \frac{1}{\eta_k} \sum_{j=1}^q (\tilde{H}_{j,k} u_{j,k} + \tilde{d}_{j,k})^T \phi_{j,k+1} \hat{y}_{k+1} \right]. \quad (5.41)$$

Then, substituting (5.32) into (5.41) yields

$$\Delta V(k) = -4\eta_k \left[1 - q\gamma_d\eta_k - \frac{\gamma_H}{2} \eta_k \sum_{j=1}^q \|u_{j,k}\|^2 \right] \|\hat{y}_{k+1}\|^2 - 4\eta_k(\alpha - 1) y_{k+1}^T \hat{y}_{k+1}. \quad (5.42)$$

To show *iii*), assume that there exists $k_s \in \mathbb{N}$ and $\varepsilon > 0$ such that for all $k \geq k_s$, $\lambda_{\min}(H_{i,k} H_{i,k}^T) > \varepsilon$. Thus, for all $k \geq k_s$, $H_{i,k} H_{i,k}^+ = I_{2\ell}$, and it follows from (5.13), (5.14), and (5.32) that for all $k \geq k_s$,

$$\begin{aligned} \hat{y}_{k+1} &= y_{k+1} + \sum_{j=1}^q \left[\phi_{j,k+1}^T (H_{j,k} H_{j,k}^+ d_{j,k} - d_{j,k}) \right] \\ &= y_{k+1}. \end{aligned} \quad (5.43)$$

Substituting (5.12) and (5.43) into (5.42) implies that for all $k \geq k_s$,

$$\begin{aligned} \Delta V(k) &= -4\eta_k \left[1 - q\gamma_d\eta_k - \frac{\gamma_H}{2} \eta_k \sum_{j=1}^q \|u_{j,k}\|^2 + \alpha - 1 \right] \|y_{k+1}\|^2 \\ &\leq -4\eta_k \left(\alpha - \frac{q\gamma_d}{\nu} - \frac{\gamma_H}{2} \right) \|y_{k+1}\|^2 \\ &= -4\eta_k c_1 \|y_{k+1}\|^2, \end{aligned} \quad (5.44)$$

where $c_1 \triangleq \alpha - q\gamma_d/\nu - \gamma_H/2$ is positive because $\alpha > \gamma_H/2 + q\gamma_d/\nu$. Thus, (5.44) implies that for all $k \geq k_s$, $\Delta V(k)$ is nonpositive. Therefore, it follows that $V(\tilde{d}_{1,k}, \dots,$

$\tilde{d}_{q,k}, \tilde{H}_{1,k}, \dots, \tilde{H}_{q,k}$) is bounded. Since, in addition, V is radially unbounded, it follows that $\tilde{d}_{i,k}$ and $\tilde{H}_{i,k}$ are bounded. Thus, $d_{i,k}$ and $H_{i,k}$ are bounded. Since $H_{i,k}$ is bounded and for all $k \geq k_s$, $\lambda_{\min}(H_{i,k}H_{i,k}^\top) > \varepsilon$, it follows that for all $k \geq k_s$, $(H_{i,k}H_{i,k}^\top)^{-1}$ exists and is bounded. Thus, for all $k \geq k_s$, $u_{i,k} = -H_{i,k}^\top(H_{i,k}H_{i,k}^\top)^{-1}d_{i,k}$. Since $H_{i,k}$, $(H_{i,k}H_{i,k}^\top)^{-1}$, and $d_{i,k}$ are bounded, it follows that $u_{i,k}$ is bounded. Thus, (5.12) and (5.44) imply that for all $k \geq k_s$,

$$\Delta V(k) \leq -c_2 \|y_{k+1}\|^2, \quad (5.45)$$

where

$$c_2 \triangleq \frac{4c_1}{\nu + \sup_{k \in \mathbb{N}} \sum_{j=1}^q \|u_{j,k}\|^2} > 0.$$

Moreover, since $V(\tilde{d}_{1,k}, \dots, \tilde{d}_{q,k}, \tilde{H}_{1,k}, \dots, \tilde{H}_{q,k})$ is positive definite, and $\Delta V(k)$ is non-positive, it follows from (5.40) and (5.45) that

$$\begin{aligned} 0 &\leq \lim_{k \rightarrow \infty} \sum_{j=k_s}^k c_2 \|y_{j+1}\|^2 \\ &\leq - \lim_{k \rightarrow \infty} \sum_{j=k_s}^k \Delta V(j) \\ &\leq V(\tilde{d}_{1,k_s}, \dots, \tilde{d}_{q,k_s}, \tilde{H}_{1,k_s}, \dots, \tilde{H}_{q,k_s}) - \lim_{k \rightarrow \infty} V(\tilde{d}_{1,k+1}, \dots, \tilde{d}_{q,k+1}, \tilde{H}_{1,k+1}, \dots, \tilde{H}_{q,k+1}) \\ &\leq V(\tilde{d}_{1,k_s}, \dots, \tilde{d}_{q,k_s}, \tilde{H}_{1,k_s}, \dots, \tilde{H}_{q,k_s}), \end{aligned}$$

where the upper and lower bounds imply that all the limits exist. Thus, $\lim_{k \rightarrow \infty} y_k = 0$, which confirms *iii*).

To show *i*) and *ii*), note that it follows from (A5.1) that $\text{rank } H_{i,*} = 2\ell$. Thus, there exist $r_1 > 0$ and $\varepsilon_1 > 0$ such that for all $H_i \in \mathbb{B}_{r_1}(\alpha H_{i,*})$, $\lambda_{\min}(H_i H_i^\top) > \varepsilon_1$. Let $r \in (0, \sqrt{r_1^2 \gamma_d / (q(\gamma_d + \gamma_H))})$, and let $\tilde{d}_{1,0}, \dots, \tilde{d}_{q,0} \in \mathbb{B}_r(0)$ and $\tilde{H}_{1,0}, \dots, \tilde{H}_{q,0} \in \mathcal{H} \cap \mathbb{B}_r(0)$. Assume for contradiction that there exists $k_1 \in \mathbb{Z}^+$ and $i_1 \in Q$ such that $\tilde{H}_{i_1, k_1} \notin \mathbb{B}_{r_1}(0)$ and for all $k \in \mathcal{K} \triangleq \{0, 1, \dots, k_1 - 1\}$, $\tilde{H}_{i,k} \in \mathbb{B}_{r_1}(0)$. Since for all $k \in \mathcal{K}$, $\tilde{H}_{i,k} \in \mathbb{B}_{r_1}(0)$, it follows that for all $k \in \mathcal{K}$, $\lambda_{\min}(H_{i,k}H_{i,k}^\top) > \varepsilon_1$. Thus, using the same process as (5.43)–(5.45) with ε replaced by ε_1 yields that for all $k \in \mathcal{K}$, $\Delta V(k) \leq 0$. Therefore, it follows from (5.40) that

$$\begin{aligned} 0 &\leq - \sum_{i=0}^{k_1-1} \Delta V(i) \\ &= V(\tilde{d}_{1,0}, \dots, \tilde{d}_{q,0}, \tilde{H}_{1,0}, \dots, \tilde{H}_{q,0}) - V(\tilde{d}_{1,k_1}, \dots, \tilde{d}_{q,k_1}, \tilde{H}_{1,k_1}, \dots, \tilde{H}_{q,k_1}) \\ &= \frac{1}{\gamma_d} \sum_{i=1}^q (\|\tilde{d}_{i,0}\|^2 - \|\tilde{d}_{i,k_1}\|^2) + \frac{1}{\gamma_H} \left(\sum_{i=1}^q \|\tilde{H}_{i,0}\|_F^2 - \|\tilde{H}_{i_1, k_1}\|_F^2 - \sum_{i \in Q \setminus \{i_1\}} \|\tilde{H}_{i, k_1}\|_F^2 \right) \\ &\leq \frac{1}{\gamma_d} \sum_{i=1}^q \|\tilde{d}_{i,0}\|^2 + \frac{1}{\gamma_H} \left(\sum_{i=1}^q \|\tilde{H}_{i,0}\|_F^2 - \|\tilde{H}_{i_1, k_1}\|_F^2 \right) \end{aligned}$$

$$\begin{aligned}
&\leq \frac{qr^2}{\gamma_d} + \frac{qr^2 - r_1^2}{\gamma_H} \\
&< \frac{q}{\gamma_d} \left[\frac{r_1^2 \gamma_d}{q(\gamma_d + \gamma_H)} \right] + \frac{1}{\gamma_H} \left(\frac{qr_1^2 \gamma_d}{q(\gamma_d + \gamma_H)} - r_1^2 \right) \\
&= 0,
\end{aligned}$$

which is a contradiction. Thus, for all $k \in \mathbb{N}$, $\tilde{H}_{i,k} \in \mathbb{B}_{r_1}(0)$, which implies that $H_{i,k} \in \mathbb{B}_{r_1}(\alpha H_{i,*})$. Therefore, for all $k \in \mathbb{N}$, $\lambda_{\min}(H_{i,k} H_{i,k}^T) > \varepsilon_1$, and it follows from *iii*) that $d_{i,k}$, $H_{i,k}$, and $u_{i,k}$ are bounded, and $\lim_{k \rightarrow \infty} y_k = 0$, which confirms *ii*).

Since for all $k \in \mathbb{N}$, $\lambda_{\min}(H_{i,k} H_{i,k}^T) > \varepsilon_1$, using the same process as (5.43)–(5.45), with ε replaced by ε_1 , it follows that for all $k \in \mathbb{N}$, $\Delta V(k) \leq 0$. Thus, the equilibrium $(\tilde{d}_{1,k}, \dots, \tilde{d}_{q,k}, \tilde{H}_{1,k}, \dots, \tilde{H}_{q,k}) \equiv 0$ is uniformly Lyapunov stable [208, Thm. 13.11], which confirms *i*).

Chapter 6

Frequency-Domain Adaptive Harmonic Control for Decentralized Control Systems

In this chapter, we present a decentralized frequency-domain adaptive harmonic control (FD-AHC), which is effective for rejection of sinusoidal disturbances of known frequencies that act on a completely unknown asymptotically-stable linear time-invariant system. In fact, this chapter extends the FD-AHC algorithm presented in Chapter 4 to address decentralized control systems. The decentralized control architecture consists of multi-input multi-output subsystems, where each local controller does not have access to any information regarding the system or the nonlocal measurements. We analyze stability and performance properties of the closed-loop for multi-input multi-output subsystems. We show that the decentralized control rejects sinusoidal disturbances asymptotically. In addition, we present a result regarding the transient properties of the decentralized controller, which provides an estimate for the convergence rate of the closed-loop system. We show that the convergence rate can be significantly improved by choice of certain control parameters. We also demonstrate the effectiveness of the controller through numerical simulations. The result of this chapter appears in [196, 197].

6.1 Introduction

Rejection of sinusoidal disturbances is a challenging control objective in many applications such as active noise cancellation [42], active balancing of rotating machinery [21], active suspension control [213], and vibration suppression of rotorcraft and spacecraft [5, 61]. The disturbance rejection problem is even more challenging if the system or the disturbances are uncertain. In addition, large-scale dynamical systems necessitate decentralized control architecture, that is, the control system must be designed with the constraint that none of local controllers has information regarding the nonlocal performance measurements [159].

For large-scale uncertain systems, decentralized adaptive control techniques that

require limited model information are proposed in [160–168]. Particularly, the technique in [162] concerns systems with strong nonlinear interconnections, and the method in [163] is applicable to large-scale dynamical systems with unknown interconnections. The methods presented in [161, 162] develop decentralized adaptive controllers that require local full-state feedback for closed-loop stabilization. These local full-state feedback adaptive methods have been extended in [169–171]. Existing decentralized control techniques for disturbance rejection are given in [144, 151, 170, 172]. However, these methods require some model information regarding the system to be controlled and may not yield perfect tonal disturbance rejection.

For an asymptotically stable linear time-invariant (LTI) system, a centralized control approach for sinusoidal disturbance rejection takes advantage of the system’s harmonic steady-state (HSS) response, that is, the remaining sinusoidal response after the transient response of the system vanishes. This technique was separately studied in [10, 20, 32, 156], and is known as ‘convergent control’ (for active rotor balancing) and ‘higher-harmonic control’ (for helicopter vibration suppression). In this chapter, we adopt the name frequency-domain higher-harmonic control (FD-HHC).

To further explain FD-HHC, consider an LTI system subject to a sinusoidal disturbance with known frequency ω . The control input generated by FD-HHC is a sinusoid with frequency ω , where the amplitude and phase are updated at discrete times. FD-HHC is a frequency-domain approach, meaning that all control computations are performed using discrete Fourier transform (DFT) of the performance measurements. The drawback of FD-HHC is that it requires an estimate of the control-to-performance transfer function evaluated at the disturbance frequency ω . In the SISO case, this estimate, which is a complex number, must have an angle within 90° of the actual value for closed-loop stability. In the MIMO case, closed-loop stability is ensured provided that the estimate is sufficiently accurate. If there are multiple disturbance frequencies, then estimates are required at each frequency. For certain applications, this transfer function can be difficult to estimate or subject to change.

To address uncertainty, adaptive HHC techniques have been developed [81, 157, 158]. However, the methods in [81, 157] require an external excitation signal to guarantee stability, and the analysis presented in [158] is limited to an averaged system. The adaptive disturbance rejection algorithms that we present in Chapters 2–5 are for unknown systems, however, these methods are centralized control schemes. In [172], a decentralized HHC technique is proposed. If the value at frequency ω of the control-to-performance transfer function is a diagonally-dominant matrix, then [172] provides some sufficient-but-not-necessary conditions for tonal disturbance rejection. Therefore, the decentralized control technique requires some model information, and is not applicable to unknown systems.

In this chapter, we present decentralized frequency-domain adaptive harmonic control (FD-AHC). Decentralized FD-AHC consists of decentralized multi-input multi-output controllers with at least as many local controls as local performance measurements. Decentralized FD-AHC is effective for rejection of known-frequency sinusoidal disturbances that act on a completely unknown asymptotically stable system. Similar to FD-HHC, decentralized FD-AHC is a frequency-domain method and uses DFT of

the local performance measurements for calculations of the local controls. We analyze stability and performance properties of decentralized FD-AHC. The main result on decentralized FD-AHC shows that the controller asymptotically rejects the disturbance. In addition, we present a result that concerns the transient properties of decentralized FD-AHC. That result provides an estimate for the convergence rate of the closed-loop system. We show that convergence rate can be significantly improved by choice of significantly large adaptive gains.

6.2 Notation

Let \mathbb{F} be either \mathbb{R} or \mathbb{C} . Let $x_{(i)}$ denote the i th element of $x \in \mathbb{F}^n$, and let $A_{(i,j)}$ denote the element in row i and column j of $A \in \mathbb{F}^{m \times n}$. Let $\|\cdot\|$ be the 2-norm on \mathbb{F}^n . The Moore-Penrose generalized inverse [201, Chap. 6.1] of $A \in \mathbb{R}^{\ell \times m}$ is denoted by $A^+ \in \mathbb{R}^{m \times \ell}$. Note that if $A \in \mathbb{R}^{\ell \times m}$ is right invertible (i.e., $\text{rank } A = \ell$), then $A^+ = A^T(AA^T)^{-1}$. Next, let A^* denote the complex conjugate transpose of $A \in \mathbb{F}^{m \times n}$, and define $\|A\|_F \triangleq \sqrt{\text{tr } A^*A}$, which is the Frobenius norm of $A \in \mathbb{F}^{m \times n}$. Let $\mathbb{R}[s]$ denote the set of polynomials with real coefficients.

We write $A > 0$ if and only if $A \in \mathbb{F}^{n \times n}$ is Hermitian positive-definite. Let $\lambda_{\min}(A)$ denote the minimum eigenvalue of the Hermitian positive-semidefinite matrix $A \in \mathbb{F}^{n \times n}$.

Define $\mathbb{N} \triangleq \{0, 1, 2, \dots\}$ and $\mathbb{Z}^+ \triangleq \mathbb{N} \setminus \{0\}$. Define the *open ball of radius $r > 0$ centered at $C \in \mathbb{C}^{m \times n}$* by $\mathbb{B}_r(C) \triangleq \{X \in \mathbb{C}^{m \times n} : \|X - C\|_F < r\}$.

6.3 Problem Formulation

Consider the LTI system

$$\dot{x}(t) = Ax(t) + D_1d(t) + \sum_{i=1}^r B_i u_i(t), \quad (6.1)$$

$$y_i(t) = C_i x(t) + D_2 d(t) + \sum_{j=1}^r D_{i,j} u_j(t), \quad (6.2)$$

where $t \geq 0$, $x(t) \in \mathbb{R}^n$ is the state, $x(0) = x_0 \in \mathbb{R}^n$ is the initial condition, $d(t) \in \mathbb{R}^p$ is the unmeasured disturbance, $A \in \mathbb{R}^{n \times n}$ is asymptotically stable, and for all $i \in \mathcal{R} \triangleq \{1, 2, \dots, r\}$, $u_i(t) \in \mathbb{R}^{m_i}$ is the control and $y_i(t) \in \mathbb{R}^{\ell_i}$ is the measured performance. Let $\omega_1, \omega_2, \dots, \omega_q > 0$, and consider the sinusoidal disturbance

$$d(t) = \sum_{j=1}^q d_{c,j} \cos \omega_j t + d_{s,j} \sin \omega_j t, \quad (6.3)$$

where for all $j \in Q \triangleq \{1, 2, \dots, q\}$, $d_{c,j}, d_{s,j} \in \mathbb{R}^p$.

We consider the decentralized disturbance rejection problem, where for each $i \in \mathcal{R}$, the control u_i can depend on the local measurement y_i , but cannot depend on nonlocal measurements $\{y_j : j \in \mathcal{R} \setminus \{i\}\}$. Our objective is to design a decentralized control

architecture such that the control u_i eliminates the effect of the disturbance d on the performance y_i . We seek to design a control that requires no model information regarding (6.1) and (6.2). Unless otherwise stated, all statements in this chapter that involve the subscript i are for all $i \in \mathcal{R}$.

Define $m \triangleq \sum_{j=1}^r m_j$, and let $G_{y_i u} : \mathbb{C} \rightarrow \mathbb{C}^{\ell_i \times m}$ and $G_{y_i d} : \mathbb{C} \rightarrow \mathbb{C}^{\ell_i \times p}$ be given by

$$\begin{aligned} G_{y_i u}(s) &\triangleq C_i(sI - A)^{-1}B + \mathcal{D}_i, \\ G_{y_i d}(s) &\triangleq C_i(sI - A)^{-1}D_1 + D_2, \end{aligned}$$

where

$$\begin{aligned} B &\triangleq [B_1 \quad \cdots \quad B_r], \\ \mathcal{D}_i &\triangleq [D_{i,1} \quad \cdots \quad D_{i,r}]. \end{aligned}$$

For simplicity of presentation, we focus on the case where d is the single-tone disturbance

$$d(t) = d_c \cos \omega t + d_s \sin \omega t. \quad (6.4)$$

However, by using separate copies of decentralized FD-AHC at each frequency, the adaptive controller presented in this chapter generalizes to the case, where d consists of multiple tones. See Section 4.6 for details. We consider multi-tone disturbances for the numerical examples presented in Section 6.6.

Define

$$M_{i,*} \triangleq G_{y_i u}(j\omega) \in \mathbb{C}^{\ell_i \times m},$$

and

$$M_* \triangleq [M_{1,*}^T \quad \cdots \quad M_{r,*}^T]^T \in \mathbb{C}^{\ell \times m},$$

where $\ell \triangleq \sum_{i=1}^r \ell_i$. We make the following assumptions:

$$(A6.1) \quad \text{rank } M_* = \ell.$$

$$(A6.2) \quad m_i \geq \ell_i.$$

$$(A6.3) \quad \omega_1, \dots, \omega_q \text{ are known.}$$

Assumption (A6.1) ensures that there exists controls u_1, \dots, u_r such that y_1, \dots, y_r tend to zero asymptotically. Assumption (A6.2) implies that the number of local actuators is at least as large as the number of local performance measurements (i.e., $m_i \geq \ell_i$). Assumption (A6.3) implies that for all $j \in \mathcal{Q}$, the disturbance frequencies ω_j are known; however, the disturbance amplitudes $d_{c,j}$ and $d_{s,j}$, and the system model (6.1) and (6.2) are completely unknown. Note that assumption (A6.1) implies (A6.2) for the case where $r = 1$ (i.e., centralized control).

For the moment, assume that, $G_{y_i u}$, $G_{y_i d}$, d_c , and d_s are known, and consider the harmonic control

$$u_i(t) = u_{i,c} \cos \omega t + u_{i,s} \sin \omega t, \quad (6.5)$$

where $u_{i,c}$, $u_{i,s} \in \mathbb{R}^{m_i}$ determine the amplitude and phase of each local control u_i . Define $\bar{u}_i \triangleq u_{i,c} - j u_{i,s}$, which is the DFT at frequency ω obtained from a sampling of u_i . In addition, define

$$\bar{u} \triangleq \left[\bar{u}_1^T \quad \cdots \quad \bar{u}_r^T \right]^T \in \mathbb{C}^m.$$

Then, the harmonic steady-state (HSS) performance of (6.1) and (6.2) with disturbance (6.4) and control (6.5) is

$$\begin{aligned} y_{i,\text{hss}}(t, \bar{u}) &\triangleq \text{Re} \left[\left(G_{y_i u}(\mathcal{J}\omega) \bar{u} + G_{y_i d}(\mathcal{J}\omega)(d_c - j d_s) \right) e^{j\omega t} \right] \\ &= \text{Re} (M_{i,*} \bar{u} + d_{i,*}) \cos \omega t - \text{Im} (M_{i,*} \bar{u} + d_{i,*}) \sin \omega t, \end{aligned} \quad (6.6)$$

where

$$d_{i,*} \triangleq G_{y_i d}(\mathcal{J}\omega)(d_c - j d_s) \in \mathbb{C}^{\ell_i}.$$

The HSS performance $y_{i,\text{hss}}$ is the steady-state response of (6.1) and (6.2) with disturbance (6.4) and control (6.5), that is, $\lim_{t \rightarrow \infty} [y_{i,\text{hss}}(t, \bar{u}) - y_i(t)] = 0$ [201, Chap. 12.12]. Define

$$\hat{y}_{i,\text{hss}}(\bar{u}) \triangleq M_{i,*} \bar{u} + d_{i,*}, \quad (6.7)$$

which is the DFT at frequency ω obtained from a sampling of $y_{i,\text{hss}}$. Moreover, define

$$\hat{y}_{\text{hss}}(\bar{u}) \triangleq \left[\hat{y}_{1,\text{hss}}^T(\bar{u}) \quad \cdots \quad \hat{y}_{r,\text{hss}}^T(\bar{u}) \right]^T \in \mathbb{C}^\ell,$$

and it follows from (6.7) that

$$\hat{y}_{\text{hss}}(\bar{u}) = M_* \bar{u} + d_*,$$

where

$$d_* \triangleq \left[d_{1,*}^T \quad \cdots \quad d_{r,*}^T \right]^T \in \mathbb{C}^\ell.$$

Define

$$y_{\text{hss}}(t, \bar{u}) \triangleq \left[y_{1,\text{hss}}^T(t, \bar{u}) \quad \cdots \quad y_{r,\text{hss}}^T(t, \bar{u}) \right]^T \in \mathbb{R}^\ell,$$

and consider the cost function

$$J(\bar{u}) \triangleq \lim_{t \rightarrow \infty} \frac{1}{t} \int_0^t \|y_{\text{hss}}(\tau, \bar{u})\|^2 d\tau, \quad (6.8)$$

which is the average power of y_{hss} . Using (6.6) and (6.7), it follows from (6.8) that

$$\begin{aligned} J(\bar{u}) &= \lim_{t \rightarrow \infty} \frac{1}{t} \int_0^t \|\text{Re } \hat{y}_{\text{hss}}(\bar{u}) \cos \omega \tau - \text{Im } \hat{y}_{\text{hss}}(\bar{u}) \sin \omega \tau\|^2 d\tau \\ &= \begin{bmatrix} \text{Re } \hat{y}_{\text{hss}}(\bar{u}) \\ \text{Im } \hat{y}_{\text{hss}}(\bar{u}) \end{bmatrix}^T \left(\lim_{t \rightarrow \infty} \frac{1}{t} \int_0^t \Omega(\tau) d\tau \right) \begin{bmatrix} \text{Re } \hat{y}_{\text{hss}}(\bar{u}) \\ \text{Im } \hat{y}_{\text{hss}}(\bar{u}) \end{bmatrix} \\ &= \frac{1}{2} \hat{y}_{\text{hss}}^*(\bar{u}) \hat{y}_{\text{hss}}(\bar{u}), \end{aligned}$$

where

$$\Omega(\tau) \triangleq \begin{bmatrix} \cos^2 \omega \tau & -(\cos \omega \tau)(\sin \omega \tau) \\ -(\cos \omega \tau)(\sin \omega \tau) & \sin^2 \omega \tau \end{bmatrix}.$$

The following result provides an expression for a control $\bar{u} = u_*$ that minimizes J . See Theorem 2.1 for details.

Theorem 6.1. Consider the cost function (6.8), and assume that (A6.1) holds. Define $u_* \triangleq -M_*^*(M_*M_*^*)^{-1}d_*$. Then, $\hat{y}_{\text{hss}}(u_*) = 0$, and $J(u_*) = 0$.

Theorem 6.1 provides an expression for a control u_* that minimizes J , but u_* requires knowledge of M_* and d_* .

In this chapter, we consider decentralized sinusoidal controls with frequency ω but where the amplitudes and phases are updated in discrete time. Let $T_s > 0$ be the update period, and for each $k \in \mathbb{N}$, let $u_{i,k} \in \mathbb{C}^m$ contain information regarding the local control amplitude and phase, which is determined from control update equations presented later. Then, for each $k \in \mathbb{N}$ and for all $t \in [kT_s, (k+1)T_s)$, the local control is

$$u_i(t) = \text{Re } u_{i,k} \cos \omega t - \text{Im } u_{i,k} \sin \omega t. \quad (6.9)$$

For each $k \in \mathbb{Z}^+$, let $y_{i,k} \in \mathbb{C}^\ell$ denote the DFT at frequency ω of the sequence obtained by sampling y_i on the interval $[(k-1)T_s, kT_s)$. If T_s is sufficiently large relative to the settling time of G_{y_i} , then for all $k \in \mathbb{N}$, $y_{i,k+1} \approx \hat{y}_{i,\text{hss}}(U_k)$ and $Y_{k+1} \approx \hat{y}_{\text{hss}}(U_k)$, where

$$\begin{aligned} U_k &\triangleq \begin{bmatrix} u_{1,k}^T & \cdots & u_{r,k}^T \end{bmatrix}^T \in \mathbb{C}^m, \\ Y_k &\triangleq \begin{bmatrix} y_{1,k}^T & \cdots & y_{r,k}^T \end{bmatrix}^T \in \mathbb{C}^\ell. \end{aligned}$$

6.4 Decentralized Frequency-Domain Adaptive Harmonic Control

We present decentralized FD-AHC, where each local control u_i does not require any information regarding d_* , M_* , or the nonlocal measurements $\{y_j : j \in \mathcal{R} \setminus \{i\}\}$. For all $k \in \mathbb{N}$, $u_{i,k}$ is given by

$$u_{i,k} \triangleq -M_{i,k}^+ d_{i,k}, \quad (6.10)$$

where $d_{i,k} \in \mathbb{C}^{\ell_i}$ and $M_{i,k} \in \mathbb{C}^{\ell_i \times m_i}$ are adaptive parameters that are determined from update equations presented below.

Consider the cost function $\mathcal{J}_{i,k} : \mathbb{C}^{\ell_i} \times \mathbb{C}^{\ell_i \times m_i} \rightarrow [0, \infty)$ defined by

$$\mathcal{J}_{i,k}(\bar{d}_i, \bar{M}_i) \triangleq \frac{1}{2} \left\| \bar{M}_i u_{i,k} + \bar{d}_i - y_{i,k+1} \right\|^2.$$

Note that $\mathcal{J}_{i,k}$ can be interpreted as a measure of how well $\bar{M}_i u_{i,k} + \bar{d}_i$ approximates the local performance $y_{i,k+1}$, which itself is approximately equal to the HSS performance $\hat{y}_{i,\text{hss}}(U_k) = M_{i,*} U_k + d_{i,*}$.

To determine the update equations, we define the gradients of $\mathcal{J}_{i,k}$ with respect to \bar{d}_i and \bar{M}_i evaluated at $\bar{d}_i = d_{i,k}$ and $\bar{M}_i = M_{i,k}$, which are given by

$$\begin{aligned} \delta_{i,k} &\triangleq \left(\frac{\partial \mathcal{J}_{i,k}}{\partial \bar{d}_i} \bigg|_{(\bar{d}_i, \bar{M}_i) = (d_{i,k}, M_{i,k})} \right)^{\text{T}} \\ &= M_{i,k} u_{i,k} + d_{i,k} - y_{i,k+1}, \end{aligned} \quad (6.11)$$

$$\begin{aligned} \Gamma_{i,k} &\triangleq \left(\frac{\partial \mathcal{J}_{i,k}}{\partial \bar{M}_i} \bigg|_{(\bar{d}_i, \bar{M}_i) = (d_{i,k}, M_{i,k})} \right)^{\text{T}} \\ &= (M_{i,k} u_{i,k} + d_{i,k} - y_{i,k+1}) u_{i,k}^*. \end{aligned} \quad (6.12)$$

Let $d_{i,\text{max}} \in (0, \infty]$ be a known but arbitrarily large upper bound on $\|d_{i,*}\|$. Let $\mu_i > 0$, $\gamma_i > 0$, and $\beta_i \geq 0$. Then, for all $k \in \mathbb{N}$, the update equations are

$$d_{i,k+1} = \begin{cases} \frac{d_{i,\text{max}}}{\|\theta_{i,k+1}\|} \theta_{i,k+1}, & \text{if } \|\theta_{i,k+1}\| > d_{i,\text{max}}, \\ \theta_{i,k+1}, & \text{otherwise,} \end{cases} \quad (6.13)$$

$$M_{i,k+1} = M_{i,k} - \gamma_i \eta_{i,k} \Gamma_{i,k}, \quad (6.14)$$

where

$$\theta_{i,k+1} \triangleq d_{i,k} - \mu_i \eta_{i,k} \delta_{i,k}, \quad (6.15)$$

$$\eta_{i,k} \triangleq \frac{1}{1 + \beta_i \|u_{i,k}\|^2}. \quad (6.16)$$

The initial conditions for (6.14) and (6.15) are $d_{i,0} \in \mathbb{C}^{\ell_i}$ and $M_{i,0} \in \mathbb{C}^{\ell_i \times m_i}$.

Thus, the adaptive controller is given by (6.9)–(6.16). The control architecture is shown in Fig. 6.1. Note that if $d_{i,\text{max}} < \infty$, then (6.13) is an orthogonal projection of the adaptive parameter $d_{i,k}$, which ensures that for all $k \in \mathbb{Z}^+$, $\|d_{i,k}\| \leq d_{i,\text{max}}$. If $d_{i,\text{max}} = \infty$, then there is no projection and $d_{i,k} = \theta_{i,k}$. In addition, note that if $\beta_i > 0$, then $\eta_{i,k}$ provides dynamic normalization for the update equations (6.14) and (6.15). If, on the other hand, $\beta_i = 0$, then for all $k \in \mathbb{N}$, $\eta_{i,k} \equiv 1$, and thus, the dynamic normalization is turned off.

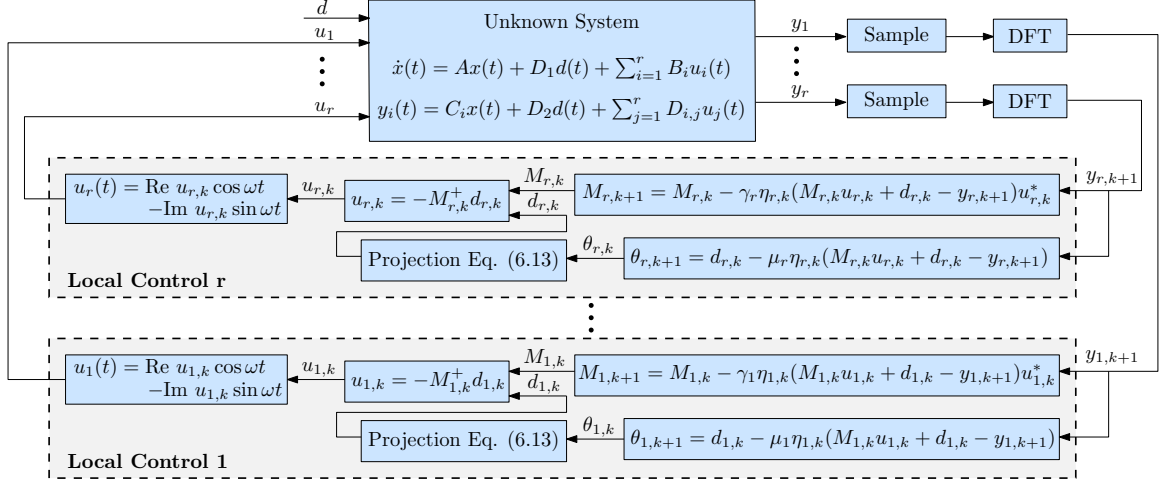


Figure 6.1: Schematic of decentralized FD-AHC with r subsystems, where each local controller has access only to local measurements.

6.5 Stability and Performance Analysis

If T_s is sufficiently large relative to the settling time of $G_{y_i u}$, then the HSS approximation $y_{i,k+1} \approx \hat{y}_{i,\text{hss}}(U_k)$ is valid. To analyze the stability of the closed-loop system, we make the HSS assumption that for all $k \in \mathbb{N}$, $y_{i,k+1} = \hat{y}_{i,\text{hss}}(U_k)$, which combined with (6.7) implies that

$$y_{i,k+1} = M_{i,*} U_k + d_{i,*}. \quad (6.17)$$

Define

$$\mathcal{S} \triangleq \left\{ (P_1, \dots, P_r, Q_1, \dots, Q_r) : P_i \in \mathbb{C}^{\ell_i \times \ell}, Q_i \in \mathbb{C}^{\ell_i \times m_i}, \right. \\ \left. P \triangleq \begin{bmatrix} P_1^T & \dots & P_r^T \end{bmatrix}^T > 0, \|P_i d_{i,*}\| \leq \|d_{i,*}\|, \text{ and } P M_* = \text{diag}(Q_1, \dots, Q_r) \right\}.$$

The following lemma concerns the existence of \mathcal{S} .

Lemma 6.1. Assume (A6.1) holds. Then, \mathcal{S} is nonempty.

The following theorem provides the stability properties of the decentralized closed-loop system (6.10)–(6.17). The proof is in Section 6.8.

Theorem 6.2. Consider the closed-loop system (6.10)–(6.17), where $d_{i,\max} \in [\|d_{i,*}\|, \infty)$, $\beta_i = 0$, and where (A6.1)–(A6.3) are satisfied. Then, there exist $\mu > 0$, and $\gamma > 0$ such that for all $\mu_i \in (0, \mu)$, and all $\gamma_i \in (0, \gamma)$, the following statements hold:

- i) For all $(P_1, \dots, P_r, Q_1, \dots, Q_r) \in \mathcal{S}$, $(d_{1,k}, \dots, d_{r,k}, M_{1,k}, \dots, M_{r,k}) \equiv (P_1 d_*, \dots, P_r d_*, Q_1, \dots, Q_r)$ is a Lyapunov stable equilibrium of (6.10)–(6.17).
- ii) For all $(P_1, \dots, P_r, Q_1, \dots, Q_r) \in \mathcal{S}$, there exists $\rho > 0$ such that for all $d_{i,0} \in \mathbb{B}_\rho(P_i d_*)$, and all $M_{i,0} \in \mathbb{B}_\rho(Q_i)$, $M_{i,k}$ and $u_{i,k}$ are bounded, and $\lim_{k \rightarrow \infty} y_{i,k} = 0$.

iii) Assume that there exists $k_s \in \mathbb{N}$, and $\varepsilon > 0$ such that for all $k \geq k_s$, $\lambda_{\min}(M_{i,k} M_{i,k}^*) > \varepsilon$. Then, for all $d_{i,0} \in \mathbb{C}^{\ell_i}$, and all $M_{i,0} \in \mathbb{C}^{\ell_i \times m_i}$, $M_{i,k}$ and $u_{i,k}$ are bounded, and $\lim_{k \rightarrow \infty} y_{i,k} = 0$.

Part *i*) of Theorem 6.2 provides Lyapunov stability of the equilibria of the closed-loop system (6.10)–(6.17). Part *ii*) guarantees local boundedness of $M_{i,k}$ and $u_{i,k}$, and local convergence of the performance $y_{i,k}$ to zero. Part *iii*) provides a sufficient condition for global boundedness of $M_{i,k}$ and $u_{i,k}$, and global convergence of the performance $y_{i,k}$ to zero. Part *iii*) invokes the assumption that there exist $k_s \in \mathbb{N}$ and $\varepsilon > 0$ such that for all $k \geq k_s$, $\lambda_{\min}(M_{i,k} M_{i,k}^*) > \varepsilon$. This assumption, which implies that $M_{i,k}$ is asymptotically full row rank, cannot be verified *a priori*. However, the assumption $\lambda_{\min}(M_{i,k} M_{i,k}^*) > \varepsilon$, for some arbitrarily small $\varepsilon > 0$, can be verified at each time step. If the condition $\lambda_{\min}(M_{i,k} M_{i,k}^*) > \varepsilon$ is violated on a time step, then $M_{i,k}$ can be perturbed to ensure $\lambda_{\min}(M_{i,k} M_{i,k}^*) > \varepsilon$. However, analyzing the stability of such a perturbation is an open problem. Nevertheless, simulations suggest that for almost all initial conditions $d_{i,0} \in \mathbb{C}^{\ell}$ and $M_{i,0} \in \mathbb{C}^{\ell \times m}$, $M_{i,k}$ is asymptotically full row rank, and thus, satisfies $\lambda_{\min}(M_{i,k} M_{i,k}^*) > \varepsilon$. In this case, part *iii*) states that the performance $y_{i,k}$ globally tends to zero.

Theorem 6.2 relies on the assumption that there exists a known $d_{i,\max} > 0$ such that $d_{i,\max} \geq \|d_{i,*}\|$. In practice, $d_{i,\max}$ can be selected arbitrarily large in order to satisfy $d_{i,\max} \geq \|d_{i,*}\|$.

The following result regards the transient properties of the closed-loop system (6.10)–(6.17). The proof follows from direct calculations.

Theorem 6.3. Consider the closed-loop system (6.10)–(6.17), where $d_{i,\max} = \infty$, $\mu_i = \gamma_i = \gamma$, and $\beta_i > 0$, and where (A6.1)–(A6.3) are satisfied. For all $d_{i,0} \in \mathbb{C}^{\ell_i}$, $M_{i,0} \in \mathbb{C}^{\ell_i \times m_i}$, and all $k \in \{\ell + 1, \ell + 2, \dots\}$, there exist $p_k \in \mathbb{R}[\gamma]$ and $q_k \in \mathbb{R}[\gamma]$ such that $\deg q_k \leq \ell k + k - \ell$, $\deg p_k \leq \ell k$, and

$$\|Y_{k+1}\| = \frac{p_k(\gamma)}{q_k(\gamma)}.$$

Numerical calculations suggest that the upperbound on the degree of the polynomials p_k and q_k , given in the Theorem 6.3, are equal to the degrees of those polynomials (i.e., $\deg q_k = \ell k + k - \ell$, $\deg p_k = \ell k$). In this case, for all $k > \ell$, there exists $c > 0$ such that

$$\|Y_{k+1}\| = c\gamma^{-k+\ell}. \quad (6.18)$$

It follows from (6.18) that if we select $\gamma > 0$ significantly large, then the rate of convergence of the performance Y_k can be improved significantly. Specifically, it follows from (6.18) that for each $k > \ell$ and all $\varepsilon > 0$, there exist $\gamma > 0$ such that $\|Y_{k+1}\| < \varepsilon$.

The following theorem provides the stability properties of the closed-loop system (6.10)–(6.17) with centralized control (i.e., $r = 1$). The proof is similar to proof of Theorem 4.2.

Theorem 6.4. Consider the closed-loop system (6.10)–(6.17), where $r = 1$, $\beta_1 > 0$, $d_{1,\max} = \infty$, and where (A6.1)–(A6.3) are satisfied. Then, for all $\mu_1 > 0$, and $\gamma_1 > 0$, the statements *i)–iii)* of Theorem 6.2 hold.

Theorem 6.4 implies that achieving asymptotic disturbance rejection with a centralized control architecture requires only dynamic normalization (i.e., $\beta_1 > 0$), and does not require projection of the adaptive parameter $d_{1,k}$ (i.e., $d_{1,\max} = \infty$). Moreover, note that Theorem 6.4 does not impose any upper bound on the gains μ_1 , and γ_1 . Using arbitrarily large gains μ_1 and γ_1 can significantly increase the rate of convergence of $y_{1,k}$ to zero.

6.6 Numerical Examples

Consider the 10-mass structure shown in Fig. 6.2, which consists of 10 masses, 11 springs, and 11 dampers. The control forces ψ_1, \dots, ψ_{10} , and the disturbance forces d_1, \dots, d_{10} , are applied to masses $\bar{m}_1, \dots, \bar{m}_{10}$, respectively. The equations of motion are given by (6.1), where

$$x(t) = \left[\xi_1(t) \quad \dot{\xi}_1(t) \quad \cdots \quad \xi_{10}(t) \quad \dot{\xi}_{10}(t) \right]^T,$$

and

$$d(t) = \left[d_1(t) \quad \cdots \quad d_{10}(t) \right]^T.$$

For all $i \in \{1, \dots, 10\}$, the non-zero elements of $A \in \mathbb{R}^{20 \times 20}$ are given by

$$\begin{aligned} A_{(2i,2i-3)} &= \frac{k_i}{\bar{m}_i}, & A_{(2i,2i-2)} &= \frac{c_i}{\bar{m}_i}, \\ A_{(2i,2i-1)} &= \frac{-(k_i + k_{i+1})}{\bar{m}_i}, & A_{(2i,2i)} &= \frac{-(c_i + c_{i+1})}{\bar{m}_i}, \\ A_{(2i,2i+1)} &= \frac{k_{i+1}}{\bar{m}_i}, & A_{(2i,2i+2)} &= \frac{c_{i+1}}{\bar{m}_i}, & A_{(2i-1,2i)} &= 1. \end{aligned}$$

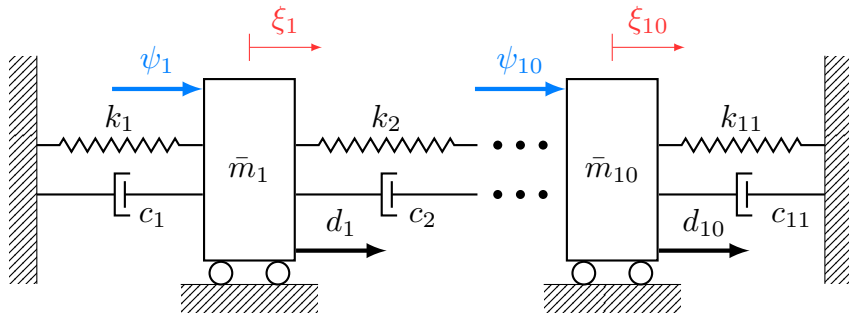


Figure 6.2: The 10-mass structure used in Examples 6.1 and 6.2.

For all $i \in \{1, \dots, 10\}$, we let $\bar{m}_i = 2$ kg, $c_i = 5i + 50$ kg/s, and $k_i = 30i + 250$ N/m. For all $i \in \{1, \dots, 10\}$,

$$d_i = 0.4(2i + 3) \cos \omega_1 t + 0.4(2i + 1) \sin \omega_2 t,$$

is a multi-tone disturbance, where $\omega_1 = 200\pi$ rad/s, and $\omega_2 = 250\pi$ rad/s. The initial conditions are $x(0) = 0$ and $d_{i,0} = 0$. The initial condition $M_{i,0}$, and parameters r , μ_i, γ_i , β_i , and $d_{i,\max}$ are specified in each example. The DFT is performed using a 10 kHz sampling frequency, and the update period is $T_s = 0.04$ s.

Example 6.1. Consider the system (6.1) and (6.2), where A is given by (6.6). Let $r = 10$, which implies $m_i = \ell_i = 1$. We let $u_i = \psi_i$, and $y_i = \xi_i + v_i$, where v_i is a zero-mean 0.001 mm-variance Gaussian white noise. Moreover, we let $\mu_i = \gamma_i = 1.5 \times 10^5$, $\beta_i = 0$, $d_{i,\max} = 10^{10}$, and $M_{i,0} = 10^2$. The control is turned on after 1 s. Figure 6.3 shows y_i and u_i , where decentralized FD-AHC asymptotically rejects the disturbance.

In this case, as shown in Fig. 6.3, the performance y_i is negligible for $t > 3$ s. Therefore, since $T_s = 0.04$ s, and control is turned on at 1 s, Fig. 6.3 implies that for all $k > (3 - 1)/0.04 = 50$, $y_{i,k}$ is negligible. On the other hand, since $\ell = 10$ and $\gamma = 1.5 \times 10^5$, (6.18) suggests that for all $k \geq 12$, $\|Y_{k+1}\|$ is negligible. However, this results does not consider measurement noise, and assumes $\beta_i > 0$. Nevertheless, numerical simulations suggest that if γ_i and μ_i are selected significantly larger than other parameters of the system and the controller, then (6.18) provides a near-exact estimate for the time and rate of convergence of $y_{i,k}$ to 0. \triangle

Example 6.2. We revisit Example 6.1, where the control is centralized. In this case, $r = 1$, which implies $m_1 = m = \ell_1 = \ell = 10$. We let $u_1 = [\psi_1 \dots \psi_{10}]^T$, and $y_1 = [\xi_1 + v_1 \dots \xi_{10} + v_{10}]^T$, where v_i is a zero-mean 0.001 mm-variance Gaussian white noise. We let $\mu_1 = \gamma_1 = 1.5 \times 10^5$, $\beta_1 = 1$, $d_{1,\max} = \infty$, and $M_{1,0} = 10^2 I_{10}$. The control is turned on after 1 s. Figure 6.3 shows $y_1 \in \mathbb{R}^{10}$ and $u_1 \in \mathbb{R}^{10}$, where decentralized FD-AHC asymptotically rejects the disturbance.

In this case, the performance $y_{1(i)}$ is negligible for $t > 3$ s, similar to the performance y_i in Fig. 6.3. Comparing stability properties and convergence time, the centralized control architecture in this case, has no advantages over the decentralized control architecture in Example 6.1. \triangle

6.7 Conclusions

We presented a MIMO decentralized frequency-domain adaptive harmonic controller, which is capable of rejecting known-frequency sinusoidal disturbances that act on a completely unknown asymptotically-stable LTI system. Decentralized FD-AHC consists of multi-input multi-output controllers, where each local controller does not have access to any information regarding the dynamic system, disturbance amplitudes and phases, or nonlocal performance measurements. We analyzed the stability and performance properties of the closed-loop for MIMO systems with as many local

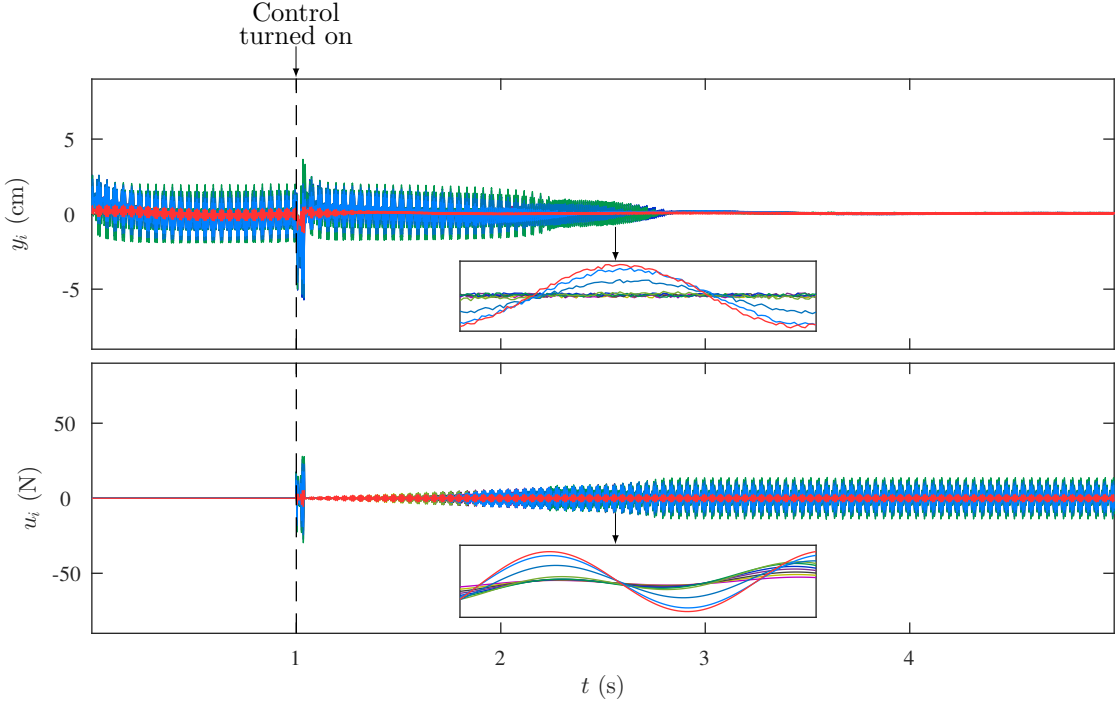


Figure 6.3: For a completely unknown system with several control inputs and several performance measurements subject to measurement noise, where only a decentralized control architecture is feasible, decentralized FD-AHC with $r = 10$ rejects the sinusoidal disturbances asymptotically. The convergence time is approximately as small as the convergence time implied by (6.18).

actuators as performance measurements. We showed that the decentralized control architecture rejects the sinusoidal disturbances asymptotically. We also presented a result that concerns the transient properties of the decentralized controller, and can be utilized to estimate the convergence rate of the closed-loop system. The results imply that convergence rate of decentralized FD-AHC can be improved remarkably by selecting significantly large adaptive gains. We also demonstrated the effectiveness of controller by numerical simulations on a mass-spring-damper system.

6.8 Proof of Theorem 6.2

Proof. Assume (A6.1) holds, and Lemma 6.1 implies that \mathcal{S} exists. Let $(P_1, \dots, P_r, Q_1, \dots, Q_r) \in \mathcal{S}$, and define

$$\tilde{d}_{i,k} \triangleq d_{i,k} - P_i d_*, \quad (6.19)$$

$$\tilde{M}_{i,k} \triangleq M_{i,k} - Q_i. \quad (6.20)$$

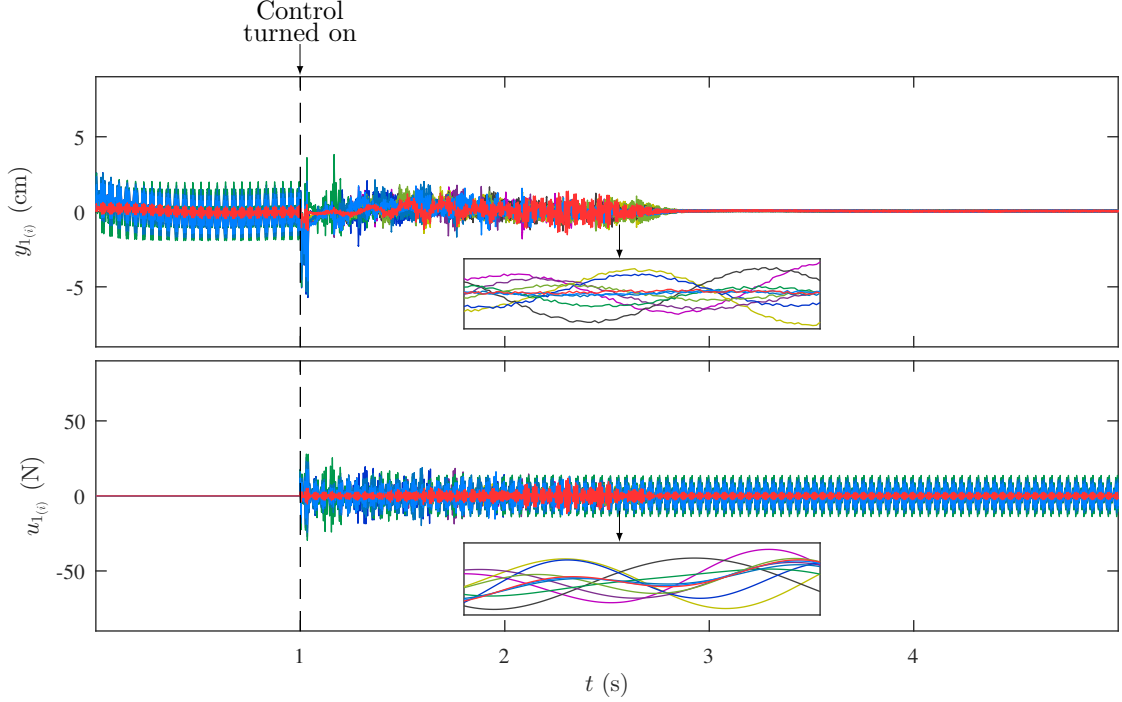


Figure 6.4: For the same unknown system used to obtain Fig. 6.3, but where a centralized control architecture is feasible, decentralized FD-AHC with $r = 1$ rejects the sinusoidal disturbances asymptotically. The convergence time is approximately equal to convergence time of the decentralized control architecture used to obtain Fig. 6.3.

Let $\beta_i = 0$. Subtracting $P_i d_*$ from both sides of (6.13), and substituting (6.11), (6.16), and (6.17) yield

$$\tilde{d}_{i,k+1} = \tilde{\theta}_{i,k+1} + \begin{cases} \left(\frac{d_{i,\max}}{\|\theta_{i,k+1}\|} - 1 \right) \theta_{i,k+1}, & \text{if } \|\theta_{i,k+1}\| > d_{i,\max}, \\ 0 & \text{otherwise,} \end{cases} \quad (6.21)$$

where

$$\tilde{\theta}_{i,k+1} \triangleq \tilde{d}_{i,k} + \mu_i \bar{y}_{i,k+1}, \quad (6.22)$$

and

$$\bar{y}_{i,k+1} \triangleq y_{i,k+1} - M_{i,k} u_{i,k} - d_{i,k}. \quad (6.23)$$

Similarly, subtracting Q_i from both sides of (6.14) and substituting (6.12), (6.16), and (6.17) yield

$$\tilde{M}_{i,k+1} = \tilde{M}_{i,k} + \gamma_i \bar{y}_{i,k+1} u_{i,k}^*. \quad (6.24)$$

Next, define the partial Lyapunov function

$$V_{i,d}(\tilde{d}_{i,k}) \triangleq \|\tilde{d}_{i,k}\|^2, \quad (6.25)$$

and the difference

$$\Delta V_{i,d}(k) \triangleq V_{i,d}(\tilde{d}_{i,k+1}) - V_{i,d}(\tilde{d}_{i,k}). \quad (6.26)$$

Since $\|P_i d_*\| \leq \|d_{i,*}\|$ by definition of \mathfrak{S} , and $\|d_{i,*}\| \leq d_{i,\max}$, it follows from (6.13) that for all $k \in \mathbb{Z}^+$, $\|\tilde{d}_{i,k}\| \leq \|\tilde{\theta}_{i,k}\|$. Thus, evaluating $\Delta V_{i,d}$ along the trajectories of (6.21), and using (6.22) yield

$$\begin{aligned} \Delta V_{i,d}(k) &= \|\tilde{d}_{i,k+1}\|^2 - \|\tilde{d}_{i,k}\|^2 \\ &\leq \|\tilde{\theta}_{i,k+1}\|^2 - \|\tilde{d}_{i,k}\|^2 \\ &= \mu_i^2 \|\bar{y}_{i,k+1}\|^2 + 2\mu_i \tilde{d}_{i,k}^* \bar{y}_{i,k+1}. \end{aligned} \quad (6.27)$$

Define the partial Lyapunov function

$$V_{i,M}(\tilde{M}_{i,k}) \triangleq \|\tilde{M}_{i,k}\|_{\mathbb{F}}^2,$$

and the difference

$$\Delta V_{i,M}(k) \triangleq V_{i,M}(\tilde{M}_{i,k+1}) - V_{i,M}(\tilde{M}_{i,k}).$$

Evaluating $\Delta V_{i,M}$ along the trajectories of (6.24) yields

$$\Delta V_{i,M}(k) = \gamma_i^2 \|u_{i,k}\|^2 \|\bar{y}_{i,k+1}\|^2 + 2\gamma_i u_{i,k}^* \tilde{M}_{i,k}^* \bar{y}_{i,k+1}. \quad (6.28)$$

Next, define the Lyapunov function

$$V(\tilde{d}_{1,k}, \dots, \tilde{d}_{r,k}, \tilde{M}_{1,k}, \dots, \tilde{M}_{r,k}) \triangleq \sum_{i=1}^r \left(\frac{1}{\mu_i} V_{i,d}(\tilde{d}_{i,k}) + \frac{1}{\gamma_i} V_{i,M}(\tilde{M}_{i,k}) \right),$$

and the difference

$$\begin{aligned} \Delta V(k) &\triangleq V(\tilde{d}_{1,k+1}, \dots, \tilde{d}_{r,k+1}, \tilde{M}_{1,k+1}, \dots, \tilde{M}_{r,k+1}) - V(\tilde{d}_{1,k}, \dots, \tilde{d}_{r,k}, \tilde{M}_{1,k}, \dots, \tilde{M}_{r,k}) \\ &= \sum_{i=1}^r \frac{1}{\mu_i} \Delta V_{i,d}(k) + \frac{1}{\gamma_i} \Delta V_{i,M}(k). \end{aligned} \quad (6.29)$$

Substituting (6.27) and (6.28) into (6.29), and using (6.19) and (6.20) yields

$$\begin{aligned} \Delta V(k) &\leq \sum_{i=1}^r \|\bar{y}_{i,k+1}\|^2 (\mu_i + \gamma_i \|u_{i,k}\|^2) + 2(u_{i,k}^* \tilde{M}_{i,k}^* + \tilde{d}_{i,k}^*) \bar{y}_{i,k+1} \\ &= \sum_{i=1}^r \|\bar{y}_{i,k+1}\|^2 (\mu_i + \gamma_i \|u_{i,k}\|^2) + 2[u_k^* (M_k^* - Q^*) + (d_k^* - d_*^* P^*)] \bar{y}_{k+1}, \end{aligned} \quad (6.30)$$

where

$$\begin{aligned} M_k &\triangleq \text{diag}(M_{1,k}, \dots, M_{r,k}) \in \mathbb{C}^{\ell \times m}, \\ Q &\triangleq \text{diag}(Q_1, \dots, Q_r) \in \mathbb{C}^{\ell \times m}, \end{aligned}$$

$$\begin{aligned}
P &\triangleq \begin{bmatrix} P_1^\top & \cdots & P_r^\top \end{bmatrix}^\top \in \mathbb{C}^{\ell \times \ell}, \\
d_k &\triangleq \begin{bmatrix} d_{1,k}^\top & \cdots & d_{r,k}^\top \end{bmatrix}^\top \in \mathbb{C}^\ell, \\
\bar{y}_k &\triangleq \begin{bmatrix} \bar{y}_{1,k}^\top & \cdots & \bar{y}_{r,k}^\top \end{bmatrix}^\top \in \mathbb{C}^\ell.
\end{aligned}$$

Since $(P_1, \dots, P_r, Q_1, \dots, Q_r) \in \mathfrak{S}$, using (6.17) and (6.23), it follows from (6.30) that

$$\Delta V(k) \leq \sum_{i=1}^r \|\bar{y}_{i,k+1}\|^2 (\mu_i + \gamma_i \|u_{i,k}\|^2) - 2[M_k u_k + d_k + P Y_{k+1}]^* \bar{y}_{k+1}. \quad (6.31)$$

To show *iii*), assume (A6.2) holds, and assume that there exists $k_s \in \mathbb{N}$ and $\varepsilon > 0$ such that for all $k \geq k_s$, $\lambda_{\min}(M_{i,k} M_{i,k}^*) > \varepsilon$. Thus, it follows that for all $k \geq k_s$, $M_{i,k} M_{i,k}^+ = I_\ell$. Therefore, (6.10) yields that for all $k \geq k_s$,

$$M_k u_k + d_k = 0, \quad (6.32)$$

which using (6.23) implies that for all $k \geq k_s$,

$$\bar{y}_{i,k+1} = y_{i,k+1}, \quad \bar{y}_{k+1} = Y_{k+1}. \quad (6.33)$$

Substituting (6.32) and (6.33) into (6.31) yields

$$\Delta V(k) \leq \sum_{i=1}^r \|y_{i,k+1}\|^2 (\mu_i + \gamma_i \|u_{i,k}\|^2) - 2\lambda_{\min}(P) \|Y_{k+1}\|^2. \quad (6.34)$$

Since (6.13) implies that for all $k \in \mathbb{Z}^+$, $\|d_{i,k}\| \leq d_{i,\max}$, it follows from (6.10) that

$$\max_{k \in \mathbb{N}} \|u_{i,k}\| < d_{i,\max}/\varepsilon, \quad (6.35)$$

which implies that $u_{i,k}$ is bounded. Using (6.35), it follows from (6.34) that for all $k \geq k_s$,

$$\Delta V(k) \leq \left(\max_{i \in \mathcal{R}} (\mu_i + \gamma_i d_{i,\max}^2 / \varepsilon^2) - 2\lambda_{\min}(P) \right) \|Y_{k+1}\|^2. \quad (6.36)$$

Let $\mu > 0$ and $\gamma > 0$ be such that

$$\max\{\mu, \gamma\} < \frac{2\lambda_{\min}(P)\varepsilon^2}{\varepsilon^2 + \max_{i \in \mathcal{R}} d_{i,\max}}, \quad (6.37)$$

and it follows from (6.36) that for all $\mu_i < \mu$, and all $\gamma_i < \gamma$,

$$\begin{aligned}
\Delta V(k) &\leq \left(\mu + \frac{\gamma}{\varepsilon^2} \max_{i \in \mathcal{R}} d_{i,\max}^2 - 2\lambda_{\min}(P) \right) \|Y_{k+1}\|^2 \\
&\leq -c_0 \|Y_{k+1}\|^2,
\end{aligned} \quad (6.38)$$

where

$$c_0 \triangleq \frac{\max\{\mu, \gamma\}}{\varepsilon^2} \left(\varepsilon^2 + \max_{i \in \mathcal{R}} d_{i, \max}^2 \right) - 2\lambda_{\min}(P) > 0.$$

Thus, it follows from (6.36) that for all $k \geq k_s$, all $\mu_i < \mu$, and all $\gamma_i < \gamma$, $\Delta V(k)$ is nonpositive, which implies that $V(\tilde{d}_{1,k}, \dots, \tilde{d}_{r,k}, \tilde{M}_{1,k}, \dots, \tilde{M}_{r,k})$ is bounded. Since, in addition, V is radially unbounded, it follows that $\tilde{d}_{i,k}$ and $\tilde{M}_{i,k}$ are bounded. Thus, $d_{i,k}$ and $M_{i,k}$ are bounded. Moreover, since $V(\tilde{d}_{1,k}, \dots, \tilde{d}_{r,k}, \tilde{M}_{1,k}, \dots, \tilde{M}_{r,k})$ is positive definite, and for all $k \geq k_s$, $\Delta V(k)$ is nonpositive, it follows from (6.29) and (6.36) that

$$\begin{aligned} 0 &\leq \lim_{k \rightarrow \infty} \sum_{j=k_s}^k c_0 \|Y_{j+1}\| \\ &\leq - \lim_{k \rightarrow \infty} \sum_{j=k_s}^k \Delta V(j) \\ &\leq V(\tilde{d}_{1,k_s}, \dots, \tilde{d}_{r,k_s}, \tilde{M}_{1,k_s}, \dots, \tilde{M}_{r,k_s}) - \lim_{k \rightarrow \infty} V(\tilde{d}_{1,k}, \dots, \tilde{d}_{r,k}, \tilde{M}_{1,k}, \dots, \tilde{M}_{r,k}) \\ &\leq V(\tilde{d}_{1,k_s}, \dots, \tilde{d}_{r,k_s}, \tilde{M}_{1,k_s}, \dots, \tilde{M}_{r,k_s}), \end{aligned}$$

where the upper and lower bounds imply that all the limits exist. Thus, $\lim_{k \rightarrow \infty} Y_k = 0$, which implies $\lim_{k \rightarrow \infty} y_{i,k} = 0$, which confirms *iii*).

To show *i*) and *ii*), note that since (A6.1) holds, Lemma 6.1 implies that there exists $(P_1, \dots, P_r, Q_1, \dots, Q_r) \in \mathcal{S}$. Moreover, since (A6.1) and (A6.2) hold, it follows that $\text{rank } Q_i = \ell_i$. Thus, there exist $\bar{\rho} > 0$ and $\bar{\varepsilon} > 0$ such that for all $M_i \in \mathbb{B}_{\bar{\rho}}(Q_i)$, $\lambda_{\min}(M_i M_i^*) > \bar{\varepsilon}$. Define

$$\mu_m \triangleq \min_{i \in \mathcal{R}} \mu_i, \quad \gamma_m \triangleq \min_{i \in \mathcal{R}} \gamma_i, \quad \gamma_M \triangleq \max_{i \in \mathcal{R}} \gamma_i.$$

Let $\rho \in (0, \bar{\rho} \sqrt{\gamma_m \mu_m / (r \gamma_M (\gamma_m + \mu_m))})$, and let $d_{i,0} \in \mathbb{B}_\rho(P_i d_*)$ and $M_{i,0} \in \mathbb{B}_\rho(Q_i)$. Assume for contradiction that there exists $k_1 \in \mathbb{Z}^+$ and $i_1 \in \mathcal{R}$ such that $\tilde{M}_{i_1, k_1} \notin \mathbb{B}_{\bar{\rho}}(0)$ and for all $k \in \mathcal{K} \triangleq \{0, 1, \dots, k_1 - 1\}$, $\tilde{M}_{i,k} \in \mathbb{B}_{\bar{\rho}}(0)$. Since for all $k \in \mathcal{K}$, $\tilde{M}_{i,k} \in \mathbb{B}_{\bar{\rho}}(0)$, it follows that for all $k \in \mathcal{K}$, $\lambda_{\min}(M_k M_k^T) > \bar{\varepsilon}$. Thus, using the same process as is in (6.32)–(6.36) with ε replaced by $\bar{\varepsilon}$ yields that there exist $\mu > 0$ and $\gamma > 0$ such that for all $\mu_i < \mu$, all $\gamma_i < \gamma$, and all $k \in \mathcal{K}$, $\Delta V(k) \leq 0$. Therefore, it follows from (6.29) that

$$\begin{aligned} 0 &\leq - \sum_{j=0}^{k_1-1} \Delta V(j) \\ &\leq V(\tilde{d}_{1,0}, \dots, \tilde{d}_{r,0}, \tilde{M}_{1,0}, \dots, \tilde{M}_{r,0}) - V(\tilde{d}_{1,k_1}, \dots, \tilde{d}_{r,k_1}, \tilde{M}_{1,k_1}, \dots, \tilde{M}_{r,k_1}) \\ &\leq \sum_{i=1}^r \left(\frac{1}{\mu_i} (\|\tilde{d}_{i,0}\|^2 - \|\tilde{d}_{i,k_1}\|^2) + \frac{1}{\gamma_i} (\|\tilde{M}_{i,0}\|_F^2 - \|\tilde{M}_{i,k_1}\|_F^2) \right) \\ &\leq \sum_{i=1}^r \left(\frac{1}{\mu_i} \|\tilde{d}_{i,0}\|^2 + \frac{1}{\gamma_i} \|\tilde{M}_{i,0}\|_F^2 \right) - \frac{1}{\gamma_{i_1}} \|\tilde{M}_{i_1, k_1}\|_F^2 \end{aligned}$$

$$\begin{aligned}
&\leq \rho^2 \sum_{i=1}^r \left(\frac{1}{\mu_i} + \frac{1}{\gamma_i} \right) - \frac{\bar{\rho}^2}{\gamma_{i_1}} \\
&\leq \frac{r\rho^2(\gamma_m + \mu_m)}{\gamma_m\mu_m} - \frac{\bar{\rho}^2}{\gamma_M} \\
&< \frac{r\gamma_m\mu_m(\gamma_m + \mu_m)\bar{\rho}^2}{r\gamma_m\mu_m(\gamma_m + \mu_m)\gamma_M} - \frac{\bar{\rho}^2}{\gamma_M} \\
&= 0,
\end{aligned}$$

which is a contradiction. Thus, for all $k \in \mathbb{N}$, $M_{i,k} \in \mathbb{B}_{\bar{\rho}}(Q_i)$. Therefore, for all $k \in \mathbb{N}$, $\lambda_{\min}(M_{i,k}M_{i,k}^*) > \bar{\varepsilon}$, and it follows from *iii*) that there exist $\mu > 0$ and $\gamma > 0$ such that for all $\mu_i < \mu$, and all $\gamma_i < \gamma$, $d_{i,k}$, $M_{i,k}$, and $u_{i,k}$ are bounded, and $\lim_{k \rightarrow \infty} y_{i,k} = 0$, which confirms *ii*).

Since for all $k \in \mathbb{N}$, $\lambda_{\min}(M_{i,k}M_{i,k}^*) > \bar{\varepsilon}$, using the same process as is in (6.32)–(6.36) with ε replaced by $\bar{\varepsilon}$, it follows that there exist $\mu > 0$ and $\gamma > 0$ such that for all $\mu_i < \mu$, all $\gamma_i < \gamma$, and all $k \in \mathbb{N}$, $\Delta V(k) \leq 0$. Thus, the equilibrium $(d_{1,k}, \dots, d_{r,k}, M_{1,k}, \dots, M_{r,k}) \equiv (P_1 d_*, \dots, P_r d_*, Q_1, \dots, Q_r)$ is Lyapunov stable, which confirms *i*). \square

Chapter 7

Frequency-Domain Adaptive Higher Harmonic Control with Unknown Disturbance Frequencies

This chapter presents frequency-domain adaptive higher harmonic control (FD-AHHC) algorithm that addresses the problem of rejecting a sinusoidal disturbance with unknown frequency that acts on an unknown multi-input multi-output (MIMO) linear time-invariant system that is asymptotically stable. In fact, this chapter extends the FD-AHHC algorithm presented in Chapter 2 to address disturbances with unknown frequency. For single-input single-output (SISO) systems, we analyze the closed-loop stability and performance of the adaptive controller. In this case, we show that the controller asymptotically rejects disturbances. We demonstrate the controller on numerical simulations of SISO and MIMO acoustic ducts. The result of this chapter appears in [200].

7.1 Introduction

The problem of sinusoidal disturbance rejection arises in a variety of applications, including noise cancellation [32, 33], rotor balancing [20], and vibration suppression for helicopters [10] and spacecraft [59]. For an accurately modeled linear-time invariant (LTI) system acted on by a sinusoidal disturbance with known frequencies, the internal-model principle can be used to design a feedback controller capable of rejecting the disturbance [116, 117, 119]. In this case, copies of the disturbance dynamics are incorporated in the feedback loop in order to achieve asymptotic disturbance rejection. If the disturbance frequencies are unknown or the system model is highly uncertain, then an internal-model controller may result in poor closed-loop performance or even instability [183]. In this case, adaptive methods can be applied to accommodate unknown disturbance frequencies or uncertain system dynamics.

First, consider the case where an accurate model of the system is known, but the frequencies of the sinusoidal disturbance are unknown. This case is related to the problem of estimating the frequency of a sinusoidal signal. Frequency estimation is

addressed with discrete-time adaptive notch filters [173–177] and related continuous-time methods [178–181]. The recent survey [182] provides a comparison of frequency-estimation techniques.

For control, the rejection of unknown-frequency sinusoids can be addressed by combining a frequency estimator with a controller capable of rejecting known-frequency sinusoids (e.g., internal-model control) [183]. Related adaptive control methods (both direct and indirect) for rejection of unknown-frequency sinusoids are presented in [147, 184–187].

Next, consider the case where an accurate model of the system is not available, but the disturbance frequencies are known. If the open-loop dynamics are asymptotically stable, then adaptive feedforward cancellation can be used [129–131]. These approaches use harmonic regressors consisting of sinusoids at the known disturbance frequencies. Adaptive feedforward approaches require certain model information or assumptions regarding the open-loop system. In the single-input single-output (SISO) case, the only model information required is the sign of the control-to-performance transfer function evaluated at the disturbance frequencies. A related approach is in [132]. However, if the system is multi-input multi-output (MIMO), then stronger assumptions (e.g., positive realness) are often invoked for stability analysis.

Another approach to rejecting known-frequency sinusoids relies on an asymptotically stable LTI system’s harmonic steady-state response, that is, the sinusoidal response that remains after the system’s transient response decays to zero. This approach was developed in [10, 20, 32], and is known as convergent control for active rotor balancing [20] and higher harmonic control (HHC) for helicopter vibration suppression [10]. We adopt the name frequency-domain higher harmonic (FD-HHC) for simplicity. FD-HHC require an estimate of the control-to-performance transfer function evaluated at the disturbance frequency. In the SISO case, this estimate, which is a single complex number, must have an angle within 90° of the true value to ensure closed-loop stability. In the MIMO case, closed-loop stability is ensured if the estimate is sufficiently accurate. If there are multiple disturbance frequencies, then estimates are required at each frequency. For certain applications, these estimates can be difficult to obtain or subject to change. To address this uncertainty, adaptive methods have been combined with FD-HHC [81, 157, 158].

Finally, consider the case where both the system model and the disturbance frequencies are unknown. In this case, adaptive feedback (rather than feedforward) control methods are capable of asymptotic disturbance rejection for both LTI systems [140–143, 188–190] and certain classes of nonlinear systems [191, 192]. However, these approaches generally rely on some model information (e.g., relative degree) and structural assumptions regarding the system (e.g., minimum phase, or state feedback). Note that [141] does not require a minimum-phase assumption, but instead relies on estimates of the nonminimum-phase zeros.

In this chapter, we extend FD-AHHC to addresses the problem of rejecting an unknown-frequency sinusoid that acts on an unknown MIMO LTI system that is asymptotically stable but need not be minimum phase. This adaptive harmonic controller requires limited model information, namely, an upper bound on the Frobenius norm of the control-to-performance transfer function evaluated at the disturbance

frequency, and upper and lower bounds on the disturbance frequency. However, all of these bounds can be arbitrarily conservative. The adaptive control in this chapter is related to the FD-AHHC method in Chapter 2, but in contrast to FD-AHHC, this chapter addresses disturbances with unknown frequency. The controller in this chapter is a frequency-domain method, meaning that some computations use discrete Fourier transform (DFT) data rather than time-domain data. The control algorithm (including DFT) is demonstrated on a numerical simulation of an acoustic duct.

7.2 Notation

Let \mathbb{F} be either \mathbb{R} or \mathbb{C} . Let $x_{(i)}$ denote the i th element of $x \in \mathbb{F}^n$. Let $\|\cdot\|$ be the 2-norm on \mathbb{F}^n . Next, let A^* denote the complex conjugate transpose of $A \in \mathbb{F}^{m \times n}$, and define $\|A\|_{\mathbb{F}} \triangleq \sqrt{\text{tr } A^*A}$, which is the Frobenius norm of $A \in \mathbb{F}^{m \times n}$. Define $\mathbb{N} \triangleq \{0, 1, 2, \dots\}$ and $\mathbb{Z}^+ \triangleq \mathbb{N} \setminus \{0\}$.

7.3 Problem Formulation

Consider the LTI system

$$\dot{x}(t) = Ax(t) + Bu(t) + D_1d(t), \quad (7.1)$$

$$y(t) = Cx(t) + Du(t) + D_2d(t), \quad (7.2)$$

where $t \geq 0$, $x(t) \in \mathbb{R}^n$ is the state, $x(0) = x_0 \in \mathbb{R}^n$ is the initial condition, $u(t) \in \mathbb{R}^m$ is the control, $y(t) \in \mathbb{R}^\ell$ is the measured performance, $d(t) \in \mathbb{R}^p$ is the unmeasured disturbance, and $A \in \mathbb{R}^{n \times n}$ is asymptotically stable. Define the transfer functions $G_{yu} : \mathbb{C} \rightarrow \mathbb{C}^{\ell \times m}$ and $G_{yd} : \mathbb{C} \rightarrow \mathbb{C}^{\ell \times p}$ by $G_{yu}(s) \triangleq C(sI - A)^{-1}B + D$ and $G_{yd}(s) \triangleq C(sI - A)^{-1}D_1 + D_2$. Let $\omega_* > 0$, and consider the tonal disturbance

$$d(t) = d_c \cos \omega_* t + d_s \sin \omega_* t, \quad (7.3)$$

where $d_c, d_s \in \mathbb{R}^p$.

The objective is to design a control u that reduces or even eliminates the effect of the disturbance d on the performance y . We make the following assumptions:

$$(A7.1) \quad \text{rank } G_{yu}(j\omega_*) = \min\{\ell, m\}.$$

$$(A7.2) \quad \text{An upper bound } \bar{M} > \|G_{yu}(j\omega_*)\|_{\mathbb{F}} \text{ is known.}$$

$$(A7.3) \quad \text{There exist known } \omega_{\min} > 0 \text{ and } \omega_{\max} > 0 \text{ such that } \omega_* \in [\omega_{\min}, \omega_{\max}].$$

The system (7.1) and (7.2), and the disturbance (7.3) are otherwise unknown.

For the moment, assume that G_{yu} , G_{yd} , ω_* , d_c , and d_s are known. In this case, consider the harmonic control

$$u(t) = \text{Re } \hat{u} \cos \hat{\omega} t - \text{Im } \hat{u} \sin \hat{\omega} t, \quad (7.4)$$

where $\hat{u} \in \mathbb{C}^m$ and $\hat{\omega} > 0$. Note that \hat{u} is the discrete Fourier transform (DFT) at frequency $\hat{\omega}$ obtained from a sampling of u over an integer number of periods. The harmonic steady-state (HSS) performance of (7.1) and (7.2) with control (7.4) is

$$\begin{aligned} y_{\text{hss}}(t, \hat{u}, \hat{\omega}) &\triangleq \operatorname{Re} \left[G_{yu}(j\hat{\omega})\hat{u}e^{j\hat{\omega}t} + d_*e^{j\omega_*t} \right] \\ &= \operatorname{Re} G_{yu}(j\hat{\omega})\hat{u} \cos \hat{\omega}t - \operatorname{Im} G_{yu}(j\hat{\omega})\hat{u} \sin \hat{\omega}t \\ &\quad + \operatorname{Re} d_* \cos \omega_*t - \operatorname{Im} d_* \sin \omega_*t, \end{aligned} \quad (7.5)$$

where $d_* \triangleq G_{yd}(j\omega)(d_c - jd_s) \in \mathbb{C}^\ell$. The HSS performance y_{hss} is the steady-state output y of (7.1) and (7.2) with control (7.4), that is, $\lim_{t \rightarrow \infty} [y_{\text{hss}}(t, \hat{u}, \hat{\omega}) - y(t)] = 0$ [201, Chap. 12.12]. Next, consider the cost function

$$J(\hat{u}, \hat{\omega}) \triangleq \lim_{t \rightarrow \infty} \frac{1}{t} \int_0^t \|y_{\text{hss}}(\tau, \hat{u}, \hat{\omega})\|^2 d\tau, \quad (7.6)$$

which is the average power of y_{hss} . It follows from (7.5) that (7.4) minimizes J only if $\hat{\omega} = \omega_*$. In this case, (7.6) implies that

$$\begin{aligned} J(\hat{u}, \omega_*) &= \lim_{t \rightarrow \infty} \frac{1}{t} \int_0^t \|\operatorname{Re} (M_*\hat{u} + d_*) \cos \omega_*\tau - \operatorname{Im} (M_*\hat{u} + d_*) \sin \omega_*\tau\|^2 d\tau \\ &= \frac{1}{2} \|M_*\hat{u} + d_*\|^2, \end{aligned} \quad (7.7)$$

where $M_* \triangleq G_{yu}(\omega_*)$. Theorem 2.1 provides an expression for a control $\hat{u} = u_*$ that minimizes J , but that control requires knowledge of ω_* , M_* , and d_* . Since these parameters are unknown, we consider a sinusoidal control where the frequency, amplitude, and phase are updated in discrete time.

7.4 FD-AHHC with Unknown Disturbance Frequency

For all $k \in \mathbb{N}$, let $\hat{\omega}_k > 0$ be an estimate of the frequency ω_* , and let $\hat{u}_k \in \mathbb{C}^m$ be an estimate of the control parameter u_* . The estimates $\hat{\omega}_k$ and \hat{u}_k are determined from update equations presented in this section. Let $n_p \in \mathbb{Z}^+ \setminus \{1\}$, and for all $k \in \mathbb{N}$, define $T_k \triangleq 2n_p\pi/\hat{\omega}_k$, which is the update period on step k . Let $t_0 = 0$, and for all $k \in \mathbb{Z}^+$, define $t_k \triangleq \sum_{j=0}^{k-1} T_j$, which is the time of the k th update. Then, for each $k \in \mathbb{N}$ and for all $t \in [t_k, t_{k+1})$, the control is

$$u(t) = \operatorname{Re} \hat{u}_k \cos \hat{\omega}_k t - \operatorname{Im} \hat{u}_k \sin \hat{\omega}_k t. \quad (7.8)$$

Let $N \in \mathbb{Z}^+$ such that $N/n_p \in \mathbb{Z}^+$. For each $k \in \mathbb{N}$, we sample y a total of N times over the interval $[t_k, t_{k+1})$. Specifically, for all $i \in \mathbb{N}$, define the sampled output

$$y_s(i) \triangleq y\left(\frac{iT_{\sigma_i}}{N} + t_{\sigma_i}\right),$$

where σ_i is the largest integer such that $\sigma_i < i/N$. Next, let $n_y \in \{1, 2, \dots, n_p - 1\}$.

For each $k \in \mathbb{N}$, let $y_{k+1} \in \mathbb{C}^\ell$ denote the DFT at $\hat{\omega}_k$ of the sequence $\{y_s(kN + i)\}_{i=N-Nn_y/n_p}^{N-1}$.

For each $k \in \mathbb{N}$ and for all $t \in [t_k, t_{k+1}]$, it follows from (7.5) that the HSS performance is

$$y_{\text{hss}}(t, \hat{u}_k, \hat{\omega}_k) = \text{Re } M_k \hat{u}_k \cos \hat{\omega}_k t - \text{Im } M_k \hat{u}_k \sin \hat{\omega}_k t + d_{\text{hss}}(t),$$

where

$$\begin{aligned} M_k &\triangleq G_{yu}(j\hat{\omega}_k) \in \mathbb{C}^{\ell \times m}, \\ d_{\text{hss}}(t) &\triangleq \text{Re } d_* \cos \omega_* t - \text{Im } d_* \sin \omega_* t. \end{aligned}$$

For each $k \in \mathbb{N}$, define

$$\begin{aligned} d_k &\triangleq \frac{2}{N} \sum_{i=0}^{N-1} \left[\text{Re } d_* \cos 2n_p \pi \omega_* \left(\frac{i}{N\hat{\omega}_k} + \sum_{j=0}^{k-1} \frac{1}{\hat{\omega}_j} \right) - \text{Im } d_* \sin 2n_p \pi \omega_* \left(\frac{i}{N\hat{\omega}_k} + \sum_{j=0}^{k-1} \frac{1}{\hat{\omega}_j} \right) \right] \\ &\quad \times \left(\cos \frac{2n_p \pi i}{N} - j \sin \frac{2n_p \pi i}{N} \right), \end{aligned} \quad (7.9)$$

which is the DFT at $\hat{\omega}_k$ of the sequence $\{d_{\text{hss}}(iT_k/N + t_k)\}_{i=0}^{N-1}$. For each $k \in \mathbb{N}$, define

$$y_{\text{hss},k+1} \triangleq M_k \hat{u}_k + d_k, \quad (7.10)$$

which is the DFT at $\hat{\omega}_k$ of the sequence $\{y_{\text{hss}}(iT_k/N + t_k), \hat{u}_k, \omega_k\}_{i=0}^{N-1}$. The DFT y_{k+1} of the sampled response y_s is an approximation of the DFT $y_{\text{hss},k+1}$ of a sampling of the HSS response $y_{\text{hss}}(t, \hat{u}_k, \hat{\omega}_k)$ on the interval $[t_k, t_{k+1}]$. If T_k is sufficiently large relative to the settling time of G_{yu} , then $y_{k+1} \approx y_{\text{hss},k+1}$. Note that $T_k = 2\pi n_p / \omega_k > 2\pi n_p / \omega_{\text{max}}$. Thus, if the integer n_p is selected sufficiently large, then $y_{k+1} \approx y_{\text{hss},k+1}$.

7.5 Adaptive Law for \hat{u}_k

Let $\mu \in (0, 1]$, $\gamma \in (0, 1]$, $\nu_1 > 0$, $\nu_2 > 0$, and $\hat{u}_0 \in \mathbb{C}^m$. Then, for all $k \in \mathbb{N}$, let

$$\hat{u}_{k+1} = \hat{u}_k - \frac{\mu}{\nu_1 + \|\hat{M}_k\|_{\text{F}}^2} \hat{M}_k^* y_{k+1}, \quad (7.11)$$

where $\hat{M}_k \in \mathbb{C}^{\ell \times m}$ is an estimate of M_* given by

$$\hat{M}_k = \begin{cases} \Theta_k, & \text{if } \|\Theta_k\|_{\text{F}} \leq \bar{M}, \\ \frac{\bar{M}}{\|\Theta_k\|_{\text{F}}} \Theta_k, & \text{otherwise,} \end{cases} \quad (7.12)$$

where

$$\Theta_k = \hat{M}_{k-1} - \eta_k \left[\hat{M}_{k-1} (\hat{u}_k - \hat{u}_{k-1}) - (y_{k+1} - y_k) \right] (\hat{u}_k - \hat{u}_{k-1})^*, \quad (7.13)$$

where $\hat{M}_0 \in \mathbb{C}^{\ell \times m} \setminus \{0\}$, and

$$\eta_k \triangleq \frac{\gamma(\nu_1 + \|\hat{M}_{k-1}\|_{\text{F}}^2)^2}{\nu_2 \mu^2 + (\nu_1 + \|\hat{M}_{k-1}\|_{\text{F}}^2)^2 \|\hat{u}_k - \hat{u}_{k-1}\|^2}. \quad (7.14)$$

The \hat{u}_k -update equation (7.11) is in the direction of the maximum rate of change of the cost function $\mathcal{J}_k(\hat{u}) = \frac{1}{2} \|\hat{M}_k \hat{u} + d_*\|_{\text{F}}^2$ with respect to \hat{u} . Note that $\mathcal{J}_k(\hat{u})$ is an approximation of the average power of y_{hss} , and $\mathcal{J}_k(\hat{u})$ equals the average power of y_{hss} if the estimates $\hat{\omega}_k$ and \hat{M}_k are equal to ω_* and M_* , respectively. Thus, (7.11) can be viewed as a gradient that updates \hat{u}_k in a direction to minimize the current estimate of the average power of y_{hss} . The magnitude of this update (i.e., the gain $\mu/(\nu_1 + \|\hat{M}_k\|_{\text{F}}^2)$) is based on the Lyapunov-like analysis in the next section. See Section 2.5 for more details on the \hat{u}_k -update equation.

The \hat{M}_k -update equations (7.12)–(7.14) are in the direction of the maximum rate of change of the cost function $\mathcal{G}_k(\hat{M}) \triangleq \frac{1}{2} \|\hat{M}(\hat{u}_k - u_{k+1}) - (y_{k+1} - y_k)\|^2$ with respect to \hat{M} . If the estimate $\hat{\omega}_k$ is equal to ω_* , then $\mathcal{G}(M_*) = 0$, that is, M_* minimizes \mathcal{G}_k . Thus, (7.12)–(7.14) can be viewed as a gradient that updates \hat{M}_k in a direction to minimize \mathcal{G}_k based on the current estimate $\hat{\omega}_k$ of ω_* . The step size η_k is based on the Lyapunov-like analysis in the next section. Note that (7.12) is a projection that ensures the estimate \hat{M}_k is bounded. See Section 2.5 for more details on the \hat{M}_k -update equations.

The adaptive parameters are $\mu \in (0, 1]$, $\gamma \in (0, 1]$, $\nu_1 > 0$, and $\nu_2 > 0$. The adaptive gains μ and γ influence the step size of the \hat{u}_k and \hat{M}_k update equations, respectively. The stability analysis in the next section demonstrates that μ and γ can be selected as large as 1. However, numerical testing suggests that smaller gains (e.g., $\mu = 0.2$ and $\gamma = 0.2$) tend to yield better performance. The parameters ν_1 and ν_2 influence the normalization of the \hat{u}_k and \hat{M}_k update equations, respectively. Numerical testing suggests $\nu_1 \ll \|\hat{M}_0\|_{\text{F}}^2$ and $\nu_2 \ll \|\hat{M}_0\|_{\text{F}}^2$ are good choices.

7.6 Adaptive Law for $\hat{\omega}_k$

For each $k \in \mathbb{N}$ and all $i \in \{0, 1, \dots, n_y N/n_p - 1\}$, define

$$\begin{aligned} \hat{d}_k(i) \triangleq & y_s(kN + N - Nn_y/n_p + i) \\ & - \left[\text{Re } y_{k+1} \cos \hat{\omega}_k(iT_k/N + t_k) - \text{Im } y_{k+1} \sin \hat{\omega}_k(iT_k/N + t_k) \right], \end{aligned}$$

which is an estimate of the disturbance sequence $\{d_{\text{hss}}(iT_k/N + t_k)\}_{i=0}^{N-1}$. Let $r_d \in \mathbb{N}$. For all $i \in \{0, 1, \dots, n_y N/n_p - 1\}$ and all $j \in \{0, 1, \dots, r_d\}$, define

$$\hat{D}_k(i + jn_y N/n_p) \triangleq \frac{\hat{d}_k(i)}{\max_i |\hat{d}_k(i)|},$$

which is the sequence $\{\hat{d}_k(i)\}_{i=0}^{Nn_y/n_p-1}$ normalized to amplitude one and repeated r_d times. Define $N_d \triangleq n_y(r_d + 1)N/n_p$. Let $\hat{\omega}_0 \in [\omega_{\min}, \omega_{\max}]$ be the initial estimate

7.7 Stability Analysis

In this section, we analyze the stability of the closed-loop system with adaptive controller. The analysis focuses on SISO systems, that is, $m = \ell = 1$. For analysis, we make the following assumptions:

$$(A7.4) \text{ For all } k \in \mathbb{N}, y_{k+1} = y_{\text{hss},k+1}.$$

$$(A7.5) \text{ There exists } c_\omega > 0, \lambda_\omega \in (0, 1), \text{ and } k_0 \in \mathbb{Z}^+ \text{ such that for all } k \geq k_0, \\ |\hat{\omega}_k - \omega_*| \leq c_\omega \lambda_\omega^{k-k_0}.$$

$$(A7.6) \text{ There exists } \varepsilon > 0 \text{ and } k_s \in \mathbb{N} \text{ such that for all } k > k_s, \hat{M}_k \neq 0.$$

Assumption (A7.4) implies that the DFT y_{k+1} of the sampled response y_s is equal to the DFT $y_{\text{hss},k+1}$ of a sampling of the HSS response $y_{\text{hss}}(t, \hat{u}_k, \hat{\omega}_k)$. As discussed earlier, if T_k is sufficiently large relative to the settling time of G_{yu} , then $y_{k+1} \approx y_{\text{hss},k+1}$. In this analysis, we assume exact equality. Assumption (A7.5) implies that the estimate $\hat{\omega}_k$ converges to ω_* exponentially. The analysis in [174] demonstrates that the adaptive notch filter (7.16)–(7.18) provides an estimate $\hat{\omega}_k$ that converges to ω_* exponentially if the sequence $\{\hat{D}_k(j)\}_{j=0}^{N_d-1}$ is sinusoidal with frequency ω_* and infinitely long (i.e., $N_d = \infty$). Assumption (A7.6) implies that the estimate \hat{M}_k is asymptotically nonzero. In the case where $\hat{\omega} \equiv \omega_*$, the results of Chapter 2 show that (A7.6) is satisfied. The next result provides the asymptotic DFT d_k . The proof is in Section 7.10.

Proposition 7.1. Consider $\{\hat{\omega}_k\}_{k=0}^\infty$, and assume it satisfies (A7.6). Then, $\bar{d} \triangleq \lim_{k \rightarrow \infty} \exp\left(2n\pi j \omega_* \sum_{j=0}^k \frac{1}{\hat{\omega}_j}\right) d_*$ exists and $\lim_{k \rightarrow \infty} d_k = \bar{d}$.

The following result provides the closed-loop stability properties of (7.1), (7.2), (7.8), and (7.11)–(7.18). This is the main analytic result of this chapter. The proof is in Section 7.11.

Theorem 7.1. Consider the open-loop system (7.1) and (7.2), and the controller (7.8) and (7.11)–(7.18), where $\ell = m = 1$, $\mu \in (0, 1]$, $\gamma \in (0, 1]$, $\nu_1 > 0$, $\nu_2 > 0$, $\alpha_k > 0$, and $\beta_k \in (0, \pi/2)$. Assume (A7.1)–(A7.6) are satisfied. Then, $\lim_{k \rightarrow \infty} u_k = -\bar{d}/M_*$ and $\lim_{k \rightarrow \infty} y_k = 0$.

7.8 Numerical Examples

Consider the acoustic duct of length $L = 2$ m shown in Fig. 7.2, where all measurements are from the left end of the duct. A disturbance speaker is at $\xi_d = 0.95$ m, while 2 control speakers are at $\xi_{\psi_1} = 0.4$ m and $\xi_{\psi_2} = 1.25$ m. All speakers have cross-sectional area $A_s = 0.0025$ m². The equation for the acoustic duct is

$$\frac{1}{c^2} \frac{\partial^2 p(\xi, t)}{\partial t^2} = \frac{\partial^2 p(\xi, t)}{\partial \xi^2} + \rho_0 \dot{\psi}_1(t) \delta(\xi - \xi_{\psi_1}) + \rho_0 \dot{\psi}_2(t) \delta(\xi - \xi_{\psi_2}) + \rho_0 \dot{d}(t) \delta(\xi - \xi_d),$$

where $p(\xi, t)$ is the acoustic pressure, δ is the Dirac delta, $c = 343$ m/s is the phase speed of the acoustic wave, ψ_1 and ψ_2 are the speaker cone velocities of the control

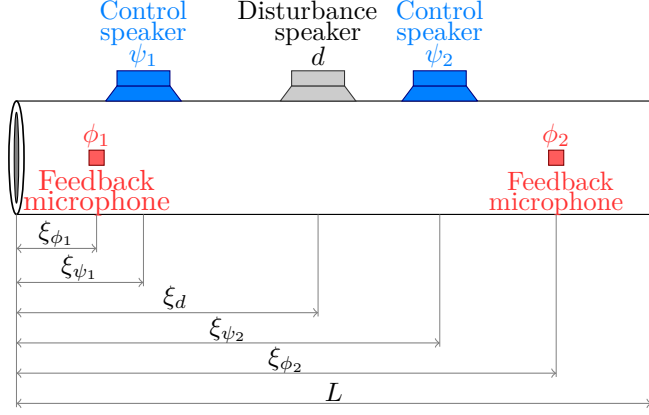


Figure 7.2: The acoustic duct used in Examples 7.1–7.4.

speakers, d is the speaker cone velocity of the disturbance speaker, and $\rho_0 = 1.21 \text{ kg/m}^2$ is the equilibrium density of air at room conditions. See [203] for more details.

Using separation of variables and retaining r modes, the solution $p(\xi, t)$ is approximated by $p(\xi, t) = \sum_{i=0}^r q_i(t)V_i(\xi)$, where for $i = 1, \dots, r$, $V_i(\xi) \triangleq c\sqrt{2/L} \sin i\pi\xi/L$, and q_i satisfies the differential equation (7.1), where

$$\begin{aligned}
 x(t) &= \left[\int_0^t q_1(\sigma) d\sigma \quad q_1(t) \quad \cdots \quad \int_0^t q_r(\sigma) d\sigma \quad q_r(t) \right]^T, \\
 A &= \text{diag} \left(\begin{bmatrix} 0 & 1 \\ -\omega_{n_1}^2 & -2\zeta_1\omega_{n_1} \end{bmatrix}, \dots, \begin{bmatrix} 0 & 1 \\ -\omega_{n_r}^2 & -2\zeta_r\omega_{n_r} \end{bmatrix} \right), \\
 B &= \frac{\rho_0}{A_s} \begin{bmatrix} 0 & V_1(\xi_{\psi_1}) & \cdots & 0 & V_r(\xi_{\psi_1}) \\ 0 & V_1(\xi_{\psi_2}) & \cdots & 0 & V_r(\xi_{\psi_2}) \end{bmatrix}^T, \\
 D_1 &= \frac{\rho_0}{A_s} \begin{bmatrix} 0 & V_1(\xi_d) & \cdots & 0 & V_r(\xi_d) \end{bmatrix}^T,
 \end{aligned}$$

and for $i = 1, \dots, r$, $\omega_{n_i} \triangleq i\pi c/L$ is the natural frequency of the i th mode, and $\zeta_i = 0.2$ is the assumed damping ratio of the i th mode.

Two feedback microphones are in the duct at $\xi_{\phi_1} = 0.3 \text{ m}$ and $\xi_{\phi_2} = 1.7 \text{ m}$, and they measure the acoustic pressures $\phi_1(t) = p(\xi_{\phi_1}, t)$ and $\phi_2(t) = p(\xi_{\phi_2}, t)$, respectively. Thus, for $i = 1, 2$, $\phi_i(t) = C_i x(t)$, where $C_i = \frac{\rho_0}{A_s} [0 \quad V_1(\xi_{\phi_i}) \quad \cdots \quad 0 \quad V_r(\xi_{\phi_i})]$. For all examples, $r = 5$ and $x(0) = 0$. The control parameters are $\mu = \gamma = 0.5$, $\nu_1 = \nu_2 = 0.01$, $n_p = 8$, $n_y = 1$, $N = 1200$, $r_d = 20$, $a_1(0) = b_1(0) = 0$, $\omega_{\min} = 1 \text{ rad/s}$, $\omega_{\max} = 10^4 \text{ rad/s}$, $\hat{\omega}_0 = 200 \text{ rad/s}$, $\hat{u}_0 = 0$, $\bar{M} = 10^6$, and \hat{M}_0 is specified in each example. In addition, $\alpha_k = T_k/N$ and $\beta_k = \min\{1, \hat{\omega}_k/100\}$. The following examples consider the acoustic duct with different control speaker and feedback microphone configurations.

Example 7.1. *SISO with step change to ω_* .* Let $u = \psi_1$, $y = \phi_1$, $\psi_2 = 0$, and $\hat{M}_0 = 0.5e^{j\frac{2\pi}{3}} M_*$. Let $d = \sin \omega_* t + 2 \cos \omega_* t$, where

$$\omega_* = \begin{cases} 600, & \text{if } t \leq 3 \text{ s}, \\ 1200, & \text{if } t > 3 \text{ s}. \end{cases}$$

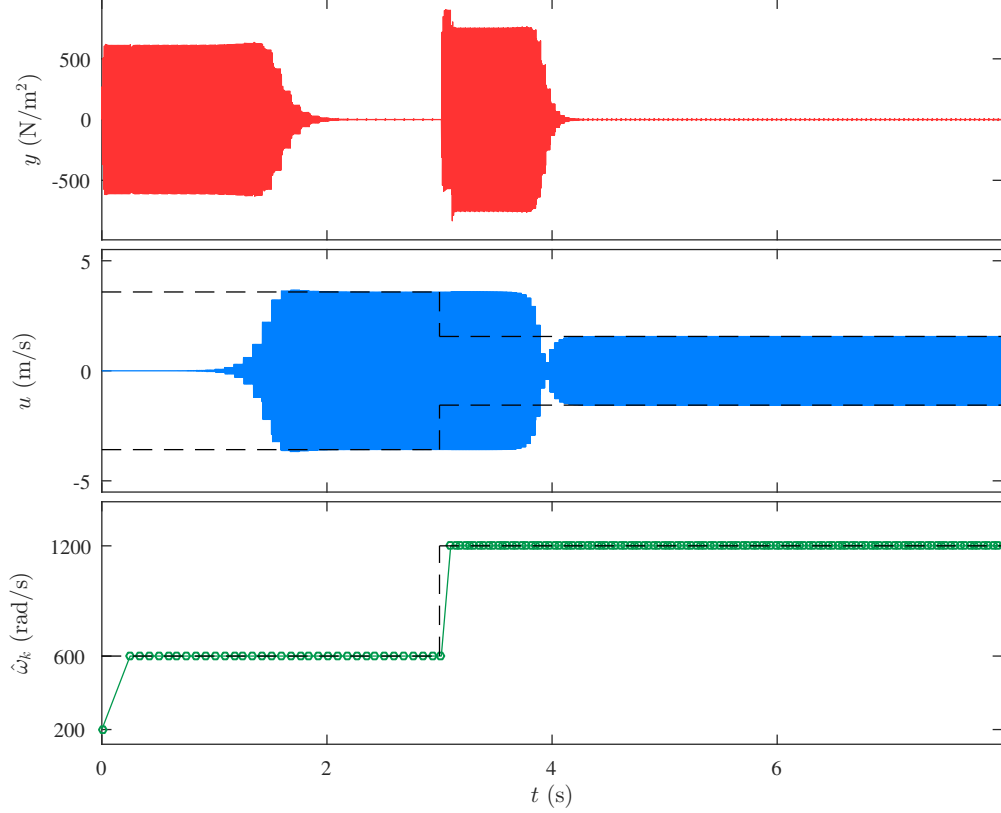


Figure 7.3: For a SISO plant with a step change in frequency, the control is capable of adapting to the change. The dashed lines in the u and $\hat{\omega}_k$ plots show $\pm|u_*|$ and ω_* , respectively.

Fig. 7.3 shows y , u , and $\hat{\omega}_k$. First $\hat{\omega}_k$ approaches 600 rad/s. After ω_* changes, the frequency estimate $\hat{\omega}_k$ converges to 1200 rad/s and the control yields asymptotic disturbance rejection, that is, y converges to 0. \triangle

Example 7.2. *SISO with measurement noise.* Let v be white Gaussian noise with 7 dBW power. We revisit Example 1 where $\omega_* = 600$ rad/s and v is added to the feedback microphone signal as a measurement noise, that is, $y = \phi_1 + v$. Fig. 7.4 shows y , u , and $\hat{\omega}_k$. The frequency estimate $\hat{\omega}_k$ converges to ω_* and the power of y is reduced relative to open loop. \triangle

Example 7.3. *Single-input two-output.* Let $u = \psi_1$, $y = [\phi_1 \ \phi_2]^T$, $\psi_2 = 0$, and $d = \sin 600t + 2 \cos 600t$. Let $\hat{M}_0 = 0.5e^{j\frac{3\pi}{4}} M_*$. Fig. 7.5 shows y , u , and $\hat{\omega}_k$. The frequency estimate $\hat{\omega}_k$ converges to ω_* and the control yields $u_k \rightarrow u_*$ as $k \rightarrow \infty$, which implies $\lim_{k \rightarrow \infty} \|y_k\|$ is minimized. \triangle

Example 7.4. *Two-input two-output.* Let $u = [\psi_1 \ \psi_2]^T$, $y = [\phi_1 \ \phi_2]^T$, and $d = \sin 600t + 2 \cos 600t$. Let $\hat{M}_0 = 0.5e^{j\frac{3\pi}{4}} M_*$. Fig. 7.6 shows y , u , and $\hat{\omega}_k$. The frequency estimate $\hat{\omega}_k$ converges to ω_* and the control yields asymptotic disturbance rejection, that is, y converges to 0. \triangle

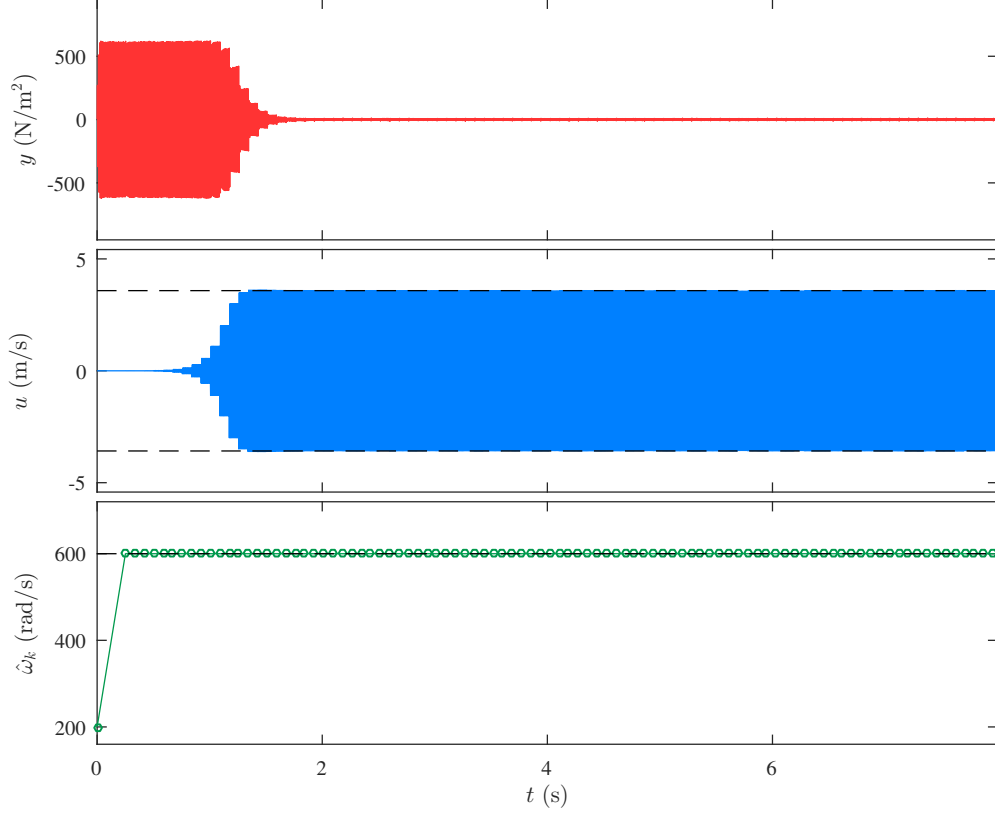


Figure 7.4: For a SISO plant subject to measurement noise, the control reduces the power of y relative to open loop. The dashed lines in the u and $\hat{\omega}_k$ plots show $\pm|u_*|$ and ω_* , respectively.

7.9 Conclusions

This chapter presented a frequency-domain adaptive higher harmonic controller that addresses the problem of rejecting an unknown-frequency sinusoid that acts on an unknown MIMO LTI system. This control combines FD-AHHC algorithm of Chapter 2 with an adaptive notch filter for frequency estimation. For SISO systems, we analyzed the closed-loop stability and performance under simplifying assumptions (A7.4)–(A7.6). Stability analyses without (A7.4)–(A7.6), and for MIMO systems is an open problem.

7.10 Proof of Proposition 7.1

Proof. First, we show $\lim_{k \rightarrow \infty} \cos\left(2n\pi\omega_* \sum_{j=0}^k \frac{1}{\hat{\omega}_j}\right)$ exists. Let $\varepsilon > 0$. Since $\lim_{k \rightarrow \infty} \hat{\omega}_k = \omega_*$, it follows that there exists $s \in \mathbb{N}$ such that

$$\left| \sum_{j=s+1}^{\infty} \frac{1}{\hat{\omega}_j} - \sum_{j=s+1}^{\infty} \frac{1}{\omega_*} \right| < \varepsilon. \quad (7.19)$$

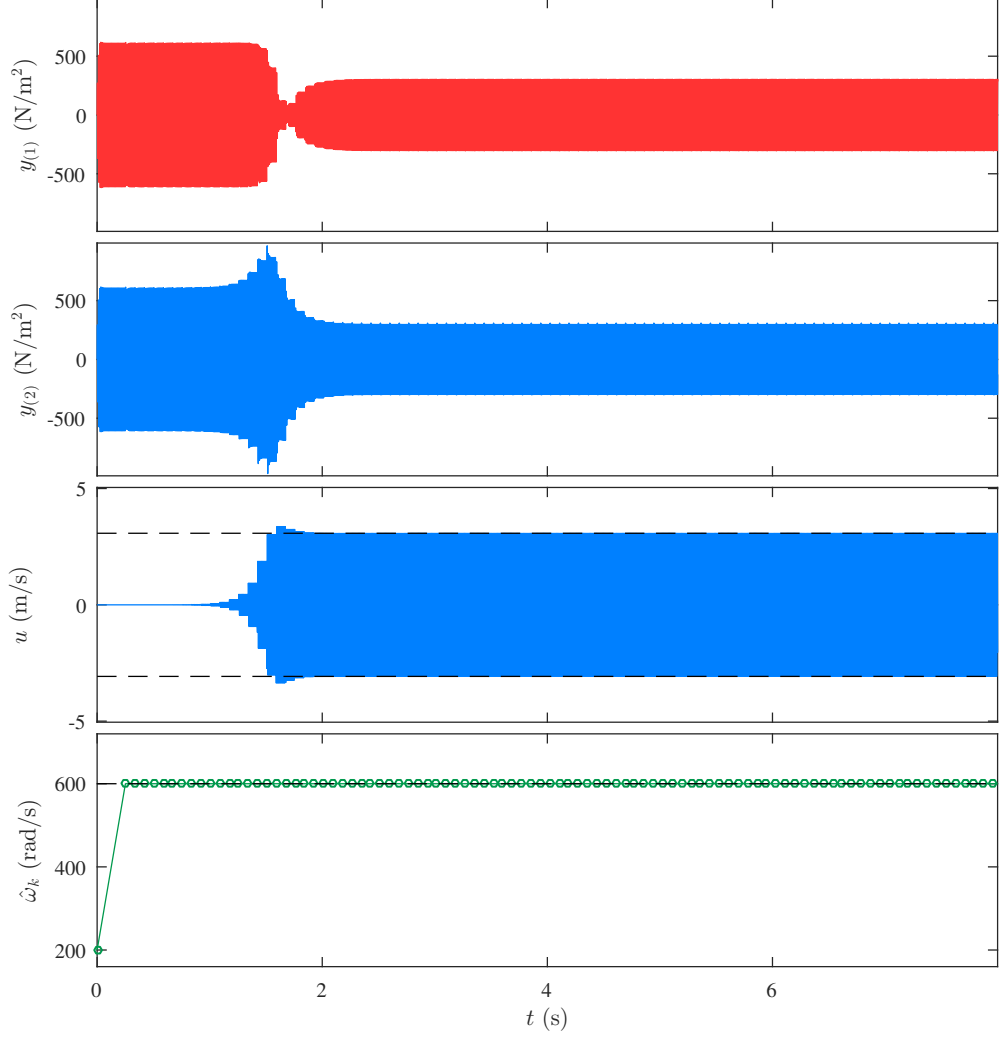


Figure 7.5: For a single-input two-output plant, the control yields $u_k \rightarrow u_*$ as $t \rightarrow \infty$, which minimizes $\lim_{k \rightarrow \infty} \|y_k\|$. The dashed lines in the u and $\hat{\omega}_k$ plots show $\pm|u_*|$ and ω_* , respectively.

Define $S_s \triangleq 2n\pi\omega_* \sum_{j=0}^s \frac{1}{\hat{\omega}_j}$, $S(k) \triangleq 2n\pi\omega_* \sum_{j=0}^k \frac{1}{\hat{\omega}_j}$, $S_{\hat{\omega}}(k) \triangleq 2n\pi\omega_* \sum_{j=s+1}^k \frac{1}{\hat{\omega}_j}$, and $S_{\omega_*}(k) \triangleq 2n\pi\omega_* \sum_{j=s+1}^k \frac{1}{\omega_*}$. It follows from direct calculation that for all $k > s$,

$$\begin{aligned}
|\cos S(k) - \cos S_s| &= |\cos(S_s + S_{\hat{\omega}}(k)) - \cos S_s| \\
&= |\cos(S_s + S_{\omega_*}(k) + S_{\hat{\omega}}(k) - S_{\omega_*}(k)) - \cos S_s| \\
&= |\cos(S_s + S_{\omega_*}(k)) \cos(S_{\hat{\omega}}(k) - S_{\omega_*}(k)) - \sin(S_s + S_{\omega_*}(k)) \sin(S_{\hat{\omega}}(k) - S_{\omega_*}(k))| \\
&= |\cos S_s (\cos(S_{\hat{\omega}}(k) - S_{\omega_*}(k)) - 1) - \sin S_s \sin(S_{\hat{\omega}}(k) - S_{\omega_*}(k))| \\
&\leq |\cos S_s| |\cos(S_{\hat{\omega}}(k) - S_{\omega_*}(k)) - 1| + |\sin S_s| |\sin(S_{\hat{\omega}}(k) - S_{\omega_*}(k))| \\
&\leq |\cos(S_{\hat{\omega}}(k) - S_{\omega_*}(k)) - 1| + |\sin(S_{\hat{\omega}}(k) - S_{\omega_*}(k))|. \tag{7.20}
\end{aligned}$$

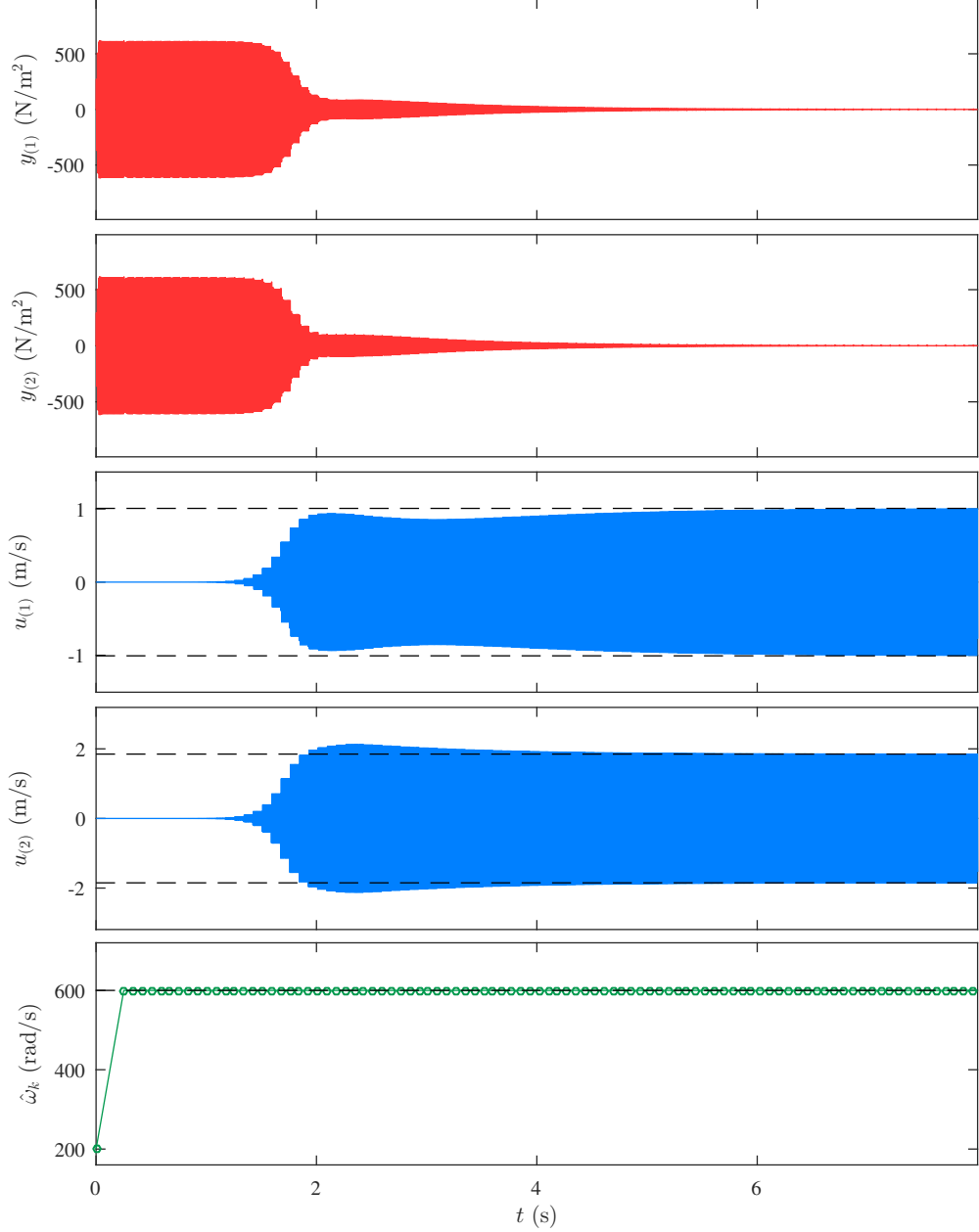


Figure 7.6: Control yields $y(t) \rightarrow 0$ as $t \rightarrow \infty$. The dashed lines in the u and $\hat{\omega}_k$ plots show $\pm|u_*|$ and ω_* , respectively.

Next, using the identities $\cos x = \sum_{j=0}^{\infty} (-1)^j \frac{x^{2j}}{(2j)!}$, $\sin x = \sum_{j=0}^{\infty} (-1)^j \frac{x^{2j+1}}{(2j+1)!}$, and $e^x = \sum_{j=0}^{\infty} \frac{x^j}{j!}$, it follows from (7.20) that

$$\begin{aligned}
 \left| \cos S(k) - \cos S_s \right| &\leq \left| \sum_{j=1}^{\infty} (-1)^j \frac{(S_{\hat{\omega}}(k) - S_{\omega_*}(k))^{2j}}{(2j)!} \right| \\
 &\quad + \left| \sum_{j=0}^{\infty} (-1)^j \frac{(S_{\hat{\omega}}(k) - S_{\omega_*}(k))^{2j+1}}{(2j+1)!} \right|. \tag{7.21}
 \end{aligned}$$

Next, taking limit of both sides of (7.21) as $k \rightarrow \infty$, and using (7.19) implies

$$\begin{aligned} \lim_{k \rightarrow \infty} |\cos S(k) - \cos S_s| &\leq \sum_{j=1}^{\infty} \frac{(2n\pi\omega_*\varepsilon)^{2j}}{(2j)!} + \sum_{j=0}^{\infty} \frac{(2n\pi\omega_*\varepsilon)^{2j+1}}{(2j+1)!} \\ &= \sum_{j=1}^{\infty} \frac{(2n\pi\omega_*\varepsilon)^j}{j!} \\ &= \exp(2n\pi\omega_*\varepsilon) - 1, \end{aligned}$$

which implies $\lim_{k \rightarrow \infty} \cos\left(2n\pi\omega_* \sum_{j=0}^k \frac{1}{\hat{\omega}_j}\right)$ exists, since ε can be arbitrary small. Similarly, we can show that $\lim_{k \rightarrow \infty} \sin\left(2n\pi\omega_* \sum_{j=0}^k \frac{1}{\hat{\omega}_j}\right)$ exists. Thus, it follows that $\bar{d} \triangleq \lim_{k \rightarrow \infty} \exp\left(2n\pi\omega_* \sum_{j=0}^k \frac{1}{\hat{\omega}_j}\right)$ exists.

Next, define $\alpha_k \triangleq \frac{2n\pi}{N} \left(\frac{\omega_*}{\hat{\omega}_k} + 1\right)$ and $\beta_k \triangleq \frac{2n\pi}{N} \left(\frac{\omega_*}{\hat{\omega}_k} - 1\right)$. It follows from (7.9) that

$$\begin{aligned} d_k &= \frac{1}{N} \cos(S_{\hat{\omega}}(k-1)) \sum_{i=0}^{N-1} [\operatorname{Re} d_*(\cos \alpha_k i + \cos \beta_k i) - \operatorname{Im} d_*(\sin \alpha_k i + \sin \beta_k i)] \\ &\quad - \frac{1}{N} \sin(S_{\hat{\omega}}(k-1)) \sum_{i=0}^{N-1} [\operatorname{Im} d_*(\cos \alpha_k i + \cos \beta_k i) + \operatorname{Re} d_*(\sin \alpha_k i + \sin \beta_k i)] \\ &\quad - \frac{j}{N} \cos(S_{\hat{\omega}}(k-1)) \sum_{i=0}^{N-1} [\operatorname{Re} d_*(\sin \alpha_k i - \sin \beta_k i) + \operatorname{Im} d_*(\cos \alpha_k i - \cos \beta_k i)] \\ &\quad + \frac{j}{N} \sin(S_{\hat{\omega}}(k-1)) \sum_{i=0}^{N-1} [\operatorname{Im} d_*(\sin \alpha_k i - \sin \beta_k i) - \operatorname{Re} d_*(\cos \alpha_k i - \cos \beta_k i)]. \quad (7.22) \end{aligned}$$

Since $\lim_{k \rightarrow \infty} \hat{\omega}_k = \omega_*$, it follows that $\lim_{k \rightarrow \infty} \alpha_k = 4n\pi/N$ and $\lim_{k \rightarrow \infty} \beta_k = 0$. Thus, it follows from (7.22) that

$$\begin{aligned} \lim_{k \rightarrow \infty} d_k &= \cos\left(2n\pi\omega_* \sum_{j=0}^{\infty} \frac{1}{\hat{\omega}_j}\right) (\operatorname{Re} d_* + j\operatorname{Im} d_*) + j \sin\left(2n\pi\omega_* \sum_{j=0}^{\infty} \frac{1}{\hat{\omega}_j}\right) (\operatorname{Re} d_* + j\operatorname{Im} d_*) \\ &= \exp\left(2n\pi\omega_* \sum_{j=0}^{\infty} \frac{1}{\hat{\omega}_j}\right) d_* \\ &= \bar{d}. \end{aligned}$$

□

7.11 Proof of Theorem 7.1.

Proof. Multiplying (7.11) by M_k , and using (A7.3) and (7.10) implies that for all $k \in \mathbb{Z}^+$,

$$y_{k+1} = y_k - \frac{\mu}{\nu_1 + |\hat{M}_{k-1}|^2} M_* \hat{M}_{k-1}^* y_k + p_k, \quad (7.23)$$

where

$$p_k \triangleq (M_k - M_{k-1})\hat{u}_{k-1} + d_k - d_{k-1} - \frac{\mu(M_k - M_*)\hat{M}_{k-1}^*y_k}{\nu_1 + |\hat{M}_{k-1}|^2} \in \mathbb{C}^\ell, \quad (7.24)$$

and $y_1 = M_0u_0 + d_0$. It follows from (7.11), (7.23), and (7.13) that

$$\Theta_k = \hat{M}_{k-1} - \frac{\gamma|\hat{M}_{k-1}|^2|y_k|^2(\hat{M}_{k-1} - M_*)}{\nu_2 + |\hat{M}_{k-1}|^2|y_k|^2} + \frac{q_k y_k^* \hat{M}_{k-1}}{(\nu_2 + |\hat{M}_{k-1}|^2|y_k|^2)^{\frac{1}{2}}}, \quad (7.25)$$

where

$$q_k \triangleq -\frac{\gamma(\nu_1 + |\hat{M}_{k-1}|^2)p_k}{\mu(\nu_2 + |\hat{M}_{k-1}|^2|y_k|^2)^{\frac{1}{2}}} \in \mathbb{C}^{\ell \times m}. \quad (7.26)$$

Define $\tilde{M}_k \triangleq \hat{M}_k - M_*$ and $\tilde{\Theta}_k \triangleq \Theta_k - M_*$, and (7.25) implies that

$$\tilde{\Theta}_k = \tilde{M}_{k-1}(1 - \Lambda_k) + \frac{q_k y_k^* \hat{M}_{k-1}}{(\nu_2 + |\hat{M}_{k-1}|^2|y_k|^2)^{\frac{1}{2}}}, \quad (7.27)$$

where $\Lambda_k \triangleq \frac{\gamma|\hat{M}_{k-1}|^2|y_k|^2}{\nu_2 + |\hat{M}_{k-1}|^2|y_k|^2}$.

Define $V_M(\tilde{M}_k) \triangleq |\tilde{M}_k|^2$, and $\Delta V_M(k) \triangleq V_M(\tilde{M}_k) - V_M(\tilde{M}_{k-1})$. It follows from (7.12) that for all $k \in \mathbb{N}$, $|\tilde{M}_k|^2 \leq |\tilde{\Theta}_k|^2$. Thus, calculating $\Delta V_M(k)$ along the trajectories of (7.27) implies that

$$\begin{aligned} \Delta V_M(k) &\leq |\tilde{\Theta}_k|^2 - |\tilde{M}_{k-1}|^2 \\ &= |\tilde{M}_{k-1}|^2(\Lambda_k^2 - 2\Lambda_k) + 2\operatorname{Re} \frac{\hat{M}_{k-1}^* y_k q_k^* \tilde{M}_{k-1}(1 - \Lambda_k)}{(\nu_2 + |\hat{M}_{k-1}|^2|y_k|^2)^{\frac{1}{2}}} + \frac{|\hat{M}_{k-1}|^2|y_k|^2|q_k|^2}{\nu_2 + |\hat{M}_{k-1}|^2|y_k|^2}. \end{aligned} \quad (7.28)$$

Next, note that

$$\begin{aligned} \Lambda_k^2 - 2\Lambda_k &= \frac{\gamma^2|\hat{M}_{k-1}|^4|y_k|^4}{(\nu_2 + |\hat{M}_{k-1}|^2|y_k|^2)^2} - \frac{\gamma|\hat{M}_{k-1}|^2|y_k|^2}{\nu_2 + |\hat{M}_{k-1}|^2|y_k|^2} \\ &\quad - \frac{\gamma|\hat{M}_{k-1}|^2|y_k|^2(\nu_2 + |\hat{M}_{k-1}|^2|y_k|^2)}{(\nu_2 + |\hat{M}_{k-1}|^2|y_k|^2)^2} \\ &= \frac{(\gamma^2 - \gamma)|\hat{M}_{k-1}|^4|y_k|^4}{(\nu_2 + |\hat{M}_{k-1}|^2|y_k|^2)^2} - \frac{\gamma|\hat{M}_{k-1}|^2|y_k|^2}{\nu_2 + |\hat{M}_{k-1}|^2|y_k|^2} - \frac{\gamma\nu_2|\hat{M}_{k-1}|^2|y_k|^2}{(\nu_2 + |\hat{M}_{k-1}|^2|y_k|^2)^2} \\ &\leq -\Lambda_k \left(1 + \frac{\nu_2}{\nu_2 + |\hat{M}_{k-1}|^2|y_k|^2} \right). \end{aligned} \quad (7.29)$$

Let $\varepsilon_M > 0$ and it follows that

$$\begin{aligned} 0 &\leq \left| \frac{q_k}{\varepsilon_M} - \varepsilon_M \frac{\hat{M}_{k-1}^* y_k \tilde{M}_{k-1} (1 - \Lambda_k)}{(\nu_2 + |\hat{M}_{k-1}|^2 |y_k|^2)^{\frac{1}{2}}} \right|^2 \\ &= \frac{|q_k|^2}{\varepsilon_M^2} - 2\operatorname{Re} \frac{\hat{M}_{k-1}^* y_k \tilde{M}_{k-1} (1 - \Lambda_k) q_k^*}{(\nu_2 + |\hat{M}_{k-1}|^2 |y_k|^2)^{\frac{1}{2}}} + \frac{\varepsilon_M^2 |\hat{M}_{k-1}|^2 |y_k|^2 |\tilde{M}_{k-1}|^2 (1 - \Lambda_k)^2}{\nu_2 + |\hat{M}_{k-1}|^2 |y_k|^2}, \end{aligned}$$

which implies

$$\begin{aligned} 2\operatorname{Re} \frac{\hat{M}_{k-1}^* y_k \tilde{M}_{k-1} (1 - \Lambda_k) q_k^*}{(\nu_2 + |\hat{M}_{k-1}|^2 |y_k|^2)^{\frac{1}{2}}} &\leq \frac{|q_k|^2}{\varepsilon_M^2} + \frac{\varepsilon_M^2 |\hat{M}_{k-1}|^2 |y_k|^2 |\tilde{M}_{k-1}|^2 (1 - \Lambda_k)^2}{\nu_2 + |\hat{M}_{k-1}|^2 |y_k|^2} \\ &= \frac{|q_k|^2}{\varepsilon_M^2} + \frac{\varepsilon_M^2 |\hat{M}_{k-1}|^2 |y_k|^2 |\tilde{M}_{k-1}|^2}{\nu_2 + |\hat{M}_{k-1}|^2 |y_k|^2} \\ &\quad \times \left(\frac{\nu_2 + (1 - \gamma) |\hat{M}_{k-1}|^2 |y_k|^2}{\nu_2 + |\hat{M}_{k-1}|^2 |y_k|^2} \right)^2 \\ &\leq \frac{|q_k|^2}{\varepsilon_M^2} + \frac{2\varepsilon_M^2 \nu_2^2 |\hat{M}_{k-1}|^2 |y_k|^2 |\tilde{M}_{k-1}|^2}{(\nu_2 + |\hat{M}_{k-1}|^2 |y_k|^2)^3} \\ &\quad + \frac{2\varepsilon_M^2 (1 - \gamma)^2 |\hat{M}_{k-1}|^6 |y_k|^6 |\tilde{M}_{k-1}|^2}{(\nu_2 + |\hat{M}_{k-1}|^2 |y_k|^2)^3} \\ &\leq \frac{|q_k|^2}{\varepsilon_M^2} + \frac{2\varepsilon_M^2 \nu_2 |\hat{M}_{k-1}|^2 |y_k|^2 |\tilde{M}_{k-1}|^2}{(\nu_2 + |\hat{M}_{k-1}|^2 |y_k|^2)^2} \\ &\quad + \frac{2\varepsilon_M^2 (1 - \gamma)^2 |\hat{M}_{k-1}|^2 |y_k|^2 |\tilde{M}_{k-1}|^2}{\nu_2 + |\hat{M}_{k-1}|^2 |y_k|^2}. \end{aligned} \quad (7.30)$$

Thus, using (7.29) and (7.30), and letting $\varepsilon_M \triangleq \frac{\sqrt{2\gamma}}{2}$, it follows from (7.28) that

$$\begin{aligned} \Delta V_M(k) &\leq - \left[\Lambda_k + \frac{\nu_2 \Lambda_k}{\nu_2 + |\hat{M}_{k-1}|^2 |y_k|^2} - \frac{2\varepsilon_M^2 \nu_2 \Lambda_k}{\gamma (\nu_2 + |\hat{M}_{k-1}|^2 |y_k|^2)} - \frac{2\varepsilon_M^2 (1 - \gamma)^2 \Lambda_k}{\gamma} \right] \\ &\quad \times |\tilde{M}_{k-1}|^2 + \left(\frac{1}{\varepsilon_M^2} + \frac{|\hat{M}_{k-1}|^2 |y_k|^2}{\nu_2 + |\hat{M}_{k-1}|^2 |y_k|^2} \right) |q_k|^2 \\ &\leq -\gamma \Lambda_k |\tilde{M}_{k-1}|^2 + \left(\frac{2 + \gamma}{\gamma} \right) |q_k|^2. \end{aligned} \quad (7.31)$$

Next, define $V_y(y_k) \triangleq |y_k|^2$ and $\Delta V_y(k) \triangleq V_y(y_{k+1}) - V_y(y_k)$. Evaluating ΔV_y along the trajectories of (7.23) yields

$$\Delta V_y(k) = |y_k|^2 \left(\frac{\mu^2 |M_*|^2 |\hat{M}_{k-1}^*|^2}{(\nu_1 + |\hat{M}_{k-1}|^2)^2} - \frac{2\mu \operatorname{Re} (M_* \hat{M}_{k-1}^*)}{\nu_1 + |\hat{M}_{k-1}|^2} \right)$$

$$+ 2\operatorname{Re} p_k^* \left(1 - \frac{\mu M_* \hat{M}_{k-1}^*}{\nu_1 + |\hat{M}_{k-1}|^2} \right) y_k + |p_k|^2. \quad (7.32)$$

Next, note that

$$-2\operatorname{Re} (M_* \hat{M}_{k-1}^*) = |\tilde{M}_{k-1}|^2 - |M_*|^2 - |\hat{M}_{k-1}|^2. \quad (7.33)$$

Let $\varepsilon_y > 0$ and it follows that

$$\begin{aligned} 0 &\leq \left| \frac{p_k}{\varepsilon_y} - \varepsilon_y \left(1 - \frac{\mu M_* \hat{M}_{k-1}^*}{\nu_1 + |\hat{M}_{k-1}|^2} \right) y_k \right|^2 \\ &= \frac{|p_k|^2}{\varepsilon_y^2} - 2\operatorname{Re} p_k^* \left(1 - \frac{\mu M_* \hat{M}_{k-1}^*}{\nu_1 + |\hat{M}_{k-1}|^2} \right) y_k \\ &\quad + \varepsilon_y^2 |y_k|^2 \left(1 + \frac{\mu^2 |M_*|^2 |\hat{M}_{k-1}^*|^2}{(\nu_1 + |\hat{M}_{k-1}|^2)^2} - \frac{2\mu \operatorname{Re} (M_* \hat{M}_{k-1}^*)}{\nu_1 + |\hat{M}_{k-1}|^2} \right), \end{aligned}$$

which implies

$$\begin{aligned} 2\operatorname{Re} p_k^* \left(1 - \frac{\mu M_* \hat{M}_{k-1}^*}{\nu_1 + |\hat{M}_{k-1}|^2} \right) y_k &\leq \frac{|p_k|^2}{\varepsilon_y^2} + \varepsilon_y^2 |y_k|^2 \\ &\quad \times \left(1 + \frac{\mu^2 |M_*|^2 |\hat{M}_{k-1}^*|^2}{(\nu_1 + |\hat{M}_{k-1}|^2)^2} - \frac{2\mu \operatorname{Re} (M_* \hat{M}_{k-1}^*)}{\nu_1 + |\hat{M}_{k-1}|^2} \right) \end{aligned} \quad (7.34)$$

Thus, using (7.33) and (7.34), it follows from (7.32) that

$$\begin{aligned} \Delta V_y(k) &\leq |y_k|^2 \left(\varepsilon_y^2 + (1 + \varepsilon_y^2) \frac{\mu^2 |M_*|^2 |\hat{M}_{k-1}^*|^2}{(\nu_1 + |\hat{M}_{k-1}|^2)^2} \right. \\ &\quad \left. + \mu (1 + \varepsilon_y^2) \frac{|\tilde{M}_{k-1}|^2 - |M_{k-1}|^2 - |M_*|^2}{\nu_1 + |\hat{M}_{k-1}|^2} \right) + \left(1 + \frac{1}{\varepsilon_y^2} \right) |p_k|^2. \end{aligned} \quad (7.35)$$

Define the Lyapunov function $V(y_k, \tilde{M}_{k-1}) \triangleq \ln(1 + aV_y(y_k)) + bV_M(\tilde{M}_{k-1})$, where $a, b > 0$ are provided later, and define the Lyapunov difference

$$\Delta V(k) \triangleq V(y_{k+1}, \tilde{M}_k) - V(y_k, \tilde{M}_{k-1}). \quad (7.36)$$

Evaluating $\Delta V(k)$ along the trajectories of (7.23) and (7.27) yields

$$\begin{aligned} \Delta V(k) &= \ln[1 + a(V_y(y_k) + \Delta V_y(k))] - \ln[1 + aV_y(y_k)] + b\Delta V_M(k) \\ &= \ln \left(1 + \frac{a\Delta V_y(k)}{1 + aV_y(y_k)} \right) + b\Delta V_M(k). \end{aligned} \quad (7.37)$$

Since for all $x > 0$, $\ln x \leq x - 1$, (7.37) implies that

$$\Delta V(k) \leq \frac{a\Delta V_y(k)}{1 + aV_y(y_k)} + b\Delta V_M(k),$$

which using (7.31) and (7.35) yields

$$\begin{aligned} \Delta V(k) &\leq \frac{-a\mu(1 + \varepsilon_y^2)|y_k|^2}{(1 + a|y_k|^2)(\nu_1 + |\hat{M}_{k-1}|^2)} \left(|M_*|^2 + |\hat{M}_{k-1}|^2 - \frac{\mu|M_*|^2|\hat{M}_{k-1}|^2}{\nu_1 + |\hat{M}_{k-1}|^2} \right) \\ &\quad - \frac{b\gamma^2|\hat{M}_{k-1}|^2|y_k|^2|\tilde{M}_{k-1}|^2}{\nu_2 + |\hat{M}_{k-1}|^2|y_k|^2} + \frac{a\mu|y_k|^2(1 + \varepsilon_y^2)|\tilde{M}_{k-1}|^2}{(1 + a|y_k|^2)(\nu_1 + |\hat{M}_{k-1}|^2)} + \frac{a\varepsilon_y^2|y_k|^2}{1 + a|y_k|^2} \\ &\quad + \frac{a\left(1 + \frac{1}{\varepsilon_y^2}\right)|p_k|^2}{1 + a|y_k|^2} + \left(\frac{2 + \gamma}{\gamma}\right)|q_k|^2. \end{aligned} \quad (7.38)$$

Let $a \triangleq \frac{\bar{M}^2}{\nu_2}$, $b \triangleq \frac{\mu\bar{M}^2(1 + \varepsilon_y^2)}{\nu_1\varepsilon_y^2\gamma^2}$, and $\varepsilon_y \triangleq \sqrt{\frac{\nu_1\mu|M_*|^2}{\nu_1 + \bar{M}^2}}$. Then, since $\mu \in (0, 1]$ and (A7.6) is satisfied, it follows from (7.12) that for all $k > k_s$, $\varepsilon < |\hat{M}_k| < \bar{M}$. Thus, it follows from (7.38) that for all $k > k_s$,

$$\begin{aligned} \Delta V(k) &\leq \frac{-\nu_1\mu\bar{M}^2(1 + \varepsilon_y^2)|y_k|^2|M_*|^2}{(\nu_2 + \bar{M}^2|y_k|^2)(\nu_1 + \bar{M}^2)^2} - \frac{b\gamma^2(2 - \gamma)\varepsilon^2|y_k|^2|\tilde{M}_{k-1}|^2}{\nu_2 + \bar{M}^2|y_k|^2} \\ &\quad + \frac{\mu\bar{M}^2(1 + \varepsilon_y^2)|y_k|^2|\tilde{M}_{k-1}|^2}{\nu_1(\nu_2 + \bar{M}^2|y_k|^2)} + \frac{\bar{M}^2\varepsilon_y^2|y_k|^2}{\nu_2 + \bar{M}^2|y_k|^2} \\ &\quad + \frac{\bar{M}^2\left(1 + \frac{1}{\varepsilon_y^2}\right)|p_k|^2}{\nu_2 + \bar{M}^2|y_k|^2} + \left(\frac{2 + \gamma}{\gamma}\right)|q_k|^2 \\ &\leq \frac{-c_1|y_k|^2}{\nu_2 + \bar{M}^2|y_k|^2} + \frac{\bar{M}^2(1 + \varepsilon_y^2)|p_k|^2}{\varepsilon_y^2(\nu_2 + \bar{M}^2|y_k|^2)} + \left(\frac{2 + \gamma}{\gamma}\right)|q_k|^2, \end{aligned} \quad (7.39)$$

where $c_1 \triangleq \frac{\nu_1\mu\bar{M}^2\varepsilon_y^2|M_*|^2}{(\nu_1 + \bar{M}^2)^2}$. Next, note that since $M_* \neq 0$ and $\hat{\omega}_k \rightarrow \omega_*$ as $k \rightarrow \infty$, it follows that there exists $k_2 \in \mathbb{N}$ such that for all $k > k_2$, $M_{k-1} \neq 0$. Thus, it follows from (A7.3) and (7.10) that for all $k > k_2$, $u_{k-1} = \frac{y_k - d_{k-1}}{M_{k-1}}$, which together with (7.24) implies

$$p_k = \left(\frac{M_k}{M_{k-1}} - 1\right)y_k + d_k - \frac{M_k}{M_{k-1}}d_{k-1} - \frac{\mu(M_k - M_*)\hat{M}_{k-1}^*y_k}{\nu_1 + |\hat{M}_{k-1}|^2},$$

which using the identity $|a + b + c|^2 \leq 3(|a|^2 + |b|^2 + |c|^2)$ yields

$$|p_k|^2 = \left| \left(\frac{M_k}{M_{k-1}} - 1\right)y_k + d_k - \frac{M_k}{M_{k-1}}d_{k-1} - \frac{\mu(M_k - M_*)\hat{M}_{k-1}^*y_k}{\nu_1 + |\hat{M}_{k-1}|^2} \right|^2$$

$$\leq 3 \left(\left| \frac{M_k}{M_{k-1}} - 1 \right|^2 |y_k|^2 + \left| d_k - \frac{M_k}{M_{k-1}} d_{k-1} \right|^2 + \frac{\mu^2 |M_k - M_*|^2 |\hat{M}_{k-1}|^2 |y_k|^2}{(\nu_1 + |\hat{M}_{k-1}|^2)^2} \right). \quad (7.40)$$

Thus, using (7.26) and (7.40), and noting that for all $k \in \mathbb{N}$, $\hat{M}_k \leq \bar{M}$, it follows from (7.39) that for all $k > \max\{k_2, k_s\}$

$$\begin{aligned} \Delta V(k) &\leq \frac{-c_1 |y_k|^2}{\nu_2 + \bar{M}^2 |y_k|^2} + \left(\frac{\bar{M}^2 (1 + \varepsilon_y^2)}{\varepsilon_y^2 (\nu_2 + \bar{M}^2 |y_k|^2)} + \left(\frac{2 + \gamma}{\gamma} \right) \left(\frac{\gamma^2 (\nu_1 + |\hat{M}_{k-1}|^2)^2}{\mu^2 (\nu_2 + |\hat{M}_{k-1}|^2 |y_k|^2)} \right) \right) \\ &\quad \times 3 \left(\left| \frac{M_k}{M_{k-1}} - 1 \right|^2 |y_k|^2 + \left| d_k - \frac{M_k}{M_{k-1}} d_{k-1} \right|^2 + \frac{\mu^2 |M_k - M_*|^2 |\hat{M}_{k-1}|^2 |y_k|^2}{(\nu_1 + |\hat{M}_{k-1}|^2)^2} \right) \\ &\leq \frac{-c_1 |y_k|^2}{\nu_2 + \bar{M}^2 |y_k|^2} + \frac{\mu^2 \bar{M}^2 (1 + \varepsilon_y^2) + \gamma \varepsilon_y^2 (2 + \gamma) (\nu_1 + \bar{M}^2)^2}{\mu^2 \varepsilon_y^2 (\nu_2 + \bar{M}^2 |y_k|^2)} \\ &\quad \times 3 \left(\left| \frac{M_k}{M_{k-1}} - 1 \right|^2 |y_k|^2 + \left| d_k - \frac{M_k}{M_{k-1}} d_{k-1} \right|^2 + \frac{\mu^2 \bar{M}^2 |M_k - M_*|^2 |y_k|^2}{\nu_1^2} \right) \\ &\leq \frac{-c_1 |y_k|^2}{\nu_2 + \bar{M}^2 |y_k|^2} + c_2 \left| \frac{M_k}{M_{k-1}} - 1 \right|^2 + c_3 \left| d_k - \frac{M_k}{M_{k-1}} d_{k-1} \right|^2 + c_4 |M_k - M_*|^2, \end{aligned} \quad (7.41)$$

where $c_2 \triangleq \frac{3(\mu^2 \bar{M}^2 (1 + \varepsilon_y^2) + \gamma \varepsilon_y^2 (2 + \gamma) (\nu_1 + \bar{M}^2)^2)}{\mu^2 \varepsilon_y^2 \bar{M}^2}$, $c_3 \triangleq \frac{c_2 \bar{M}^2}{\nu_2}$, and $c_4 \triangleq \frac{c_2 \mu^2 \bar{M}^2}{\nu_1^2}$. Since V is positive definite, it follows from (7.36), (7.41) and Lemma 7.1 in Section 7.12 that there exists $k_1 > \max\{k_2, k_s\}$ such that

$$\begin{aligned} 0 &\leq \sum_{i=k_1}^{\infty} \frac{c_1 |y_i|^2}{\nu_2 + \bar{M}^2 |y_i|^2} \\ &\leq \sum_{k=k_1}^{\infty} \left(c_2 \left| \frac{M_i}{M_{i-1}} - 1 \right|^2 + c_3 \left| d_i - \frac{M_i}{M_{i-1}} d_{i-1} \right|^2 + c_4 |M_i - M_*|^2 - \Delta V(i) \right) \\ &\leq \sum_{k=k_1}^{\infty} \left(c_2 \left| \frac{M_i}{M_{i-1}} - 1 \right|^2 + c_3 \left| d_i - \frac{M_i}{M_{i-1}} d_{i-1} \right|^2 + c_4 |M_i - M_*|^2 \right) \\ &\quad + V(y_{k_1}, \tilde{M}_{k_1-1}) - \lim_{k \rightarrow \infty} V(y_k, \tilde{M}_{k-1}) \\ &\leq \sum_{k=k_1}^{\infty} \left(c_2 \left| \frac{M_i}{M_{i-1}} - 1 \right|^2 + c_3 \left| d_i - \frac{M_i}{M_{i-1}} d_{i-1} \right|^2 + c_4 |M_i - M_*|^2 \right) + V(y_{k_1}, \tilde{M}_{k_1-1}), \end{aligned}$$

where the upper and lower bounds imply that all the limits exist. Thus,

$$\lim_{k \rightarrow \infty} \frac{c_1 |y_k|^2}{\nu_2 + \bar{M}^2 |y_k|^2} = 0,$$

which implies that $\lim_{k \rightarrow \infty} y_k = 0$. □

7.12 Lemma 7.1 Used in Proof of Theorem 7.1

Lemma 7.1. Consider the sequence $\{\hat{\omega}_k\}_{k=0}^\infty$, and assume it satisfies (A7.5). Then, the following statements hold:

- i)* $\sum_{i=k_1}^\infty |M_i - M_*|^2$ exists.
- ii)* $\sum_{i=k_1}^\infty \left| \frac{M_i}{M_{i-1}} - 1 \right|^2$ exists.
- iii)* $\sum_{i=k_1}^\infty \left| d_i - \frac{M_i}{M_{i-1}} d_{i-1} \right|^2$ exists.

Proof. Note that $G_{yu}(j\omega)$ is a Lipschitz continuous function of ω , that is, there exists $L_G > 0$ such that for all $\omega_1, \omega_2 > 0$,

$$|G_{yu}(j\omega_1) - G_{yu}(j\omega_2)| \leq L_G |\omega_1 - \omega_2|. \quad (7.42)$$

To show *i)*, since (A7.5) is satisfied, it follows from (7.42), that for all $k_1 > k_0$,

$$\begin{aligned} \sum_{i=k_1}^\infty |M_i - M_*|^2 &= \sum_{i=k_1}^\infty |G_{yu}(j\omega_i) - G_{yu}(j\omega_*)|^2 \\ &\leq L_G^2 \sum_{i=k_1}^\infty |\hat{\omega}_i - \omega_*|^2 \\ &\leq c_\omega^2 L_G^2 \sum_{i=k_1}^\infty \lambda_\omega^{2(i-k_0)} \\ &= \frac{c_\omega^2 L_G^2 \lambda_\omega^{2(k_1-k_0)}}{1 - \lambda_\omega^2}, \end{aligned}$$

which confirms *i)*.

To show *ii)*, note that it follows from (A7.5) that for all $k > k_0$,

$$|\hat{\omega}_k - \hat{\omega}_{k-1}| \leq c_\omega (\lambda_\omega^{k-k_0} + \lambda_\omega^{k-1-k_0}). \quad (7.43)$$

Furthermore, note that (A7.5) implies that $\lim_{k \rightarrow \infty} \hat{\omega}_k = \omega_*$. Thus, there exists $k_3 \in \mathbb{N}$ such that for all $k \geq k_3$, $M_{k-1} \neq 0$. Thus, it follows that there exist $\varepsilon > 0$ such that for all $k \geq k_3$, $|M_{k-1}| > \varepsilon$. Therefore, it follows from (7.42), and (7.43) that for all $k_1 \geq \max\{k_0, k_3\}$,

$$\begin{aligned} \sum_{i=k_1}^\infty \left| \frac{M_i}{M_{i-1}} - 1 \right|^2 &= \sum_{i=k_1}^\infty \left| \frac{G_{yu}(j\omega_i) - G_{yu}(j\omega_{i-1})}{G_{yu}(j\omega_{i-1})} \right|^2 \\ &\leq L_G^2 \sum_{i=k_1}^\infty \frac{|\hat{\omega}_i - \hat{\omega}_{i-1}|^2}{\varepsilon^2} \end{aligned}$$

$$\begin{aligned}
&\leq \frac{c_\omega^2 L_G^2}{\varepsilon^2} \sum_{i=k_1}^{\infty} \left(\lambda_\omega^{2i-2k_0} + 2\lambda_\omega^{2i-2k_0-1} + \lambda_\omega^{2i-2k_0-2} \right) \\
&= \frac{c_\omega^2 L_G^2 (\lambda_\omega^2 + 2\lambda_\omega + 1)}{\varepsilon^2} \sum_{i=k_1}^{\infty} \lambda_\omega^{2i-2k_0-2} \\
&= \frac{c_\omega^2 L_G^2 (1 + \lambda_\omega)^2 \lambda_\omega^{2k_1-2k_0-2}}{\varepsilon^2 (1 - \lambda_\omega)^2} \\
&= \frac{c_\omega^2 L_G^2 (1 + \lambda_\omega) \lambda_\omega^{2k_1-2k_0-2}}{\varepsilon^2 (1 - \lambda_\omega)},
\end{aligned}$$

which confirms *ii*).

To show *iii*), note that Fact 7.1 states that $\bar{d} = \lim_{k \rightarrow \infty} d_k$ exists. Moreover, since $\lim_{k \rightarrow \infty} \frac{M_k}{M_{k-1}} = 1$, it follows that $\lim_{k \rightarrow \infty} \frac{M_k}{M_{k-1}} d_{k-1} = \bar{d}$. Thus, there exists $\delta > 0$ and $k_4 \in \mathbb{N}$ such that for all $k > k_4$, $|d_k - \bar{d}| < \delta$ and $|\frac{M_k}{M_{k-1}} d_{k-1} - \bar{d}| < \delta$. Thus, it follows from (A7.5) that there exists $L_d > 0$, such that for all $k_1 > \max\{k_4, k_0\}$,

$$|d_{k_1} - \bar{d}| \leq L_d |\hat{\omega}_{k_1} - \omega_*| \leq L_d c_\omega \lambda_\omega^{k_1 - k_0}, \quad (7.44)$$

$$\left| \frac{M_{k_1}}{M_{k_1-1}} d_{k_1-1} - \bar{d} \right| \leq L_d |\hat{\omega}_{k_1} - \omega_*| \leq L_d c_\omega \lambda_\omega^{k_1 - k_0}. \quad (7.45)$$

Next, note that

$$\begin{aligned}
\sum_{i=k_1}^{\infty} \left| d_i - \frac{M_i}{M_{i-1}} d_{i-1} \right|^2 &= \sum_{i=k_1}^{\infty} \left| d_i - \bar{d} + \bar{d} - \frac{M_i}{M_{i-1}} d_{i-1} \right|^2 \\
&\leq 2 \sum_{i=k_1}^{\infty} |d_i - \bar{d}|^2 + 2 \sum_{i=k_1}^{\infty} \left| \frac{M_i}{M_{i-1}} d_{i-1} - \bar{d} \right|^2.
\end{aligned} \quad (7.46)$$

Moreover, it follows from (7.44) that

$$\begin{aligned}
\sum_{i=k_1}^{\infty} |d_i - \bar{d}|^2 &\leq L_d^2 c_\omega^2 \sum_{i=k_1}^{\infty} \lambda_\omega^{2i-2k_0} \\
&= \frac{L_d^2 c_\omega^2 \lambda_\omega^{2k_1-2k_0}}{1 - \lambda_\omega^2},
\end{aligned} \quad (7.47)$$

and it follows from (7.45) that

$$\begin{aligned}
\sum_{i=k_1}^{\infty} \left| \frac{M_i}{M_{i-1}} d_{i-1} - \bar{d} \right|^2 &\leq L_d^2 c_\omega^2 \sum_{i=k_1}^{\infty} \lambda_\omega^{2i-2k_0} \\
&= \frac{L_d^2 c_\omega^2 \lambda_\omega^{2k_1-2k_0}}{1 - \lambda_\omega^2}.
\end{aligned} \quad (7.48)$$

Thus, using (7.47) and (7.48), it follows from (7.46) that

$$\sum_{i=k_1}^{\infty} \left| d_i - \frac{M_i}{M_{i-1}} d_{i-1} \right|^2 \leq \frac{4L_d^2 c_\omega^2 \lambda_\omega^2}{1 - \lambda_\omega^2},$$

which confirms *iii*). □

Chapter 8

Conclusions and Future Work

We presented a variety of new adaptive control algorithms that address the problem of rejecting sinusoids with known frequencies that act on an unknown asymptotically stable linear time-invariant system. To implement these algorithms, minimal or no system model information is required. These algorithms were developed in discrete time, meaning that the control computations use sampled-date measurements. Moreover, these algorithms were developed in both frequency and time domains. We demonstrated effectiveness of the adaptive controllers through stability and performance analysis, numerical simulations, and experimental testings. We also presented extensions to these algorithms that address decentralized control system implementations as well as unknown disturbance frequencies.

8.1 Trade-offs for Adaptive Algorithms

We present a comparison of adaptive control algorithms of this dissertation. Figure 8.1 summarizes the trade-offs between adaptive algorithms.

Frequency-Domain vs. Time-Domain:

The adaptive control algorithms developed in Chapters 2, 4, 6, and 7 are in frequency domain, meaning that all control computations use discrete Fourier transform data (DFT), whereas the algorithms in Chapters 3 and 5 are in time domain.

Frequency-domain algorithms are less susceptible to measurement noise. These algorithms are also less influenced by the system's transient response, because DFT can often extract the harmonic steady-state response even if the system is not at steady state. In other words, DFT can filter out the non-sinusoidal part of a system's response during transient, and thus T_s can be selected smaller than the settling time of the system (e.g., See Example 1.1 and Fig. 1.3, where T_s for FD-HHC is selected smaller than settling time of the helicopter system).

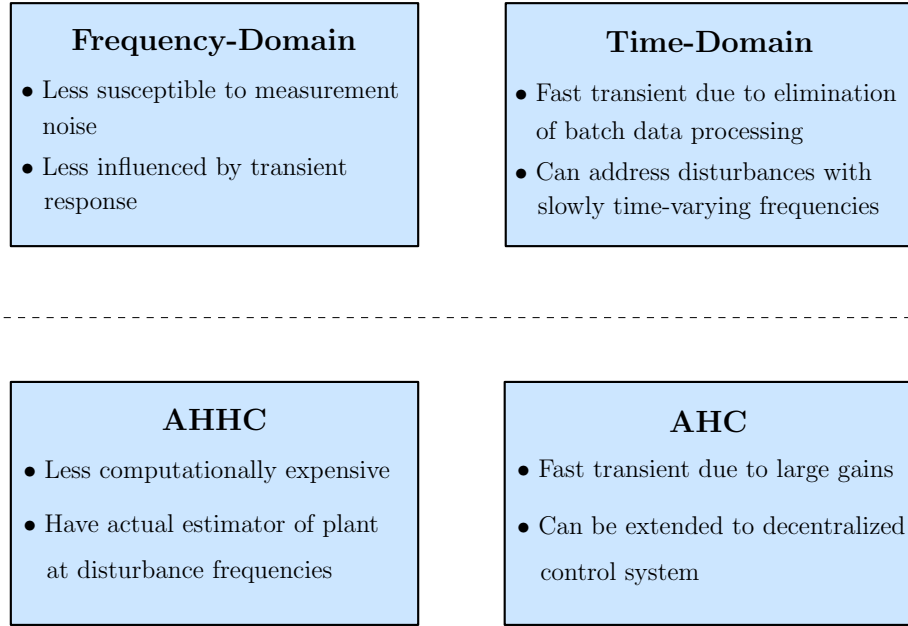


Figure 8.1: Trade-offs for adaptive algorithms of this dissertation

Alternatively, time-domain methods can yield faster convergence (e.g., see Examples 3.1 and 3.2), and can accommodate disturbances with slowly time-varying frequencies (e.g., see Example 5.4). Therefore, for each disturbance rejection task, depending on the characteristics of dynamic system and external disturbances, the choice between a frequency-domain and a time-domain algorithm can affect the effectiveness of implementation.

AHHC vs. AHC:

The control algorithms in Chapters 4, 5, and 6 are named AHC, whereas the algorithms of Chapters 2, 3, and 7 are named AHHC.

Note that AHHC algorithms can be less computationally expensive since they do not require online matrix inversion. In addition, for AHHC, we developed update equations for an adaptive estimate of the control-to-performance transfer function at disturbance frequency, that is, M_k for FD-AHHC and H_k for TD-AHHC. The update equations for the control parameter u_k depends on the adaptive estimates M_k or H_k . Roughly speaking, Propositions 2.1 and 3.2 imply that in terms of Frobenius norm, the adaptive estimates M_k or H_k move toward their ideal values M_* or H_* .

Alternatively, AHC has other benefits. Note that Theorems 4.2 and 5.2 do not impose upper bounds on the gains μ and γ for FD-AHC, and the gains γ_d and γ_H for TD-AHC. Thus, AHC can use large gains and yield faster convergence compared to AHHC. Also, note that AHC can be extended to systems with decentralized control architecture. In Chapter 6, we presented a decentralized extension of FD-AHC. Similar decentralized extension can be developed for TD-AHC. However, the extension of AHHC algorithms to decentralized case is an open problem.

8.2 Concluding Remarks

We summarize some remarks regarding the main characteristics of the adaptive control algorithms of this dissertation.

Adaptive Estimation and Control:

In Sections 3.5 and 3.6, we presented and analyzed a new control method named TD-HHC, which we consider as the time-domain counterpart of the existing FD-HHC algorithm in Section 2.4. Although these two methods have relatively good robustness to changes in the system's dynamics, we consider them as non-adaptive methods, because both require knowledge of sufficiently accurate fixed estimates of the control-to-performance transfer function at the disturbance frequencies; and they both use fixed gains in the control parameter update equations. Therefore, both FD-HHC and TD-HHC can cause closed-loop instabilities if changes in the dynamic system are not sufficiently small. On the other hand, we developed adaptive versions of FD-HHC and TD-HHC named FD-AHHC and TD-AHHC, respectively, in Sections 2.5 and 3.7, which do not require any model information since both FD-AHHC or TD-AHHC use adaptive estimates rather than fixed estimates. It is worthwhile to note that introducing FD-AHHC and TD-AHHC does not render FD-HHC and TD-HHC pointless control methods. For certain applications, where the dynamic system does not change too much, using FD-HHC or TD-HHC can be more efficient compared to the use of FD-AHHC or TD-AHHC, because both FD-AHHC and TD-AHHC are computationally more expensive than FD-HHC and TD-HHC. Also, note that introducing adaption in a control system can aggravate actuator saturation, or can cause adaptive parameter drift, both of which, can cause closed-loop instabilities if not taken care of.

Actuator Saturation:

Actuator saturation is a common practical issue in feedback control systems, which happens if magnitude of the computed control is larger than the actuator's maximum deliverable magnitude. Ignoring actuator saturation in the design can result in degraded performance or even instability. Addressing actuator saturation becomes even more imperative in adaptive control design, because unforeseen changes in the dynamic system or unexpectedly large-amplitude disturbances can readily cause actuator saturation. For adaptive control methods of this dissertation, we presented modifications to the control update equations aimed at addressing the problem of actuator saturation. These modifications are in Section 3.10 for TD-HHC and TD-AHHC, and in Section 5.7 for TD-AHC. Similar modifications can address actuator saturation for other algorithms of this dissertation.

Computational Complexity:

Computational complexity of the adaptive controllers of this dissertation is com-

parable to other adaptive feedforward methods (e.g., [81, 157, 158]). Also, we note that all control methods in this dissertation are developed in discrete time, and thus, control calculations are required only every T_s seconds— T_s is the control update period. Therefore, T_s can be increased as necessary to accommodate the computational capabilities of the control hardware. Although, increasing T_s tends to increase convergence time, for FD-AHC and TD-AHC the gains used in the update equations can be increased (since their gains are not upper-bounded) to achieve desired convergence time. This property is illustrated in Example 5.1.

Disturbances with Known-but-Time-Varying Frequencies:

In contrast to frequency-domain control methods, time-domain methods do not require batch data processing (e.g., DFT). This feature of time-domain methods provides the possibility of their successful implementation for systems subject to disturbances with known-but-time-varying frequencies. Numerical simulations suggest that the adaptive controllers of this dissertation that are developed in time domain (i.e., TD-HHC, TD-AHHC, and TD-AHC) are effective for rejection of disturbances with time-varying frequencies if the time variation is known, and the rate of change of the frequencies is sufficiently small. One such demonstration of this time-domain feature is in Example 5.4 for TD-AHC algorithm.

Inaccurate Knowledge of Disturbance Frequencies:

If the frequencies of harmonic control differ from the frequencies of disturbance, the adaptive control algorithms of this dissertation are still applicable and can achieve disturbance attenuation, provided that the difference between the frequencies of disturbance and control is sufficiently small. Experiment 5.6 demonstrates one such scenario.

Decentralized Control Architecture:

We presented decentralized FD-AHC in Chapter 6, which is the extension of the new FD-AHC algorithm that we introduced in Chapter 4. Similar to TD-AHC algorithm presented in Chapter 5, FD-AHC benefits from arbitrarily large adaptive gains in its update equations, which can significantly improve the convergence time. For decentralized FD-AHC, Theorem 6.2 requires sufficiently small gains for Lyapunov stability and global convergence. However, numerical simulations suggest that similar to FD-AHC and TD-AHC, sufficiently small gains are not necessary for successful implementation of decentralized FD-AHC. In other words, numerical simulations suggest that decentralized FD-AHC benefits from arbitrarily large gains as well as FD-AHC and TD-AHC.

Note that, although not presented, TD-AHC can be also extended to decentralized control systems (i.e., similar to decentralized FD-AHC). However, for AHHC algorithms, extension to decentralized control systems is an open problem.

Disturbances with Unknown Frequencies:

In Chapter 7, we extended the result of Chapter 2 to address the case of disturbances with unknown frequencies. In fact, we coupled an exponentially-fast frequency estimator with FD-AHHC, and in Theorem 7.1 we validated the design through analysis. Although, Theorem 7.1 concerns a specific exponentially-fast frequency estimator coupled with FD-AHHC, its statement can be shown to be true for other exponentially-fast frequency estimators coupled with FD-AHHC or other adaptive algorithms of this dissertation. In fact, numerical simulations suggest that not only exponentially-fast frequency estimators but also other frequency estimators that asymptotically converge to the disturbance frequency can be coupled with our adaptive control methods to address the rejection of sinusoids with unknown frequencies.

8.3 Recommendations for Future Work

In Chapter 7, we extended FD-AHHC to address disturbances with unknown frequencies. It might be worthwhile to seek for other ways of extending FD-AHHC or other algorithms of this dissertation to the case of unknown-frequency disturbances. Moreover, modifications to the adaptive algorithm of this dissertation might be helpful for certain applications. One can investigate the incorporation of windowing techniques, recursive least squares parameter estimation, and multi-rate update approaches. Also, the extension of AHHC algorithms to systems with decentralized control architecture is an open problem. In addition, it might be beneficial to study the possibility of extending the adaptive controllers of this dissertation to nonlinear systems.

Bibliography

- [1] W. F. Paul and K. C. Mard, "Vibration damped helicopter rotor," Nov. 17 1970, US Patent 3,540,809.
- [2] F. J. McHugh and J. Shaw, "Helicopter vibration reduction with higher harmonic blade pitch," *J. Amer. Helicopter Society*, vol. 23, no. 4, pp. 26–35, 1978.
- [3] J. Shaw and N. Albion, "Active control of the helicopter rotor for vibration reduction," *J. Amer. Helicopter Society*, vol. 26, no. 3, pp. 32–39, 1981.
- [4] E. R. Wood, R. W. Powers, J. H. Cline, and C. E. Hammond, "On developing and flight testing a higher harmonic control system," *J. Amer. Helicopter Society*, vol. 30, no. 1, pp. 3–20, 1985.
- [5] G. Goodwin, R. Evans, R. Leal, and R. Feik, "Sinusoidal disturbance rejection with application to helicopter flight data estimation," *IEEE Trans. Acoust. Speech Sig. Proc.*, vol. 34, no. 3, pp. 479–484, 1986.
- [6] P. P. Friedmann, "Helicopter vibration reduction using structural optimization with aeroelastic/multidisciplinary constraints-a survey," *J. Aircraft*, vol. 28, no. 1, pp. 8–21, 1991.
- [7] S. R. Hall and N. M. Wereley, "Performance of higher harmonic control algorithms for helicopter vibration reduction," *J. Guid. Contr. Dyn.*, vol. 16, no. 4, pp. 793–797, 1993.
- [8] T. A. Millott and P. P. Friedmann, "Vibration reduction in helicopter rotors using an actively controlled partial span trailing edge flap located on the blade," 1994.
- [9] J. T. Pearson and R. M. Goodall, "Adaptive schemes for the active control of helicopter structural response," *IEEE Trans. Contr. Sys. Tech.*, vol. 2, no. 2, pp. 61–72, 1994.
- [10] P. P. Friedmann and T. A. Millott, "Vibration reduction in rotorcraft using active control: A comparison of various approaches," *J. Guid. Contr. Dyn.*, vol. 18, no. 4, pp. 664–673, 1995.
- [11] M. Lovera, P. Colaneri, C. Malpica, and R. Celi, "Discrete-time, closed-loop aeromechanical stability analysis of helicopters with higher harmonic control," *J. Guid. Contr. Dyn.*, vol. 30, no. 5, pp. 1249–1260, 2007.

- [12] C. Malpica, "Contributions to the dynamics of helicopters with active rotor controls," Ph.D. dissertation, 2008.
- [13] R. Mura and M. Lovera, "Baseline vibration attenuation in helicopters: robust mimo-hhc control," *IFAC Proc. Volumes*, vol. 47, no. 3, pp. 8855–8860, 2014.
- [14] P. M. Küfmann and C. Brillante, "In-flight tracking and vibration control using the dlr's multiple swashplate system," *CEAS Aeronautical Journal*, vol. 8, no. 4, pp. 637–652, 2017.
- [15] W. A. Welsh, "Helicopter vibration reduction," in *Morphing Wing Technologies*, A. Concilio, I. Dimino, L. Lecce, and R. Pecora, Eds. Butterworth-Heinemann, 2018, pp. 865 – 892.
- [16] H. Merritt, "Theory of self-excited machine-tool chatter: contribution to machine-tool chatter research," *J. Eng. Indust.*, vol. 87, no. 4, pp. 447–454, 1965.
- [17] C. L. Nachtigal and N. H. Cook, "Active control of machine-tool chatter," *J. Basic Engineering*, vol. 92, no. 2, pp. 238–244, 1970.
- [18] M. Rahman and Y. Ito, "Stability analysis of chatter vibration in turning processes," *J. Sound Vibration*, vol. 102, no. 4, pp. 515–525, 1985.
- [19] M. Tsai, S. Takata, M. Inui, F. Kimura, and T. Sata, "Prediction of chatter vibration by means of a model-based cutting simulation system," *CIRP Annals-Manufacturing Technology*, vol. 39, no. 1, pp. 447–450, 1990.
- [20] C. R. Knospe, R. W. Hope, S. M. Tamer, and S. J. Fedigan, "Robustness of adaptive unbalance control of rotors with magnetic bearings," *J. Vibration Contr.*, vol. 2, no. 2, pp. 33–52, 1996.
- [21] S. Zhou and J. Shi, "Active balancing and vibration control of rotating machinery: a survey," *Shock and Vibration Digest*, vol. 33, no. 5, pp. 361–371, 2001.
- [22] S. W. Dyer, J. Shi, J. Ni, and K.-K. Shin, "Robust optimal influence-coefficient control of multiple-plane active rotor balancing systems," *J. Dynam. Sys. Measur. Contr.*, vol. 124, no. 1, pp. 41–46, 2002.
- [23] B. Hredzak and G. Guo, "New electromechanical balancing device for active imbalance compensation," *J. Sound Vibration*, vol. 294, no. 4-5, pp. 737–751, 2006.
- [24] M. Chen and C. R. Knospe, "Control approaches to the suppression of machining chatter using active magnetic bearings," *IEEE Trans. Control Sys. Tech.*, vol. 15, no. 2, pp. 220–232, 2007.

- [25] T. R. Grochmal and A. F. Lynch, "Precision tracking of a rotating shaft with magnetic bearings by nonlinear decoupled disturbance observers," *IEEE Trans. Contr. Sys. Tech.*, vol. 15, no. 6, pp. 1112–1121, 2007.
- [26] M. De Queiroz, "An active identification method of rotor unbalance parameters," *J. Vibration and Contr.*, vol. 15, no. 9, pp. 1365–1374, 2009.
- [27] A. Lees, J. Sinha, and M. Friswell, "Model-based identification of rotating machines," *Mechanical Sys. Sig. Proc.*, vol. 23, no. 6, pp. 1884–1893, 2009.
- [28] J. Kejian, Z. Changsheng, and T. Ming, "A uniform control method for imbalance compensation and automation balancing in active magnetic bearing-rotor systems," *J. Dyn. Sys. Meas. Contr.*, vol. 134, no. 2, p. 021006, 2012.
- [29] S. Zheng, B. Han, Y. Wang, and J. Zhou, "Optimization of damping compensation for a flexible rotor system with active magnetic bearing considering gyroscopic effect," *IEEE/ASME Trans. Mechatronics*, vol. 20, no. 3, pp. 1130–1137, 2015.
- [30] X. Xu, J. Fang, G. Liu, and H. Zhang, "Model development and harmonic current reduction in active magnetic bearing systems with rotor imbalance and sensor runout," *J. Vibration Contr.*, vol. 21, no. 13, pp. 2520–2535, 2015.
- [31] C. Peng, J. Sun, X. Song, and J. Fang, "Frequency-varying current harmonics for active magnetic bearing via multiple resonant controllers," *IEEE Trans. Indust. Electro.*, vol. 64, no. 1, pp. 517–526, 2017.
- [32] S. J. Elliott, C. C. Boucher, and P. A. Nelson, "The behavior of a multiple channel active control system," *IEEE Trans. Sig. Proc.*, vol. 40, no. 5, pp. 1041–1052, 1992.
- [33] S. J. Elliott and P. A. Nelson, "Active noise control," *IEEE Sig. Proc. Mag.*, vol. 10, no. 4, pp. 12–35, 1993.
- [34] S. M. Kuo and D. Morgan, *Active noise control systems: algorithms and DSP implementations*. John Wiley & Sons, Inc., 1995.
- [35] N. J. Bershad and J. C. M. Bermudez, "Sinusoidal interference rejection analysis of an lms adaptive feedforward controller with a noisy periodic reference," *IEEE Trans. Sig. Proc.*, vol. 46, no. 5, pp. 1298–1313, 1998.
- [36] S. M. Kuo and D. R. Morgan, "Active noise control: a tutorial review," *Proc. IEEE*, vol. 87, no. 6, pp. 943–973, 1999.
- [37] M. Bodson, J. S. Jensen, and S. C. Douglas, "Active noise control for periodic disturbances," *IEEE Trans. Contr. Sys. Tech.*, vol. 9, no. 1, pp. 200–205, 2001.
- [38] S. M. Kuo and H.-T. Wu, "Nonlinear adaptive bilinear filters for active noise control systems," *IEEE Trans. Circ. Sys. I*, vol. 52, no. 3, pp. 617–624, 2005.

- [39] M. T. Akhtar, M. Abe, and M. Kawamata, "A new variable step size lms algorithm-based method for improved online secondary path modeling in active noise control systems," *IEEE Trans. Audio Speech Lang. Proc.*, vol. 14, no. 2, pp. 720–726, 2006.
- [40] B. Yousefzadeh, M. Mahjoob, N. Mohammadi, and A. Shahsavari, "An experimental study of sound transmission loss (stl) measurement techniques using an impedance tube," *J. Acoustical Society Amer.*, vol. 123, no. 5, p. 3119, 2008.
- [41] M. Mahjoob, N. Mohammadi, and S. Malakooti, "An investigation into the acoustic insulation of triple-layered panels containing newtonian fluids: theory and experiment," *Applied Acoustics*, vol. 70, no. 1, pp. 165–171, 2009.
- [42] C. Hansen, S. Snyder, X. Qiu, L. Brooks, and D. Moreau, *Active control of noise and vibration*. CRC press, 2012.
- [43] N. V. George and A. Gonzalez, "Convex combination of nonlinear adaptive filters for active noise control," *Applied Acoustics*, vol. 76, pp. 157–161, 2014.
- [44] M. Akraminia, M. Mahjoob, and M. Tatari, "Active noise control using adaptive polynomial gaussian winowed wavelet networks," *J. Vibration Contr.*, vol. 21, no. 15, pp. 3020–3033, 2015.
- [45] M. Akraminia and M. J. Mahjoob, "Adaptive feedback active noise control using wavelet frames: simulation and experimental results," *J. Vibration Contr.*, vol. 22, no. 7, pp. 1895–1912, 2016.
- [46] M. Akraminia, M. J. Mahjoob, and M. Tatari, "Nonlinear active noise control using adaptive wavelet filters," *Amer. Scientific Research J. Eng. Tech. Sci.*, vol. 37, no. 1, pp. 287–304, 2017.
- [47] E. M. Ku, "Adaptive modeling of secondary path in an active noise control system," 2017, US Patent App. 15/616,332.
- [48] M. Akraminia, M. J. Mahjoob, and A. H. Niazi, "Feedforward active noise control using wavelet frames: simulation and experimental results," *J. Vibration Cont.*, vol. 23, no. 4, pp. 555–573, 2017.
- [49] N. Kwatra, J. D. Hendrix, and J. L. Melanson, "Systems and methods for adaptive active noise cancellation for multiple-driver personal audio device," Jul. 3 2018, US Patent App. 10/013,966.
- [50] T. Soharton, "Development of impedance simulation fixtures for spacecraft vibration tests," 1969.
- [51] N. Formica, L. B. Crema, C. Galeazzi, and F. Morganti, "Vibration control of satellite panels by means of piezoelectric elements," *WIT Trans. Built Environment*, vol. 22, 1970.

- [52] G. Fleischer and P. Likins, "Results of flexible spacecraft attitude control studies utilizing hybrid coordinates," *J. Spacecraft Rockets*, vol. 8, no. 3, pp. 264–273, 1971.
- [53] J. Canavin, "The control of spacecraft vibrations using multivariable output feedback," in *Astrodynamics Conferece*, 1978, p. 1419.
- [54] L. Meirovitch and H. Oz, "Modal-space control of large flexible spacecraft possessing ignorable coordinates," *J. Guid. Contr. Dynam.*, vol. 3, no. 6, pp. 569–577, 1980.
- [55] A. Von Flotow, "Traveling wave control for large spacecraft structures," *J. Guid. Contr. Dynam.*, vol. 9, no. 4, pp. 462–468, 1986.
- [56] L. Meirovitch and R. Quinn, "Maneuvering and vibration control of flexible spacecraft," 1987.
- [57] G. Song, N. V. Buck, and B. N. Agrawal, "Spacecraft vibration reduction using pulse-width pulse-frequency modulated input shaper," *J. Guid. Contr. Dyn.*, vol. 22, no. 3, pp. 433–440, 1999.
- [58] Q. Hu and G. Ma, "Variable structure control and active vibration suppression of flexible spacecraft during attitude maneuver," *Aerospace Science and Technology*, vol. 9, no. 4, pp. 307–317, 2005.
- [59] J. Lau, S. S. Joshi, B. N. Agrawal, and J.-W. Kim, "Investigation of periodic-disturbance identification and rejection in spacecraft," *J. Guid. Contr. Dyn.*, vol. 29, no. 4, pp. 792–798, 2006.
- [60] Q. Hu, P. Shi, and H. Gao, "Adaptive variable structure and commanding shaped vibration control of flexible spacecraft," *J. Guid. Contr. Dynam.*, vol. 30, no. 3, pp. 804–815, 2007.
- [61] Z. Chen and J. Huang, "Attitude tracking and disturbance rejection of rigid spacecraft by adaptive control," *IEEE Trans. Auto. Contr.*, vol. 54, no. 3, pp. 600–605, 2009.
- [62] Y. Jiang, Q. Hu, and G. Ma, "Adaptive backstepping fault-tolerant control for flexible spacecraft with unknown bounded disturbances and actuator failures," *ISA Transactions*, vol. 49, no. 1, pp. 57–69, 2010.
- [63] T. Sales, D. Rade, and L. De Souza, "Passive vibration control of flexible spacecraft using shunted piezoelectric transducers," *Aerospace Science and Technology*, vol. 29, no. 1, pp. 403–412, 2013.
- [64] W. He and S. S. Ge, "Dynamic modeling and vibration control of a flexible satellite," *IEEE Trans. Aerospace Electro. Sys.*, vol. 51, no. 2, pp. 1422–1431, 2015.

- [65] K. Yang, Y.-W. Zhang, H. Ding, T.-Z. Yang, Y. Li, and L.-Q. Chen, “Nonlinear energy sink for whole-spacecraft vibration reduction,” *J. Vibration Acoustics*, vol. 139, no. 2, p. 021011, 2017.
- [66] M. Malekzadeh and H. Karimpour, “Adaptive super twisting vibration control of a flexible spacecraft with state rate estimation,” *J. Sound Vibration*, vol. 422, pp. 300–317, 2018.
- [67] D. W. Rickert, “Method of suppressing seek-excited vibration in a disk drive or similar servo system,” Oct. 16 1984, US Patent 4,477,755.
- [68] Y. Mizoshita, S. Hasegawa, and K. Takaishi, “Vibration minimized access control for disk drives,” *IEEE Trans. Magnetics*, vol. 32, no. 3, pp. 1793–1798, 1996.
- [69] Y. Soeno, S. Ichikawa, T. Tsuna, Y. Sato, and I. Sato, “Piezoelectric piggy-back microactuator for hard disk drive,” *IEEE Trans. Magnetics*, vol. 35, no. 2, pp. 983–987, 1999.
- [70] I. Shen, “Recent vibration issues in computer hard disk drives,” *J. Magnetism and Magnetic Materials*, vol. 209, no. 1-3, pp. 6–9, 2000.
- [71] T. Atsumi, T. Arisaka, T. Shimizu, and T. Yamaguchi, “Vibration servo control design for mechanical resonant modes of a hard-disk-drive actuator,” *JSME Int. J. Series C Mechanical Systems, Machine Elements and Manufacturing*, vol. 46, no. 3, pp. 819–827, 2003.
- [72] K. Oldham, X. Huang, A. Chahwan, and R. Horowitz, “Design, fabrication, and control of a high-aspect ratio microactuator for vibration suppression in a hard disk drive,” *IFAC Proceedings Volumes*, vol. 38, no. 1, pp. 13–18, 2005.
- [73] R. Horowitz, Y. Li, K. Oldham, S. Kon, and X. Huang, “Dual-stage servo systems and vibration compensation in computer hard disk drives,” *Contr. Eng. Practice*, vol. 15, no. 3, pp. 291–305, 2007.
- [74] T. Atsumi, A. Okuyama, and S. Nakagawa, “Vibration control above the nyquist frequency in hard disk drives,” *IEEE Trans. Indust. Electro.*, vol. 55, no. 10, pp. 3751–3757, 2008.
- [75] T. Atsumi, “Disturbance suppression beyond nyquist frequency in hard disk drives,” *Mechatronics*, vol. 20, no. 1, pp. 67–73, 2010.
- [76] J.-H. She, X. Xin, and Y. Pan, “Equivalent-input-disturbance approach analysis and application to disturbance rejection in dual-stage feed drive control system,” *IEEE/ASME Trans. Mechatronics*, vol. 16, no. 2, pp. 330–340, 2011.
- [77] D. Huang, V. Venkataramanan, J.-X. Xu *et al.*, “Contact-induced vibration in dual-stage hard disk drive servo systems and its compensator design,” *IEEE Trans. Indust. Electro.*, vol. 61, no. 8, pp. 4052–4060, 2014.

- [78] T. Yamaguchi, M. Hirata, and J. C. K. Pang, *High-speed precision motion control*. CRC press, 2017.
- [79] J.-S. Lee, S.-Y. Lim, I. Kim, W. Jeong, S. Park, and H. Yang, “An adaptive disturbance rejection method with stability enhancement using adjustable dead zone for hard disk drives,” *IEEE Trans. Magnetics*, vol. 53, no. 3, 2017.
- [80] S. Yabui, “Compensation and identification for external disturbances in head positioning systems of hard disk drives based on a data-based design method,” *Mechanical Sys. Sig. Proc.*, vol. 115, pp. 434–449, 2019.
- [81] D. Patt, J. Chandrasekar, D. S. Bernstein, and P. P. Friedmann, “Higher-harmonic-control algorithm for helicopter vibration reduction revisited,” *J. Guid. Contr. Dyn.*, vol. 28, no. 5, pp. 918–930, 2005.
- [82] M. Kamaldar and J. B. Hoagg, “Adaptive harmonic steady-state control for rejection of sinusoidal disturbances acting on a completely unknown system,” *Int. J. Adapt. Contr. Sig. Proc.*, vol. 31, no. 9, pp. 1308–1326, 2017.
- [83] N. K. Gupta, “Frequency-shaped cost functionals-extension of linear-quadratic-gaussian design methods,” *J. Guid. Contr. Dyn.*, vol. 3, no. 6, pp. 529–535, 1980.
- [84] W. Johnson, *Helicopter theory*. Courier Corporation, 2012.
- [85] A. C. Veca, “Vibration effects on helicopter reliability and maintainability,” United Technologies Corp., Stratford CT, Sikorsky Aircraft DIV, Tech. Rep., 1973.
- [86] A. Bayoumi, W. Ranson, L. Eisner, and L. Grant, “Cost and effectiveness analysis of the ah-64 and uh-60 on-board vibrations monitoring system,” in *Aerospace Conference*. IEEE, 2005, pp. 3921–3940.
- [87] “Aeronautical design standard, standard practice, requirements for rotorcraft vibration specifications, modeling and testing,” *ADS-27A-SP*, May 2, 2006.
- [88] A. R. Bramwell, D. Balmford, and G. Done, *Bramwell’s helicopter dynamics*. Elsevier, 2001.
- [89] R. L. Bielawa, *Rotary wing structural dynamics and aeroelasticity*. American Institute of Aeronautics and Astronautics, 2006.
- [90] W. A. G. Ferdinand, “Double row roller bearing,” Nov. 29 1949, US Patent 2,489,342.
- [91] J. J. O’Leary, “Reduction in vibration of the ch-47c helicopter using a variable tuning vibration absorber,” *Shock and Vibration Bulletin*, vol. 40, pp. 191–202, 1969.

- [92] T. Millott, R. Goodman, J. Wong, W. Welsh, J. Correia, and C. Cassil, "Risk reduction flight test of a pre-production active vibration control system for the uh-60m," in *Annual Forum Proceedings, American Helicopter Society*, vol. 59, no. 1. American Helicopter Society, Inc., 2003, pp. 223–230.
- [93] R. Taylor, P. Zwicke, P. Gold, and W. Miao, "Analytical design and evaluation of an active control system for helicopter vibration reduction and gust response alleviation," 1980.
- [94] J.-D. Moon, B.-S. Kim, and S.-H. Lee, "Development of the active balancing device for high-speed spindle system using influence coefficients," *Int. J. Machine Tools Manufac.*, vol. 46, no. 9, pp. 978–987, 2006.
- [95] A. Sinervo and A. Arkkio, "Rotor radial position control and its effect on the total efficiency of a bearingless induction motor with a cage rotor," *IEEE Trans. Magnetics*, vol. 50, no. 4, pp. 1–9, 2014.
- [96] L. Eriksson, M. Allie, C. Bremigan, and J. Gilbert, "The use of active noise control for industrial fan noise," *ASME Paper*, 1988.
- [97] S. Elliott, P. Nelson, I. Stothers, C. Boucher, and J. Evers, "In-flight experiments on the active control of propeller-induced cabin noise," in *12th Aeroacoustic Conference*, 1990, p. 1047.
- [98] R. L. Chance, "Earmuff apparatus for use with headsets," Jun. 2 1987, US Patent 4,669,129.
- [99] T. Kimura, "Noise-cancelling headphone," Oct. 25 2011, US Patent 8,045,726.
- [100] H. Coanda, "Procédé de protection contre les bruits," *French Patent No. 722 274*, 1930.
- [101] P. Lueg, "Verfahren zur dämpfung von schallschwingungen," *German patent*, no. 655, p. 508, 1933.
- [102] H. F. Olson and E. G. May, "Electronic sound absorber," *J. Acoustical Society Amer.*, vol. 25, no. 6, pp. 1130–1136, 1953.
- [103] H. F. Olson, "Electronic control of noise, vibration, and reverberation," *J. Acoustical Society of America*, vol. 28, no. 5, pp. 966–972, 1956.
- [104] W. B. Conover, "Fighting noise with noise," *Noise Control*, vol. 2, no. 2, pp. 78–92, 1956.
- [105] K. Ahuja and J. Stevens, "Recent advances in active noise control," *AIAA J.*, vol. 29, no. 7, pp. 1058–1067, 1991.
- [106] N. V. George and G. Panda, "Advances in active noise control: A survey, with emphasis on recent nonlinear techniques," *Sig. Proc.*, vol. 93, no. 2, pp. 363–377, 2013.

- [107] S. Di Gennaro, “Output stabilization of flexible spacecraft with active vibration suppression,” *IEEE Trans. Aero. Electro. Sys.*, vol. 39, no. 3, pp. 747–759, 2003.
- [108] G. H. Hu Q, Shi P, “Adaptive variable structure and commanding shaped vibration control of flexible spacecraft,” *J. Guid. Contr. Dyn.*, vol. 30, no. 3, pp. 804–815, 2007.
- [109] D. Hyland, J. Junkins, and R. Longman, “Active control technology for large space structures,” *J. Guid. Contr. Dyn.*, vol. 16, no. 5, pp. 801–821, 1993.
- [110] S. Korkmaz, “A review of active structural control: challenges for engineering informatics,” *Computers & Structures*, vol. 89, no. 23-24, pp. 2113–2132, 2011.
- [111] Q. W. Jia, “Disturbance rejection through disturbance observer with adaptive frequency estimation,” *IEEE Trans. Magnetics*, vol. 45, no. 6, pp. 2675–2678, 2009.
- [112] L. Guo and Y.-J. Chen, “Disk flutter and its impact on hdd servo performance,” *IEEE Trans. Magnetics*, vol. 37, no. 2, pp. 866–870, 2001.
- [113] R. Ehrlich and D. Curran, “Major hdd tmr sources and projected scaling with tpi,” *IEEE Trans. Magnetics*, vol. 35, no. 2, pp. 885–891, 1999.
- [114] J. S. McAllister, “The effect of disk platter resonances on track misregistration in 3.5 inch disk drives,” *IEEE Trans. Magnetics*, vol. 32, no. 3, pp. 1762–1766, 1996.
- [115] C. D. Johnson, “Accommodation of external disturbances in linear regulator and servomechanism problems,” *IEEE Trans. Autom. Contr.*, vol. 16, pp. 635–644, 1971.
- [116] E. J. Davison, “The robust control of a servomechanism problem for linear time-invariant multivariable systems,” *IEEE Trans. Autom. Contr.*, vol. 21, pp. 25–34, 1976.
- [117] B. A. Francis, A. Sebakhy, and W. M. Wonham, “Synthesis of multivariable regulators: The internal model principle,” *J. Appl. Math. Optim.*, vol. 1, pp. 64–86, 1974.
- [118] I. D. Landau, A. Constantinescu, and D. Rey, “Adaptive narrow band disturbance rejection applied to an active suspension—an internal model principle approach,” *Automatica*, vol. 41, no. 4, pp. 563–574, 2005.
- [119] J. B. Hoagg, M. A. Santillo, and D. S. Bernstein, “Internal model control in the shift and delta domains,” *IEEE Trans. Autom. Contr.*, vol. 53, pp. 1066–1072, 2008.
- [120] D. Carnevale, S. Galeani, M. Sassano, and A. Astolfi, “Robust hybrid estimation and rejection of multi-frequency signals,” *Int. J. Adapt. Contr. Sig. Proc.*, vol. 30, no. 12, pp. 1649–1673, 2016.

- [121] W.-H. Chen, J. Yang, L. Guo, and S. Li, “Disturbance-observer-based control and related methods—An overview,” *IEEE Trans. Indust. Electr.*, vol. 63, no. 2, pp. 1083–1095, 2016.
- [122] L. Guo and W.-H. Chen, “Disturbance attenuation and rejection for systems with nonlinearity via DOBC approach,” *Int. J. Robust Nonlin. Contr.*, vol. 15, no. 3, pp. 109–125, 2005.
- [123] J. Yang, S. Li, and X. Yu, “Sliding-mode control for systems with mismatched uncertainties via a disturbance observer,” *IEEE Trans. Indust. Electr.*, vol. 60, no. 1, pp. 160–169, 2013.
- [124] X. Yao and L. Guo, “Composite anti-disturbance control for markovian jump nonlinear systems via disturbance observer,” *Automatica*, vol. 49, no. 8, pp. 2538–2545, 2013.
- [125] S. Li, H. Sun, J. Yang, and X. Yu, “Continuous finite-time output regulation for disturbed systems under mismatching condition,” *IEEE Trans. Autom. Contr.*, vol. 60, no. 1, pp. 277–282, 2015.
- [126] W. Kim, H. Kim, C. C. Chung, and M. Tomizuka, “Adaptive output regulation for the rejection of a periodic disturbance with an unknown frequency,” *IEEE Trans. Contr. Sys. Tech.*, vol. 19, no. 5, pp. 1296–1304, 2011.
- [127] A. A. Bobtsov and A. A. Pyrkin, “Cancellation of unknown multiharmonic disturbance for nonlinear plant with input delay,” *Int. J. Adapt. Contr. Sig. Proc.*, vol. 26, no. 4, pp. 302–315, 2012.
- [128] S. Li, J. Yang, W.-H. Chen, and X. Chen, *Disturbance observer-based control: methods and applications*. CRC press, 2014.
- [129] M. Bodson, A. Sacks, and P. Khosla, “Harmonic generation in adaptive feedforward cancellation schemes,” *IEEE Trans. Autom. Contr.*, vol. 39, no. 9, pp. 1939–1944, 1994.
- [130] W. Messner and M. Bodson, “Design of adaptive feedforward algorithms using internal model equivalence,” *Int. J. Adapt. Contr. Sig. Proc.*, vol. 9, pp. 199–212, 1995.
- [131] D. S. Bayard, “A general theory of linear time-invariant adaptive feedforward systems with harmonic regressors,” *IEEE Trans. Autom. Contr.*, vol. 45, no. 11, pp. 1983–1996, 2000.
- [132] R. Marino and P. Tomei, “Output regulation for unknown stable linear systems,” *IEEE Trans. Autom. Contr.*, vol. 60, no. 8, pp. 2213–2218, 2015.
- [133] R. Marino and P. Tomei, “Hybrid adaptive multi-sinusoidal disturbance cancellation,” *IEEE Trans. Autom. Contr.*, 2016.

- [134] S. Jafari and P. A. Ioannou, “Robust adaptive attenuation of unknown periodic disturbances in uncertain multi-input multi-output systems,” *Automatica*, vol. 70, pp. 32–42, 2016.
- [135] S. Jafari and P. A. Ioannou, “Rejection of unknown periodic disturbances for continuous-time MIMO systems with dynamic uncertainties,” *Int. J. Adapt. Contr. Sig. Proc.*, vol. 30, no. 12, pp. 1674–1688, 2016.
- [136] R. Venugopal and D. S. Bernstein, “Adaptive disturbance rejection using AR-MARKOV/Toeplitz models,” *IEEE Trans. Contr. Sys. Tech.*, vol. 8, no. 2, pp. 257–269, 2000.
- [137] G. Pin, “A direct approach for the frequency-adaptive feedforward cancellation of harmonic disturbances,” *IEEE Trans. Sig. Proc.*, vol. 58, no. 7, pp. 3523–3530, 2010.
- [138] G. Fedele, “A fractional-order repetitive controller for periodic disturbance rejection,” *IEEE Trans. Autom. Contr.*, 2017.
- [139] M. Bodson, “Rejection of periodic disturbances of unknown and time-varying frequencies,” *Int. J. Adapt. Contr. Sig. Proc.*, vol. 19, pp. 67–88, 2005.
- [140] J. B. Hoagg, M. A. Santillo, and D. S. Bernstein, “Discrete-time adaptive command following and disturbance rejection with unknown exogenous dynamics,” *IEEE Trans. Autom. Contr.*, vol. 53, pp. 912–928, 2008.
- [141] J. B. Hoagg and D. S. Bernstein, “Retrospective cost model reference adaptive control for nonminimum-phase systems,” *J. Guid. Contr. Dyn.*, vol. 35, no. 6, pp. 1767–1786, 2012.
- [142] H. I. Basturk and M. Krstic, “State derivative feedback for adaptive cancellation of unmatched disturbances in unknown strict-feedback LTI systems,” *Automatica*, vol. 50, no. 10, pp. 2539–2545, 2014.
- [143] H. I. Basturk and M. Krstic, “Adaptive sinusoidal disturbance cancellation for unknown LTI systems despite input delay,” *Automatica*, vol. 58, pp. 131–138, 2015.
- [144] J. B. Hoagg and T. M. Seigler, “Decentralized filtered dynamic inversion for uncertain minimum-phase systems,” *Automatica*, vol. 61, pp. 192–200, 2015.
- [145] J. B. Hoagg and T. M. Seigler, “Filtered feedback linearization for nonlinear systems with unknown disturbances,” *Sys. Contr. Lett.*, vol. 62, no. 8, pp. 613–625, 2013.
- [146] J. B. Hoagg and T. M. Seigler, “Filtered-dynamic-inversion control for unknown minimum-phase systems with unknown-and-unmeasured disturbances,” *Int. J. Contr.*, vol. 86, no. 3, pp. 449–468, 2013.

- [147] X. Guo and M. Bodson, "Analysis and implementation of an adaptive algorithm for the rejection of multiple sinusoidal disturbances," *IEEE Trans. Contr. Sys. Tech.*, vol. 17, no. 1, pp. 40–50, 2009.
- [148] H. M. Bagherpoor and F. R. Salmasi, "Robust model reference adaptive output feedback tracking for uncertain linear systems with actuator fault based on reinforced dead-zone modification," *ISA Transactions*, vol. 57, pp. 51–56, 2015.
- [149] A. M. Boker and H. K. Khalil, "Semi-global output feedback stabilization of non-minimum phase nonlinear systems," *IEEE Trans. Autom. Contr.*, 2016.
- [150] Y. Zhu, M. Krstic, and H. Su, "Adaptive output feedback control for uncertain linear time-delay systems," *IEEE Trans. Autom. Contr.*, vol. 62, no. 2, pp. 545–560, 2017.
- [151] A. H. Ghasemi, J. B. Hoagg, and T. M. Seigler, "Decentralized filtered feedback linearization for uncertain nonlinear systems," *Int. J. Robust Nonlin. Contr.*, vol. 28, no. 4, pp. 1496–1506, 2018.
- [152] B. Widrow and S. D. Sterns, *Adaptive Signal Processing*. Prentice Hall, 1985.
- [153] E. Bjarnason, "Analysis of the filtered-X algorithm," *IEEE Trans. Speech Audio Process.*, vol. 3, no. 6, pp. 504–514, 1995.
- [154] S. M. Kuo and D. Vijayan, "A secondary path modeling technique for active noise control systems," *IEEE Trans. Speech Audio Process.*, vol. 5, no. 4, pp. 374–377, 1997.
- [155] M. Zhang, H. Lan, and W. Ser, "Cross-updated active noise control system with online secondary path modeling," *IEEE Trans. Speech Audio Process.*, vol. 9, no. 5, pp. 598–602, 2001.
- [156] J. T. Pearson, R. M. Goodall, and I. Lyndon, "Active control of helicopter vibration," *Computer Contr. Eng. J.*, vol. 5, pp. 277–284, 1994.
- [157] J. Chandrasekar, L. Liu, D. Patt, P. P. Friedmann, and D. S. Bernstein, "Adaptive harmonic steady-state control for disturbance rejection," *IEEE Trans. Contr. Sys. Tech.*, vol. 14, no. 6, pp. 993–1007, 2006.
- [158] S. Pigg and M. Bodson, "Adaptive algorithms for the rejection of sinusoidal disturbances acting on unknown plants," *IEEE Trans. Contr. Sys. Tech.*, vol. 18, no. 4, pp. 822–836, 2010.
- [159] L. Bakule, "Decentralized control: An overview," *Annual Reviews in Control*, vol. 32, no. 1, pp. 87–98, 2008.
- [160] P. Ioannou, "Decentralized adaptive control of interconnected systems," *IEEE Trans. Autom. Contr.*, vol. 31, no. 4, pp. 291–298, 1986.

- [161] D. T. Gavel and D. D. Siljak, "Decentralized adaptive control: structural conditions for stability," *IEEE Trans. Autom. Contr.*, vol. 34, no. 4, pp. 413–426, 1989.
- [162] L. Shi and S. K. Singh, "Decentralized adaptive controller design for large-scale systems with higher-order interconnections," *IEEE Trans. Autom. Contr.*, vol. 37, no. 8, pp. 1106–1118, 1992.
- [163] S. Jain and F. Khorrami, "Decentralized adaptive control of a class of large-scale interconnected nonlinear systems," *IEEE Trans. Auto. Contr.*, vol. 42, no. 2, pp. 136–154, 1997.
- [164] C. Wen and Y. C. Soh, "Decentralized model reference adaptive control without restriction on subsystem relative degrees," *IEEE Trans. Autom. Contr.*, vol. 44, no. 7, pp. 1464–1469, 1999.
- [165] Y. Guo, Z.-P. Jiang, and D. J. Hill, "Decentralized robust disturbance attenuation for a class of large-scale nonlinear systems," *Sys. Contr. Lett.*, vol. 37, no. 2, pp. 71–85, 1999.
- [166] K. S. Narendra and N. O. Olegg, "Exact output tracking in decentralized adaptive control systems," *IEEE Trans. Autom. Contr.*, vol. 47, no. 2, pp. 390–395, 2002.
- [167] P. Krishnamurthy and F. Khorrami, "Decentralized control and disturbance attenuation for large-scale nonlinear systems in generalized output-feedback canonical form," *Automatica*, vol. 39, no. 11, pp. 1923–1933, 2003.
- [168] J. Zhou, "Decentralized adaptive control for large-scale time-delay systems with dead-zone input," *Automatica*, vol. 44, no. 7, pp. 1790–1799, 2008.
- [169] K. S. Narendra, N. O. Olegg, and S. Mukhopadhyay, "Decentralised adaptive control with partial communication," *IEE Proc. Contr. Theory Appl.*, vol. 153, no. 5, pp. 546–555, 2006.
- [170] J. D. Polston and J. B. Hoagg, "Decentralized adaptive command following and disturbance rejection for subsystems with local full-state feedback," *Int. J. Adapt. Contr. Sig. Proc.*, vol. 29, no. 5, pp. 581–602, 2015.
- [171] P. R. Pagilla, R. V. Dwivedula, and N. B. Siraskar, "A decentralized model reference adaptive controller for large-scale systems," *IEEE/ASME Trans. Mechatronics*, vol. 12, no. 2, pp. 154–163, 2007.
- [172] S. J. Elliott and C. C. Boucher, "Interaction between multiple feedforward active control systems," *IEEE Trans. Speech Audio Proc.*, vol. 2, no. 4, pp. 521–530, 1994.
- [173] D. Rao and S.-Y. Kung, "Adaptive notch filtering for the retrieval of sinusoids in noise," *IEEE Trans. Acoustics, Speech, Sig. Proc.*, vol. 32, no. 4, pp. 791–802, 1984.

- [174] P. A. Regalia, “An improved lattice-based adaptive IIR notch filter,” *IEEE Trans. Sig. Proc.*, vol. 39, no. 9, pp. 2124–2128, 1991.
- [175] B. S. Chen, T.-Y. Yang, and B.-H. Lin, “Adaptive notch filter by direct frequency estimation,” *Sig. Proc.*, vol. 27, no. 2, pp. 161–176, 1992.
- [176] G. Li, “A stable and efficient adaptive notch filter for direct frequency estimation,” *IEEE Trans. Sig. Proc.*, vol. 45, no. 8, pp. 2001–2009, 1997.
- [177] M. Mojiri and A. R. Bakhshai, “Stability analysis of periodic orbit of an adaptive notch filter for frequency estimation of a periodic signal,” *Automatica*, vol. 43, no. 3, pp. 450–455, 2007.
- [178] G. Obregon-Pulido, B. Castillo-Toledo, A. Loukianov *et al.*, “A globally convergent estimator for n-frequencies,” *IEEE Trans. Autom. Contr.*, vol. 47, no. 5, pp. 857–863, 2002.
- [179] X. Xia, “Global frequency estimation using adaptive identifiers,” *IEEE Trans. Autom. Contr.*, vol. 47, no. 7, pp. 1188–1193, 2002.
- [180] M. Hou *et al.*, “Amplitude and frequency estimator of a sinusoid,” *IEEE Trans. Autom. Contr.*, vol. 50, no. 6, pp. 855–858, 2005.
- [181] A. A. Bobtsov, “New approach to the problem of globally convergent frequency estimator,” *Int. J. Adapt. Contr. Sig. Proc.*, vol. 22, no. 3, pp. 306–317, 2008.
- [182] R. Marino and P. Tomei, “Adaptive notch filters are local adaptive observers,” *Int. J. Adapt. Contr. Sig. Proc.*, vol. 30, pp. 128–146, 2016.
- [183] M. Bodson and S. C. Douglas, “Adaptive algorithms for the rejection of sinusoidal disturbances with unknown frequencies,” *Automatica*, vol. 33, no. 12, pp. 2213–2221, 1997.
- [184] R. Marino, G. L. Santosuosso, and P. Tomei, “Robust adaptive compensation of biased sinusoidal disturbances with unknown frequency,” *Automatica*, vol. 39, no. 10, pp. 1755–1761, 2003.
- [185] R. Marino and P. Tomei, “Output regulation for linear minimum phase systems with unknown order exosystem,” *IEEE Trans. Autom. Contr.*, vol. 52, no. 10, pp. 2000–2005, 2007.
- [186] L. J. Brown and Q. Zhang, “Periodic disturbance cancellation with uncertain frequency,” *Automatica*, vol. 40, no. 4, pp. 631–637, 2004.
- [187] Z. Wu, M. Liu, and F. B. Amara, “Youla parameterized adaptive regulation against unknown multiple narrow-band disturbances,” *Trans. Institute Meas. Contr.*, vol. 36, no. 2, pp. 206–215, 2014.
- [188] G. C. Goodwin and K. S. Sin, *Adaptive Filtering, Prediction, and Control*. Prentice Hall, 1984.

- [189] R. Marino and P. Tomei, “An adaptive learning regulator for uncertain minimum phase systems with undermodeled unknown exosystems,” *Automatica*, vol. 47, no. 4, pp. 739–747, 2011.
- [190] R. Marino and P. Tomei, “Adaptive disturbance rejection for unknown stable linear systems,” *Trans. Institute Meas. Contr.*, vol. 38, no. 6, pp. 640–647, 2016.
- [191] L. Liu, Z. Chen, and J. Huang, “Parameter convergence and minimal internal model with an adaptive output regulation problem,” *Automatica*, vol. 45, no. 5, pp. 1306–1311, 2009.
- [192] L. Liu, Z. Chen, and J. Huang, “Global disturbance rejection of lower triangular systems with an unknown linear exosystem,” *IEEE Trans. Autom. Contr.*, vol. 56, no. 7, pp. 1690–1695, 2011.
- [193] M. Kamaldar and J. B. Hoagg, “Multivariable adaptive harmonic steady-state control for rejection of sinusoidal disturbances acting on an unknown system,” in *Proc. Amer. Contr. Conf.*, 2016, pp. 1631–1636.
- [194] M. Kamaldar and J. B. Hoagg, “Time-domain adaptive harmonic control for sinusoidal disturbances rejection,” in *Proc. Amer. Contr. Conf. IEEE*, 2018, pp. 5430–5435.
- [195] M. Kamaldar and J. B. Hoagg, “Time-domain adaptive higher harmonic control for rejection of sinusoidal disturbances acting on an unknown system,” *Contr. Eng. Practice*, 2019 (to be submitted).
- [196] M. Kamaldar and J. B. Hoagg, “Decentralized adaptive harmonic control for rejection of sinusoidal disturbances acting on an unknown system,” in *Proc. Amer. Contr. Conf. IEEE*, 2019 (under review).
- [197] M. Kamaldar and J. B. Hoagg, “Decentralized adaptive harmonic control for sinusoidal disturbance rejection,” *AIAA J. Guid. Contr. Dyn.*, 2019 (to be submitted).
- [198] M. Kamaldar and J. B. Hoagg, “Time-domain adaptive harmonic control for rejection of sinusoidal disturbances acting on an unknown discrete-time system,” in *Proc. Amer. Contr. Conf. IEEE*, 2017, pp. 5690–5695.
- [199] M. Kamaldar and J. B. Hoagg, “Adaptive harmonic control for rejection of sinusoidal disturbances acting on an unknown system,” *IEEE Trans. Contr. Sys. Tech.*, 2018.
- [200] M. Kamaldar and J. B. Hoagg, “Adaptive control for rejection of a sinusoidal disturbance with unknown frequency acting on an unknown system,” in *Proc. Amer. Contr. Conf. IEEE*, 2017, pp. 5696–5701.
- [201] D. S. Bernstein, *Matrix Mathematics*. Princeton Univ. Press, 2009.

- [202] D. H. Brandwood, “A complex gradient operator and its application in adaptive array theory,” *IEE Proceedings F (Communications, Radar and Signal Processing)*, vol. 130, no. 1, pp. 11–16, 1983.
- [203] J. Hong, J. C. Ackers, R. Venugopal, M. N. Lee, A. G. Sparks, P. D. Washbaugh, and D. S. Bernstein, “Modeling, identification, and feedback control of noise in an acoustic duct,” *IEEE Trans. Contr. Sys. Tech.*, vol. 4, pp. 283–291, 1996.
- [204] A. Esbrook, X. Tan, and H. K. Khalil, “An indirect adaptive servocompensator for signals of unknown frequencies with application to nanopositioning,” *Automatica*, vol. 49, no. 7, pp. 2006–2016, 2013.
- [205] P. Tomei, “Multi-sinusoidal disturbance rejection for discrete-time uncertain stable systems,” *Automatica*, vol. 79, pp. 144–151, 2017.
- [206] A. Bobtsov, A. Pyrkin, and S. Kolyubin, “Simple output feedback adaptive control based on passification principle,” *Int. J. Adapt. Contr. Sig. Proc.*, vol. 28, no. 7-8, pp. 620–632, 2014.
- [207] D. S. Bernstein, *Matrix Mathematics*, 2nd ed. Princeton University Press, 2009.
- [208] W. M. Haddad and V. Chellaboina, *Nonlinear Dynamical Systems and Control*. Princeton University Press, 2008.
- [209] P. Ioannou and B. Fidan, *Adaptive Control Tutorial*. SIAM, 2006.
- [210] K. J. Åström and B. Wittenmark, *Adaptive Control*. Courier Corporation, 2013.
- [211] P. K. Meher, J. Valls, T.-B. Juang, K. Sridharan, and K. Maharatna, “50 years of CORDIC: Algorithms, architectures, and applications,” *IEEE Trans. Circ. Sys.*, vol. 56, no. 9, pp. 1893–1907, 2009.
- [212] S. Pigg and M. Bodson, “Adaptive harmonic steady-state disturbance rejection with frequency tracking,” *Asian J. Contr.*, vol. 15, no. 1, pp. 1–10, 2013.
- [213] W. Sun, Y. Zhao, J. Li, L. Zhang, and H. Gao, “Active suspension control with frequency band constraints and actuator input delay,” *IEEE Trans. Indust. Electr.*, vol. 59, no. 1, pp. 530–537, 2012.

Vita

Mohammadreza Kamaldar was born in Shiraz, Iran, in 1987. He received the B.S.E. degree in mechanical engineering from Shiraz University, Shiraz, Iran, in 2009, and the M.S.E. degree in mechanical engineering from the University of Tehran, Tehran, Iran, in 2011. He started his Ph.D. studies in mechanical engineering at the University of Kentucky in 2013. His current research interests include adaptive control of mechatronic systems.